Program and Abstract Volume

LPI Contribution No. 1673

LUNAR AND PLANETARY INSTITUTE

USRA

Third International Planetary Dunes Workshop: Remote Sensing and Data Analysis of Planetary Dunes

June 12–15, 2012 • Lowell Observatory • Flagstaff, Arizona

Sponsors

National Aeronautics and Space Administration

Universities Space Research Association

Lunar and Planetary Institute

NASA's Planetary Dunes Program

Conveners

Timothy Titus
U.S. Geological Survey

Scientific Organizing Committee

Timothy Titus
U.S. Geological Survey

Mary Bourke
Planetary Science Institute

Lori Fenton
Carl Sagan Center at the SETI Institute

Rose Hayward
U.S. Geological Survey

Nick Lancaster
Desert Research Institute

Briony Horgan
Arizona State University

Dave Rubin
U.S. Geological Survey

Lunar and Planetary Institute 3600 Bay Area Boulevard Houston TX 77058-1113

LPI Contribution No. 1673

Compiled in 2012 by

Meeting and Publication Services
Lunar and Planetary Institute
USRA Houston
3600 Bay Area Boulevard, Houston TX 77058-1113

The Lunar and Planetary Institute is operated by the Universities Space Research Association under a cooperative agreement with the Science Mission Directorate of the National Aeronautics and Space Administration.

Abstracts in this volume may be cited as

Author A. B. (2011) Title of abstract. In Third International Planetary Dunes Workshop: Remote Sensing and Data Analysis of Planetary Dunes, p. XX. LPI Contribution No. 1673, Lunar and Planetary Institute, Houston.

ISSN No. 0161-5297

Preface

This volume contains abstracts that have been accepted for presentation at the Third International Planetary Dunes Workshop: Remote Sensing and Data Analysis of Planetary Dunes, June 12–15, 2012, Flagstaff, Arizona.

Administration and publications support for this meeting were provided by the staff of the Meeting and Publication Services Department at the Lunar and Planetary Institute.

Contents

Program

Tuesday, June 12, 2012
RON GREELEY MEMORIAL KEYNOTE DEDICATION
8:30 a.m. Giclas Lecture Hall

Workshop introduction and the Ron Greeley Dedication keynote presentation.

Chairs: **Timothy Titus**
James Zimbelman

8:30 a.m. Titus T. N. *
Workshop Introduction

8:35 a.m. Zimbelman J. R. *
"The Answer is Blowin' in the Wind": The Remarkable Aeolian Career of Ronald Greeley **[#7002]**

Tuesday, June 12, 2012
GLOBAL DUNE INVENTORIES AND DETECTION
9:00 a.m. Giclas Lecture Hall

Dunes are found on Earth, Mars, Venus, and Titan.
This reviews global inventories and dune detection methods.

Chairs: **Claire Newman**
Alice Le Gall

9:00 a.m. Ewing R. C. *
Source-to-Sink: Comparison of Boundary Conditions for Planetary Aeolian Systems **[#7022]**

9:30 a.m. Kreslavsky M. A. * Bondarenko N. V.
Aeolian Transport and Aeolian Deposits on Venus: An Overview of Remote Sensing Observations **[#7008]**

10:00 a.m. Le Gall A. * Rodriguez S. Garcia A. Radebaugh J. Lorenz R. D. Lopes R. M. C. Hayes A. Reflet E.
Titan's Dunes by the Numbers **[#7037]**

10:30 a.m. Newman C. E. * Richardson M. I. Rubin D. M. Lancaster N.
General Circulation Model Predictions of Dunes on Mars and Titan Using PlanetWRF **[#7009]**

11:00 a.m. Bandeira L. * Pina P. Marques J. S. Saraiva J.
Supervised Learning Strategies for Automated Detection of Martian Dune Fields **[#7039]**

11:30 a.m. DISCUSSION

Tuesday, June 12, 2012
BEDFORM MORPHOLOGY
1:00 p.m. Giclas Lecture Hall

From measurement of terrestrial dunes and ripples to the statistical study of dune field development and automated detection of bedform change, this session covers many aspects of bedform morphology.

Chairs: **Mark Bishop**
Dan Blumberg

1:00 p.m. Valdez A. *
Observations on Dune Behavior at Great Sand Dunes National Park, Colorado **[#7048]**

1:30 p.m. de Silva S. L. * Bridges N. T. Zimbelman J. R. Spagnuolo M. G. Burr D. M. Scheidt S. Ortiz A.
Investigating the Coarsest Gravel Ripples in Earth — Field Relationships, Sedimentological Character and Implications for Mars **[#7035]**

2:00 p.m. Zimbelman J. R. * Scheidt S. P.
Topographic Profiles Across a Large Reversing Dune, to Aid in Evaluating the Reversing Dune Hypothesis for TARs on Mars **[#7003]**

2:30 p.m. Bishop M. A. *
The Relationships Between Dune-Dune Interactions, Boundary Conditions and Dune Field Development, Al Liwa Basin, the Empty Quarter **[#7011]**

3:00 p.m. BREAK

3:30 p.m. Vaz D. A. * Silvestro S.
An Object Based Approach for the Mapping and Characterization of Mars Ripples **[#7019]**

4:00 p.m. Blumberg D. G. * August Y.
Radar Observations of Planetary Dune Analogues and Assessing Their Stability Using Synthetic Aperture Radar **[#7006]**

4:30 p.m. DISCUSSION

Tuesday, June 12, 2012
AEOLIAN SANDSTONES — KEYNOTE PRESENTATION
AND INSIGHTS FOR THE FIELD TRIP
5:00 p.m. Giclas Lecture Hall

Chairs: **David Rubin**
Mary Bourke

5:00 p.m. Edgar L. A. *
Reconstruction of Eolian Bedforms and Paleocurrents at Meridiani Planum, Mars **[#7027]**

5:30 p.m. Rubin D. *
Field Trip Expectations and Preparation

6:00 p.m. DISCUSSION

Tuesday, June 12, 2012
POSTER SESSION
6:30 p.m. Rotunda Museum

Rodriguez S. Le Mouélic S. Barnes J. W. Hirtzig M. Rannou P. Sotin C. Brown R. H. Bow J. Vixie G. Cornet T. Bourgeois O. Narteau C. Courrech du Pont S. Le Gall A. Reffet E. Griffith C. A. Jauman R. Stephan K. Buratti B. J. Clark R. N. Baines K. H. Nicholson P. D. Coustenis A.
Equinoctial Atmospheric Activity over Titan Dune Fields Revealed by Cassini/VIMS **[#7029]**

Hayes A. G. Ewing R. C. Lucas A. McCormick C. Troy S. Ballard C.
Determining Timescales of the Dune Forming Winds on Titan **[#7057]**

Lorenz R. D.
Timescales of Dune Obliteration and Repair on Titan **[#7014]**

Diniega S.
Venusian Dunes — Where are They? An Update **[#7015]**

Draut A. E. Rubin D. M.
Interactions Between Subaqueous and Aeolian Sedimentary Systems **[#7004]**

Bridges N. T. de Silva S. L. Zimbelman J. R. Lorenz R. D.
Formation Conditions for Coarse-Grained Megaripples on Earth and Mars: Lessons from the Argentinean Puna and Wind Tunnel Experiments **[#7010]**

Dinwiddie C. L. Michaels T. I. Hooper D. M. Stillman D. E.
Environmental Conditions and Meteorologic Context for Modification of the Great Kobuk Sand Dunes, Northwestern Alaska **[#7033]**

Scheidt S. P.
Sand Transport Pathways of Dark Dunes in the Sperrgebiet: Sand Composition and Dune Migration Rates from ASTER Data **[#7051]**

Demitroff M. Cicali M. Smith J. Demitroff A. N.
Ancient Eolian Landforms and Features from a Terrestrial Mid-Latitude Periglacial Environment **[#7041]**

Hooper D. M. Dinwiddie C. L. McGinnis R. N.
Meltwater-Induced Debris Flows on Cold-Climate Aeolian Dunes and the Implications for Analogous Processes on Mars **[#7046]**

Cox C. Isherwood R. Reitz A. Krahenbuhl R. Andrews-Hanna J. C. Valdez A.
Geophysical Analysis of the Crestone "Crater", Great Sand Dunes National Park, Colorado **[#7042]**

Titus T. N. Cushing G. E.
Thermal Diffusivity Experiment at the Grand Falls Dune Field **[#7044]**

Bachman S. R. Titus T. N. Edwards C. S.
Mineral Analysis of Martian Dunes: Constraining Possible Sediment Source **[#7032]**

Berman D. C. Balme M. R. Michaels T. I.
Investigations of Transverse Aeolian Ridges on Mars **[#7025]**

Mattson S. Bridges N. T. Kirk R. L. Howington-Kraus E. Mogk N. Ojha L.
Studying Martian Dune Changes with HiRISE DTMs and Orthoimages **[#7030]**

Wednesday, June 13, 2012
FIELD TRIP TO STUDY SEDIMENTARY FEATURES IN THE AEOLIAN NAVAJO AND ENTRADA SANDSTONES NEAR PAGE, ARIZONA
7:30 a.m. USGS Parking Lot

The trip is expected to last approximately 7–8 hours with an additional 4 hours of travel and dinner time. We will stop for dinner in Page at 6:00 p.m. Light snacks and lunch will be provided for the trip.

Important Note About Parking

USGS Parking Lot, Gemini Dr., Flagstaff AZ 86001

Please park your vehicle on the north side of the parking lot.
Alternative parking is available just outside the USGS campus on Gemini Drive,
or in the Buffalo Park parking lot at the end of Gemini Drive.

Thursday, June 14, 2012
TRANSPORT, WINDS, AND BEDFORM DYNAMICS
8:30 a.m. Giclas Lecture Hall

From the scale of ripples to sand seas, we will discuss techniques to quantify the evolution of bedforms and dune fields in response to incident flows.

Chairs: **Hezi Yizhaq**
Tim Michaels

8:30 a.m. Yizhaq H. * Kok J.
Basaltic Sand Ripples in Eagle Crater as Indirect Evidence for the Hysteresis Effect in Martian Saltation **[#7023]**

9:00 a.m. Rubin D. M. *
A Unifying Model for Planform Straightness of Ripples and Dunes in Air and Water **[#7020]**

9:30 a.m. Fenton L. K. * Beyer R. A.
Reconstructing the Formative Winds of a Dune Field in Ganges Chasma, Mars, by Bootstrapping with the Rule of Maximum Gross Bedform-Normal Transport **[#7028]**

10:00 a.m. Reffet E. * Courrech du Pont S. Hersen P. Douady S.
Evolution of Laboratory Dunefields Analogs **[#7043]**

10:30 a.m. Michaels T. I. *
Towards a Better Understanding of Longer-Term Aeolian Processes on Earth via Dynamical Downscaling **[#7045]**

11:00 a.m. Radebaugh J. * Lorenz R. D. Le Gall A.
Dunes on Titan at the Beginning of the Cassini Solstice Mission **[#7031]**

11:30 a.m. DISCUSSION

Thursday, June 14, 2012
DUNE COMPOSITION AND SEDIMENT SOURCES
1:00 p.m. Giclas Lecture Hall

This session showcases ongoing work to understand the origin and transport pathways of dune sediments using remote sensing, with a focus on dunes sourced from volcaniclastic sediments.

Chairs: **Laura Kerber**
Daniela Tirsch

1:00 p.m. Tirsch D. * Jaumann R.
On the Sources of Dark Dune Sands on Mars **[#7017]**

1:30 p.m. Horgan B. * Clarke D. Bell J. F. III
Evidence for Glass-Rich Pyroclastics in Martian Dunes **[#7050]**

2:00 p.m. Burr D. M. * Zimbelman J. R. de Silva S. L. Bridges N. T. Chojnacki M. Qualls F. B.
Testing the Volcaniclastic Hypothesis for Martian Dune Sediments: The Medusae Fossae Formation, Mars, and Andean Ignimbrites, Earth **[#7024]**

2:30 p.m. Chojnacki M. * Moersch J. E. Burr D. M. Wray J. J.
Potential Sediment Sources and Pathways in Valles Marineris Dune Fields: Implications for Martian Aeolian Systems **[#7040]**

3:00 p.m. BREAK

Thursday, June 14, 2012
CRYO-AEOLIAN PROCESSES AND LANDFORMS
3:30 p.m. Giclas Lecture Hall

Studies that relate the important role of ice in the evolution of planetary aeolian systems.

Chairs: **Cynthia Dinwiddie**
Devon Burr

3:30 p.m. Lorenz R. D. * Valdez A.
Observations of Niveo-Aeolian Activity at Great Sand Dunes National Park and Preserve (GSDNPP) **[#7013]**

4:00 p.m. Dinwiddie C. L. * McGinnis R. N. Jr. Stillman D. E. Bjella K. L. Grimm R. E.
Internal Sedimentary Structure and Aqueous-Phase Distribution of the Great Kobuk Sand Dunes, Northwestern Alaska: Insights from an Arctic Aeolian Analog Site **[#7034]**

4:30 p.m. Putzig N. E. * Bowers L. M. Mellon M. T. Herkenhoff K. E. Phillips R. J.
Thermal Effects of Physical Heterogeneity in Olympia Undae **[#7054]**

5:00 p.m. Smith I. B. * Holt J. W.
The Northern Spiral Troughs of Mars as Cyclic Steps: A Framework for Using Observations of Active Processes to Calculate Migration and Accumulation Rates on the NPLD **[#7047]**

5:30 p.m. DISCUSSION

Friday, June 15, 2012
RECENT BEDFORM MIGRATION ON MARS
8:30 a.m. Giclas Lecture Hall

Given the abundant data indicating present-day bedform migration on mars, we will discuss the current status of these investigations and possible implications for aeolian processes on this windy planet.

Chairs: **Matthew Chojnacki**
Lynn Neakrase

8:30 a.m. Geissler P. E. * Banks M. E. Bridges N. T. Silvestro S. HiRISE Science Team
HiRISE Observations of Sand Dune Motion on Mars: Emerging Global Trends **[#7053]**

9:00 a.m. Silvestro S. * Vaz D. A. Rossi A. P. Flahaut J. Fenton L. K. Ewing R. C. Geissler P. E.
Active Aeolian Processes Along Curiosity's Traverse **[#7036]**

9:30 a.m. Ayoub F. * Bridges N. T. Avouac J.-P. Leprince S. Lucas A.
Measuring Sand Flux and its Seasonality from a Time Series of HiRISE Images **[#7026]**

10:00 a.m. Bourke M. C. * Parteli E. J. R. Byrne S. Berman D. C.
Dune Migration in the North Polar Region of Mars **[#7007]**

10:30 a.m. DISCUSSION

Friday, June 15, 2012
SESSION REVIEWS AND WORKSHOP ACCOMPLISHMENTS
11:00 a.m. Giclas Lecture Hall

Session synopsis, discussion of workshop accomplishments, and deciding the top 10 recommendations for the EOS meeting proceedings article.

Chairs: **Timothy Titus**

11:00 a.m. Co-Chairs
Session Synopsis

11:30 a.m. Titus T. N. *
Deciding the Top Ten for EOS

12:00 p.m. MEETING ADJOURNS

MEASURING SAND FLUX AND ITS SEASONALITY FROM A TIME SERIES OF HIRISE IMAGES

F. Ayoub[1] , N.T. Bridges[2] , J-P. Avouac[1] , S. Leprince[1] , A. Lucas[1], [1]Division of Geological and Planetary Sciences, California Institute of Technology, Pasadena, CA 91125 (fayoub@gps.caltech.edu), [2]Applied Physics Laboratory, 11100 Johns Hopkins Road, Laurel, MD 20723

Introduction: The volumetric transport rate of sand, or flux, is a fundamental parameter that affects the rate of landscape modification through surface covering and removal, and abrasion of rocks and landforms. This is particularly the case on Mars, where aeolian processes are the dominant geomorphic agents. Measuring sand flux on Mars was previously not possible because of the lack of high spatial and temporal resolution images, and of quantitative techniques, for making displacement and accurate topographic measurements. These limitations have now been overcome because, 1) It is found that many dunes and ripples on Mars are mobile in High Resolution Imaging Science Experiment (HiRISE) images [1-4], and 2) the application of precise image registration and correlation methods permits the quantification of movement to sub-pixel precision that, when combined with topographic data, permits the derivation of reptation and saltation sand flux [5].

Here, we first measure the migration rate of sand ripples and dune lee fronts at Nili Patera, Mars over a 105 days, and derive the reptation and total fluxes. Second, the seasonal variation of the sand flux is assessed from the processing of a time-series of images spanning almost a Mars year. Third, from the extraction of two DEMs acquired 390 days apart, we measure dune migration rate. The dunes have unexpectedly high sand fluxes similar to those in Victoria Valley, Antarctica, implying that rates of landscape modification on Mars and Earth are similar.

Methods: Recent advances in image registration and correlation techniques permit the quantitative measurement of changes down to the sub-pixel level. This has been implemented in the COSI-Corr tool suite, which provides quantitative surface dynamics measurements via automatic and precise ortho-rectification, co-registration, and sub-pixel correlation of images [6]. Under a Mars Data Analysis Program effort, we have used COSI-Corr on HiRISE images, with the goal of quantifying bedform changes on Nili Patera dune field, where unambiguous ripple motion has been identified.

Four images were used in the first part of our analysis (Table 1 – 4 first rows). ESP_017762_1890 (subsequently designated *S*1) and ESP_018039_1890 (*S2*) were processed to make a stereo-derived digital elevation model (DEM). PSP_004339_1890 (*T*1) and PSP_005684_1890 (*T*2) were draped onto the DEM to make an orthorectified model. In processing orthorectified images *T*1 and *T*2 through COSI-Corr, the displacement of ripples across the entire dune field in the overlap region was computed (Figure 1). In addition, using the registered image *S*1 and comparing to *T*2, the displacement of dune lee fronts was measured.

Image ID	L_s(°)	Date Acquired	ΔDays
PSP_004339_1890	268	6/30/07	0
PSP_005684_1890	330	10/13/07	105
ESP_017762_1890	89	5/11/10	941
ESP_018039_1890	99	6/2/10	22
ESP_020729_1890	207	12/28/10	209
ESP_021652_1890	252	03/10/11	72
ESP_022364_1890	287	05/05/11	56
ESP_023076_1890	319	06/29/11	55
ESP_023353_1890	331	07/21/11	22
ESP_023564_1890	340	08/06/11	33
ESP_023920_1890	354	09/03/11	28

Table 1: HiRISE images used in the analysis

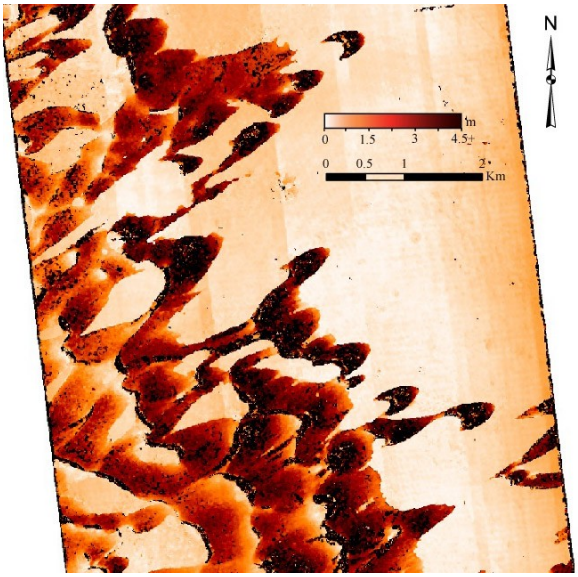

Figure 1: Map of the ripple migration amplitude over 105 days at Nili Patera. Displacement as large as 4m could be measured. The entire dune field is subject to ripple migration.

Interpretation: The ripple and dune migration rates are related, as they both reflect sand transport, and can be used to estimate sand flux [7,8]. The dune migration rates derived from lee front advancement are approximately 5 times larger than the ripple-derived

rates. The higher values characterize the contribution of the saltation sand flux that is not considered in the correlation of ripples-to-dunes-derived fluxes.

Sand fluxes at the dune crests is comparable to sand fluxes for dunes in Victoria Valley, Antarctica, based on their crest heights and migration rates [9]. Terrestrial studies show that bulk and interdune sand fluxes are about 1/3 that of the crest flux [10], such that typical fluxes in Nili should be ~2.3 m^3/m/yr.

Seasonal variability: Once the methodology was established on the previous pair of image acquired in 2007, the same technique was applied to a time-series of eight images acquired in 2010-2011 (Table 1) which covers a period of more than 2/3 of a Mars year. The objective was to assess the variation of the ripple migration, and the associated sand flux, over time. Pairs of sequential images, *i.e.*, ESP_018039 and ESP_020729, ESP_020729 and ESP_021652, and so forth, were processed in COSI-Corr for a total of seven displacement maps obtained. Using a Principal Component Analysis (PCA) on the time-series of ripple displacement maps, the seasonal variation of the ripple migration rate was estimated. Around 65% of the variance is explained by the first component of the PCA. This rate is directly related to the sand flux as seen in the first part of this study.

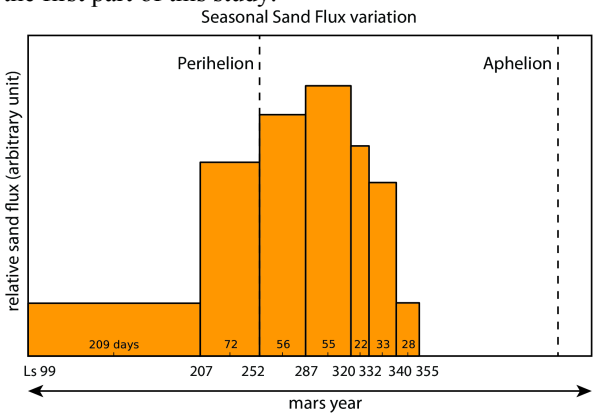

Figure 2: Relative average sand flux observed between the acquisition dates, function of the time of a mars year starting 06/02/10. A strong sand flux activity is observed around perihelion. Around 1/3 of the year cannot be measured due to absence of data.

Figure 2 represents the variability of the ripple migration rate for the seven pairs. Although we do not have a temporal coverage of a full Mars year, we clearly observe a variation of the migration rate, or sand flux, with a peak in activity that corresponds to the perihelion season. These measurements suggest that the migration rate, or sand activity, is permanent over the year, with a high activity around the perihelion season that spans ~1/3 of a year. The orientation of the ripple displacement is stable in time at ~115 degrees from the North direction (counter-clockwise), suggesting also that the wind direction is quite constant in the area, consistent with earlier studies [1,4].

Dune migration from DEM comparison: In addition to the time-series a second stereo pair of images was acquired in 2011, 390 days after the first stereo pair. The DEM extraction was operated using SOCET-SET with the same post-spacing resolution than the first DEM. The objective is to detect and measure dune migration, as opposed to ripple migration, by comparing the two DEMs. Prior to comparison, the DEMs registration, which was not precise enough out of SOCET-SET, was improved by wrapping the second DEM onto the first one using the bedrock only as a support for registration. The registration residual was estimated at around 40cm RMSE and is mostly due to residual in CCD registration and uncorrected attitudes. Once the DEMs were registered, a few topographic profiles on the dunes were extracted (Figure 3). The good registration of the bedrock and misalignment of the dunes reveal a dune migration of up to 1 meter per Earth year for the fastest dunes. An ongoing work is to automatically retrieve the full dune migration map from the DEMs.

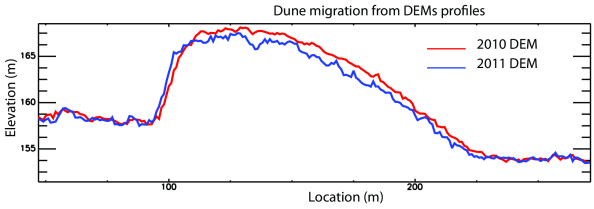

Figure 3: Comparison of dune profiles extracted from registered 1-m post-spacing DEMs that were acquired 390 days apart. A migration of about 1m can be observed in that time span.

References: [1] Silvestro, S. et al. (2010), *GRL, 37*. doi:10.1029/2010GL044743. [2] Chojnacki, et al. (2011), *JGR, 116*, doi:10.1029/2010JE003675. [3] Hansen, C.J. et al. (2011), *Science, 331,* 575-578. [4] Bridges, N.T. et al. (2012), *Geology, 40*, 31-34. [5] Bridges, N.T. et al. (2012), Nature, in press. [6] Leprince, S. et al. (2007), *IEEE Tran Geosci. Rem. Sens., 45*, 1529-1558. [7] Claudin, P. and B. Andreotti, B. (2006), *EPSL, 252*, 30-44. [8] Andreotti, B. et al. (2006), *Phy. Rev. Lett., 96*, 028001. [9] Bourke, M.C. et al. (2009), *Geomorph., 109,* 148-160. [10] Ould Ahmedou, D. et al. (2007), *JGR, 112*, doi:10.1029/2006JF000500.

MINERAL ANALYSIS OF MARTIAN DUNES: CONSTRAINING POSSIBLE SEDIMENT SOURCE. S.R. Bachman[1,2], T.N. Titus[2], C.S. Edwards[3] [1]Northern Arizona University, Flagstaff, AZ, 86001 (savbachman@sbcglobal.net), [2]U.S.G.S., Astrogeology Science Center, 2255 N. Gemini Dr., Flagstaff, AZ 86001, [3]Arizona State University, Tempe, AZ, 85287.

Introduction: Mars is an arid planet with few active geomorphic changes. The principle geomorphologic process in an arid environment is shear wind velocities [1]. These aeolian processes erode bedrock creating unconsolidated sediment that is readily transported. Bedrock on Mars is composed primarily of two types of solidified magmas; one is basalt which is lower in silica content than the other, silica rich, andesitic-basalt [2]. When these lavas solidify, unique minerals nucleate into crystals. The minerals that form are determined by the lava cooling rate and composition of the magma. Comparative mineral compositions of dunes and their surroundings may suggest whether the source of the dune sediment is local or global. Here we explore the spatial variability of mineral compositions of Martian dunes and discuss the implications for sediment sources.

Technique: Six dune fields were chosen from the Mars Global Digital Dune Database [3] in the latitude band 65°N to 65°S (Table 1). These dunes were analyzed using emissivity spectra from the Thermal Emission Spectrometer (TES) [4]. It was necessary to find dunes with high temperatures so that the thermal spectra collected by TES would have a high signal-to-noise ratio [5]. The averaged spectrum of each dune field was deconvolved into its mineral end-members using SMA in the programming environment DaVinci (http://davinci.asu.edu).

Table 1: Spectral library compiled of the mineral end members used during this study. These include igneous basalt type minerals: plagioclase, olivine, pyroxene, and quartz.

Acidalia Type Surface	**Microcline**
Albite	**Oligoclase**
Andesine	**Olivine Fo10**
Anorthite	**Olivine Fo35**
Anorthoclase	**Olivine Fo68**
Augite	**Quartz**
Diopside	**Syrtis Type Surface**
Enstatite	

Mineral comparisons on and off the dune field were used to identify mineral abundances on the dune and were compared to mineral abundances surrounding the dune field. A variety of minerals were selected from the ASU spectral library (SPECLIB) based on expected mineral compositions previously researched by others (e.g., [6,7] Table 1). In this study, we focused on olivine Fo35 and anorthoclase.

Analysis: The six dune fields chosen for this study show the greatest variance in olivine Fo35 which is iron rich, and anorthoclase which is an aluminum rich feldspar. All of the dune fields except field #4 are located within impact craters (Fig. 1, Table 2). Mineral abundances of the dune fields were compared to the mineral abundances of regions within 10 km north and south of each field. Based on the changes in abundance from the dune site to the surrounding areas, sediment sources were defined as local or non-local, where local means the dune field's mineral composition is similar to its' immediate surroundings.

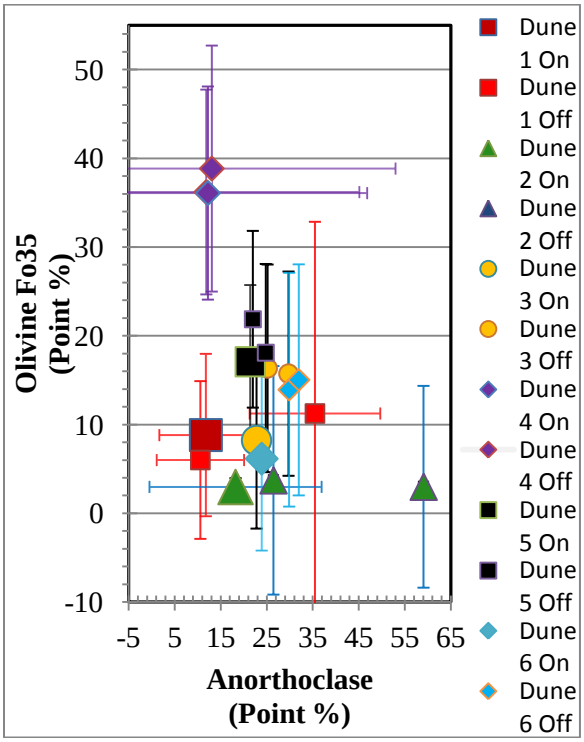

Figure 1: Graphical presentation of olivine Fo35 and anorthoclase abundances compared on and off of each dune field.

The mineral abundances in dune field #1 are consistent with the mineral abundances of the surrounding regions suggesting that the sediment source is local.

Dune field #2 contained small amounts of olivine similar to its surroundings. Anorthoclase abundances were significantly lower on the dune field when compared to surroundings. The lower dune field abundance may suggest a non-localized source for anorthoclase. However; a small crater located adjacent

to the dune field may be an additional source for sediment of different mineral compositions which was measured by TES in this study.

Dune fields #3 and #6 were the most similar in mineral abundance to each other and their surroundings. The abundance of olivine on the dune is less than the surroundings. Anorthoclase abundances remain somewhat constant. The olivine variance of the dune region is indicative of a non-localized source.

The composition of dune field #4 is similar to its surroundings, suggesting that it was derived from a local source.

The abundances of both minerals in dune field #5 varied by small amounts, suggestive of a local sediment source.

Conclusion: Using anorthoclase and olivine Fo35 to compare compositions of dunes and their surroundings, sediment sources were found to be local or non-local. Three dune fields are composed of local sediment. This was concluded by the abundances being evenly dispersed over the dune regions. Two dune fields have variations in mineral abundances over the dune regions which indicate non-local transport. One dune field has a unique abundance of anorthoclase, but the sediment source is undetermined. Future research into sediment transport could potentially be used to map global wind pathways over the surface of Mars.

Acknowledgements: I would like to thank Rose Hayward and Justin Hagerty for their insightful comments.

References: [1] Bridges et al. (2011) LPSC XLII. [2] Bandfield, J. L. (2002), Geophys. Res., 107 (E6), 5042, doi:10.1029/2001JE001510. [3] Hayward, et al., (2009) JGR 114.E11012; [4] Christensen et al. (2001) JGR 106(E10) 23,823-23,871; [5] Smith, et al. (2000) JGR 105(E4), 9589-9607. [6] Cornwall et al. (2010) 2nd IPDW, Abstract #2016; [7] Edwards et al. (2008) JGR 113.E11003.

	Dune ID	Lat/ Long	Olivine Fo35 On	Off North	Off South	Anorthoclase On	Off North	Off South	Local/Non-Local
1	1279-148	125.7/ -13.8	8.82	11.25	6.01	11.81	35.51	10.62	Local
2	2461-581	246.1/ -58.9	2.97	2.99	3.72	18.26	59.09	26.49	Undetermined
3	2086-603	208.5/ -60.3	8.22	16.34	15.74	22.82	25.22	29.77	Non-local
4	3124-080	311.6/ -7.8	36.09	38.85	36.21	12.26	13.11	11.91	Local
5	0194-468	19.5/ -46.8	17.08	21.87	18.1	21.45	22.02	24.83	Local
6	1640-615	164.4/ -61.4	6.16	13.93	15.04	23.95	29.89	32.00	Non-local

Table 2: Comparative mineral analysis for each dune, indicating local or non-local sediment source which is based off the abundance found of each mineral on and off the dune. The mineral abundances in this table are recorded as precentages.

SUPERVISED LEARNING STRATEGIES FOR AUTOMATED DETECTION OF MARTIAN DUNE FIELDS. L. Bandeira[1], P. Pina[1], J. S. Marques[2] and J. Saraiva[1], [1]CERENA / IST (Av. Rovisco Pais, 1049-001 Lisboa, Portugal; lpcbandeira@ist.utl.pt), [2]ISR / IST (Av. Rovisco Pais, 1049-001 Lisboa, Portugal).

Introduction: The knowledge on sand dunes on Mars has increased significantly with the availability of very high resolution (VHR) images of the surface, namely, MOC N/A and HiRISE [1]. Assessing the global distribution, shape and other characteristics of dunes with a higher detail can lead to an improved understanding of the interactions between the atmosphere and the surface of the planet [2]. The sheer quantity of data to be analyzed suggests that the use of automated methods can play an important role in fully exploiting the information that is being collected by automated probes. Thus, there are published studies using automatic procedures on temporal change detection [3, 4], determination of dune heights [5], morphologies [6] and spatial patterns [7], often considering analogies with terrestrial dunes. There is an automated method [8] using texture features and a neural network based classifier to identify terrestrial dunes on images with tens of meters but with performances below 70%. We have been addressing the development of automated methods for the delineation and characterization of dune fields, with good results on VHR images of Mars [9, 10]. In here, after a short reminder of our methodology, we report the most recent advances achieved.

Methodology: The supervised learning strategy followed in our approach is based on the tiling of an image into relatively small square cells, which are then classified. These simple geometric shape makes the analysis very fast and leads to a non-iterative solution which is compatible with the large amount of data to be processed. This task is done through the extraction and analysis of local information (image features) along the regular grid of the tiled image. To benefit from context and diminish the dependence on specific factors such as illumination, an aggregation of the local features of neighbouring cells is performed within a block, i.e., a region constituted by 3×3 cells, and that constitutes the detection window of the methodology [11]. This block window is moved along the whole grid with a cell-sized step in order to analyse the complete image. For the mathematical formalism and additional details, consult our previous publication [10].

For this work we test the method with two different classifiers: Support-Vector Machine (SVM), as in previous works, and Random Forests (RF), that models the classification problem using multiple decision trees trained from random subsets of data [12].

Dataset: In order to demonstrate the generalized application of supervised learning strategies we continue to enlarge our dataset, now constituted by 230 MOC N/A images distributed around the surface of the planet. All have a spatial resolution better than 6.80 m/pixel, down to 1.45 m/pixel, in order to detect in detail small dune fields. About 70% of the images constituting the dataset (160 out of 230 images) include examples of the major types of dunes, according to the literature [13-15]: barchans (13%), barchanoid (19%), transverse (2%), dome (6%), linear (8%), star (1%), sand sheet (5%) and others (17%). These 160 images were visually analysed, in order to construct a ground-truth for each of them by manually drawing the contours of the dunes. The other 70 images (30% of the dataset) contain other geomorphological structures that can be confounded with dunes (channels, crater rims, textured terrain, among others).

To compare the ground-truth with the result produced by the automated classifiers, both must be in the same format. Thus, we had to tile each ground-truth exactly like its corresponding original image. Furthermore, we had to consider three types of cells: 'non-dune', 'dune' and 'unclassifiable'. To assign one of these labels to a cell, we computed the area occupied by dune terrain in the block from which it is the centre: if this area is less than 10% of the number of pixels of the block, the cell is 'non-dune'; if it is higher than 30%, the cell is 'dune'; if the area is between 10 and 30%, we decided not to classify it.

Results: The performance of each classifier is evaluated through the computation of the probabilities of false negatives ($p_{FN} = FN/(FN+TP)$), false positives ($p_{FP} = FP/(FP+TN)$) and of a global error ($p_{error} = p_N.p_{FP} + p_P.p_{FN}$), where FN stands for the number of false negative cells, TN the number of true negative cells, FP the number of false positive cells, TP the number of true positive cells, N the total number of negative cells and P the total number of positive cells.

The classification output is illustrated globally in Fig. 1 on an entire MOC image and in detail in Fig. 2 on several images to illustrate successful and insuccessfull examples of the approach. The results we have obtained for the whole set of images confirm that this methodology is a valid contribution to the

automated mapping of dune fields on remotely sensed images. There are 370,019 cells to be classified in the 230 images, and the average global error obtained is 0.11. Moreover, we employed a cross-validation procedure where the dataset was divided in five groups, and each of those was used in turn to test the methodology (while the other four were, in each run, used for training). The five groups were built in such a way as to have a comparable number of positive 'dune' examples. The results for these five runs are similar and illustrate the robustness of the methodology: the lowest probability of error is 0.09, the highest is 0.14.

Table I – Classification performances.

	p_{FP}	p_{FN}	p_{error}
SVM	0.11	0.09	0.11
RF	0.12	0.08	0.10

We have also evaluated the classification performance by type of dune. Barchan and barchanoid types achieve the best performance with a probability of error of 0.09; on the other hand the star dunes, show the worst probability of error, but even this is only about 0.21, which we believe is due to a poor representation in the dataset.

Conclusion: The performance of our methodology, based on gradient histograms coupled with either a SVM or a RF classifier, can be considered very good, with an average of error of about 11%. This fact reinforces the idea that advances made towards the classifiers may continue to lead to marginal gains in the detection of dune fields, indicating that the main area of future intervention should be on the extraction of other types of features combined with a multi-scale approach to better describe the whole pattern spectra of Martian dunes.

References: [1] Bourke MC et al (2010) *Geomorph, 121,* 1-14. [2] Fenton LK and Hayward RK (2010) *Geomorph, 121,* 98-121. [3] Silvestro S et al (2010) *GRL, 37,* L20203. [5] Silvestro S et al (2011) *GRL,* 38, L20201, [5] Bourke MC et al (2006) *Geomorph, 81,* 440-452. [6] Ewing RC et al (2006) *ESPL, 31,* 1176-1191. [7] Bishop MA (2010) *Geomorph, 120,* 186-194. [8] Chowdhury PR et al (2011) *IEEE JSTARS, 4,* 171-184. [9] Bandeira L et al (2010) *LNCS, 6112,* 306-315. [10] Bandeira L et al (2011) *IEEE GRSL, 8,* 626-630. [11] Dalal N and Triggs B (2005) *Proc. CVPR,* 886-893. [12] Breiman L (2001) *ML,* 45, 5–32. [13] Mckee ED (1979) Univ. Press Pacific, Honolulu. [14] Hayward R et al (2007) *JGR, 112,* E1107. [15] Hayward R (2011) *ESPL,* 36(14), 1967-1972.

Acknowledgments: Work supported by FCT (Portugal), through project ANIMAR (PTDC/CTE-SPA/110909). LB and JS acknowledge finantial support in the form of BPD and BD grants from FCT.

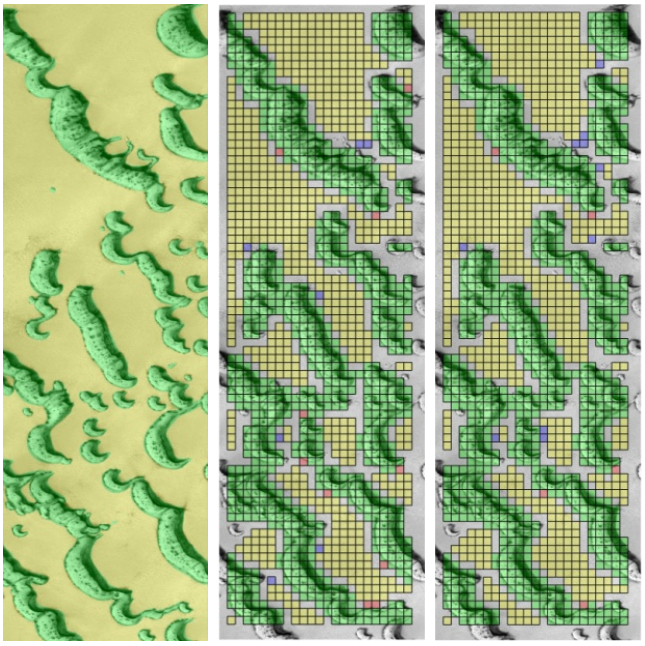

(a) (b) (c)

Fig. 1. Example of automated dune classification on E18-00494 image: (a) ground-truth; (b) SVM and (c) RF outputs (*TP* in green, *TN* in yellow, *FN* in red and *FP* in blue). [image credits: MSSS/NASA/JPL].

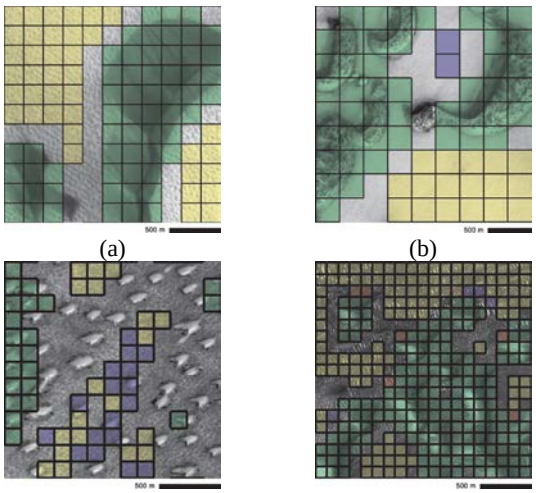

(a) (b) (c) (d)

Fig. 2. Details of correct detections (a, b) and unsolved problems (c, d) in images differently zoomed (each cell is 40 pixels wide): (a) E03-02056. (b) R18-01147. (c) R17-02607. (d) E03-00618 (colours have the same meaning of Fig.1) [image credits: MSSS/NASA/JPL).

INVESTIGATIONS OF TRANSVERSE AEOLIAN RIDGES ON MARS. Daniel C. Berman[1], Matthew R. Balme[1], and Timothy I. Michaels[2], [1]Planetary Science Institute, 1700 E. Ft. Lowell Rd., Suite 106, Tucson, AZ 85719; [2]Southwest Research Institute, 1050 Walnut Street, Suite 300, Boulder, CO 80302; bermandc@psi.edu.

Introduction: As noted first from Viking Oribter images [1,2] and more recently from Mars Global Surveyor (MGS) Mars Orbiter Camera (MOC) narrow-angle (NA) images [3,4], a population of aeolian bedforms exists that is morphologically and dimensionally distinct from Large Dark Dunes (LDD) fields, being generally brighter than, or of similar albedo to, the surrounding terrain [3]. These features are significantly smaller than the dark dunes (Fig. 1), appear to form normal to local winds, and tend to have simple, transverse, "ripple-like" morphologies. Whether these small martian bedforms represent extremely large ripples, small transverse dunes, or something entirely different is currently under debate, and so they have been designated "Transverse Aeolian Ridges" [5].

TARs are one of the most common landforms on Mars. As the smallest aeolian landforms observed from orbit, TARs are clearly important for understanding meso- and small-scale interactions between the surface and atmosphere. TARs are also indicative of the weathering and sediment transport regime on Mars and an understanding of their morphologies, morphometries, and composition can provide information on the composition, mobility, and availability of aeolian sediments on Mars. Moreover, the spatial distribution of TARs provides information about where on Mars aeolian sediments are concentrated. If we can determine if TARs were active only in the past, or whether TARs are mobile under today's wind conditions, then we can begin to assess when and where TARs are/were active over Mars' recent geological history. Thus TARs have the potential for being indicators/records of climate change on Mars.

Methodology: In this work we focus on the local/regional scale and thus have identified six regional study areas, each 5° by 5°, to investigate the behavior of TARs in detail; one in the northern hemisphere, three in the equatorial band, and two in the southern hemisphere. All HiRISE, CTX, and MOC images for each study area have been downloaded from the PDS, processed in ISIS, and ingested into an ArcGIS database. By exploring sediment sources, climate, and local topography/geology as potential factors, we can constrain potential formation mechanisms.

Mapping of surficial deposits: Surficial sediment deposit maps of each study area are being produced to trace sediment from source to sink, and to investigate whether LDDs and TARs share sediment sources and pathways. Initial results for one study area are shown in Fig. 2. Note that TARs are mostly found near LDDs or dark deposits, indicating a related source. Note also that nearly all of the deposits are found in local topographic lows, or sediment traps.

We are mapping TARs in terms of morphology and morphometry. For each of the study areas we are mapping the surficial deposits with a focus on sediment pathways, sediment sources, and interactions/associations between TARs and LDDs. We are primarily using CTX data for this task. We are mapping 1) TARs (including orientations, degree of saturation and morphological characteristics as described by [6,7], 2) LDDs and dark aeolian deposits, 3) possible sediment sources (e.g., layered terrains, dissected terrains or mass wasting deposits), and 4) the underlying geology for context. These maps can then be used to examine sediment transport pathways, constraining sediment sources for TARs [8].

Morphologic and morphometric analyses: We seek to determine what factors control the morphology and morphometry of TARs. We are producing Digital Terrain Models (DTMs) from HiRISE stereo pairs for each study area to conduct morphologic and morphometric analyses of TARs. The first of these is completed and a portion is shown in Fig. 3. Figure 4 shows the profile of one TAR bedform as measured from the DTM, showing a bedform height of 3 meters and a width of 35 meters. We are taking height and width measurements for large numbers of TAR bedforms within each DTM to assist in calculating TAR volumes as a function of classification in order to estimate their sediment buget. We are also performing statistical analyses of TAR surface areas, degree of TAR clustering, and TAR equivalent sediment thickness and spacing. We are calculating the range of values, mean, and standard deviation for TAR lengths, widths, length/width ratios, heights, wavelength, and bedform saturation.

Comparison with local/regional meteorology, topography, and geology: By comparing the distribution of TARs with local/regional meteorology (using mesoscale regional climate models), topography, and geology within our study areas, we can search for correlation with climate model data and look for effects of local topography on wind

speed/direction and TAR distribution. Preliminary results show good correlation.

Compositional analyses: Compositional studies are being carried out using THEMIS, OMEGA, and CRISM data to: 1) constrain the composition of TAR materials themselves, and 2) compare the composition of TARs to the composition of local LDDs and to local layered terrains (or other terrain units). We are testing the hypothesis that TARs are derived from local sources by comparing the composition of the bedforms to that of the terrain on which they rest. We are searching for evidence of compositional uniqueness within the dunes that could potentially contradict this hypothesis, and possibly be linked to a distal source region.

Crater counting and changes in high-resolution images: We are conducting crater count analyses on contiguous TAR fields, LDDs, and other associated terrains in HiRISE and CTX images in order to estimate formation ages. Investigating formation ages of TARs and TAR fields, and how they move and evolve over time can help us determine whether TARs are forming under current climate conditions, or are indurated/cemented and thus indicators of past climates. We are exploring how TARs evolve under the current climate regime by using time series high-resolution images to search for changes in morphology and position of TARs with time.

References: [1] Thomas P. (1981) *Icarus 48*, 76-90. [2] Thomas P. et al. (1999) *Nature 397*, 592-594. [3] Malin M.C. and Edgett K.S. (2001) *JGR 106*, 23,429-23,570. [4] Wilson, S.A. and Zimbelman J.R. (2004) *JGR 109*. [5] Bourke M.C. et al. (2003) *LPSC XXXIV*. [6] Balme M.R. et al. (2008) *Geomorphology 101*, 703-720. [7] Berman D.C. et al. (2009) *Icarus 213*, 116-130. [8] Bourke M.C. et al. (2004) *JGR 109*.

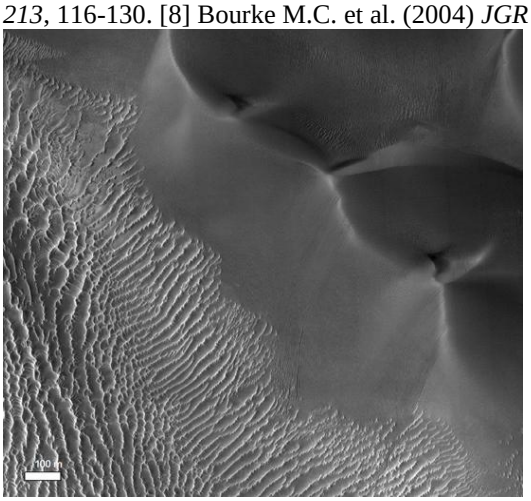

Figure 12. Example of TARs (lower left) alongside LDDs (upper right). HiRISE image PSP_003325_1355.

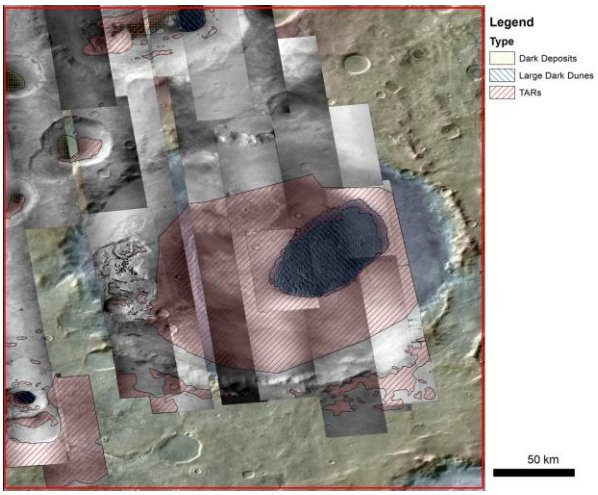

Figure 2. Study area in southern hemisphere around Proctor crater showing mapped regions containing TARs, Large Dark Dunes, and dark aeolian deposits.

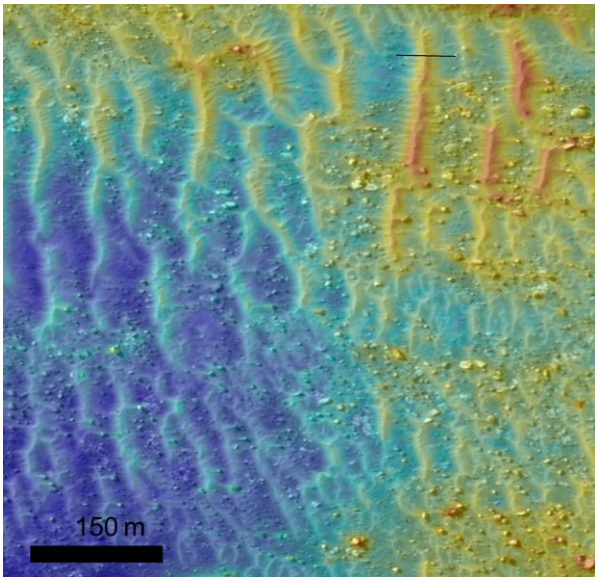

Figure 3. Portion of DTM of HiRISE images ESP_024449_1320 and ESP_024515_1320 with line indicating location of profile in Figure 4.

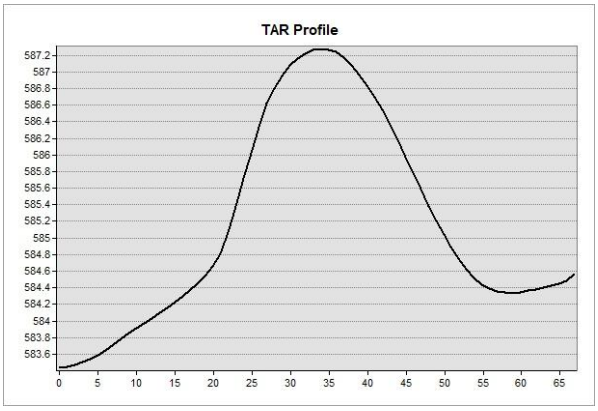

Figure 4. Profile of TAR bedform from DTM.

THE RELATIONSHIPS BETWEEN DUNE-DUNE INTERACTIONS, BOUNDARY CONDITIONS AND DUNE FIELD DEVELOPMENT, AL LIWA BASIN, THE EMPTY QUARTER. Mark. A. Bishop[1,2], [1]Planetary Science Institute, 1700 E. Fort Lowell, Suite 106, Tucson, AZ 85719, USA, [2]Planetary Science Institute Outreach, 43 Devon Street South, Goodwood, SA, 5034, Australia bishop@psi.edu.

Introduction: Within the greater Ar Rub' al Khali (Empty Quarter) sand sea lies an internal depocentre, the Al Liwa basin, which comprises a variety of mega-scale dune types. Crescentic dunes dominant the north of the basin while megadunes of stellate or star form are a major landform of the south-eastern reaches [1]. Their development into dune fields is determined by the style and rate of dune-dune interactions, the boundary conditions imposed by a multi-modal wind regime, fluctuating groundwater levels, and sediment availability under an assortment of climatic conditions throughout the Quaternary. As a result, dune field patterns are a collective response to these perturbations in space, time and environment. The *R*-statistic is a collective measure of these responses, and is a metric capable of identifying the degree of pattern maturity of the aeolian system, and the pathways from which patterns evolve.

Dune Field Development:

Dune Field Geography. The spatial signature of the southerly located star dunes within the Al Liwa basin (ALB) is characterized by two definitive patterns of organization: the first, one of complete spatial randomness, the other, a low degree of spatial uniformity. In isolation, these results appear to be unrelated to those for crescentic dunes of the region in which a significantly higher degree of pattern dispersion is the norm (Fig.1).

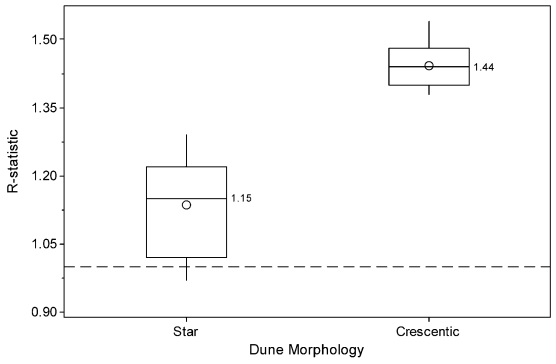

Figure 1. Box plots showing the distribution of the nearest neighbour statistic for the mega -star and -barchanoid dunes of the Liwa basin.

Dune Field Density. Metrics of dune density across the ALB demonstrate that the range of values per unit area has significantly less variation for crescentic forms compared with the more diverse range shown with star dunes (Fig. 2); a characteristic that also associates with the less organized and random state of the patterns. Median density values, $2.24_{crescentics}$ *cf.* 4.00_{stars}, show an approximate twofold increase in the number of star dunes relative to crescentic forms. These density values relate directly to dimensional changes for the dunes, whereby the southern star dune fields comprise substantially smaller individual dunes than the barchanoids of the northern basin (Fig. 3).

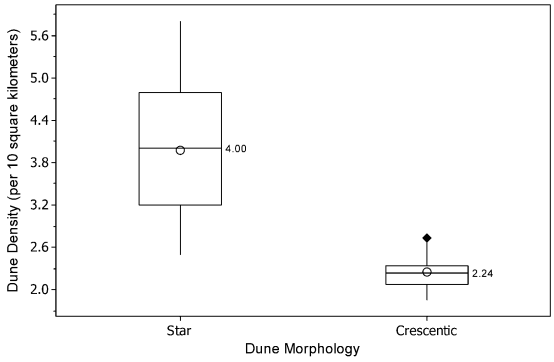

Figure 2. Boxplots showing near-normal distributions of dune density for star and crescentic morphologies (◊ symbol is an outlier).

Figure 2 demonstrates that the overlap of the lower and upper 'whiskers' for star and crescentic forms respectively, reflects the transition of dune type and the north-to-south variability of dune density. Greatest variability found with the star dunes may relate to a changing, regenerative environment in contrast to the predominantly constructive setting for the northerly located crescentic dunes.

Dune-Dune Interactions. Synergetic patterns and the overarching evolutionary pathway for dunes of the ALB are shown in Figure 3. (A) Linked barchanoid ridges with overriding superimposed crescentic dunes show a dimpled or scalloped surface texture. Although lateral linking (LL) is pervasive, broad-scale merging or coalescence (M), merging by off-centre collision (O-CC), and calving (Ca) are also seen here. (B) Linked ridges show asymmetric form as they 'stretch' towards the south-east under the influence of a secondary oblique wind. Calved dunes are prevalent upon the interdunes. (C) Crescentic form becomes negligible as embryonic star dunes develop. Note the decrease in overall dune size, and increase in dune number per unit

area. (D) Both individual (simple) and compound assemblages of star dunes occur in the south-eastern sector of the basin. Any sustained semblance to barchanoid morphology no longer occurs. However, haloes surrounding the primary dune structures comprise barchan, barchanoid, and embryonic star dunes. Calving appears to occur from the arms of the primary dunes, and suggests a regenerative, disequilibrated aeolian environment involving defect creation and migration.

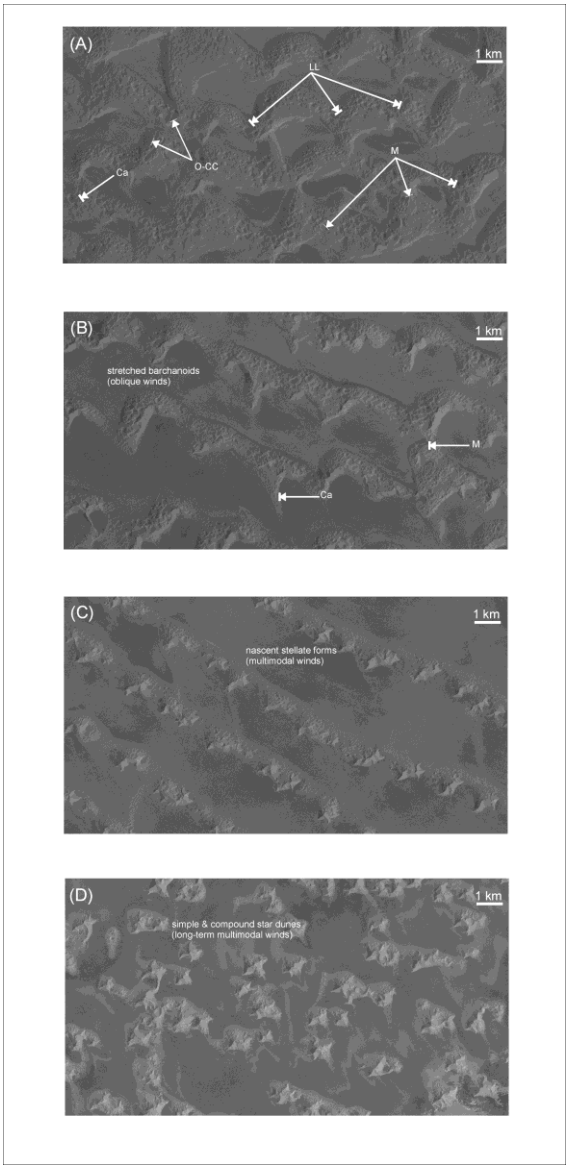

Figure 3. A Landsat ETM$^+$ pan-band (15 m) selection of dune types north-to-south for the Al Liwa basin.

Conclusions: When spatial statistical measures are integrated with the theoretical understanding of dune-dune interactions and the involvement of environmental agents, the complex morphodynamic pathways and linkages between regional dune fields is better understood. In this case, both constructive (e.g. merging, lateral linking) and regenerative activity (e.g. calving) have played important roles in the development of dune size, and associated adjustments in spacing, and dune numbers, and subsequently dune field patterns. Although apparently contrary characteristics exist between the crescentic dominated fields in the north compared with the star dune fields in the south, a morphodynamic synergy exists between dune types across the region. S*ynergetic patterns* are emblematic of this vast dunescape, whereby transitional geographic, morphologic, dimensional and environmental modifications exist between the mega- crescentic and -stellate dunes of the Empty Quarter. In conjunction with a multidirectional wind regime, the more random nature of the southern star dune fields may be a consequence of the synergy between groundwater-to-surface geography, and sediment availability from the more northerly locales. Hydrological processes are fundamental elements in the preservation of aeolian sequences and an ensuing decrease in dune sand mobility. For the ALB, successive climatic (hydrologic) influences saw the northern dune fields become ever enlarging megaforms that were obstacles to distal sediment transport. This in turn decreased the sediment yield available to the more southern dune fields, further limiting their development. Significantly, the location of piezometric surface(s) relative to the dune base may also assist in the forcing of pattern homogeneity or heterogeneity across a dune field, and subsequently the entire sand sea: variations in field patterns also being a result of the shape and extent of the watertable's upper boundary. As such, self-organization is restrained from reaching the end-member configuration defined by the highest indices for the nearest neighbour statistic. The inability for dune fields to produce a spatial signature that exceeds $R \sim 1.5x$, suggests that a combination of dune size and the limitations imposed by the space between dunes (*i.e*. dune density), as well as the degree of dune sand induration (*i.e*. sand availability and mobility) are key attributes in the regulation and evolution of field patterns and the ease at which dunes and their respective fields, grow, move and multiply.

In turn, such synergies may assist at better illuminating the geologic and climatic histories of the many hundreds of dune fields scattered across Mars, as well as offer insight into the equatorial sand seas of Titan.

References: [1] Bishop M. A. (2010) *Geomorphology, 120,* 186-194.

Radar observations of planetary dune analogues and assessing their stability using synthetic aperture radar.
D.G. Blumberg and Y. August, Department of Geography and Environmental Development, Ben-Gurion University of the Negev, Beer-Sheva Israel (blumberg@bgu.ac.il).

Introduction: Monitoring geomorphic changes on other planets is always a puzzle while on Earth measuring geomorphological dynamics can involve field work, i.e., ground truth. Dunes, wind streaks and other aeolian morphologies have been identified on Earth, Mars, Venus and Titan. These morphologies can be subjected to rapid and continuous changes when the surface is not stabilized by vegetation or crust and the wind is sufficiently strong. Thus, these sand bodies can change rapidly responding to the wind regime, rainfall, and sand particle availability. Identifying these changes by remote sensing (or even on the ground) is not straightforward because the entire surface may change concurrently.

In this paper we demonstrate how synthetic aperture radar interferometry (InSAR) can be used to identify changes in dunes using the coherence which is normally a measure of phase noise prohibiting interferometric studies. We demonstrate this for dunes along the Negev and Sinai border region. This paper will show how ERS data were used to map the stability, and loss of it, over time ranges spanning from 1 day intervals to 2 years when eventually the entire surface changed including the, so called, stable areas. This methodology has advantages as it does not show potential mobility but rather the true mobility or stability. It is applicable to planetary landscapes where there is no other indication of stability. Moreover, the methodology can be used also to measure the stability of surfaces susceptible to other mechanisms of landscape changes.

Synthetic aperture radar: Synthetic-aperture radar (SAR) is a method for the acquisition of images by actively illuminating a target scene with microwaves (λ~ 1 cm to 1 m) and integrating multiple radar images along a flight track to yield higher-resolution images than would be possible by a real aperture radar antenna. SAR amplitude images provide information on the surface geometry including slopes and roughness and the surface dielectric constant.

Spaceborne platforms such as ERS, and Radarsat, and the previously flown 1994 SIR-C/X-SAR exhibit single-look resolutions of 5-8 m in range and 15-20 m in azimuth and new spaceborne platforms such as the German TerraSAR-X, the Israeli TecSAR, and the Italian Comos Sky-med all exhibit resolution capibilities of at least 1 m. Mostly, data are processed to multilook images, which are produced by averaging single images of the same area to create a reduced speckle image (with lower spatial resolution.) Hence, the SAR spatial resolutions is as fine and at times superior to those known on current civilian VIS/NIR platforms and provide complementary information about the target scene. Another advantage of SAR system is the ability to acquire observations during both day and night and through all weather conditions, the results are systematic observation of the area of interest.

Radar coherence The radar phase is also affected by other factors, which together make the raw SAR phase image essentially arbitrary, with no correlation from pixel to pixel. Coherence is one of the products of the SAR interferometric process and it represents the magnitude of the complex correlation of both amplitude and phase information from two interferometric signals. The coherence is used to measure interferometry SAR data quality. Because each pixel in a SAR image is formed by the coherent sum of the backscatter from thousands of cells on the scale of the radar wavelength, temporal decorrelation can also be caused by the relative motion of the scattering cells within the SAR resolution (for example dunes can do so.)Thus, coherent change detection should provide an indication for dune motion
The first step of this work was to develop a methodology to precisely register all the SAR images. Our algorithm co-registered the images to a registration of better than 0.1 parts of a pixel. The second step was the coherence map creation. The coherence image of interferometric pair is shown in Figure 3 and figure 4. Clearly, the absolute coherence values are ranged between greater than 0.0 and less than 1.0, where values near 0.0 present totally decorrelated areas while the absolute coherence value near 1.0 represents a perfect coherence and the interpretation is stable area.

Results: LThe interferogram was converted into a color code map and the coherence converted into a three layer color map where one layer shows coherence of one day, the second of 10 months, and the third of almost two years. Decorrelation appears as salt and pepper pixels detached from the fringe pattern. The dune areas of the Northern Negev show high correlation over time caused by the fact that there is a biogenic crust on most of this area and little, if any, grazing. The area to the west demonstrates decorrelation starting within one day for small areas on the crest of the dunes. Within ten months the entire area of the Sinai side is decorrelated whilst the Negev (the Israeli side of the border) still maintains at high correlation

Conclusions: Radar remote sensing is a very useful toll in geomorphic studies and mapping. The additive value regarding the structure and geometry of dunes can and needs to be exploited. Moreover, beyond the amplitude imagery the phase information provide a unique capability of generating interferograms. Alongside the interferograms, temporal coherence maps are generated classically a measure of noise. These temporal coherence maps provide original and unique information compared with traditional optical and radar imagery. Dune motion is of interest in geomorphology studies especially of arid regions. Using the coherence maps, one can actually extract information regarding the dune motion. It is, thus, a useful tool for the mapping of dune activity.

This paper demonstrated an area with two very different land use policies yet identical climate showing dune changes on one side of the international boundary over short time periods and stable dunes on the other, over a long time periods.

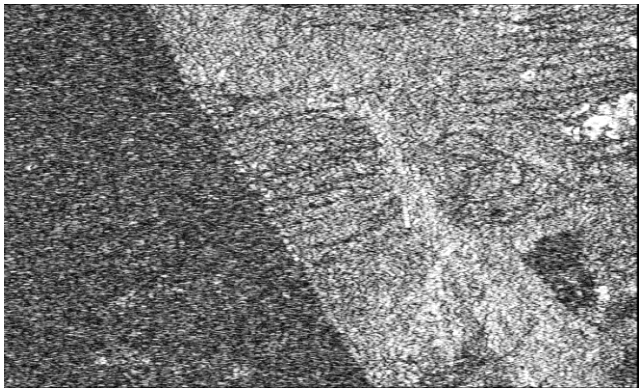

The above figure shows the coherence map of the interferometric pair of images acquired between 1995-07-14 and 1996-05-24. In this set the Egyptian side, Sinai is to the west, is decorrelated and has shown motion of the dunes.

DUNE MIGRATION IN THE NORTH POLAR REGION OF MARS. M.C. Bourke[1] and E.J.R. Parteli[2], S. Byrne[3], and D. Berman[1]. [1]Planetary Science Institute, Tucson, Arizona mbourke@psi.edu, [2]Institute for Multiscale Simulation, University of Erlangen-Nürnberg, 91052 Erlangen, Germany. [3]Lunar and Planetary Laboratory, University of Arizona.

Introduction: It has recently been established that sand is mobile under the current Martian climate, including at the North Pole [1,2]. Here we present a detailed study of the morphometry and migration of barchan and dome dunes in the North Polar Region of Mars.

Study Area: The dunes are located at the head of an unnamed Polar Cavi located at 83.5°N, 118.9°E (Figure 1). Previous studies at this site have shown that the dunes are sourced from the Basal Unit exposed in the adjacent Cavi wall. In addition, the dunes are enriched with gypsum derived from the Upper Layered Deposits [3]. The dunefield is composed of barchan and barchanoid dunes that traverse a number of topographic steps away from the Cavi head wall.

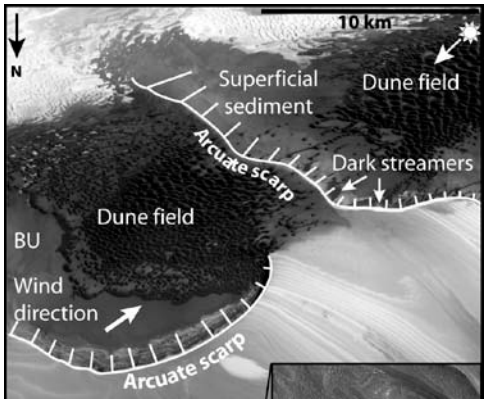

Figure 1. Location of the study area after Masse et al. (2010)

Methods: Dune width and length of 34 dunes were measured from 25 cm/pixel resolution HiRISE Images. In order to estimate dune heights, a HiRISE stereo pair was processed in ISIS and imported into BAE Systems Socet Set software. Multi-Sensor Triangulation was then used to solve for relative and absolute horizontal orientation (by measuring tie points) and the pair was then controlled to a MOLA DEM and MOLA Track points for vertical orientation. We were then able to extract true elevations for x,y points. The height of 22 dunes was estimated in this way.

Change in dune morphology and position was mapped using HiRISE images taken at two time steps. PSP_001593_2635 was taken November 28th 2006 and ESP_019143_2635 was taken August 27th, 2010, covering a total of 1.99 Mars years (3.75 Earth years).

In order to measure dune displacement distances, subsets of HiRISE images were cropped around individual sample dunes and georectified in ARC GIS. The interdune polygonal surface and rocks were used as tie points. Two measurements of displacement were made for each dune: the change in the dune centroid and the maximum advancement in the dune brink.

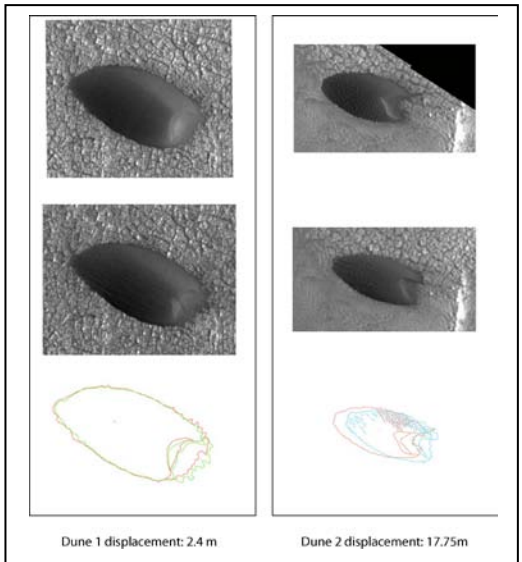

Figure 2. Example of displacement of two dunes. Between 2006 (top) and 2010 (bot)

Dune Simulations: We applied the dune model of Sauermann et al. [4-6] to reproduce the shape of the Cavi dunes. Our aim is to use the model to

estimate the average wind speed and grain size through comparing simulation results with morphology of the Cavi dunes.

This approach is similar to that of Parteli *et al.* [7], but with the difference that now the grain diameter (d) is an unknown to be determined from the modeling. In contrast to Parteli *et al.* [7] d was assumed to be 500 μm [8], while the interdune flux (q_{in}) was not known. Here we assume q_{in} to be 20% of the saturated flux (q_s), which is a reasonable value for fields of barchan dunes moving on the bedrock [9]. In summary, there are two unknowns we want to fit from the model results: the average shear velocity u_* of sand-moving winds at Cavi and the grain diameter d.

Results:

Dune Morphometry. Dunes are on average 170 m long and 121 m wide. Mean dune height is 18 m and is positively correlated with dune width (R^2 = 0.71). 68% of the sample dunes are asymmetric suggesting that, similar to Earth, barchan asymmetry is a morphological norm.

Dune Displacement. Although data are few, it has been established that asymmetric barchans migrate at rates comparable to non-asymmetric barchans in the same region [10]. Dunes at the Cavi sample site have migrated 5 m on average over 2 Mars Years. The individual dune rates are highly variable, measuring between 0.57 and 17.7 m. Dune displacement distances decrease with dune height, but the relationship is poorly correlated.

Dune Modeling: The threshold wind speed at Cavi estimated using the equation of [11] for d = 380 μm and Cavi atmospheric conditions is u_{*t} = 1.31 m/s. Using this value of u_{*t} and the pair d = 380μm, u_* = 2.33 m/s, the saturated flux $Q_s \approx 0.14$ kg m^{-1} s^{-1} — in comparison, on Earth $q_s \approx 0.015$ kg m^{-1} s^{-1} under typical u_* = 0.4 m/s. The bulk sand flux at Cavi is $Q_s = q_s/[0.62\rho_{grains}] \approx 2237.4$ m^2/year.

Conclusion:

- Dunes in the North Polar Region are migrating under the current climate regime.
- Rates are variable and may be influenced by topography, proximity to other dunes but not dune form.
- The smallest dunes have migrated the greatest distance. These include both dome dunes and dunes that are transitional forms between dome and barchan.
- Modeling of dunes using observational data from Mars can be used to obtain information on grain diameter and wind speed.

Acknowledgements: This work is funded by NASA MDAP Grant # NNX10AQ35G

References

[1] Bridges, N.T. *et al.*, (2011) *Geology*.
[2] Hansen, C. *et al.*, (2011) *Science* 331 (575), DOI: 10.1126/science.1197636.
[3] Massé, M. *et al.*, (2010) *Icarus* 209 (2), 434-451.
[4] Sauermann, G. *et al.*, (2001) *Physical Review E - Statistical, Nonlinear, and Soft Matter Physics* 64 (3 I), 313051-3130510.
[5] Kroy, K. *et al.*, (2002) *Physical Review* E66 (031302).
[6] Durán, O. *et al.*, (2010) *Earth Surface Processes and Landforms* 35 (13), 1591-1600.
[7] Parteli, E.J.R. *et al.*, (2007) *Physical Review E - Statistical, Nonlinear, and Soft Matter Physics* 75 (1)(011301).
[8] Edgett, K.S. *et al.*, (1991) *Journal of Geophysical Research (Planets)* 96 (E5), 22,765-22,776.
[9] Fryberger, S.G. *et al.*, (1984) *Sedimentology* 31 (3), 413-431.
[10] Bourke, M.C., (2010) *Icarus* 205 (1), 183-197, doi:10.1016/j.icarus.2009.08.023.
[11] Iverson, J.D. *et al.*, (1982) *Sedimentology* 29, 111-119.

FORMATION CONDITIONS FOR COARSE-GRAINED MEGARIPPLES ON EARTH AND MARS: LESSONS FROM THE ARGENTINEAN PUNA AND WIND TUNNEL EXPERIMENTS

N.T. Bridges[1], S.L. de Silva[2], J.R. Zimbelman[3], R.D. Lorenz[1] ; [1]Applied Physics Laboratory, 11100 Johns Hopkins Road, Laurel, MD 20723 (nathan.bridges@jhuapl.edu); [2]Deparment of Geosciences, Oregon State University, Corvallis, OR 97331-5506; [3]Center for Earth and Planetary Studies, Smithsonian Institution, Washington, D.C. 20013-7012

Introduction

The Martian surface contains a diversity of aeolian landforms, attesting to the effectiveness of wind as a major geomorphic agent despite the lower atmospheric pressure, gravity, and frequency of threshold winds compared to Earth. Rover observations have documented sand mobility at the field scale [1,2] and HiRISE has shown many dunes and ripples undergoing active migration [3]. The understanding of the formation mechanisms, rates, and particle fluxes of Martian aeolian bedforms is informed by terrestrial analog field work, commonly augmented with wind tunnel and modeling studies. Martian dunes and ripples have fairly close terrestrial morphometric analogs, emphasizing the role of saltation and impact splash in both environments. However, "Transverse Aeolian Ridges" (TARs) are a class of Martian bedform for which a viable terrestrial analog is much harder to find. With sizes and morphometric properties intermediate between dunes and ripples, TARs have been proposed as large megaripples formed via impact splash and creep, reversing dunes, or both [4-6].

Gravel megaripple fields of Catamarca, Argentina [7-9] are located in one of the windiest parts of the Argentinean Puna and may be the best terrestrial analog for TARs. In the region of the Cerro-Blanco caldera complex, late Pleistocene ignimbrites ranging in age from 13,000 to 70,000 years dominate the landscape [8,10]. These rhyolitic ignimbrites are weakly to moderately indurated and have been wind eroded to produce prominent yardangs and demoiselles. They contain about 5% by volume of lithic clasts with densities ranging from 2.6 to 3 g/cm^3, and up to 10% crystal-poor pumice clasts with densities of ~0.8 to 1.3 g/cm^3. Erosion liberates these clasts and the crystals from the matrix ash. The ash is quickly elutriated away, leaving a lag of crystals and clasts dominated by older ignimbrites, lavas, basement metamorphic-rich lithics, and pumice fragments.

We have been studying the Puna gravel megaripples and local wind conditions in an attempt to better understand potential TAR formation on Mars. Here we describe preliminary results from in situ wind profile measurement, time-lapse imaging, and simple wind tunnel studies.

Methods and Initial Results

Wind Profile Measurements

Wind profile measurements were conducted in December, 2010. Three anemometers were set up on at logarithmic spacings up to 1.6 meters. A semi-log fit to the profile data shows a roughness height (z_0) of a few centimeters for a range of freestream wind speeds and field conditions. The derived roughness heights are similar to typical gravel sizes at the ripple crests, indicating that at least some grains can be saltated if wind speeds are high enough. Friction speeds (u^*) were below that needed to move pumice. This is consistent with our qualitative observations that local sand was saltating, but no clasts were moving, indicating conditions were below threshold for the major megaripple components. However, in the winter, winds are probably more active, consistent with changes seen in our time-lapse imaging (below).

Time-lapse imaging

Time-lapse cameras were placed at three locations. However, only one camera, anchored on a coarse-grained ripple at "White Lake Field," worked over a long enough time span to return interesting data. It took pictures every 2.875 (-50%, +100%) hours over ~9-10 months (image time-tagging was not automatic, but will be reconstructed later) Comparison of images acquired in December, 2010 and ~July, 2011 show displacement, removal, and addition of clasts up to several centimeters in size. Most of these look like pumice [Fig. 1].

Fig. 1: Removal and addition of large pumice fragments as seen in time lapse images acquired in December 2010 (top) and ~July 2011 (bottom) at the "White Lake Field" site (S26°30.865', W67°42.053'). Arrows point to some changes in clasts between the two images.

Wind tunnel investigation

Experiments were conducted at the Arizona State University wind tunnel in January, 2012. It operates at standard pressure and temperature, with a fan and

motor system able to achieve free stream winds up to 30 m s^{-1}. It has dimensions of 13 (length) x 1.2 (width) x 0.9 m (height). A upwind motorized hopper can drop sand into the windstream. The test sections is coated with fine sand paper (average grain size = 120 µm). Upwind the tunnel is smooth plywood. Initially we had intended to simulate the field z_0 and u^* (adjusted for atmospheric density) determined from the wind profile data and collected samples by coating the tunnel floor with materials of similar sizes to those in the Puna. Because of calibration issues at the tunnel, we were not confident that the wind speed profile could be measured. So, we instead did first order measurements of *relative* threshold wind speeds of various field materials by placing them in the test section. Wind speed was gradually ramped up and threshold stages (vibrating, rolling, saltating) were noted, with simultaneous side-mounted video and overhead time-lapse imaging. Fluid and impact threshold were simulated, with the latter using quartz and scoria sand dropped from the upwind hopper.

Data are scattered (Fig. 2), but, based on our observations, we are confident more trends will result with further analysis (for example, clast size and shape have not been differentiated in Fig. 2). However, clear threshold stages are apparent, with even large pumice grains capable of being saltated. We also documented clear material segregation and clumping into ripple-like forms (Fig. 3).

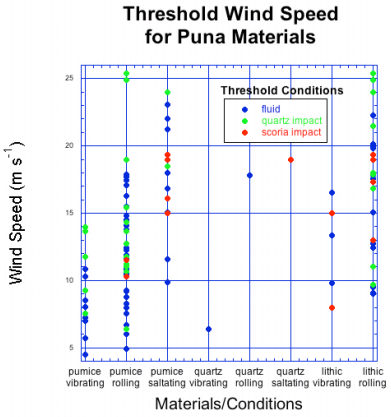

Fig. 2: Freestream threshold speeds for field materials measured in the ASU wind tunnel.

Discussion

More robust field and wind tunnel studies are planned for this project that will provide quantitative measurements of threshold friction speed for various materials and estimates of gravel ripple changes. Our preliminary observations nevertheless provide some important information on megaripple formation conditions in the Puna and insight into Martian processes. Large pumices and lithics can move at wind speeds that clearly occur in the region. If the time-lapse 2010-11 images are representative, ripple material movement is an ongoing process and is probably most effective in the winter.

Fig. 3: Initial and final stages of wind tunnel tests to determine freestream threshold of large pumices, lithics, and gravels. Sunset crater ash (> 800 µm) was saltated the length of the wind tunnel to simulate impact threshold conditions of pumice-like materials. Note the clumping of materials into ripple-like forms.

There is strong evidence that the Puna ripples are concentrated at the peaks of swales on the eroded bedrock ignimbrite surface (reflecting differential induration by exsolved gasses that passed through cooling cracks) [11]. The observed clast transport is therefore inconsistent with a model in which 1) ripple materials remain in place, or 2) the ripples gradually migrate across the landscape. Rather, the position of the megaripples may remain relatively constant, with clasts periodically removed from one megaripple and then blown downstream onto another. Such a model for dynamic, yet emplaced, megaripples may be operative on Mars. TARs have not been observed to migrate in contrast to some dunes and ripples [3] and it has been inferred that those distal to large dunes are inactive under present conditions [12], perhaps an unsurprising result if TARs are indeed megaripples armored with coarse grains like those that characterize plains ripples in Terra Meridiani [1]. This may also explain why some Martian large traverse bedforms are aligned on the crests of periodic bedrock ridges that have been hypothesized to have formed from aeolian erosion [13]. Continued studies of the Puna megaripples will provide further insight on these enigmatic Mars landforms.

References [1] Sullivan, R. et al. (2005), *Nature, 436*, 58-61. [2] Sullivan, R. et al. (2008), *J. Geophys. Res., 113*, doi:1029/2008JE003101. [3] Bridges, N.T. et al. (2012), *Geology, 40*, 31-34. [4] Bourke, M.C. et al. (2003), *Lun. Planet. Sci. XXXIV*, 2090. [5] Balme, M. et al. (2008), *Geomorphology, 101*, 703-720. [6] Zimbelman, J.R. (2010), *Geomorphology, 121*, 22-29. [7] Milana, J.P. (2009), *Geology, 37*, 343-346. [8] de Silva, S.L. (2010), *Geology,* doi:10.1130/G30780C.1. [9] Milana, J.P. et al. (2010), *Geology*, doi:10.1130/G31354Y.1. [10] Ortiz, A., (2012), *Thesis de Grado, Univ. of Salta.* [11] de Silva, S.L. and J. Bailer (2011), *AGU Fall 2011 Meeting, V31A-2509*. [12] Berman, D.C. et al. (2011), *Icarus, 213*, 116-130. [13] Montgomery, D.R. et al. (2012), *J. Geophys. Res., 117*, doi:10.1029/2011JE003970.

TESTING THE VOLCANICLASTIC HYPOTHESIS FOR MARTIAN DUNE SEDIMENTS: THE MEDUSAE FOSSAE FORMATION, MARS, AND ANDEAN IGNIMBRITES, EARTH. D. M. Burr[1], J. R. Zimbelman[2], S. L. de Silva[3], N. T. Bridges[4], M. Chojnacki[1], and F. B. Qualls[1] [1]University of Tennessee Knoxville, Knoxville, TN (dburr1@utk.edu), [2]Smithsonian Institution, Washington, D.C. 20013-7012, [3]Oregon State University, Corvallis, OR 97331, [4]JHUAPL, Laurel, MD 20723.

Introduction: Dark dunes have been observed on Mars since the Mariner and Viking missions [1], and the Mars global dune data base [2] shows them to be widespread. Most terrestrial sand is formed by comminution of granitic material into durable quartz grains [1], but Mars apparently lacks appreciable amounts of this parent material [*e.g.*, 3]. Previous work traces dune sand to polar layered deposits [4,5] or local sedimentary units [6], but a mechanism for global sand distribution has not been identified.

One hypothesis for the origin of dark dune-forming sand on Mars is as volcaniclastic deposits [7], which are widely distributed [*e.g.*, 8]. Inferred volcaniclastic deposits include the Medusae Fossae Formation (MFF) [*e.g.*, 8,9], with dark dunes documented in the western MFF (wMFF) [10]. Thus, comparison of the wMFF and terrestrial volcaniclastic deposits and their dune-forming sediments allows us to test the volcaniclastic hypothesis for the source of dark dune sand on Mars.

Data and methods: For the wMFF, we used data from the Context Camera (CTX; res. 6m/px;[11]) and the Compact Reconnaissance Imaging Spectrometers for Mars (CRISM;[12]) for feature identification, and gridded Mars Orbiter Laser Altimeter (MOLA;[13]) data for topographic information. On Earth, we used remote images in conjunction with field observations.

Dark dunes in the wMFF: The MFF is a 2.1×10^6 km^2 equatorial unit with multi-scale layering, whose pervasive erosional scarps and yardangs demonstrate its friable, particulate nature and the prevalence of aeolian sand transport [*e.g.*, 14]. The two lobes of the wMFF (Fig. 1) stretch from the dichotomy boundary into the Cerberus lava plains with total relief of ~1500m, and host fields of dark bedforms. These bedforms are preferentially located in low elevations, primarily in the trough between the wMFF and southern highlands (Fig. 1), and exhibit barchan, barchanoid, mound, and echo dune morphologies with rippled surface textures [10] characteristic of Martian dunes [15]. Thermal inertia values are consistent with (sub-)mm sized sand [10]. On these bases of morphology, texture, and thermal inertia, these bedforms are interpreted as aeolian dunes [10].

Evidence for the MFF as the source for the dark dunes. Dune orientations indicate their emplacement by northerly (N-to-S) winds [10]. Given the strong concentration of dunes in the south wMFF, this northerly direction of sediment transport is consistent with the wMFF as the sand source. Another possible source is the Cerberus lava plains to the north and east, but the roughness and topography of the wMFF would limit sediment influx from that direction. Catabatic winds down Elysium Mons could have transported volcaniclastic sediment from the north, but sediment transport pathways from this direction are not apparent. Evidence in support of the MFF as the sand source includes erosional scarps that decrease in albedo down slope to dunes at their base (Fig. 2). On these bases, we hypothesize that erosion of the wMFF liberates dark dune sediments, with deflation of lighter and lighter-toned material [10].

Andean ignimbrites as MFF analogs: To examine this hypothesis, we consider dark dunes in Andean ignimbrites [16,17], proposed as analogs for the MFF [9]. Andean ignimbrites are late Neogene to Quaternary-age ash flow tuffs that extend from southern Peru and Bolivia to central Chile and Argentina [18 and refs. therein]. In the northwestern Catamarca province, Argentina (26°36'S 67°30'W), the light-toned Campo Piedra Pomez ignimbrite (CPP) [18,19] is extensively eroded into yardangs like the MFF [9], and likewise yields dark dune-forming sediments (Fig. 3;[20]). These similarities between the wMFF and CPP provide a basis for using CPP dark dunes as analogs for the wMFF dark dunes.

Dark dunes in the CPP: The erosional morphology of the CPP controls dune-forming sediments, which are located between yardangs [20], as in the wMFF. These deposits also form extensive sheets with rippled surface texture, as seen on wMFF dunes. Comparative componentry and granulometry of particles within the CPP and of the superposed dark sediments are consistent with the dark sediments being derived from the ignimbrite.The source of these clasts is mainly surface derived – picked up by the pyroclastic flow as it travelled – although some sediments may have come from the conduit as the erupting mixture made its way to the surface [20].

Although most volcanism on Mars appears to have been basaltic instead of felsic [*e.g.*, 3, 21 and refs. therein], basaltic volcanism under the low gravity and atmospheric pressure of Mars is postulated to have produced pyroclastic flows [*e.g.*, 22, 23]. The derivation of dark sediments from the CPP (Fig. 3) demonstrates that dark bedforms may be derived from light-toned deposits. The pervasive dust over the MFF makes determination of true albedo uncertain, but terrestrial basaltic ignimbrites [e.g., 24, 25] are commonly darker that felsic ignimbrites, making the derivation of dark sediments from the wMFF even more plausible.

Hypothesis testing/future work: If dark dune sand is sourced in the wMFF, then other regions of the MFF should host dark dunes. However, the central and eastern MFF do not show extensive dark dunes, possibly because of their higher stratigraphic position. Examination of hypothesized Martian ignimbrites of various elevations for dark dunes investigate this idea.

Implications: If the MFF is the source for locally derived dark dunes, this finding implies that other dark dunes also originate in Martian volcanoclastic rocks. The mafic composition of the wMFF dark dunes [10] is similar to that of other dunes on Mars. Vast expanses of the Martian surface show evidence of having been mantled and, in places, subsequently exhumed [26]. Although the origin of the mantle is not known, a major component of the light-toned mantles could be ignimbrites. Light-toned layered deposits, hypothesized to be ignimbrites, are extensive in the equatorial region of Mars, with a total exposed area of ~2.9×10^6 km^2 [7]. These hypothesized ignimbrites would provide a ready source for dark dune sands. Their large extent would obviate the need for global transport and, in face of the rapid breakdown during transport of aeolian sand, could explain the wide-spread distribution of dark dunes on Mars.

References: [1] Greeley R. and Iversen J. D. (1985) Wind as a Geological Process, 333 pp., Cambridge Univ. Press. [2] Hayward R. K. et al. (2007) *JGR, 112*, E11007, 10.1029/2007JE002943. [3] Bandfield J.L. (2002) *JGR, 107*, Cite ID 5042. [4] Thomas P. and Weitz C. (1989) *Icarus, 81*, 185-215. [5] Langevin Y. et al. (2005) Science, 307(5715), 1584–1586, doi:10.1126/science.1109091. [6] Fenton L. K. (2005) *JGR, 110*, E11004. [7] Edgett K.S. and Lancaster N. (1993) *J. Arid Environments, 25(3)*, 271-297. [8] Hynek et al. (2003) *JGR 108*(E9) 5111. [9] Mandt, K. et al. (2009) *Icarus, 204*, 471–477. [10] Burr et al. (2011) *LPS XLII*, 1582. [11] Malin M. C. et al. (2007) *JGR, 112*, E05S04. [12] Murchie S.L. et al. (2009) *JGR, 114*, E003344. [13] M. Zuber et al., (1992) *JGR, 97*, 9981. [14] Bradley B. et al. (2002) *JGR 107(E8)*, 5058. [15] Bridges N. T. et al. (2007) *GRL, 34(23)*, L23205. [16] de Silva S.L. (1989) *JVGR 37*, 93-131. [17] Cas R.A.E. et al. (2011) *Bull. Volcanol. 73*, 1583-1609. [18] de Silva S. L. et al. (2006) *Geol. Soc. Spec. Publ., 269*, 47– 64. [19] de Silva S. L. et al. (2011) *LPS XLII*, #2421. [20] de Silva S.L. et al. (2012) *LPS XLIII*, #2038. [21] McSween H. Y. et al. (2006) *JGR 111*, E02S10. [22] Wilson L. and Head J.W. (2007) *JVGR 163*, 83-97.[23] Wilson L. and Heslop S.E. (1990) *JGR 95*, 17309-17314. [24] Freundt and Schmincke (1995) *JGR 100*, B1, 455-474. [25] Watkins S.D. et al. (2002) *JVGR 118*, 173-203. [26] Malin, M.C. and K.S. Edgett (2001) *JGR 106*, 23,429-23,570.

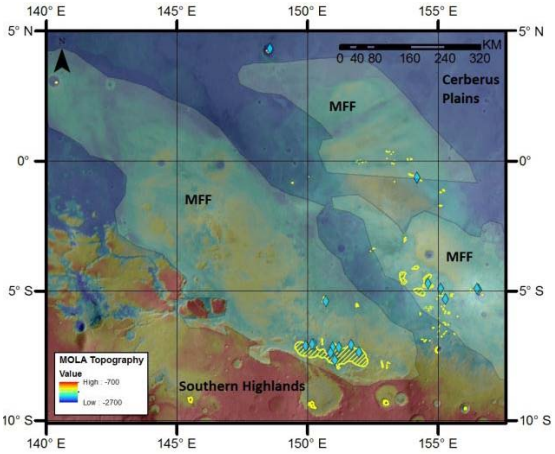

Fig. 1: wMFF study area, showing the locations of dark dunes (yellow hatching). Sites from which thermal inertia values were derived (blue diamonds) are indicated [10].

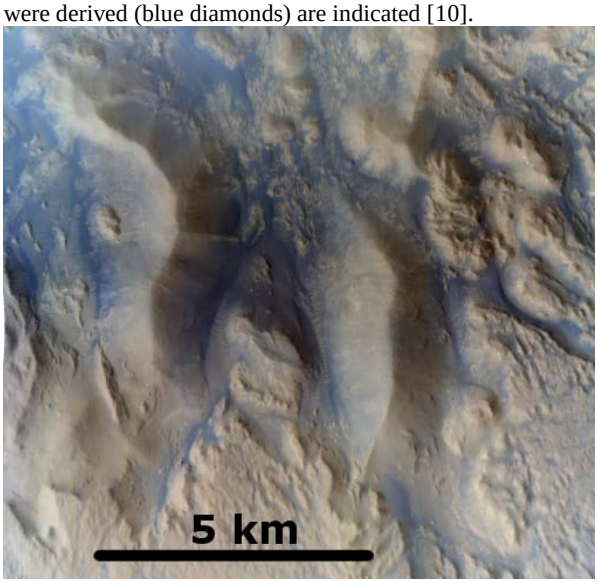

Fig. 2: CRISM FRT63A8 (nr -7.7, 151E) in enhanced color (R=590nm, G=530nm, B=440nm) showing erosional scarps that decrease in albedo downward to dark dunes at their bases.

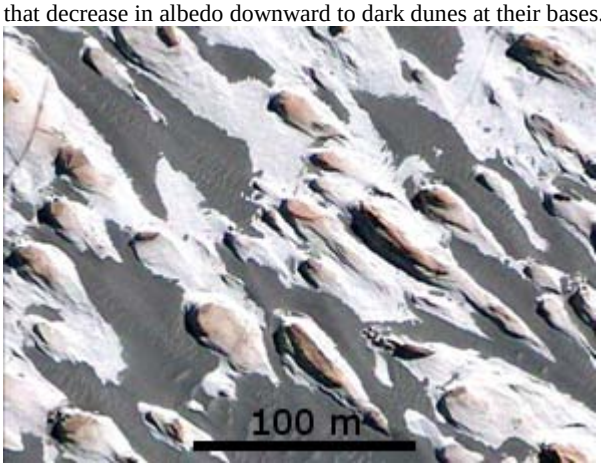

Fig. 3: Image of yardangs formed in the CPP with intervening dark dunes, Catamarca, Argentina. Credit: Google Earth.

SURFACE AND ORBITAL MONITORING OF THE "GREELEY DUNE FIELD" IN ENDEAVOUR CRATER, MERIDIANI PLANUM, MARS. M. Chojnacki[1], J.R. Johnson[2], J.E. Moersch[1], and J.F. Bell III[3], [1]Department of Earth and Planetary Sciences, University of Tennessee, Knoxville, TN (chojan1@utk.edu), [2]Johns Hopkins University Applied Physics Laboratory, Laurel, MD, [3]School of Earth and Space Exploration, Arizona State University, Tempe, AZ.

Introduction and Context: Reports from orbital observation have clearly documented evidence for contemporary Martian ripple and dune mobility events [1–3]. These events demonstrate that the threshold wind speed for entrainment was exceeded under current conditions in these locations. However, the timing (what season) and duration of sand movement are poorly constrained due to the infrequent temporal coverage of orbital observations.

Meridiani Planum exhibits ample evidence in orbital images and ground-based observations by the Mars Exploration Rover (MER) Opportunity for aeolian activity, with dunes, ripples, and dark streaks [4–5]. The 2011 arrival of Opportunity at the western rim of Endeavour crater (Cape York) provided an excellent chance to look for activity over a multi-season time span in the same low albedo dunefield (Fig. 1) where orbital observations documented changes over the past decade [2]. Here we report the first results from a dedicated Pancam campaign to monitor these dunes and to document any aeolian surface changes more frequently than is possible with orbital observations alone.

Endeavour crater has two populations of duneforms. The eastern bedforms consists of poorly developed transverse and dome dunes, which were the focus of earlier studies due to the large degree of apparent activity (*e.g.,* deflation and/or translation of eight small dome dunes) observed in MGS-MRO images [2]. These dunes are >11 km downrange from Opportunity at Cape York and are partially obscured by the interior crater's hummocky surface. The western dune field (Fig. 2) consists of 26 barchans and one large barchanoid compound dune (Figs. 1 & 3). The ~20 resolvable duneforms, informally named the "Greeley Dune Field" after late planetary scientist Ronald Greeley, are 6–8 km downrange from Cape York and are the subject of this abstract.

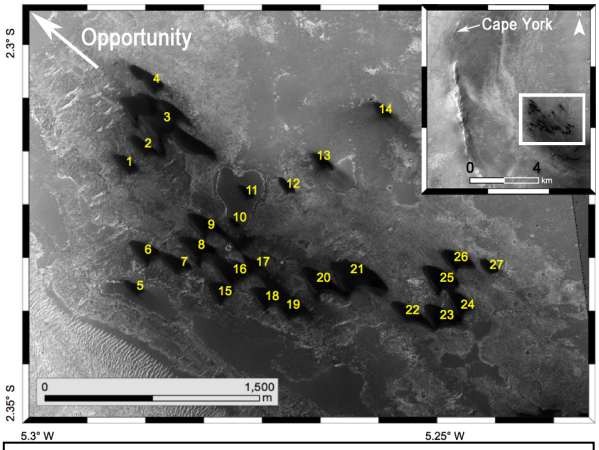

Fig. 2. HiRISE image PSP_005779_1775 of Endeavour crater's western dune field. Inset shows a CTX mosaic with the dune field's location relative to Cape York.

Methods: For our investigation of dune variability, we used orbital images from the MRO Context Camera (CTX) [6] and the High Resolution Imaging Science Experiment (HiRISE) [7]. Surface observations used Pancam [8] images of the crater interior and western dune field. As part of the Opportunity winter campaign, ten dune field images (as of April 2012) were acquired every ~20 sols (L_s=3°–89°), usually as late afternoon observations, using various filter combinations to look for evidence of surface changes. These included two "super resolution" sequences [9] that slightly improve Pancam's native resolution (0.28 mrad/pixel).

Results and Interpretations: *Dune Morphology*.

Individual dune morphology and projected heights are resolvable in Pancam images using various filter combinations and super resolution (Figs. 1 & 4). Opportunity's viewing azimuth was/is oriented roughly parallel to the dunes' paleo-transport direction (*i.e.*, paleo-downind), as inferred from evidence listed below. Thus, the crestlines of these dunes as projected

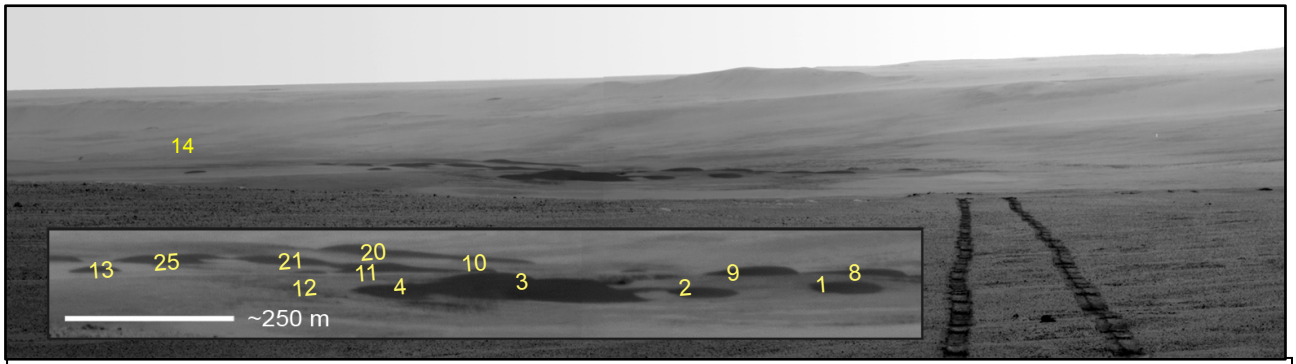

Fig 1. Southeastward Pancam "super resolution" view of the Endeavour crater interior and the "Greeley Dune Field". Acquired on Sol 2759 (sequences P2568 and P2569) from Cape York. The largest visible barchanoid dune is shown centered in the inset. Numeric labels identify the same dunes that are seen from orbit in Fig 2.

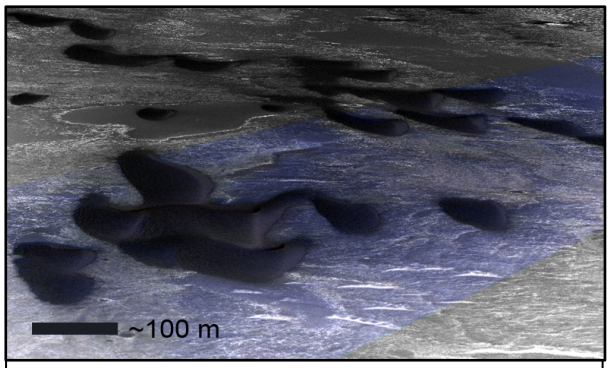

Fig. 3. A color HiRISE (PSP_005779_1775) southeastward prospective view (at a similar azimuth as Pancam images) using an HRSC DTM [10] of the closest dunes (dunes 1–4) to Opportunity.

in Opportunity's images are good approximations for their transverse (to the wind) profiles. Qualitatively, the crestlines appear symmetric about their centers and Gaussian in their slopes. Similarly, HiRISE nadir-viewing images show these dunes to have relatively symmetric planform shapes and a lack of horn extensions (Figs. 1 & 3). Together these properties may be resulting from dune equilibrium (*i.e.,* coupling between wind flow, shear stress, and morphology) within a unidirectional wind regime [11–12].

Wind Regimes and Evidence for Activity. As was observed in previous studies [2,3,13], slip face orientations and the timing/orientation of local dark/light streaks suggest a southern autumn northwesterly wind regime, consistent with mesoscale wind modeling. Partial support for this wind regime came from paired-HiRISE observations (2007–2008) where notable dark streaks emanating SSE from one isolated barchan (Fig. 2, dune #14) at this time of season (see [2, Fig. 4]). By the time of Opportunity's arrival at Cape York, at the onset of southern winter, this dune's SSE-oriented dark streak was still resolvable (Fig. 4a). This dark streak appears to have faded in several later observations. Analysis of abundant CTX images can also resolve changes in dune dark streaks and would predict a ~180° shift in the streak-orientation with a southeasterly (southern winter-spring) wind regime [2,3,13]. With the arrival of southern spring, continued Pancam monitoring of the dark streak may be able to detect and monitor this shift.

Although there has been no unambiguous evidence for dune translation/deflation from Pancam some additional hints at aeolian activity were found between Pancam super resolution sub-frames (not shown, Sol 2759 sequence P2569) with evidence for a dust-lifting event just south of the dune fields. From wind tunnel experiments, local gusts capable of entraining dust were should also have been sufficient to initiate sand saltation [14]. Likewise, dust-cleaning events around the same time at Cape York resulted in notable increases in solar array power.

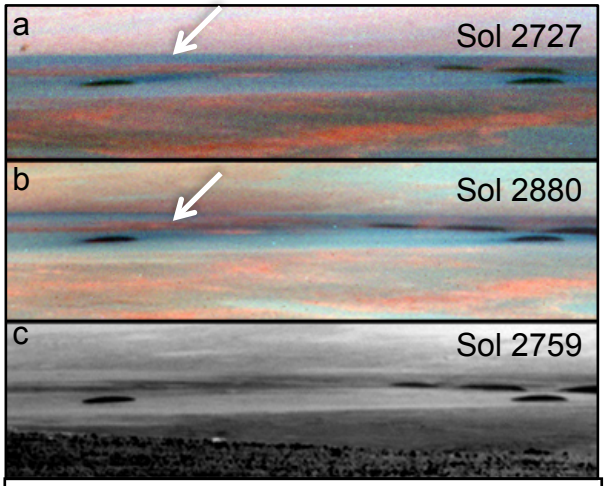

Fig 4. (a-b) Southeastward Pancam false-color views of the "Greeley Dune Field" using filters at 753, 535, and 432 nm. Sol 2727 (L_s=6°) and sol 2880 (L_s=77°) were both acquired in the late afternoon (13:45-14:45 LST) and under similar lighting conditions. (c) Similar view using super resolution (Fig. 1) for comparison. Dune #14 (left) is ~55 m wide. Note that images were taken from different locations ~500 m apart along Cape York, resulting in some viewing parallax.

Discussion and Future Observations: Once available solar power increases enough from its winter low, Opportunity may depart to Cape Tribulation and new science targets. A southward traverse would shorten the distance to the dunes and increase Pancam's sensitivity to small dune changes. The western dunes, although on average volumetrically larger than the eastern dunes, do possess some smaller barchans of a similar scale (~50 m wide) as those known to deflate completely elsewhere in the crater (see [2, Fig. 2]). Likewise those earlier orbital studies deduced migrations rates of ~7 m per Martian year averaged over the 2.3 year temporal baseline available for two small eastern dunes [2]. This rate would imply ~1.5 m of translation over the ~90-sol baseline of Opportunity's observations if the dunes move a uniform rate. This small amount of translation, projected into the Pancam image plane, would be below the threshold for detectability for changes in the images. Further Pancam observations will be needed to attempt to determine whether dune movement is gradual or (perhaps more likely) episodic, and what the actual rate of movement is during periods of activity.

References: [1] Silvestro et al. (2010) GRL, 37, 2010GL044743. [2] Chojnacki et al. (2011) JGR, 116, 2010JE003675. [3] Bridges et al. (2012) Geology, 40, 31-34. [4] Geissler et al. (2008) JGR, 113, 2008JE003102. [5] Johnson et al. (2011) EPSC-DPS, 6, 1205. [6] Malin et al. (2007) JGR, 112, E05S04. [7] McEwen et al. (2007) JGR, 112, E05S02. [8] Bell et al. (2003) JGR, 108, 2003JE002070. [9] Bell et al. (2006) JGR, 111, 2005JE002444. [10] Neukum, et al. (2004) ESA SP - 1240, 17–35. [11] Hesp and Hastings (1998) Geomorph., 22, 193–204. [12] Bourke (2010) Geomorp., 205, icarus.2009.08.023. [13] Sullivan et al. (2005) Nature, 436, nature03641. [14] Greeley et al. (1980) GRL, 7, 121–124.

POTENTIAL SEDIMENT SOURCES AND PATHWAYS IN VALLES MARINERIS DUNE FIELDS: IMPLICATIONS FOR MARTIAN AEOLIAN SYSTEMS. M. Chojnacki[1], J. E. Moersch[1], D. M. Burr[1], and J. J. Wray[2], [1]Planetary Geosciences Institute, Department of Earth and Planetary Sciences, University of Tennessee, Knoxville, TN 37996 (chojan1@utk.edu), [2]School of Earth and Atmospheric Sciences, Georgia Institute of Technology, GA, 30332.

Introduction and Motivation: As one of the primary Martian sediment sinks, the Valles Marineris (VM) holds nearly a quarter of the global inventory of dune area on Mars [1–2]. The sediment comprising the VM dune fields may have been derived from a variety of potential sediment sources (PSS) (*e.g.*, interior layered deposits (ILDs), spur-and-gully walls, extra-rift sources). Here we expand on the recent documentation that some VM dune fields (Fig. 1) are likely locally-derived from a variety of lithologic sources [3].

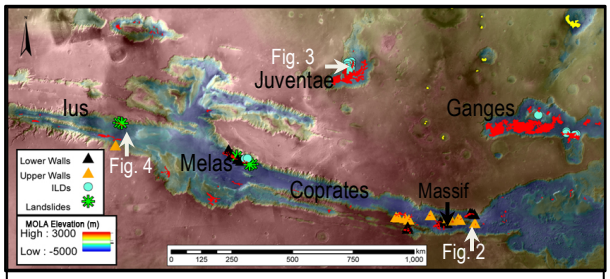

Fig. 1. Valles Marineris (red) and extra-rift (yellow) dune fields in relation to potential sand sources, as inferred from morphologic, spectral, and/or thermophysical evidence. MOC-WA with MOLA elevation overlaid. Note massif in Coprates is partially obscured by polygons.

Data: Geologic context for the dune fields was provided by the CTX [4] and HiRISE [5] cameras. Topography of dune and outcrop surfaces was determined from HRSC camera digital terrain models (DTMs) [6]. Thermal inertia (TI) data from the THEMIS imager [7] were derived to create thermophysical unit maps and infer particle sizes [8]. We used CRISM [9] visible to near-infrared reflectance spectra to determine compositions of dunes and potential source materials.

Results:

Extra-Rift PSS: In order to constrain the provenance of VM dune fields, a survey was performed on the ~1000 km region surrounding them. This scale was chosen because it encompasses the estimated maximum transport distance of basaltic sand grain particles due to mechanical weathering [10 and refs. therein]. We identified 22 dune fields, primarily in Lunae Palus and Margaritifer Sinus, 19 of which are small (2–70 km^2, ~1600 km^2 total). The total area of these dunes is <8% of the dune field area mapped within VM. The majority of these crater-confined dune fields are found with paleo-wind indicators (i.e., slip faces, dark streaks) suggestive of transport away from VM, with a few exceptions northeast of the rift. To date, no dune fields have been located within ~200 km of the VM rim (Fig. 1).

Spur-and-Gully Wall PSS: Coprates and Melas chasmata (Fig. 1) contain ~12% of the VM dune field areal inventory, with a rich diversity of dune morphologies and topographic relationships. Dunes are often in close proximity to or atop wall material that has been deposited by mass wasting. For example, Fig. 2 shows a ~800-m-tall, steep (30–40°) wall scarp and associated talus above a floor dune field. This lower wall segment is interpreted as massively-layered flood basalts [12]. CRISM spectra of both the dunes and lower-wall scree show evidence for both olivine-bearing basalt and high-calcium pyroxene (HCP). In contrast, other wall spurs in that figure display spectral characteristics that match those of low-calcium pyroxene (LCP) and Fe/Mg-smectite [12], and dune fields west of this location have dominantly olivine-bearing compositions [3]. TI values of the dune surfaces closest to the scarp are ~370 $Jm^{-2}K^{-1}s^{-1/2}$, consistent with coarse sand, whereas TI monotonically decreases paleo-downwind (as inferred by slip faces orientation).

Falling dunes (a type of topographically constrained duneform) in VM are most commonly located within Coprates Chasma gullies adjacent to dark-toned upper-wall PSS [13]. Most of these coarse-grained (as inferred from TI) dunes occur on a topographically isolated 200-km-long massif (Fig. 1) where extra-rift sources are not likely. CRISM spectra of local falling dunes and adjacent upslope outcrops match each other with variable basaltic spectra, but are distinct from spectra of lower-wall PSS.

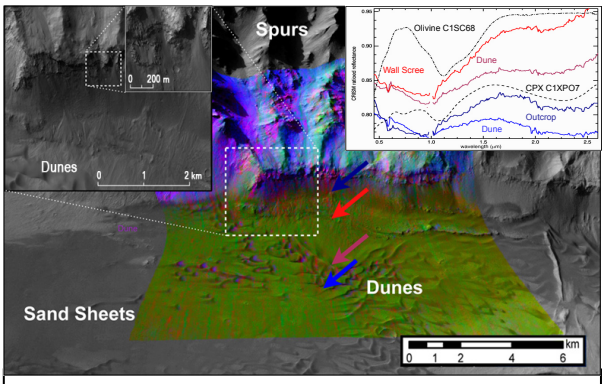

Fig. 2. A CTX perspective view of Coprates Chasma dune-wall relationships using a HRSC DTM colorized with CRISM (FRT 21CB0 where HCPINDEX (red), OLINDEX (green), and LCPINDEX (blue) [11]). (inset) HiRISE (ESP_025731_1655) views of select locations along the steep ~30–40°-scree-slopes above dunes. CRISM spectra (inset) of dunes and PSSs. Note that lab spectra (black dashed) are in units of reflectance.

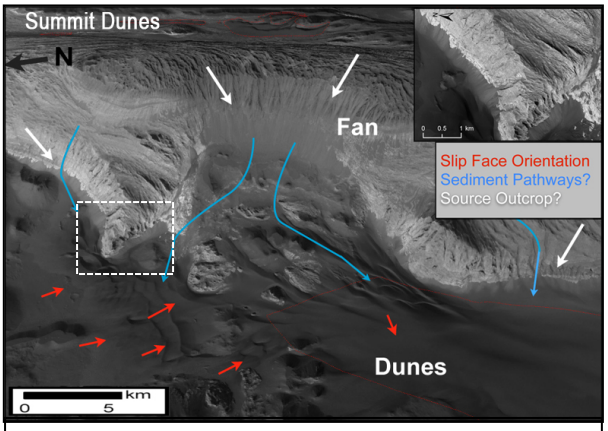

Fig. 3. Eastward perspective view of Juventae Chasma ILDs in relation to several dune fields (CTX using a HRSC DTM). CRISM observation show HCP associated with fans, floor dunes, and sand sheets to the south, whereas summit dunes are olivine-bearing [3].

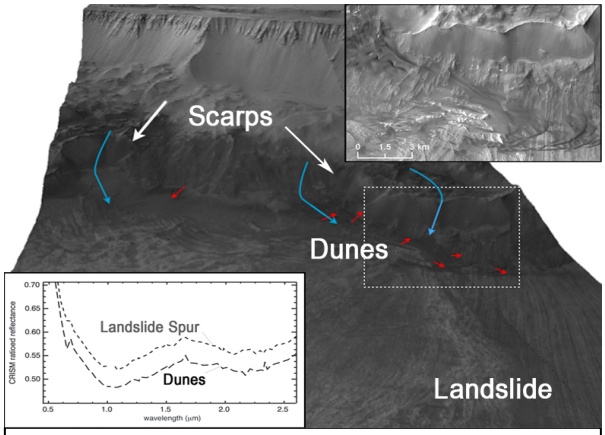

Fig. 4. CTX perspective view of Ius Chasma landslides and dunes (CTX using a HRSC DTM). CRISM multispectral spectra of scarps and dunes, consistent with HCP, are similar. Annotations are the same as Fig. 3.

ILD PSS: Juventae and Ganges chasmata both host massive ergs and smaller dune fields (~80% of total VM dune field area) in close association with ILDs. These massive layered deposits, although usually associated with hydrated sulfates, are also partially composed of mafic mineralogies [3,11,14]. For example, one topographically-isolated dune field found atop the summit of a Juventae Chasma ILD (Fig. 3) possess a spectra (consistent with olivine) similar to that of a regional mantling unit and was interpreted as evidence for local provenance [3]. Here, as with Ganges Mensa and other VM ILDs, morphologic evidence for mass-wasting of fans can be found [1,15]. Additional mid-toned material is observed on the slope to the west, where barchanoid dunes and sand sheets are located (Fig. 3, inset). Dunes, sand sheets to the south, and the ILD-sourced fans have the same broad absorption features at ~1.1 and ~2.3 μm, consistent with HCP [3].

Landslide PSS. Several VM dune fields are superposed on late Amazonian (<1 Ga) landslides [16], primarily located in Ius, Melas, and Hebes chasmata. One example, in Ius Chasma (Fig. 1), shows a small landslide dune field adjacent to eroding landslide scarps (Fig. 4). CRISM multispectral observations of both scarp material and dunes show absorption features indicative of HCP-bearing basalt.

Interpretations: A variety of findings indicate local sources provide sediment for the dunes. Spectral pairing between dune and outcrop/talus surfaces are consistent with local derivation of dune sediment from Coprates wall (Fig. 2), Juventae ILD (Fig. 3) and Ius landslide scarp (Fig. 4) materials. In Coprates chasma, we interpret the thermophysical trend below the scarp as evidence for the deflation of finer sand particles leeward of the PSS, although mechanical breakdown may also be a factor. The falling dunes spectra, along with previous morphologic and thermophysical evidence [13], suggest discrete, local (<10 km) sediment pathways from wall gullies down to chasm floors as a source for larger floor dune fields.

Discussion and Summary: Numerous observations in VM link specific outcrop materials to individual dune fields. However, given the long history of VM, multiple sources, including other dunes and extra-rift material, also seem likely. Eastern Coprates Chasma provides robust evidence for local derivation of aeolian sediment from specific stratigraphic levels of local spur-and-gully walls. Mantling units and fan material of ILDs in Juventae Chasma show evidence as sources for separate yet adjacent and spatially large dune populations. These examples of spectrally distinct dune fields in close proximity (~10 km) to one another argue for discrete, relatively unmixed sediment sources, counter to the notion that Martian sands and (by extension) dark soils have been globally homogenized [17]. Future work will continue to test the hypothesis for local provenance of VM dune fields.

We speculate that several mechanisms are responsible for the breakdown of VM PSS geologic units, depending on the location and starting compositions: susceptibility of basalt to thermal stress (*i.e.,* thermal stress fatigue, thermal shock) [18], impact gardening, aeolian erosion, and ancient weakening of bedrock due to a aqueous alteration/digenesis [12], all compounded by gravity driven processes. The high relief and exposure of the strata of VM may be driving factors in sourcing sediment for widespread aeolian bedforms across the rift.

References: [1] Chojnacki and Moersch (2009) LPS XL, 2486. [2] Fenton and Hayward (2010) Geomorph., 121, 98–121. [3] Chojnacki et al. (2012) LPS XLIII, 2444. [4] Malin et al. (2007) JGR, 112, E05S04. [5] McEwen et al. (2007) JGR, 112, E05S02. [6] Neukum, et al. (2004) ESA SP-1240, 17–35. [7] Christensen et al. (2004) Space Sci. Rev., 110, 85–130. [8] Piqueux and Christensen (2009) JGR, 114, E09005. [9] Murchie et al. (2007) JGR, 112, E05S03. [10] Rogers and Christensen (2003) JGR, 108, E45003. [11] Pelkey et al. (2007) JGR, 112, E08S14. [12] Murchie et al. (2009) JGR, 114, E00D06. [13] Chojnacki et al. (2010) GRL, 37, L08201. [14] Mangold et al. (2008) Icarus, 194, 519-543. [15] Chojnacki and Hynek (2008) JGR, 113, E12005. [16] Quantin et al. (2004) Icarus, 172, 555– 572. [17]. Soderblom and Bell (2008) in The Martian Surface, pp. 3–20, Cambridge Univ. Press. [18] Hall (1999) Geomorph., 31, 47–63.

COMBINING DUNE FIELD ANALYSIS WITH WIND MODEL RESULTS TO UNDERSTAND RECENT EVOLUTION OF HYPERBOREAE UNDAE, MARS. S. Christian[1], G. Kocurek[1], A. Spiga[2]; [1]Jackson School of Geosciences, University of Texas, Austin, TX 78512 (schristian@utexas.edu). [2]Laboratoire de Météorologie Dynamique, Université Pierre et Marie Curie, France.

Introduction: Remotely analyzing dune fields to interpret formative wind regimes and regional climatic events is not straightforward [1], particularly when the field demonstrates seemingly inconsistent dune morphologies [2]. Hyperboreae Undae (HU), one of several dune fields surrounding the north polar plateau of Mars, Planum Boreum [3] (Fig. 1), has well-known examples of coexisting barchan and linear dunes [2, 3] (Fig. 2). This apparently incompatible dune configuration has been explained by change from bimodal to unimodal wind regime due to topographic influence [4] or temporal change in wind regime coupled with dune induration [2]. While the first hypothesis cannot explain the side-by-side existence of the two morphologies as seen in HU (Fig. 2a), the second is difficult to test when reconstructing dune field history.

An alternative approach to explaining the formation and evolution of HU utilizes results from mesoscale wind models of the north polar region [5] and morphological analysis of the modern dunes. Crestline trends are predicted from modeled, modern wind vectors using gross bedform-normal calculations; modeled trends are then compared to empirical trends to constrain the timing of recent dune field evolution. Dune morphologies are analyzed to better understand current modification of pre-existing dune forms.

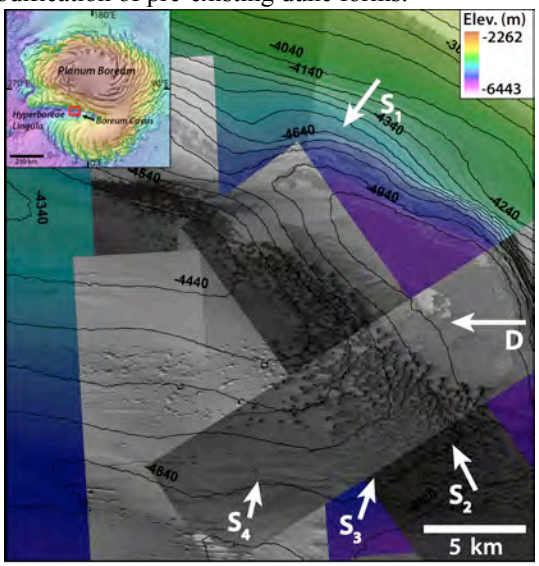

Figure 1. Dominant (D) and subordinate (S) wind vectors are from [5]. Dune distribution is shown in HiRISE imagery coregistered with MOLA topography (contoured at 100 m intervals). Inset shows the study site location.

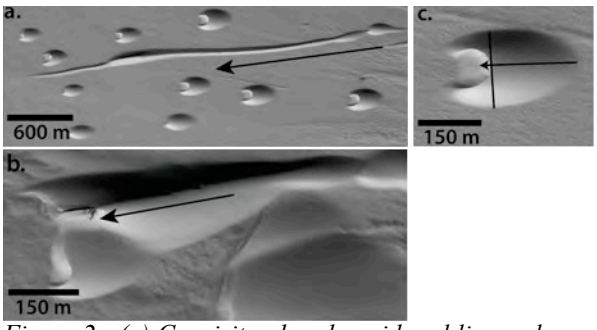

Figure 2. (a) Coexisitng barchanoid and linear dunes in HU. (b) Axes of linear-type dunes demonstrate local transport direction (black arrows). (c) Crestline trend and transport directions derived from a barchan dune.

Results of this study demonstrate that the dunes in HU are consistent with the modern wind regime in Chasma Boreale. Furthermore, variation of common dune forms (eg., barchans without lee faces and straight-crested linear dunes (Fig. 2)) appears linked to morphological parameters and may be partly explained by preferential erosion of narrower dunes.

Methods: The study site in HU is at the head of Boreum Cavus (Fig. 1). High Resolution Imaging Science Experiment (HiRISE) images were co-registered with Mars Orbiter Laser Altimeter (MOLA) data (Fig. 1) using ESRI's ArcGIS.

It is generally accepted that dune crestlines orient as perpendicular as possible to all constructive winds [e.g. 6, 7]. This principle of gross bedform-normal transport allows prediction of crestline trends with known wind direction. Wind vectors over Planum Boreum produced by spingtime (L_s = 61°) atmospheric modeling [5] (Fig. 1) provide direction and magnitude estimates of the modern winds entering Chasma Boreale at Boreum Cavus. Using modeled vectors, a resultant wind vector was calculated and crestline trend was predicted (Fig. 3). For comparison, the crestline trend of 40 barchans was measured (Figs. 2 and 3), and the values were averaged. Additionally, average transport direction was measured parallel to the long axes of 10 linear-type dunes (Figs. 2 and 3).

To study dune modification, 300 dunes were divided into 4 morphologies: barchans, indurated barchans [2], linear-type dunes, and coalesced dune forms. Barchans display two well-developed defects (Fig. 2c), indurated barchans resemble elongate domes (Fig. 2a), linear-type dunes are prominently elongated in one direction (Fig. 2a), and coalesced dune forms have

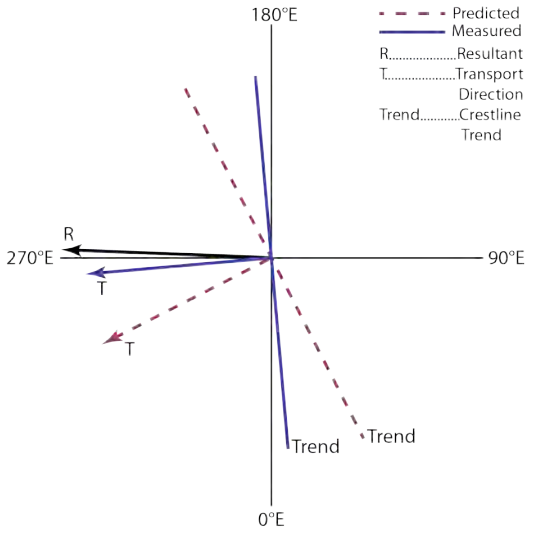

Figure 3. Crestline trend and transport direction predicted by a gross bedform-normal calculation using 4 pairs of dominants and subordinant winds after [5]. Predicted values are 22° away from measured values for crestline trend and transport direction. The resultant modeled wind vector, R, for springtime winds [5] is 7° away from measured transport direction.

elements of multiple morphologies (Fig. 2b). Morphology was plotted against maximum stoss slope width (Fig. 4), which was measured perpendicular to measured transport direction at the widest point. This measurement was chosen as a means to gauge a dune's ability to trap sediment and continue accumulation.

Results: The distribution of dunes at the study site closely follows elevation contours and appears to be influenced by topography. Noticeably, low and high points in the study site are mostly devoid of dunes (Fig. 1), which indicates low sediment supply, low sediment availability, and/or a wind transport capacity inconsistent with dune development [8].

Assuming net transport direction parallel to the long axes of linear-type dunes, measured transport direction is towards 275°, and average crestline trend is 185° (Fig. 3). Modeled wind vectors towards 323°, 270°, 207°, 161°, and 167° (Fig. 1) [5] yield a resultant vector towards 268°. The difference between modeled resultant wind vector and measured transport direction is 7°, strongly suggesting that the dunes of HU are equilibrated with the modern wind regime.

The average of four gross bedform-normal calculations using the dominant easterly wind and 4 subordinate winds (Fig. 1) yields a predicted average crestline trend of 207° and transport direction of 297° (Fig. 3). The predicted crestline trend varies from the measured trend by 22°. The difference is most likely a result of including only springtime winds in the calculation.

Dune morphology correlates with maximum stoss slope width (Fig. 4). Particularly, dunes ~ 100 m wide

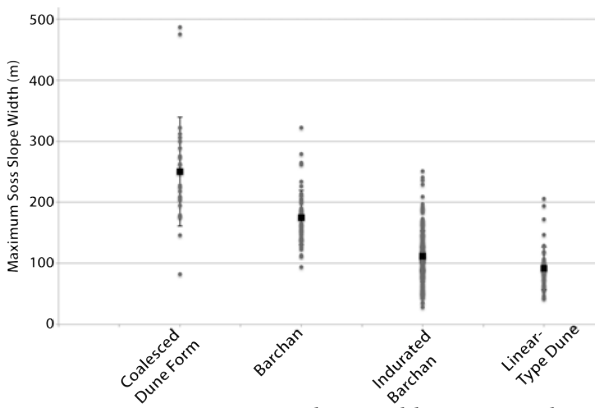

Figure 4. Maximum stoss slope width corresponds to dune morphology. Black boxes are the mean width with error bars giving 1 standard deviation.

appear to express an indurated barchan [2] or straight-crested, lee dune morphology (Fig. 4). The similar mean maximum stoss slope width values between indurated barchans and linear-type dunes suggests the two morphologies are related. Furthermore, the maintenance of a defined lee face by wider barchan dunes suggest sediment is being lost at the crest from indurated barchans, making them erosional features.

Conclusions: Comparisons between measured crestline trends and trends predicted by modeling of modern winds demonstrate that the dunes of Hyperboreae Undae are equilibrated with the modern wind regime. The unique dune morphologies of HU can possibly be explained by their ability to trap and retain sediment, which is estimated using maximum stoss slope width.

Future Work: Current calculations only take into account modern springtime winds in Chasma Boreale. Seasonal influence must be explored. Comparison of HU's bedform trends with those calculated from Planum Boreum cavi unit [3, 9] outcrops can provide insight into the evolution of wind regimes throughout the construction of the Chasma Boreale region [10].

Acknowledgements: This work was supported by the National Park Service as part of the Chihuahuan Desert Network Inventory and Monitoring Program.

References: [1] Ewing, R.C. et al. (2010) *JGR,* doi:10.1029/2009JE003526. [2] Schatz, V. et al. (2006) *JGR*, doi:10.1029/2005JE002514. [3] Tanaka, K.L. et al. (2008) *Icarus*, *196*, 318-358. [4] Edgett, K.S., and Blumberg, D.G. (1994) *Icarus, 112*, 448-464. [5] Spiga, A., et al. (2011) *Icarus, 212*, 504-519. [6] Rubin, D.M., and Hunter, R.E. (1987) *Science, 237*, 276-278. [7] Rubin, D.M., and Ikeda, H. (1990) *Sedimentology, 37*, 673-684. [8] Eastwood, E., et al. (2011) *Sedimentology, 58*, 1391-1406. [9] Kocurek, G., et al. (2011) *MPSE 5*, Abstract #6020. [10] Holt, J.W. et al. (2010) *Nature, 465*, 446-449.

POSSIBLE SEASONAL INDURATION OF SOUTHERN MID-LATITUDE DUNE FIELDS ON MARS. Carin Cornwall[1] and Stephen Wood[1], Molly Johnson, [1]Department of Earth and Space Sciences, University of Washington, Seattle, Washington, USA (carinc@uw.edu, sewood@uw.edu).

Introduction: Dune fields are highly sensitive to both circulation patterns and wind strengths and therfore preserve a unique record of the wind regime in which they formed. Due to their abundance and distribution over a wide range of latitudes, dune fields are valuable in studying global circulation patterns and help constrain Global Circulation Models (GCMs) [1]. Dune fields are also sensitive to climate change. Previous wind regimes may be preserved if the dunes are indurated due to a geochemical cement or ice [2, 3, 4, 5]. And the nature of the induration itself can provide insight into past and present climate processes.

There are many dune geometries on Mars that appear to be misaligned under the current wind regime [6]. These dune fields may be indurated and indicate past atmospheric circulation patterns [2, 4, 6, 7]. Many dune fields on Mars may contain layers of interbedded sand, snow, and ice [3]. The seasonal cap extends down to latitudes as low as -50° in the southern hemisphere during the autumn and winter seasons [8]. A number of dune fields are confined to craters in the southern highlands and may incorporate seasonal snow and ice deposits by processes such as diffusion of water vapor into pore spaces [9], burial, or simultaneous transportation and deposition of snow and ice [3].

We propose that some southern mid to high-latitude dune fields (~40°S to 60°S) may be niveo-aeolian deposits, composed of layers of snow, ice and sand. We expect many dunes to be wholly or partially indurated during the autumn, winter and early spring seasons. Thermal inertia values may indicate the presence of snow and ice in the near surface during the autumn, winter and early spring seasons and support the idea of niveo-aeolian deposits.

Data: This study uses a combination of data from the Thermal Emission Imaging System (THEMIS), Compact Reconnaissance Imaging Spectrometer for Mars (CRISM), high-resolution Mars Orbiter Camera (MOC) and Mars Reconnaissance Orbiter Context Camera (CTX) images to investigate the presence of snow and ice within dune fields in the southern mid-latitudes.

Analysis: We use a series of THEMIS early morning images, ranging from 3 AM to 5 AM to derive thermal inertia values for dune fields throughout the Martian year to examine variations in thermal inertia. THEMIS observations are restricted to those having a low dust and ice opacity in order to ensure accurate estimates in thermal inertia throughout the Martian year. CRISM images are used to confirm the presence or absence of ice on the dune field as well as the surrounding area. MOC and CTX images are used to monitor the presence of frost on dune fields in autumn and winter and provide any visible indications of thawing in the spring (dark spots, flow features etc. [e.g. 10]).

We utilize a 1-D thermal model, similar to the Kieffer/Viking Thermal Model, to derive apparent thermal inertia values from THEMIS temperatures that takes into account slope and azimuth of dune surfaces as well as seasonal deposition of CO_2 frost. A second model, the MaxRTCM (Maxwellian Regolith Thermal Conductivity Model) [11], was used to calculate the thermal conductivity of particles as a function of grain size, also taking into account seasonal variations of temperature and atmospheric pressure, non-spherical particle shape, thermal conductivity of basalt, and porosity. These thermal conductivity values were then converted into thermal inertia values to compare with THEMIS-derived values.

Results. We show the preliminary results of thermal inertia values derived for the Kaiser crater dune field. A previous study of Kaiser crater dune morphology suggested that the dune field might be a niveo-aeolian deposit [3]. If this is the case, we expect thermal inertia values to vary seasonally, increasing in the autumn and winter seasons with the addition of new snow and ice, then decreasing in the spring as the seasonal cap recedes. If ice remains in the pore space after the seasonal cap recedes, we expect thermal inertia values to remain elevated and reflect induration. Figure 1 shows the temperature variation of a portion of the Kaiser crater dune field for Ls 41, 211, and 314. Figure 2 shows the seasonal thermal inertia variation of the dune field based on temperature data from seven THEMIS observations, including the three from Figure 1. Figure 2 also shows thermal inertia values derived from MaxRTCM-calculated thermal conductivity for 500 μm diameter basalt particles at temperatures and pressures corresponding to each THEMIS image. Our results show an interesting seasonal variation in thermal inertia values that indicates a strong dependence upon temperature, as suggested by Piqueux and Christensen [12]. More work needs to be done to account for the effects of near-surface ground ice on THEMIS-derived thermal inertia values to determine if these variations may be due in part to the presence of niveo-aeolian deposits.

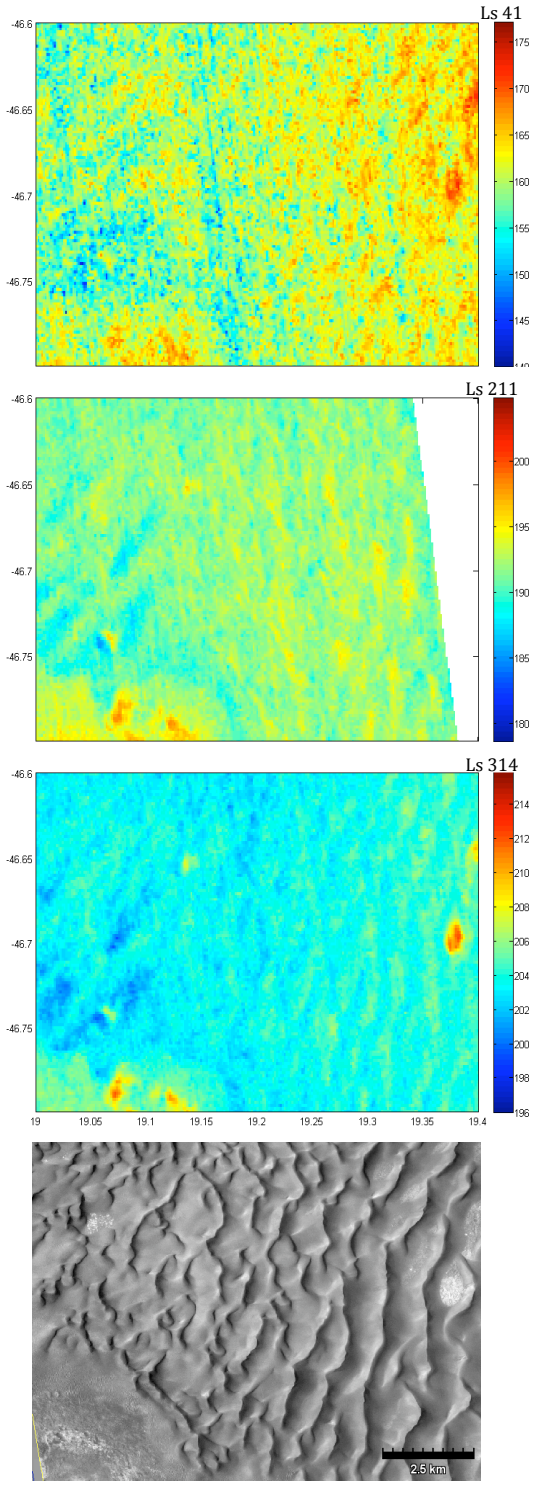

Figure 1. Temperature variations in Kelvin for a portion of the Kaiser crater dune field and a high resolution CTX image (B05_011527_1329_XN_47S340W) of the featured area. Top image corresponds to Ls 41 (late autumn), middle image; Ls 211 (spring), and bottom image; Ls 314 (summer).

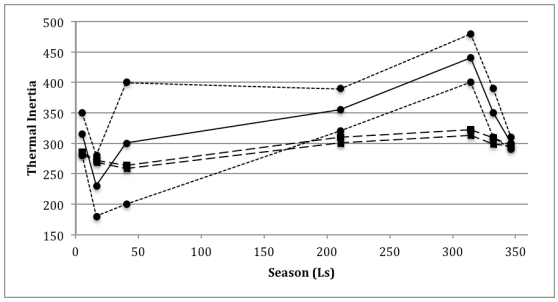

Figure 2. Graph of thermal inertia values derived from temperatures from 7 THEMIS observations. The solid line corresponds to average apparent thermal inertia values, where the dotted lines are the maximum and minimum values. The dashed lines correspond to minimum and maximum values of thermal inertia derived from thermal conductivity values calculated using MaxRTCM [11], assuming a porosity of 40%, sphericity of 0.85 and roundness of 0.60.

Conclusions. Preliminary results show an interesting seasonal variation in thermal inertia values for the Kaiser crater dune field. Results suggest a strong temperature dependence, where some of the variation may be accounted for by changes in CO_2 gas conductivity in the pore space [11, 12]. Further modeling will be made to determine if some component of these variations are due to seasonal induration of the sand or if these variations can be explained by contributions from ground ice heat storage and/or temperature-dependent conductivity of regolith particles and pore gas. If thermal inertia variations persist, these southern mid-latitude dune fields may be seasonally indurated and can potentially be classified as niveo-aeolian deposits, providing a unique record of a past wind regime on Mars, or insight into current climate processes.

References: [1] Hayward R. K. et al. (2009) JGR, 114, E11012. [2] Bourke M. C. (2004) Eos, Transactions, Fall Meeting Suppl., 85, abs #P21B-01. [3] Bourke M. C. (2005) LPSC XXXVI, abs. #2373. [4] Schatz V. et al. (2006) JGR, 111, doi:10.1029/2005JE002514. [5] Gardin E. et al. (2011) Icarus, 212, 590-596. [6] Fenton L. K. and Hayward R. K. (2010) Geomorph, 121, 98-121. [7] Malin M. C. and Edgett K. S. (2001) JGR, 106, 23,429-23,570. [8] James et al. (1979) J. Geophys. Res., 84, 2889-2922. [9] Mellon M. T. and B. M. Jakosky (1995) J. Geophys. Res, 100, 11,781-11799. [10] Gardin E. et al. (2010) JGR, 115, doi:10.1029/2009JE003515. [11] Wood S. (2011) LPSC XXXXII, abs. #2795. [12] Piqueux, S. and P. R. Christensen (2011) J. Geophys. Res., 116, doi:10.1029/2011JE003805.

GEOPHYSICAL ANALYSIS OF THE CRESTONE "CRATER", GREAT SAND DUNES NATIONAL PARK, COLORADO. C. Cox[1], R. Isherwood[1], A. Reitz[1], R. Krahenbuhl[1], J. C. Andrews-Hanna[1] and A. Valdez[2], [1]Colorado School of Mines Department of Geophysics, 1500 Illinois St, Golden, CO 80401 (jcahanna@mines.edu) [2]Great Sand Dunes National Park and Preserve, 11500 Highway 150, Mosca, CO 81146-9798, USA (andrew_valdez@nps.gov)

Introduction: In the northwest of Great Sand Dunes National Park, outside of Crestone, Colorado at 37°54'40.0"N, 105° 39'10.9"W, exists a controversial crater-like feature of unknown origin (Figure 1). This small (100 m diameter) raised-rim depression, dubbed the Crestone Crater, is suspected to be of either impact or aeolian origin. The word "crater" will be used throughout this study, but this is meant in a descriptive sense independent of the formation mechanism. Previous studies supported an aeolian origin, possibly produced by a blowout [1], based on the surface expression of the crater and a single drill core that did not find meteoritic material.

Here we report on the results of geophysical surveys conducted by Colorado School of Mines undergraduate students (Cox, Ishwerwood, & Reitz). This project was motivated by the Second International Planetary Dunes Workshop in Alamosa, CO during a field trip that visited the Crestone Crater. The main objectives of the study were to determine the subsurface structure of the putative crater as revealed by geophysical property contrasts. The survey included gravity, magnetics, and DC-resistivity measurements over the crater.

The proposed aeolian and impact origins for the crater would be expected to result in different subsurface properties as revealed in the geophysical survey. In particular, an origin of the depression as an aeolian blowout would not be expected to result in any subsurface structure correlated with the topographic expression of the crater, since the low-energy removal of material would have had little effect at depth. In contrast, an impact origin would be expected to significantly modify the properties of the subsurface from the passage of the shockwave and the excavation flow. The results of this preliminary survey lend some support to an impact origin, but are not conclusive.

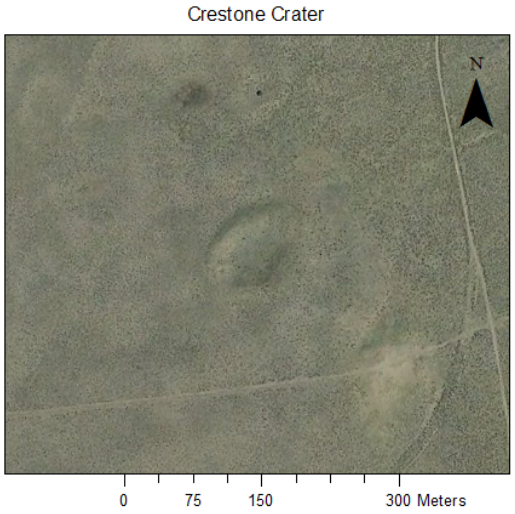

Figure 1. Aerial view of the Crestone crater.

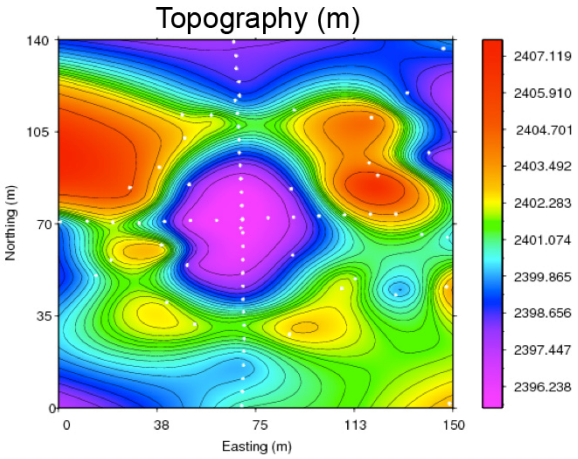

Figure 2. Interpolated topographic map of the Crestone crater (white dots represent data points).

Survey and results: The data was collected over two consecutive weekends early 2010. The survey consisted of topographic surveying of select points, two 1D gravity transects, a grid of 15 lines of magnetics measurements, and a grid of 9 lines of DC resistivity measurements. The DC resistivity and magnetics data were inverted to yield 3D maps of the subsurface resistivity and magnetic susceptibility. The gravity data was processed to yield the Bouguer anomaly using the measured surface topography.

The topography reveals an elliptical depression with a raised rim (Figure 2). Both the DC resistivity and magnetics survey reveal subsurface anomalies at depth that correlate with the surface expression of the crater (Figures 3 and 4). In the resistivity data inversion, a ring shape appears at depth that correlates with the raised topographic rim. Similarly, the Bouguer gravity anomaly reveals a relative gravity high at the center of the crater, anti-correlated with the topography (Figure 5). This is indicative of a positive density anomaly below the crater floor

Conclusions: This preliminary geophysical survey of the Crestone crater has revealed a unique geophysical signature in the subsurface that is correlated with the surface expression. This is contrary to the expectations for an aeolian origin, but may be consistent with the effects of an impact. However, the results of this study remain inconclusive, as no diagnostic evidence for an impact has been found in this or previous work. Future work should include surveys of aeolian features in the vicinity for comparison. A geomorphic comparison of the Crestone crater with small impact craters in aeolian environments on Mars would also help to shed light on its origin. If the feature is an impact crater, it is unique both due to its small size and its preservation in unconsolidated sediments. Understanding the preservation and modification of craters in aeolian environments on Earth may help to understand similar craters on Mars and to draw inferences regarding the degree of recent aeolian activity there.

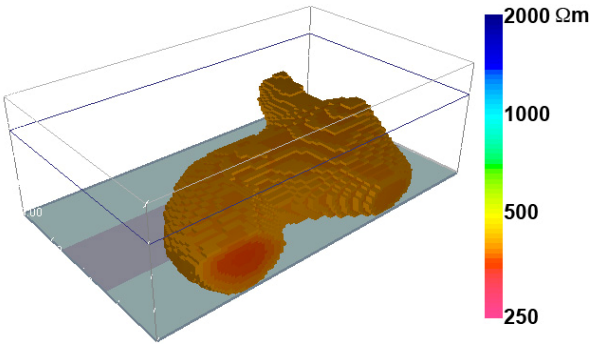

Figure 3. Results of the 3D DC resistivity inversion (note only half of crater was surveyed)

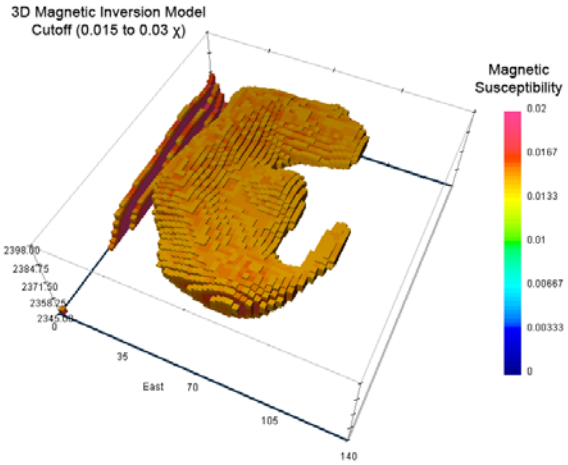

Figure 4. 3D magnetic susceptibility model from inversion of magnetics data.

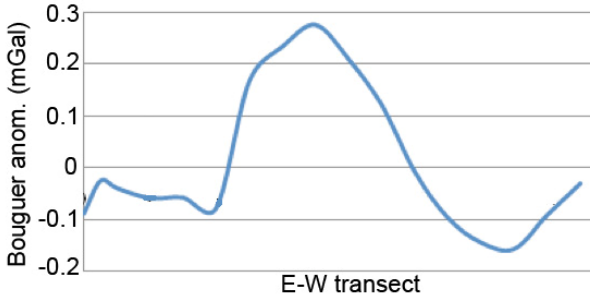

Figure 5. Bouguer gravity profile along the east-west survey line.

References: [1] Marvin, U. B. and T. C. Marvin A re-examination of the crater near Crestone, Colorado. Meteorics, 3(1):1-10, 1966.

ANCIENT EOLIAN LANDFORMS AND FEATURES FROM A TERRESTRIAL MID-LATITUDE PERIGLACIAL ENVIRONMENT . M. Demitroff[1], M. Cicali[2,3], J. Smith[4], and A.N. Demitroff[2], [1]University of Delaware, Department of Geography, 216 Pearson Hall, Newark, DE 19716 (mdemitrf@udel.edu), [2]Richard Stockton College of New Jersey, School of Natural Sciences and Mathematics, Environmental Science Program, 101 Vera King Farris Drive, Galloway, NJ 08205, [3]URS - FAA William J. Hughes Technical Center, ANG-E332, Atlantic City, NJ 08405, [4]Nature Conservancy, Delaware Bayshore Office, 2350 Route 47, Delmont, NJ 08314.

Introduction: The "Pine Barrens" region of southern New Jersey has recently been the focus of intensive examination of evidence for deep seasonal frost and permafrost [1,2,3]. Surprisingly little is known of the Mid-Atlantic States' cold, nonglacial (periglacial) history, a dynamic dry, windy, and poorly vegetated environment subject to abrupt changes. Conditions in southern New Jersey during the Late Glacial Maximum have few modern terrestrial analogs. Cryostratigraphic studies of the region's Coastal Plain has revealed Pleistocene periglacial relicts that could provide serviceable analogs for Mars eolian research.

Remote Sensing: Laser altimetry provided survey through the region's dense vegetation to reveal the underlying terrain. Down-looking airborne light detection and ranging (LiDAR) point cloud data were used to reveal bare-earth ground terrain. This was performed using high resolution LiDAR (1 meter) geodetically corrected data captured in early April 2010. The LiDAR data enabled the separation and extraction of surface vegetation from the measured bare-earth ground surface. The geodetically controlled bare-earth point cloud matrices and surfaces were modeled and analyzed using Quick Terrain Modeler (QtModeler) version 7.1.5. Through this analyses, it was evident strong density-driven katabatic winds from the Laurentide Ice Sheet and enhanced westerlies sculpted Pine Barrens ground through sand deposition and deflation. Subtle en-echelon parabolic dunes and sand sheets were formed, remnants of a sand-starved eolian system. South Jersey sediments were often frozen when winds were strongest [4]. Eolian landforms interacted with the local paleohydrology. In some places dunes occluded, dammed (Figure 1), or avulsed drainageways, in others fluvial channels cut across and reshaped ancient eolian bed forms. Numerous playa-like deflation hollows have been recorded [5].

Fieldwork: A suite of macrostructures observed in the field, abundantly expressed in local sand and gravel operations, also provided evidence of past permafrost and rigorous periglacial conditions. Ventifacts were abundant, often present in lag pavements. Cracks of primary infill ranged from small desiccation fissures in fragipan to somewhat enigmatic ground or soil wedges produced under deep-seasonal frost (cryodesiccation) to large (+2.5 m depth) thermal-contraction sand-wedge casts [1,4,6]. Along with features associated with a cooling climate (e.g., permafrost aggradation) were features of climate amelioration (e.g., permafrost degradation). Subsidence structures attributable to melt of ground ice, such as modified sand wedges and sediment-filled pots (bulb-like wedge intersections), were also commonplace. Fragipan, a densified soil horizon, was coincident with the prior permafrost table [2]. Cryogenic weathering of silicates, a process best developed in the active layer of permafrost regions, was represented in local paleosols [7,8].

Conclusion: Examination of Pine Barrens periglacial phenomena will add to the range of Earth analogs for Mars dune studies, especially concerning mid-latitudinal climate change dynamics. The frozen ground of Mars and New Jersey both experienced: 1) diurnal cycles of high-amplitude temperature change across the freezing point; and 2) polycyclic warming and cooling episodes possibly related to Milankovitch cycles. By comparison, Antarctica or Baffin Island may share a very cold Mars-like environment, but these high-latitude Earth analogs have been relatively quiescent from a geomorphological perspective. South Jersey's periglacial features provided good representation of the effects of the polycyclic nature of global climate change, in a location far more accessible than high-latitude locations like Greenland or Antarctica. Similarities between the mid-latitude regions of Earth and Mars during cold climatic intervals will help us better understand the past geologic temperature record of both realms, and help predict future changes as a consequence.

References: [1] French H. M. et al. (2003) *Permafrost Periglac., 14,* 259–274. [2] French H. M. et al. (2005) *Permafrost Periglac., 16,* 173–186. [3] Newell W. L. and DeJong B. D. (2011) *Geol. Soc. London, Spec. Pub. 354,* 259–276. [4] French H. M. and Demitroff M. (2003) *Proc. GANJ XX,* 117–142. [5] French H. M. and Demitroff M. (2001) *Permafrost Periglac., 12,* 337–350. [6] Demitroff M. et al. (2008) *Proc. NICOP,* 355–360. [7] Demitroff M. et al. (2007) *Proc. Cryogenic Resources of Polar Regions*. 139–141. [8] French H. M. et al. (2009) *Earth's Cryosphere, 13,* 17–28. [9] NJDEP (1931) Airplane Atlas Sheet 222. [10] French H. M. et al. (2007) *Permafrost Periglac., 18,* 49–59.

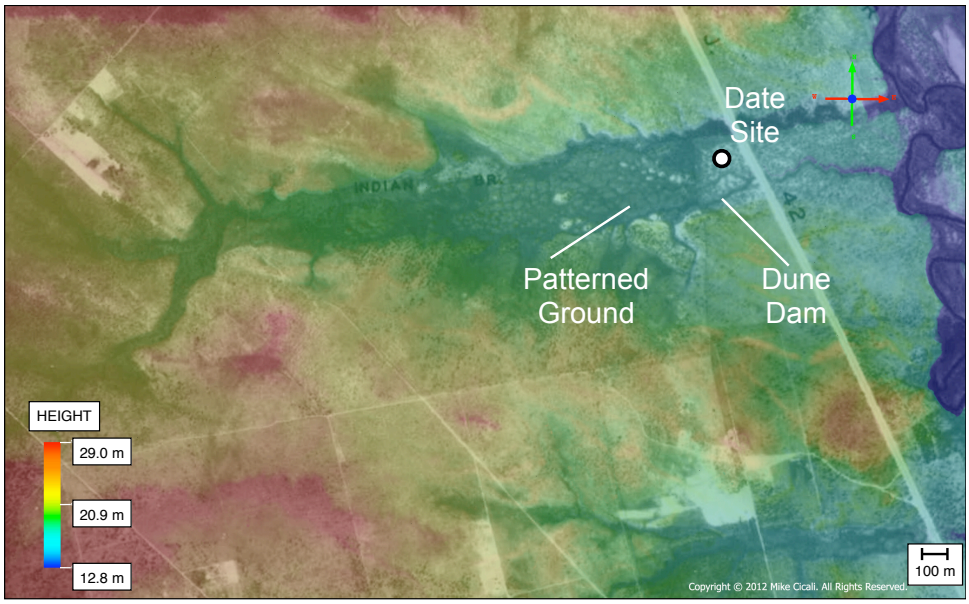

Figure 1: LiDAR image of a completely dune blocked paleochannel at Indian Branch (1–3 m infill), an event that has been luminescence dated to 28.16 ± 2.80 ka BP. A layer from 1931 aerial photomosaics [9] has been added to show fossil patterned ground polygons behind the dam. Damming coincided with MIS 3 climate amelioration and regional development of thermokarst terrain. Location 39 33 20.22, -74 48 47.26.

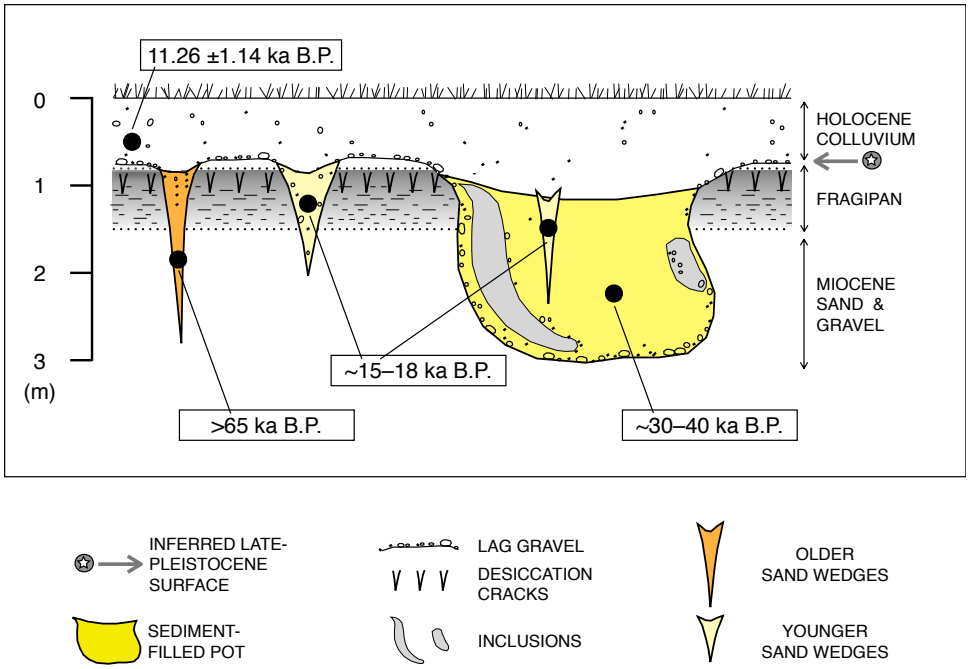

Figure 2: Typical Late-Pleistocene and Holocene terrace stratigraphy of the Pine Barrens, southern New Jersey. The smaller wind-faceted pebbles are commonly found beneath Holocene colluvium and above Late Tertiary-age sand and gravel. The sketch shows Late Pleistocene periglacial features, including ≥MIS-4 and MIS-2 frost cracks, a MIS-3 thermokarst thaw bulb with inclusions, fragipan fissures capped by cover sand, and Holocene (Pleistocene-transitional?) colluvium. Modified from [10].

INVESTIGATING THE COARSEST GRAVEL RIPPLES ON EARTH – FIELD RELATIONSHIPS, SEDIMENTOLOGICAL CHARACTER AND IMPLICATIONS FOR MARS. S. L. de Silva[1], N. T. Bridges[2], J. R. Zimbelman[3], M.G. Spagnuolo[4], D.M. Burr[5]; S.Scheidt[3], A. Ortiz[6] [1]Oregon State University, Corvallis, OR 97331 (desilvas@geo.oregonstate.edu), [2]CEPS/NASM MRC 315, Smithsonian Institution, Washington D.C. 20013-7012. [3] JHUAPL, Laurel, MD 20723, [4]University of Buenos Aires, Argentina, [5]University of Tennessee Knoxville, Knoxville, TN 37919, [6]Universidad de Salta, Salta, Argentina

Introduction: Coarse gravel megaripples in the Puna of Argentina represent some of the most extreme aeolian bedforms on Earth in terms of particle properties and formation conditions [1, 2]. These gravel ripples are built on a bedrock of ignimbrites and composed of a bimodal association of dense (>2 g cm^{-3}) lava and metamorphic clasts up to 2.5cm in diameter and pumice clasts (<1.5 g cm^{-3}) up to 5 cm in diameter, making these the coarsest grained ripples yet described on Earth (Figure 1). While the mechanisms of origin and formation are debated [1,2,3], it is clear that these ripples must represent extreme conditions that define an end member of the spectrum of granule ripples on Earth. The relevance to Mars is threefold: First, these aeolian gravel bedforms consist of materials that have similar equivalent weight to those composing the granule ripples at Meridiani Planum, Mars. Second, the spatial relationships among these Puna megaripples, topography, and bedrock are analogous to relationships among Transverse Aeolian Ridges (TARs), topography, and bedrock on Mars. Third, the gravels are locally derived and may point to an alternative source to globally transported dark dune sediments on Mars [4,5]. We report here the progress we have made studying these megaripples, conducted under the auspices of NASA MFRP grant NNX10AP79G. We dedicate this work to the memory of our collaborator Ron Greeley.

Geologic Background: The gravel megaripple fields of Catamarca, Argentina are located in one of the windiest parts of the Argentinean Puna. The gravel ripples are distributed in five distinct fields in close proximity to each other, centered around 26°45'S 67°45'W. The fields vary in areal extent from 300 km^2 to 50 km^2, representing the largest areas of coarse gravel ripples yet described on Earth [1,2]. Each field is located in a separate "basin" demarked by bounding volcanic and basement (metamorphic) highlands and is distinct in componentry and macroscopic appearance, reflecting variable sources of the lithic clasts. The largest of the fields is Campo Piedra Pomez that is built on the bedrock of the 70 ka Campo Piedra Pomez ignimbrite (CPP). Here dark megaripples prevail [4,5]. The largest and coarsest megaripples are found in the Purulla and White Lake fields, while the White Barchan field hosts the smallest quartz-dominated megaripples.

Observations and Interpretations. The megaripple fields display amplitudes up to 2m and wavelengths of up to 30m (Figure 1). Common to all the fields is that the bedrock rhyolitic ignimbrites are weakly to moderately indurated and have been abraded by wind-blown sediment to produce prominent yardangs and demoiselles. Yardang development in the Purulla field is limited by the poor induration of the ignimbrite.

Figure 1. Large lithic dominated gravel megaripple bedforms of the Purulla field. Wind from bottom right. Note concentration of large pumice on the lee side of the bedform and person for scale. Amplitude of the topography is ~2m and the wavelength is almost 30m.

Figure 2. Detail of the gravel bedforms at Purulla. Wind direction is out of the page. The crest is dominated by lithic clasts up to 2cm and the lee-side (bottom left) is dominated by pumice up to 5 cm.

In some fields, the gravel bedforms consist of lithics derived exclusively from erosion of the bedrock

ignimbrite. In others, the source is a mixture of local bedrock ignimbrite and surrounding highlands. Pumice is derived from the local ignimbrite exclusively. Profiles of the ripples made using laser profiling and Brunton measurements show significant variability, with ripples in the Purulla area showing more symmetry between lee and stoss slopes than those in the Campo Piedra Pomez.

A key feature of these fields is that the eroded surface of the ignimbrite bedrock on which the gravels develop is distinctively wavy and scalloped at the 1 to 2m vertical and 10m horizontal scale. Gravels appear to collect on the erosional surface in the swales or troughs between yardangs and vary from areally extensive sheets through diffuse lenses to distinct bedforms. The best developed bedforms appear to nucleate and develop on the crest of the surface topography. This relationship is confirmed by trenching into the bedforms, which reveals that the largest gravel bedforms make up only 30cm of the 2m amplitude of the megripple topography. The upper 20cm is dominated by crudely bedded coarse gravels, while the lower portion contains significantly more sandy material. The coarsest particles are concentrated at the surface and peak of the ripple. Large pumice, up to 2.5x the size of associated lithic fragments, is loosely concentrated on the lee of the bedform. No evidence of slip faces were found in the sections we made, confirming that these bedforms are indeed ripples and not dunes. Rare internal sandy beds suggest ephemeral sand sheets swept through the area.

A model for the origin of the Coarse Gravel Megaripples in the Puna of Argentina: Componentry supports the macro- and mesoscale observations that the origin of the gravels is from erosion of the bedrock ignimbrite augmented locally by input from surrounding highlands [5]. Locally there is abundant evidence that the gravels that constitute the megaripples are a lag material that developed on the eroded bedrock ignimbrite surface. The strong association of the discrete megaripple bedforms with local topographic "highs" and pumice with the gravels suggests that organization of the gravels into bedforms was influenced by these two factors. The concentration of pumice on the lee side of the bedforms implies a symbiotic relationship between gravel bedform and pumice. We suggest that saltation of pumice (and sand) results in reptation of gravel through impact energy transfer. Undulose topography on the bedrock surface may set up local turbulence and Bernoulli effects that might promote accumulation of gravel on crests. Bedforms start to nucleate and stabilize on highs, setting up a feedback between the bedform, airflow, and lee-side accumulation of saltating pumice. Once the bedform stabilizes it produces a lee-side wind shadow zone that allows pumice to concentrate. As the bedform stabilizes, flow separation results in formation of vortices that deepen the troughs. This stabilized bedform is an equilibrium surface that is only modified if the bedforms are disrupted during rare extreme conditions. Thus we envisage an evolution of the surface from bedrock => yardangs => gravel sheets => gravel bedforms => stable megaripples that cap bedrock ridges.

Implications for Mars: The predominance of aeolian (wind-driven) activity as a surface-modifying agent on Mars has been recognized throughout the history of telescopic, satellite, and robotic investigation of the planet. The most obvious expressions of aeolian processes are manifested in dunes, yardangs (aerodynamic ridges in bedrock) [6,7], sand ripples [8,9], and Transverse Aeolian Ridges (TARs) [10].

Granule ripples on Earth have been suggested as potential analogs for ripple-like TARs on Mars [11]. Moreover, dark dunes on Mars have been hypothesized as volcaniclastic sediments [12], including those of the western Medusae Fossae Formation (MFF) [e.g., 4]. Thus, comparison between TARs and western MFF on Mars and terrestrial volcaniclastic bedform-forming sediments allows us to offer insight into aeolian processes on Mars and the origin of TARs.

Beyond helping understand the bimodal granule ripples imaged by rovers at Meridiani [13], our observations in the Puna may help reconcile current models of TARs with the recognition that some periodic bedrock ridges (PBR) may be produced by erosion [14]. The flow separation model presented for PBRs is not unlike that which we envisage for the Puna megaripples.

Moreover, if the Martian dark gravel/sand is locally derived, as we suggest for dark megaripples in the CPP of the Puna, this derivation would obviate the need for large scale atmospheric transport of dark sediment [4,5]. It may be that much dark sand elsewhere on Mars, prior to transport to its present location, could have been derived from ancient volcanoclastic mantles that have subsequently been stripped away.

References: [1] Milana, 2009; *Geology* 2009;37;343-346 doi:10.1130/G25382A.1 [2] de Silva, 2010, Geology, doi: 10.1130/G30780C.1. [3] Milana et al 2010, Geology, doi: 10.1130/G31354Y.1 [4] Burr et al. (2011) *LPS XLII*, 1582 [5] de Silva S.L. et al. (2012) *LPS XLIII, #*2038. [6] Ward, 1979; Journal of Geophysical Research 84: 8147-8166. [7] Mandt, K., de Silva, S.L., Zimbleman, J.R., and Crown, D.A. Journal of Geophysical Research VOL. 113, E12011, doi:10.1029/2008JE003076. [8] Sullivan, R. et al. (2007), Lun. Planet. Sci. XXXVIII, 2048. [9] Silvestro, S. et al. (2010), Geophysical Research Letters, 37. [10] Bourke et al., 2003. *Lunar and Planetary Science XXXIV*, Lunar and Planetary Institute, 321 Houston (CD-ROM), Abstract 2090. [11] Zimbelman J. R. (2010) *Geomorphology* 121, 22-29, 10.1016/j.geomorph.2009.05.012. [12] Edgett K.S. and Lancaster N. (1993) *J. Arid Environments, 25(3),* 271-297. [13] Sullivan et al., 2005 *Nature* 436, doi: 10.1038/nature03641. [14] Montgomery, D.R. et al. (2012), *J. Geophys. Res., 117*, doi:10.1029/2011JE003970.

Venusian dunes – where are they? An update. Serina Diniega[1] (serina.diniega@jpl.nasa.gov), [1]Jet Propulsion Laboratory, California Institute of Technology, Pasadena, CA.

Introduction: With Venus' thick atmosphere, it seems likely that aeolian features such as streaks, yardangs, ripples, and dunes should be common. Magellan synthetic aperture rader images of the surface did yield numerous wind streaks and a few possible yardangs [1], but only a handful of dune fields [1-2] -- far fewer than were expected [2-3]. This overview study will present current observations of dune fields (focusing on Magellan and any updates from Venus Express) and will then explore implications these observations (or lack thereof) yield about the Venusian environmental conditions and active surface processes.

Previously Identified Dune Fields: A survey of Magellan images covering 80% of the Venus surface with a resolution of 75m yielded two dune fields [1]:

- Aglaonice at 25°S, 340°E covers 1290 km^2. Dune orientation indicates a westward wind flow, which is supported by associated bright and dark wind streaks.
- Fortuna-Meshkenet (Figure 1) at 67°N, 90°E covers 17,120 km^2. Dune orientation and nearby bright wind streaks indicate a northwest-west wind flow.

Figure 1. Magellan image of the Fortuna-Meshkenet dune field. Taken from [1].

Possible Reasons for the Paucity of Dunes: A lack of observations of dunes and ripples can result from two situations: (1) these features do not exist or (2) these features are not visible in current observations.

For point (1), there are two types of limitations that will prevent dunes and ripples from forming:

- *Wind-limited:* wind-tunnel experiments indicate that sand-sized particles should be easily entrained at moderate wind speeds (~1 m/s) [4], so a lack of saltation-formed landforms would imply that Venusian surface winds are very low/inconsistent.
- *Supply-limited:* dunes and ripples will not form unless a minimum-sized pile of sand can accumulate. This can be prevented by having either no zones of accumulation (which seems unlikely given there are impact craters and other low topography regions) or a very small sand supply (which would imply the lack of surface erosion processes yielding sand-sized particles).

However, these results are not consistent with the observation of wind-streaks and other aeolian features [1] – the existence of which suggests that some saltation/wind-driven erosion has occurred, or observations of fines and sand-sized particles at Venera landing sites [5].

For point (2), issues could arise with respect to:

- *sufficient contrast from background materials*: as we are considering radar images, this involves look-angle effects (slip-faces must be oriented near-normal to the radar mean, which implies that N-S trending dunes primarily will be visible in Magellan imagery [2]) as well as composition/dielectric/roughness differences.
- *image resolution*: Wind-tunnel experiments done under Venusian atmospheric conditions yielded transverse dunes with wavelengths of 10-20 cm [4], which is consistent with the minimum dune size predicted by general dune models [6]. Magellan images had a resolution of 75m – several orders of magnitude larger. So unless "microdunes" grow significantly, they will be difficult to detect.

Acknowledgements: SD was supported by an appointment to the NASA Postdoctoral Program, administered by Oak Ridge Associated Universities, at Caltech/JPL under a contract with NASA.

References: [1] Greeley R., et al. (1992) *JGR, 97(E8)*, 13319-13345. [2] Weitz C.M., et al. (1992) *LPSC XXIII*, Abstract 1511. [3] Weitz C.M., et al. (1994) *Icarus, 112(1)*, 282-295. [4] Greeley R., et al. (1991) *Icarus, 90*, 123-128. [5] Garvin, J.B., et al. (1984) *JGR, 89*, 3381-3399. [6] Claudin P., et al. (2006) *E&PSL, 252*, 30-44.

INTERNAL SEDIMENTARY STRUCTURE AND AQUEOUS-PHASE DISTRIBUTION OF THE GREAT KOBUK SAND DUNES, NORTHWESTERN ALASKA: INSIGHTS FROM AN ARCTIC AEOLIAN ANALOG SITE. C. L. Dinwiddie,[1] R. N. McGinnis,[1] D. E. Stillman,[2] K. L. Bjella,[3] and R. E. Grimm[2] [1]Geosciences and Engineering Division, Southwest Research Institute®, 6220 Culebra Road, San Antonio, TX 78238, [2]Space Science and Engineering Division, Southwest Research Institute, 1050 Walnut Street, Suite 300, Boulder, CO 80302, [3]Cold Regions Research and Engineering Laboratory, U. S. Army Corps of Engineers, Ft. Wainwright, Alaska 99703.

Introduction: We are studying the stratigraphy and aqueous-phase distribution of the high-latitude, cold-climate Great Kobuk Sand Dunes (GKSD) (Fig. 1) of northwestern Alaska as potentially analogous to extraterrestrial æolian dunes affected by permafrost [1–3 and references therein] and other volatiles. Our team acquired a suite of geophysical, shallow borehole, ground temperature, and topographic data from the field in late-March 2010 [1–3]—long before mean daily surface temperatures rose to 0ºC [4].

Observations: Interdunes, small dunes, lee slopes, and most of the stoss slopes of large dunes are completely snow-covered for approximately 70% of each year, yet crests of the largest dunes remain exposed to atmospheric forcing throughout much of the winter season. Estimates based upon remote sensing {Fig. 4 in [5]} suggest that large dunes migrate faster here than smaller dunes—a distinctly atypical behavior.

Reversing dune signatures [6] that would document reactivation surfaces from brief, summer-season wind reversals are not evident in ground-penetrating radar (GPR) profiles that reveal the internal sedimentary structure of the dunes. Wind reversals do not produce flat-topped dunes or complex internal bounding surfaces like those observed at the Packard dune field in Antarctica [7]. Rather, simple, high-angle and generally west-dipping cross-strata (i.e., grainfall and grainflow laminae) are prevalent within the dunes, with erosional truncation on eastern stoss slopes and deposition on western lee slopes. Higher order bounding surfaces are dominated by Stokes surfaces [8] near the base of dunes where wind scoured the sand to an irregular, flat-lying plain at the top of the capillary fringe, slightly above the level of the regional groundwater table.

GPR, OhmMapper capacitively coupled resistivity, and shallow borehole data directly or indirectly identified and provided support for the variable thickness of the seasonally frozen active layer in the dunefield. The active layer is ~4 m thick beneath dune crests, and <2 m thick beneath interdunes [1, 2]. Unfrozen water lies beneath the active layer, either within a regional aquifer or within a perched water zone (Fig. 1). OhmMapper data show that the highest resistivity values are within the frozen active layer and the lowest are below a hydrologic GPR reflector, especially beneath interdunes [2]. The ever-present, near-surface hydrologic GPR reflector closely matches the position of the 5000 Ω·m resistivity contour at the dunefield margin and below interdunes, but better matches the ~50,000 Ω·m contour in dune uplands [2]. While the near-surface hydrologic reflector does not mirror topography exactly, it does so generally even in the uplands, which differs from warm-climate dune fields characterized by relatively flat-lying water tables.

Interpretations: Arctic dunes have relatively slow migration rates [e.g., 5] compared to warm-climate dunes, and large arctic dunes may display atypical rapid migration rates relative to small arctic dunes because of the frequent absence of snowcover near large dune crests and the presence and duration of longterm snowcover on interdunes, stoss slopes, and small dune crests. The dominant, sand-transporting winds at the GKSD are polar easterlies from November to April [4], but snow-covered sand is largely decoupled from these cold season winds. GPR data confirm the dominance of easterly cold-season winds in dune construction [4]. The lack of preservation of reversing dune signatures is consistent with the transport-dampening effects of warm-season rains that also frequently occur during the brief summer wind reversal.

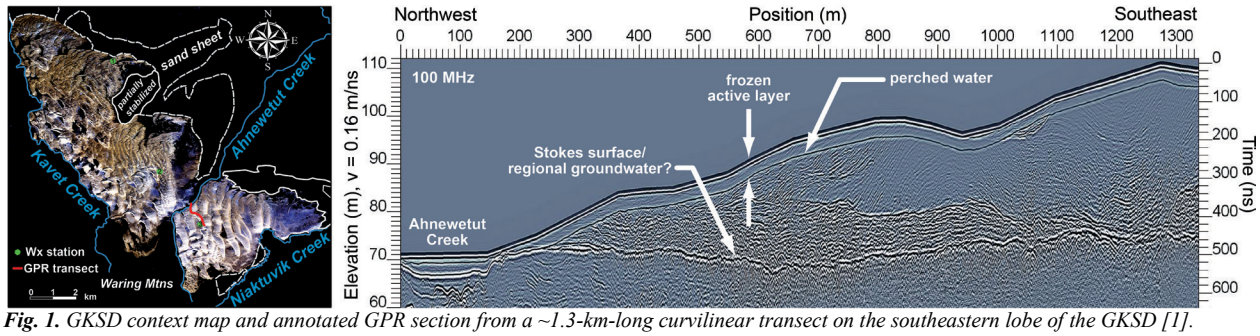

Fig. 1. *GKSD context map and annotated GPR section from a ~1.3-km-long curvilinear transect on the southeastern lobe of the GKSD [1].*

Given that these dunes are composed of fine sand {i.e., 167 μm [2]}, one would expect them to drain rapidly and the regional water table to be relatively flat, similar to those associated with warm-climate dunes. The hydrogeologic anisotropy of the layered, steeply sloping grainfall and grainflow bedforms is understood to shed water in the vadose zone preferentially and downslope [9] through lateral flow diversion. We think that we have imaged near-surface regional groundwater at the lowland dunefield margins and below interdunes, but that near-surface liquid water in the dune uplands must be perched above a relatively continuous, low permeability unit (Fig. 1). The pseudo-topographic mirroring behavior of the near-surface hydrologic GPR reflector and certain resistivity contours, along with the depths of free water or moist, unfrozen sand observed in boreholes altogether suggest that the near-surface presence of liquid water within dune uplands is thermally controlled, and that it is very likely perched upon a syngenetic permeability barrier. But what is this barrier that develops in virtual dynamic equilibrium with slow dune migration?

We suggest that this low-permeability perching unit developed through cryodessication and may be composed of (i) an ice-rich lens oriented normal to the direction of heat flow in the transition zone at the base of the active layer [10], (ii) calcrete [11], and (iii) other fines deposited through thermal regelation [12]. Cryodessication can produce both ice lenses and calcrete deposits at the base of the active layer where upward freezing from a permafrost table or downward freezing from the land surface occur [13–15]. Secondary precipitation of $CaCO_3$ occurs during slow, progressive, seasonally closed (to the input of atmospheric CO_2)-system freezing—a solute concentration process by which both the partial pressure of CO_2 and calcite saturation index increase as a result of (i) vapor migration toward freezing fronts and (ii) ion exclusion in ice formation [14–17]. Carbonate grains and phyllosilicates comprise 7% and 5% of the GKSD sands, and widespread calcrete has been observed [e.g., 11]. Thermal regelation is a process associated with frost heaving whereby a growing ice lens preferentially segregates fine soil particles below it. Because fine particles are spatially segregated by seasonal freezing, an initially marginally frost-susceptible sediment (such as the fine, dirty GKSD sand) may gradually transform into a more strongly frost-susceptible sediment [18].

Conclusions: Our data suggest that the GKSD are a wet æolian system [19]. Although they are exposed to a semi-arid climate, the presence of near-continuous permafrost in this region results in considerable near-surface moisture. The GKSD and surrounding land are vulnerable to accelerating permafrost degradation because the continuous permafrost zone boundary, which lies nearby [20–22], is migrating northward in response to a warming climate.

We hypothesize that mechanical arrest of dune movement at the GKSD is due especially to the combined influences of long-lived, wind-shielding niveo-æolian deposits, the seasonally frozen active layer, warm-season rains, a regional aquifer beneath interdunes and perched liquid water within the dune uplands [1, 2].

The high-latitude, cold-climate GKSD are an excellent U.S.-based terrestrial analog for cold-season study of the hydrocryologic controls on high-latitude niveo-æolian transport. It is important for in-depth investigations of the GKSD to continue while the arctic analogy is still defensible, given the anticipated effects of a warming climate on the permafrost of this region. This arctic analog site may provide less beneficial information in future decades than it can today.

References: [1] Dinwiddie C. L. et al. (2011) *XXXXII LPS*, Abstract 2501. [2] Dinwiddie C. L. et al. (2011) *5th Mars Polar Sci Conf*, Abstract 6035. [3] Dinwiddie C. L. et al. (2010) *2nd International Planetary Dunes Wkshp*, Abstract 2029. [4] Dinwiddie C. L. et al. (2012) *3rd International Planetary Dunes Wkshp*, this volume. [5] Necsoiu M. et al. (2009) *Remote Sens Environ*, *113*, 2441–2447. [6] Koster E. A. and Galloway J. P. (1984) *4th International Conf Permafrost*, National Academy Press, Washington, D.C., 323. [7] Bristow C. S. et al. (2010) *Earth Planet Sci Lett, 289,* 30–42. [8] Fryberger S. G. et al. (1988) *Sedimentol, 35,* 21–41. [9] Bagnold R. A. (1941) *The physics of blown sand and desert dunes*. Dover, Mineola, NY. [10] Shur Y. et al. (2005) *Permafrost Periglac Process, 16,* 5–17. [11] Dijkmans J. W. A. et al. (1986) *Arctic Alpine Res, 18,* 377–387. [12] Faraday M. (1860) *Proceedings of the Royal Society of London, 10,* 440–450. [13] Fairchild I. J. et al. (2004) Chapter 13 in *Earth's Glacial Record*. Cambridge University Press, Cambridge. [14] Cerling T. E. (1984) *Earth Planet Sci Lett, 71,* 229–240. [15] Vogt T. and Corte A. E. (1996) *Sedimentol, 43,* 53–64. [16] Sharp M. et al. (1990) *Arctic Alpine Res, 22,* 141–152. [17] Killawee J. A. et al. (1998) *Geochimica et Cosmochimica Acta, 62,* 3637–3655. [18] van Vliet-Lanoë B. (1988) *J Quat Sci, 3,* 85–96. [19] Kocurek G. and Havholm K. G. (1993) *Siciliclastic Sequence Stratigraphy*, AAPG Mem, 58, 393–409. [20] Ferrians O. J. (1965) *Permafrost map of Alaska.* USGS Misc. Geologic Investigations Map I-445. [21] Jorgenson T. et al. (2008) *9th International Conf Permafrost*, 121–122. [22] Gruber S. (2012) *The Cryosphere*, *6*, 221–233.

Acknowledgements: NASA Mars Fundamental Research grant NNX08AN65G funded this work. Any opinions, findings, and conclusions or recommendations expressed are those of the authors and do not necessarily reflect the views of NASA. The authors thank S. Kantner for invaluable field knowledge and D. M. Hooper for data collection assistance, C. Wood for use of his private allotment, J. Kincaid and A. Williams for logistical support, and the National Park Service for research permit KOVA-2010-SCI-0001.

ENVIRONMENTAL CONDITIONS AND METEOROLOGIC CONTEXT FOR MODIFICATION OF THE GREAT KOBUK SAND DUNES, NORTHWESTERN ALASKA.

C. L. Dinwiddie,[1] T. I. Michaels,[2] D. M. Hooper,[1] and D. E. Stillman[2] [1]Geosciences and Engineering Division, Southwest Research Institute®, 6220 Culebra Road, San Antonio, TX 78238, [2]Space Science and Engineering Division, Southwest Research Institute, 1050 Walnut Street, Suite 300, Boulder, CO 80302

Introduction: We are studying meteorologic and niveo-æolian controls on cold-climate sand mobility, transport, and geomorphology at the Great Kobuk Sand Dunes (GKSD) in Alaska [1–5] as potentially analogous to those occurring on high-latitude Martian dunes [2–5 and references therein]. Here we summarize longer-term average meteorologic forcings near the GKSD that are relevant to dunefield modification, and document selected local *in situ* meteorologic data collected in March 2010. In so doing, we estimate the threshold wind speed and demonstrate that debris flow and gully formation on the GKSD, which we observed in the field [5], *does not* require mean daily surface temperatures above or even near the melting point of water.

Setting: The 62 km^2 GKSD lie ~50 km north of the Arctic Circle and ~160 km inland from Kotzebue Sound within an east–west basin between the Baird and Waring Mountains {Fig. 1 in [4]}. The Waring Mountains are a topographic trap against which dunes climb at the southwestern margin of the field. Many of the dunes migrate west-northwest; we estimated that migration rates fall within the narrow range of 0.5 to 1.5 m/yr [1], which is relatively slow for dunes on Earth. Dune forms include transverse, barchanoid, longitudinal, and star, among others, and range in elevation from 30 to 175 m amsl. The GKSD and surrounding land are vulnerable to accelerating permafrost degradation because the continuous permafrost zone boundary that lies nearby [6–8] is migrating northward in response to a warming climate.

Longer-term climate data: A relatively continuous, ~18-yr time series from the Kavet Creek Remote Automated Weather Station (RAWS; located at 72 m amsl and 3.6 to 19 km from the northwestern and southeastern margins of the dune field) provides relatively long-term meteorologic data {**Fig. 1**; [9]}. The GKSD experience long cold winters and brief warm summers; mean annual air temperature is –4°C [**Fig. 1(A)**]. Mean daily air temperature falls to 0°C near the end of September, after nighttime ground frost has returned. Mean daily maximum air temperature falls to 0°C ~2 weeks later, after which air temperature remains below freezing for the season. Mean daily air temperature rises to 0°C near the end of April, after daytime ground thawing has begun. RAWS-measured mean annual precipitation [**Fig. 1(B)**] is 67% of the PRISM model's estimate [10] at this location; the difference is attributed to snow water equivalent. Snow

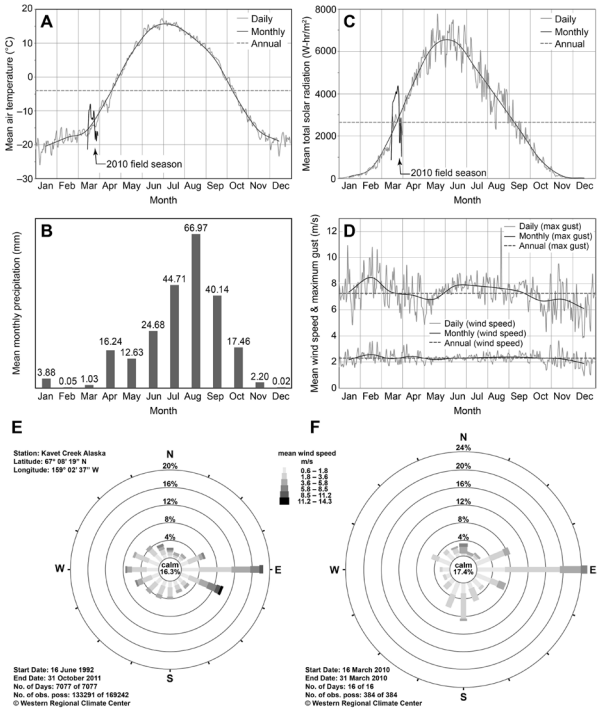

Fig. 1. *Kavet Creek RAWS climate data.* ***(A)*** *Mean daily, monthly, and annual air temperature.* ***(B)*** *Mean monthly precipitation.* ***(C)*** *Mean total solar radiation.* ***(D)*** *Mean daily, monthly, and annual wind speed.* ***(E)*** *Mean annual wind rose.* ***(F)*** *Mean wind rose during March 2010 fieldwork. Data credit [9].*

partially to fully blankets the dunes for ~70% of the year; rainfall peaks in August.

The strongest daily mean winds are out of the east-southeast from November to April, and average-to-intermediate-strength winds are frequently out of the west from May to July. A mixed wind regime occurs during the transitional months of August–October. Wind speed variance appears to be correlated with solar radiation [**Fig. 1(C, D)**]; winds are often light and variable during the sunless days of winter, and wind speed variance is lowest during the 38 days of constant summer daylight. The wind regime (measured at 6.1 m AGL) is bimodal at the macroscale [**Fig. 1(E)**], where the dominant, sand-transporting winds are polar easterlies from November to April (despite snowcover), and a brief westerly wind reversal coincides with summer transport-dampening rains. Active dune migration likely is limited, therefore, to the windy months of early autumn and late winter to early spring. Mean annual maximum wind gust speed is 7.3 ± 1.1 m/s, with gusts up to 40 m/s in the record.

All months except solsticial June and December experience strong but relatively infrequent northerly winds. Significant day-to-day variations in wind direction and strength are commonplace at all seasons due to the quasi-cyclic modulations induced by baroclinic storm systems.

***In situ* environmental data:** We deployed a portable, multilevel meteorological station to three locations {Wx1, Wx2, and Wx3 [4, their Fig. 2 inset]} during our field campaign. This customized system provides the types of boundary layer atmospheric flux data that are needed to assess æolian erosion potential. We measured 2D (horizontal) mean wind velocity, air temperature, barometric pressure, and relative humidity at 10 sec intervals at 50, 100, and 200 cm AGL, as well as mean net solar radiative flux at 2 min intervals. We also measured ground temperatures at 0, 5, 10, 20, 50 and 100 cm BGL at 2 min intervals, and the number of particle impacts on and kinetic energy imparted to an erosion sensor per 10 sec interval.

Resulting data streams (e.g., **Figs. 2, 3**) are useful for characterizing microclimates, identifying subgrid-scale processes that influence æolian transport, and supporting atmospheric modeling (to be demonstrated at the workshop) by providing a measure of whether the nested numerical models capture important processes. Additionally, particle flux data demonstrate sand saltation above snow-free crests (Wx2 and Wx3 locations) and suggest a saltation threshold (**Fig. 2**).

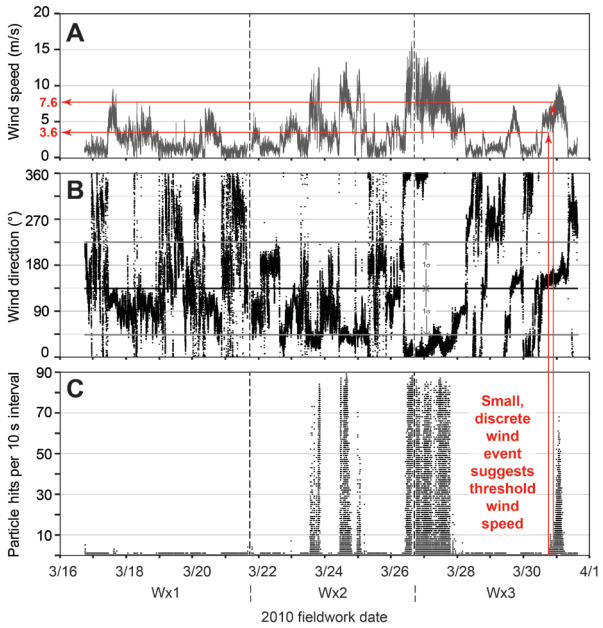

Fig. 2. In situ *wind and particle flux data from snow-covered station Wx1 and snowfree stations Wx2 and Wx3.* ***(A)*** *10-sec mean wind speed at 2m.* ***(B)*** *10-sec mean wind direction; overall mean azimuth and standard deviation.* ***(C)*** *Particle hits per 10-sec interval. A small, 2.44 hr-long wind event on 30 March had a mean and standard deviation of 5.7 ± 0.7 m/s and caused 504 impacts.*

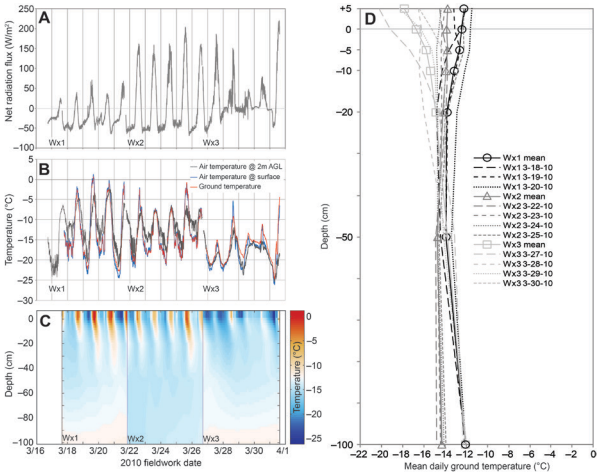

Fig. 3. In situ *environmental data.* ***(A)*** *Net radiative flux.* ***(B)*** *Air and ground surface temperatures.* ***(C)*** *Air, surface, and subsurface ground temperatures to 1 m depth.* ***(D)*** *Mean daily air, surface, and subsurface ground temperatures to 1 m depth.*

Debris flow observations: Fresh debris flows and gullies on lee slopes were photographed on 25 and 30 March [5] when the mean daily surface temperature was never greater than −12.3ºC; [**Fig. 3(C, D)**]. Surface temperatures such as these are either colder than or else comparable to austral Antarctic summer temperatures when æolian Mars-analog field expeditions to that continent are most common.

Conclusions: Meteorologic datasets help elucidate the processes that maintain and sculpt dunefields. The high-latitude, cold-climate GKSD are an excellent U.S.-based Mars analog for cold-season study of dune gully and debris flow processes [5], as well as for study of hydrocryologic controls on high-latitude æolian transport [e.g., 3, 4]. It is important for in-depth investigations of the GKSD to continue in the near-term, while the arctic analogy is still defensible.

References: [1] Necsoiu, M. et al. (2009) *Remote Sens Environ*, *113*, 2441–2447. [2] Dinwiddie, C. L. et al. (2010) *2nd International Planetary Dunes Workshop*, Abstract 2029. [3] Dinwiddie, C. L. et al. (2011) *5th Mars Polar Science Conference*, Abstract 6035. [4] Dinwiddie, C. L. et al. (2011) *XXXXII LPS*, Abstract 2501. [5] Hooper, D. M. et al. (2012) *XXXXIII LPS*, Abstract 2040. [6] Ferrians, O. J. (1965) *Permafrost map of Alaska.* USGS Misc. Geologic Investigations Map I-445. [7] Jorgenson, T. et al. (2008) *9th International Conference on Permafrost*, 121–122. [8] Gruber, S. (2012) *The Cryosphere*, *6*, 221–233. [9] WRCC (2011) *Kavet Creek Alaska (RAWS)*. Western Regional Climate Center, Reno, Nevada. [10] Gibson, W. (2009) *Mean Precipitation for Alaska 1971–2000.* National Park Service, Alaska Regional Office GIS Team. Geospatial Dataset 2170508.

Acknowledgements: This research was funded by SwRI® IR&D grant 20.R8136 and NASA MFR grant NNX08AN65G, and was subject to U.S. NPS research permit KOVA-2010-SCI-0001. We are grateful to have been provided: data support by S. Stothoff; field support by S. Kantner, R. McGinnis and K. Bjella; logistical support by J. Kincaid; and a private allotment belonging to C. Wood.

Interactions between subaqueous and aeolian sedimentary systems

Amy E. Draut* and David M. Rubin
U.S. Geological Survey, 400 Natural Bridges Drive, Santa Cruz, CA 95060
*Corresponding author: adraut@usgs.gov

Interaction between subaqueous and aeolian sedimentary systems occurs widely on Earth's surface, spanning spatial and temporal scales that vary according to global and regional climate, among other factors, and are evident from both modern and ancient settings. The best-studied examples of such connectivity are arguably those from coastal regions, where beach conditions affect sediment supply to aeolian dunes, and from desert playas and dry lake beds that act as aeolian dust sources. Aeolian deposits also can form as wind reworks sediment from alluvial fans and crevasse-splay deposits at river-mouth deltas. Fluvial–aeolian sediment interactions play an important role in many arid and semiarid regions worldwide, though links between rivers and aeolian dunes have received somewhat less attention in scientific literature. Rivers in arid and semiarid lands commonly serve as sources and sinks of aeolian sediment, but because aeolian and fluvial processes traditionally have been studied separately, relatively little is known about their interaction and controlling factors. On Earth, coupling between fluvial sediment supply and aeolian sediment reworking also can affect dryland ecosystems. This presentation will highlight various examples of subaqueous-aeolian sediment interaction on Earth. The author seeks input and discussion on possible analogous linked sedimentary and geomorphic processes from elsewhere in the solar system, with the view that similar sediment-transport connectivity could be important in other settings to a greater degree than has yet been recognized.

RECONSTRUCTION OF EOLIAN BEDFORMS AND PALEOCURRENTS AT MERIDIANI PLANUM, MARS. L. A. Edgar[1], [1]California Institute of Technology, Pasadena, CA (ledgar@caltech.edu).

Introduction: Over the past eight years, the Mars Exploration Rover *Opportunity* has investigated several impact craters at Meridiani Planum, studying the exposed sedimentary rocks in an effort to better understand the role of aqueous and atmospheric activity in its geologic history. Bedrock exposures at Eagle, Endurance, and Erebus craters reveal a complex sedimentary history, involving eolian sediment transport and deposition, followed by episodic inundation by shallow surface water, evaporation, exposure, and desiccation [1-4]. Bedrock outcrops exposed at Eagle and Endurance craters make up the Burns formation, represented by eolian dune, sand sheet, and interdune facies. The strata exposed at Eagle and Endurace craters is interpreted to represent a progressive increase in the influence of groundwater and surface water during deposition [2]. This wetting-upward trend contrasts with the overall drying-upward trend as seen at Erebus crater, at a slightly higher stratigraphic level [4]. This series of outcrops may comprise a full climatic cycle, from dry to wet to dry conditions, as one moves stratigraphically upward from the strata at Eagle crater through the strata at Erebus crater [4].

After completing its exploration at Erebus crater, *Opportunity* explored much larger bedrock outcrops at Victoria crater. It became clear that both depositional and diagenetic processes acted regionally in extent [5] and that most primary sedimentary bedforms are also of very large magnitude. This is important because it facilitates a greater understanding of the processes controlling deposition as well as the scale of the depositional environment. The work described here focuses on the reconstruction of eolian bedforms and paleocurrents from large-scale outcrops at Victoria crater, and an extended understanding of the climatic history at Meridiani Planum.

Geologic Setting: Victoria crater lies 6 km southeast from the original *Opportunity* landing site in Eagle crater. The plains surrounding Victoria crater are ~10 m higher in elevation than those surrounding previously explored Endurance crater, suggesting that Victoria crater exposes a stratigraphically higher section (assuming flat dip of strata). The outcrop exposed at Victoria crater may lie at the same elevation as the uppermost unit in Erebus crater, allowing for possible stratigraphic correlation between these two locations. Victoria crater has a scalloped rim produced by erosion and downhill movement of crater wall material, which results in a series of alcoves and promontories exposing more than 10 m of well-bedded sedimentary rocks.

Prior to ingress, *Opportunity* spent several months traversing the rim of the crater. Observations of outcrops at several promontories reveal large-scale cross-stratification with bedsets of at least several meters in thickness [5]. Analysis of cross-bedding geometries indicates reversing paleowind directions oriented in a dominantly north–south direction [6]. Detailed measurements of the stratigraphy were taken by the Panoramic Camera (Pancam) and Microscopic Imager (MI) as *Opportunity* descended into the crater at Duck Bay.

Stratigraphy at Duck Bay and Cape Verde: *Opportunity's* ingress path in Duck Bay intersects three stratigraphic units, named Lyell, Smith and Steno, in ascending stratigraphic order. The units consist of sulfate-rich cross-bedded sandstone, interpreted as fossil eolian dunes. Smith is a light-toned band that lines much of the upper rim of the crater. Smith is interpreted as a diagenetic band, exhibiting a lighter tone and poor expression of lamination consistent with recrystallization. Evidence of the diagenetic unit reworked in the impact breccia indicates that Smith formed prior to the crater impact. The contact between Smith and Lyell is gradational, and the darker tone and well-defined stratification of Lyell gradually fade upward. A clear erosional contact distinguishes Smith from the overlying Steno unit. Strike and dip measurements suggest that this truncation surface between Steno and Smith has a dip of ~10^{o} to the southeast [7]. Bedding measured within Lyell dips to the southwest, while bedding measured within Steno dips to the southeast. These units define the "Reference Section" for Victoria crater. They can be traced visibly around much of Duck Bay, but cannot be directly correlated with the nearest promontory, Cape Verde, which is separated by a large area of breccia.

After completing observations of the Duck Bay strata, *Opportunity* made a close approach to the outcrop at Cape Verde. Cape Verde exposes a light-toned band overprinting well-laminated sandstone with low-angle cross-bedding. In some places, small climbing ripples are super-imposed on the larger dune cross-stratification. The base of the Cape Verde cliff face contains a truncation surface dipping ~10^{o} to the southeast. It is inferred that the erosional contact at the base of Steno correlates with the erosional surface at the base of Cape Verde. Although these surfaces lie at different elevations, they have a similar 10^{o} dip into

the crater and projection of this dip shows the potential continuity of the surface between elevations. This surface indicates deposition at the same time between locations, but on pre-existing topography, and represents an architectural element larger than the scale of the cross-bedding [7].

Reconstruction of Eolian Bedforms: The erosional surface exposed in the ingress path and at Cape Verde may be interpreted as a bounding surface produced by migration of dunes on a larger bedform (cf., [8]). The compound bedform (smaller dunes migrating over a larger dune) may be termed a draa. Consideration of cross-bedding geometry produces additional insight. Strata below the erosional surface, both at Duck Bay and at Cape Verde, dip to the southwest, while the strata above the surface dip to the southeast. This leads to two possible interpretations. The different dip directions may be interpreted as remnants of three-dimensional sinuous crested dunes migrating southward. Trough cross-bedding produced by three-dimensional sinuous crested dunes is observed at nearby promontory Cape St. Mary, although the scale of the bedsets is much smaller [6].

Alternatively, the different dip directions could be indicative of different dune-migration directions, from which paleo-wind directions may be inferred. This interpretation is consistent with observations of terrestrial draas, which may contain reactivation surfaces representing the migration of dunes across a draa in different directions [9]. Detailed paleocurrent analysis indicates that a pattern of reversing transport direction is observed at other locations around Victoria crater, and also with juxtaposition of cross-bedsets across larger-scale surfaces [6]. Furthermore, bedform modeling [10] of these inferred conditions produces results that match the stratal geometries observed at Duck Bay and Cape Verde.

Given the available data, we are unable to distinguish between these two hypotheses, but both scenarios suggest paleowind directions from north to south. In the case of a large bedform with superimposed bedforms that reverse migration direction, the orientation of the erosional surface (rather than the cross-strata above the surface) may serve as a better indicator of the local orientation of the bedform surface when it was formed. The erosional surface at Duck Bay and Cape Verde is important in that it exposes a larger-scale bedform than had previously been seen at Meridiani Planum. If it represents the migration of dunes across a draa, then three orders of bedforms are observed: ripples, dunes, and draas. Draas are typical of modern ergs (sand seas), often occurring in the centers of well-developed ergs, where sand cover is thickest [11-12].

Conclusions: The strata exposed at Duck Bay and Cape Verde indicate deposition in an eolian dune environment, with further modifications though diagenesis. Correlation between Duck Bay and Cape Verde reveals an erosional surface that is interpreted to represent the migration of dunes across a draa, and its orientation indicates that the draa was migrating from northwest to southeast at the time that the surface was formed. The stratal geometry above and below the erosional surface indicates dune migration in opposing directions or by southward migrating three-dimensional bedforms. Additionally, the presence of three orders of bedforms and a complex wind regime indicates that the strata may have been part of a large sand sea, with no evidence for aqueous deposition, as observed at Eagle and Endurance craters. Victoria crater not only reveals the regional extent of processes seen elsewhere in Meridiani Planum, but the greater size of its outcrop exposures reveals the building of ever-larger eolian bedforms.

References: [1] Squyres S. W. et al. (2004) *Science*, *306*, 1709–1714. [2] Grotzinger J. P. et al. (2005) *EPSL*, *240*, 11-72. [3] Grotzinger J. P. et al. (2006) *Geology*, *34*, 1085-1088. [4] Metz J. M. et al. (2009) *JSR*, *79*, 247-264. [5] Squyres S. W. et al. (2009) *Science*, *324*, 1058-1061. [6] Hayes A. G. et al. (2011) *JGR*, *116*, 2010JE003688. [7] Edgar L. A. et al. (2010) *LPS LXXII* Abstract #2626. [8] Fryberger S. G. (1993) *GSL Special Publications*, *73*, 167–197. [9] McKee E. D. (1966) *Sedimentology*, *7*, 1–61. [10] Rubin D. M. and Carter C. L. (2005) *USGS Open-File Report* 2005–1272. [11] Wilson I. G. (1971) *Geographical Journal*, *137*, 180–199. [12] Havholm K. G. and Kocurek G. (1988) *Sedimentology*, *35*, 649–669.

Source-To-Sink: Comparison of Boundary Conditions for Planetary Aeolian Systems R.C. Ewing
[1] University of Alabama, Department of Geological Sciences, Box 870338, Tuscaloosa, AL 35487, rcewing@ua.edu

Introduction: Aeolian sand dunes figure prominently into the landscapes of Earth, Mars, and Titan and have been recognized on the surface of Venus [1,2,3,4]. Sedimentary deposits interpreted as aeolian in origin are found in the rock records of Earth and Mars[]. The widspread occurance of aeolian dunes on these worlds and within their deep-time depositional records suggests that aeolian systems are and likely have been a default depositional environment for the Solar System.

This presentation explores the hypothesis that boundary conditions specific to each world create differences in the production, transport, accumulation and preservation of aeolian sediment, but dunes and dunefield patterns remain largely similar [5]. This hypothesis is cast within an aeolian sediment source-to-sink framework with examples from Earth and Mars and questions and tentative expectations for Pluto and worlds with tenuous atmospheres.

References: [1] Kocurek (1999) *Aeolian Env. and Landforms, Eds. A.S. Goudie, I Livingston and S. Stokes*. [2] Hayward et al. (2007) *JGR, 112, E11007* [3] Lorenz et al. (2006) *Science, 312, 724* [4] Greeley et al. (1992) *JGR 97(E8), 13,319-13,345.* [5] Kocurek and Ewing (2012), SEPM Special Publication 11.

RECONSTRUCTING THE FORMATIVE WINDS OF A DUNE FIELD IN GANGES CHASMA, MARS, BY BOOTSTRAPPING WITH THE RULE OF MAXIMUM GROSS BEDFORM-NORMAL TRANSPORT.

L. K. Fenton[1] and R. A. Beyer[1,2], [1]Carl Sagan Center at the SETI Institute, 189 Bernardo Ave, Mountain View, CA, 94043, USA, (lfenton@carlsagancenter.org), [2]NASA Ames Research Center, Moffett Field, CA 94035, USA.

Introduction: The widespread presence of bedforms on the surface of Mars holds a largely untapped potential for reconstructing their formative wind regimes, which are critical for understanding patterns of sediment transport and climate change. We quantitatively apply the concept of maximum gross bedform-normal transport (MGBNT) in a dune field in Ganges Chasma on Mars, showing that dune morphology reveals winds not easily distinguishable without use of this approach.

Bootstrapping with the Rule of Maximum Gross Bedform-Normal Transport: Experimental studies have shown that the orientation of a bedform is aligned as transverse as possible to all incident, sediment-bearing flows [1, 2]. Mathematically, the gross bedform-normal transport T across any potential bedform trend can be represented as the sum of N transport vectors Q_i (e.g., measured sand fluxes) projected onto the gross bedform-normal transport:

$$T = \sum_{i=1}^{N} Q_i \left|\sin\alpha_i\right|$$

where α_i is the angle between each transport vector Q_i and the bedform trend. The bedform will develop so that it is aligned orthogonal to the maximum gross bedform-normal transport T_m (see Fig. 1).

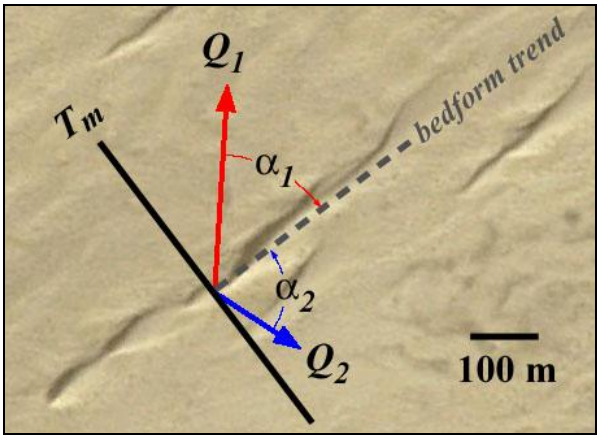

Figure 1. Bedforms are aligned orthogonal to the maximum gross bedform-normal transport, T_m.

The bedform trend is distinct from the resultant transport direction (i.e., the vector sum of all transport vectors Q_i), which may be orthogonal, parallel, or oblique to the bedform trend (resulting in transverse, longitudinal, and oblique dunes, respectively). In conditions in which the direction and relative strengths of incident sand-bearing winds are known, the rule of MGBNT allows prediction of bedform type and orientation.

However, there are few locations on Mars where the wind regime is known with enough accuracy to determine the local bedform morphology. On Mars, local winds may occasionally be inferred from unidirectional wind markers, such as yardangs and wind streaks. Using MGBNT, the relative sand transport capacity of such winds can be determined by comparison with dune crestline orientation (i.e., the relative magnitude of the transport vectors Q_i can be determined by calculating the set of angles α_i that produce the maximum gross bedform-normal transport T_m).

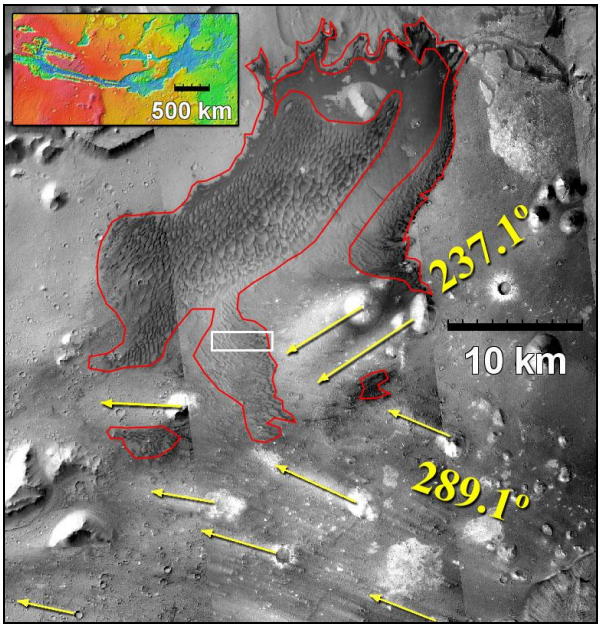

Figure 2. A dune field in Ganges Chasma, showing with two sets of wind streaks formed from sand-transporting winds. The white box shows the location of Fig. 3.

If nearby dunes appear to be shaped by a more complex wind regime than that implied by unidirectional wind markers, then it is possible to constrain the formative wind regime using a process here termed "reverse-MGBNT". In this case, the concept of MGBNT is used to determine the possible range of incident winds that would combine with known winds to produce the observed dune crestlines (i.e., possible transport vectors Q_i are identified by their capacity to produce the observed bedform trend). The solution is nonunique, but the wind regime can often be con-

strained by dune morphology. By assuming that such identified winds are now "known", one can reapply them elsewhere in the same dune field with the rule of MGBNT in a bootstrapping process.

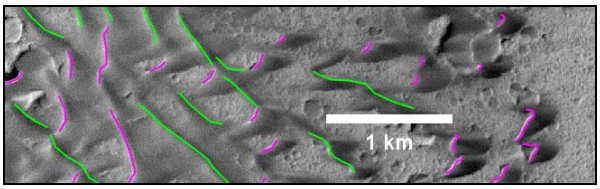

Figure 3. A portion of the dune field from Fig. 2, showing two sets of crestlines: barchanoid dunes in magenta and oblique or linear dunes in green.

Example in Ganges Chasma: Figure 2 shows the largest dune field on the floor of Ganges Chasma, which is one of several large canyons in Valles Marineris (see inset). The dune field spans 305 km^2, with its main body extending NE-SW, parallel to the local chasma wall. Hundreds of wind streaks, yardangs, wind scours, and barchans in the chasma indicate that the net sand transport is towards the west, parallel to the walls [3]. In the region of the dune field, there are two sets of wind streaks: a prominent set flowing WNW (289.1º) and a less distinct set flowing SW (237.1º). Figure 3 shows a small portion of the southeast edge of the dune field, with two sets of dune crestlines outlined (a total of eight different sets, not shown, were identified in the dune field). Each set of dune crestlines was produced by a different combination of transport winds (Q_i).

Magenta crestlines. Magenta crestlines outline a population of barchans, barchanoid, and transverse dunes in the southeastern portion of the dune field. Because of their morphology, it is likely that they were formed by winds with strong easterly components, so we use MGBNT to determine if the two wind-streak-forming winds could have produced these dunes, and in what proportion.

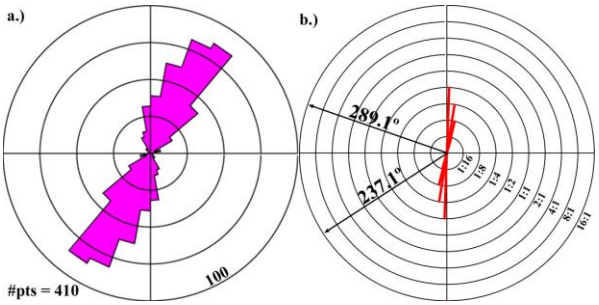

Figure 4. a.) A histogram of the mean orientations of magenta crestlines and b.) matching MGBNT crestlines produced by the two wind-streak-forming winds. Circles indicate varying relative strengths of the two winds (ratios are shown as 237.1º:289.1º).

Figure 4a shows a histogram of the magenta crestlines, which have a strong mode oriented NE-SW. The two wind-streak-forming winds, Q_1 and Q_2 in this example, combine to produce transverse dunes that best align with the magenta crestlines when the WNW-flowing wind (289.1º) dominates by at least a factor of two (with ratios of 1:2, 1:4, 1:8, and 1:16 in Fig. 4b).

Green crestlines: Green crestlines correspond to dunes that appear to be either oblique or longitudinal, with net transport towards the northwest. This is a case where reverse-GBNT can be used to constrain formative wind directions. It is possible that either or both of the two wind-streak-forming winds created these dunes, but at least one more sand-transporting wind must have contributed to produce the observed morphology. Building on the results from MGBNT analysis of the barchanoid dunes, we solve for all possible winds that could combine with the 289.1º winds to produce the green crestlines.

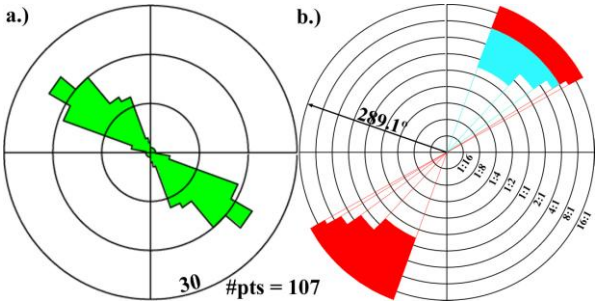

Figure 5. a.) A histogram of the mean orientations of green crestlines and b.) possible formative winds that produce the crestlines (red = transverse, blue = oblique).

Figure 5a shows a histogram of the green crestlines. Figure 5b shows possible combinations of winds that, together with the WNW-flowing wind, produce crestlines that align with those of Fig. 5a. Winds blowing to the SW (lower left quadrant) may be ruled out because dune morphology indicates a net transport towards the NW, which would not be the case if SW-flowing winds dominated dune formation. Assuming that only two winds form these dunes (likely an oversimplification), and that they are oblique, reverse-MGBNT indicates that they were formed by winds blowing toward the NE, with a transport magnitude 2-8 times that of the WNW-flowing wind streak winds.

Conclusions: In the absence of meteorological data, the principle of gross bedform-normal transport can be used to analyze dune fields remotely to determine the primary dune-building winds. Two sets of dune crests in a dune field in Ganges Chasma indicate formative winds blowing towards the WNW and NE, producing both barchanoid and oblique dunes.

References: [1] Rubin D. M. and Hunter R. E. (1987) *Science*, *237*, 276-278. [2] Rubin, D. M. and Ikeda H. (1990) *Sedimentology*, *37*, 673-684. [3] Fenton L. K. et al. (2012) *LPS XLIII*, Abstract #2441.

HiRISE OBSERVATIONS OF SAND DUNE MOTION ON MARS: EMERGING GLOBAL TRENDS. P. E. Geissler[1], M. E. Banks[2], N. T. Bridges[3], S. Silvestro[4] and the HiRISE Science Team, [1]US Geological Survey, Flagstaff AZ 86001 USA (pgeissler@usgs.gov), [2]Center for Earth and Planetary Studies, Smithsonian Air and Space Museum, Washington, DC 20013, USA, [3]Johns Hopkins University, Applied Physics Laboratory, 11100 Johns Hopkins Road, Laurel, Maryland 20723, USA, [4]Carl Sagan Center, SETI Institute, 189 N. Bernardo Avenue, Suite 100 Mountain View, CA, 94043, USA.

Introduction: Little was known about the extent and magnitude of sand dune motion on Mars prior to the arrival of Mars Reconnaissance Orbiter (MRO). Several searches for dune motion based on prior mission data had been carried out with negative results [1-3], and only one detection of dune disappearance was achieved [4], leaving the observational lower limit for planet-wide sand flux near zero. Repeated imaging observations at resolutions up to 25 cm/pixel by the HiRISE camera on MRO have now documented sand dune movement in several locations [5-8]. Other pairs of repeated HiRISE sand dune observations have failed to show any evidence of changes. Definitive detection or non-detection of sand dune motion requires repeated imaging under similar illumination conditions at intervals of 1 or more martian years, and has been achieved so far in only a limited number of locations. Although the total number of repeated observations of sand dunes is still small, we can begin to draw inferences about the global distribution of shifting sand dunes, at the peril of the vagaries of the statistics of small numbers.

Geographic Distribution: Figure 1 shows a map of the best documented detections and non-detections of sand dune movement on Mars to date. This map clearly indicates that the observations available are still very sparse. Only 40 definitive detections of sand dune movement have so far been made, out of a total of just 64 qualifying image pairs. Coverage remains uneven in both latitude and longitude. Note for example that there are no detections or non-detections in the latitude range from 30 to 65 degrees north. Many of these targets were deliberately chosen because of the ease of visibility of any changes, for example among dark sand dunes overlying bright dust or bedrock substrates. The data omit observations of transverse aeolian ridges (TARs), which are morphologically distinct from sand dunes and have not been observed to change.

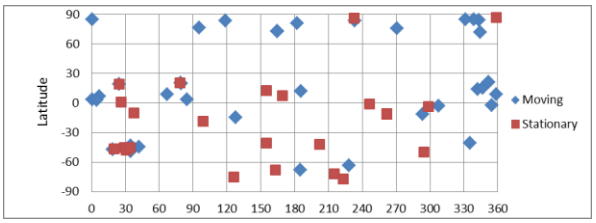

Figure 1: Spatial distribution of dune movement detections (blue) and non-detections (red).

Latitudinal Distribution. Figure 2 shows the observations summed by latitude, represented as the fraction of observations demonstrating dune movement in each latitude bin. Also shown on this chart is the latitudinal distribution of the occurrence of sand dunes in each bin, expressed as a fraction of the total areal coverage of dunes, taken from the Mars Global Digital Dune Database statistics provided by the Mars-Dunes.org Consortium [9]. Although sand dunes in general are strongly concentrated in the southern highlands, the preliminary figures suggest that detections of dune motion tend to be most common at equatorial latitudes (and northern polar latitudes, of course).

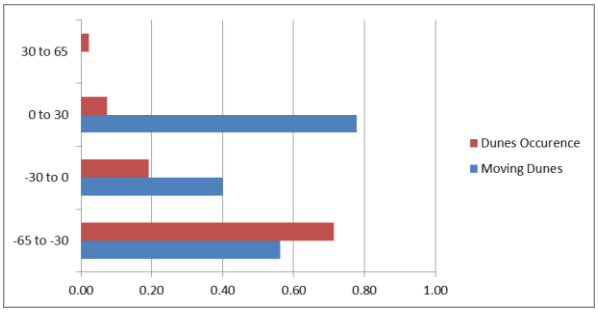

Figure 2. Latitudinal distribution of the fraction of dunes in motion (blue) vs. areal coverage of dunes (red).

Elevation Distribution. Figure 3 breaks the observations down by elevation, expressed as km above the 6 mbar datum. These preliminary numbers suggest that dune motion detections are more prevalent at lower elevations, while non-detections are more prevalent at higher elevations.

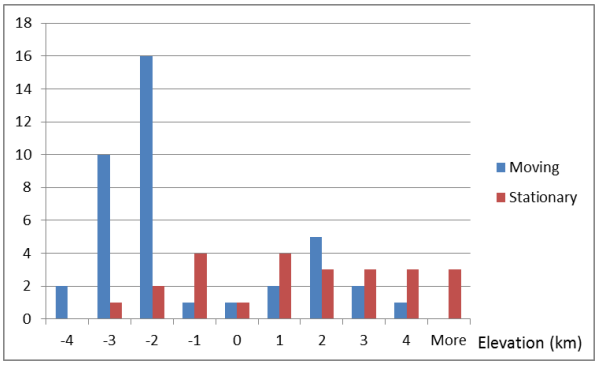

Figure 3. Elevation distribution of dune motion detections (blue) vs. non-detections (red).

Displacement Rates and Sand Fluxes: Various HiRISE observations have documented erosion and deposition of sand patches, movement of small ripples on the backs of sand dunes, and advances of the slip faces of individual barchans. Rates of ripple movement are best established, and range from 0.2 to 1.2 m per Earth year. Slip faces in Meridiani Planum have been observed to advance up to 0.25 m per Earth year [10]. The best documented dune field is in Nili Patera, where a series of HiRISE images has monitored sand motion at frequent intervals over a period of over 2 martian years. These images demonstrate frequent avalanches cascading down the slip faces of active dunes, and show the gradual advance of the slip faces as they are overtaken by the faster ripples. A digital elevation model constrains the volumetric changes in the Nili Patera dune fields [11]. Using this model together with terrestrial analogies, estimates can be made of the sand flux needed to produce the observed changes [12]. The results suggest sand fluxes on order of several cubic meters per meter per year, similar to sand fluxes in Victoria Valley, Antarctica [ibid.].

Discussion: That martian sands were mobile was long suspected for a variety of reasons, including the fresh appearance of the dunes and the lack of impact craters on their surfaces. However, HiRISE is the first experiment to quantify the extent and magnitude of sand dune motion on the planet, beyond giving an upper limit. The results suggest ubiquitous sand movement on Mars, from the equator to sub-polar latitudes, and sand fluxes comparable to terrestrial dune fields. These findings impact our understanding of landscape modification under current climatic conditions, and generate new questions concerning the modern day sources of martian sands.

Our analysis of the dune motion survey to date suggests that the more active dunes away from the north pole are found at low elevations near the equator of Mars. We speculate that the sands are more easily moved by the denser atmosphere at lower elevations, and by the strong seasonal winds crossing the equator. Continued monitoring of martian dune fields by HiRISE will decide whether these suggestions of global trends are sustained.

References: [1] Zimbelman, J. R. (2000) *GRL*, doi:10.1029/1999GL008399. [2] Malin, M. C., and Edgett, K.S. (2001), *JGR*, doi:10.1029/2000JE001455. [3] Williams, K. K. (2006), *LPSC* 37, Abstract #2322. [4] Bourke, M.C., et al. (2008), *Geomorphology*, doi:10.1016/j.geomorph.2007.05.012. [5] Silvestro, S., et al. (2010) *GRL*, doi:10.1029/2010GL044743. [6] Chojnacki, M., et al. *JGR*, doi:10.1029/2010JE003675. [7] Hansen, C.J., et al. (2011), *Science*, doi:10.1126/science.1197636. [8] Bridges, N.T. et al., *Geology*, doi:10.1130/G32373.1. [9] Hayward, R. et al. (2007), *JGR*, doi:10.1029/2007JE002943. [10] Geissler, P. et al. (2011) *LPSC* 42, abstract # 2537. [11] Mattson, S. et al., this meeting. [12] Bridges, N. T. (2012) *LPSC* 43, abstract #1322.

DETERMINING TIMESCALES OF THE DUNE FORMING WINDS ON TITAN.

A. G. Hayes[1], R. C. Ewing[2], A. Lucas[3], C. McCormick[2], S. Troy[2], and C. Ballard[1]. [1]Department of Earth and Planetary Sciences, University of California, Berkeley CA [2] Department of Geologic Sciences, University of Alambama, Tuscaloosa AL [3] Division of Geological and Planetary Sciences, California Insitute of Technology, Pasadena CA.

Abstract: Titan's linear dunes are a unique and robust record of past and present climatic conditions. The timescales (seasonal vs. milankovich) and direction of the surface winds that generated the dunes are two important components of climate. This work addresses challenges and outstanding questions pertaining to these climate components. We use Cassini Synthetic Aperture Radar (SAR) data to examine the interactions between the dunes and their environment in order to test the hypothesis that dune on Titan maybe in equilibrium with longer term (Milankovich) cyclic variations in the wind regime.

It is difficult to **not** form a line in the sand when a fluid moves loose granular particles of any composition. This statement reflects the paradigm of nearly the last 30 years of aeolian research on the formation of laboratory-to-landscape scale bedforms, indicating that patterns will emerge from grain interactions and self-organization regardless of differences in the fundamental variables affecting sediment transport such as gravity, fluid density and particle composition (Anderson, 1990; Werner, 1999; Kocurek et al., 2010). What is surprising, however, is that the individual patterns characteristics (e.g., length and spacing) are also independent of these environmental parameters. Building off the work of Ewing and Kocurek (2010), our initial analysis shows that the fundamental pattern parameters of dune fields found on Earth, Mars, and Titan are remarkably self-similar over a wide range of scales (Figure 1). Furthermore, dune fields that are not in equilibrium with respect to wind regime, sediment supply and sediment availability have pattern variables that are distinct from those that are in equilibrium, providing a method of discovery of degraded dune patterns. These observations provide a basis for applying established pattern analysis methods and models from Earth-based studies (Werner and Kocurek, 1997; 1999; Ewing et al., 2006; Ewing and Kocurek, 2010) to studies of Titan.

Previous work on Titan's dunes has established that the dunes are well-organized with regularly spaced crestlines at ~2 km, crestline lengths of 50+ km, approximate east -west orientations and crest heights reaching ~100 m (Lorenz et al, 2006; Radebaugh et al, 2010). Global variability in dune width and spacing are correlated with both latitude and elevation (Savage, 2010; LeGall et al., 2011; 2012). Variation in dune morphology is apparent from barchanoid forms that coincide with a decrease in sediment availability (Radebaugh et al, 2010). Despite the large amount of geomorphic .

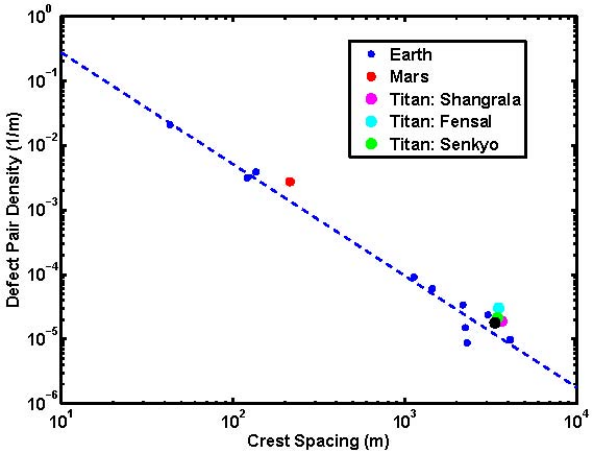

Figure 1: : Logarithmic plot of dune pattern vairables crest spacing vs. defect density on Earth, Mars and Titan. Defect density is the inverse of the average dune crest length. Note that the data points follow a similar power law relationship, irrespective of environmental conditions.

mapping done on Titan's dunes and the many successful contributions that have resulted from this work (e.g., Lorenz, 2006; Radebaugh, 2008; 2010), a mechanistically consistent explanation of the winds that generated dune field patterns is still missing. To date, interpretations of the dune forming surface winds on Titan have varied widely from unidirectional to obtuse bimodal (see review in Rubin and Hesp, 2009) and importantly, these cycling of these winds has been assumed to be seasonal. GCM studies find that seasonally varying westerly winds are meteorologically difficult to generate and the leading GCM-based hypothesis for the dune forming winds is that a tri-model wind regime, which has not yet been observed to generate linear bedforms (Rubin and Hunter 1987), may be responsible for the formation of Titan's dunes (Tokano et al. 2010). In summary, the current state of knowledge of the dune forming winds on Titan does not consider the possibility that Titan's dunes maybe in equilibrium with longer-term (Milankovich) cyclic variations in the wind regime.

In this work, we apply the crestline re-orientation model developed by Werner and Kocurek [Geology, 1997] to the equatorial dune fields of Titan. We use Cassini SAR images processed through a de-noising algorithm recently developed by Lucas et al. [LPSC,

2012] to measure variations in pattern parameters (crest spacing, crest length and defect density, which is the number of defect pairs per total crest length) both within and between Titan's dune fields to describe

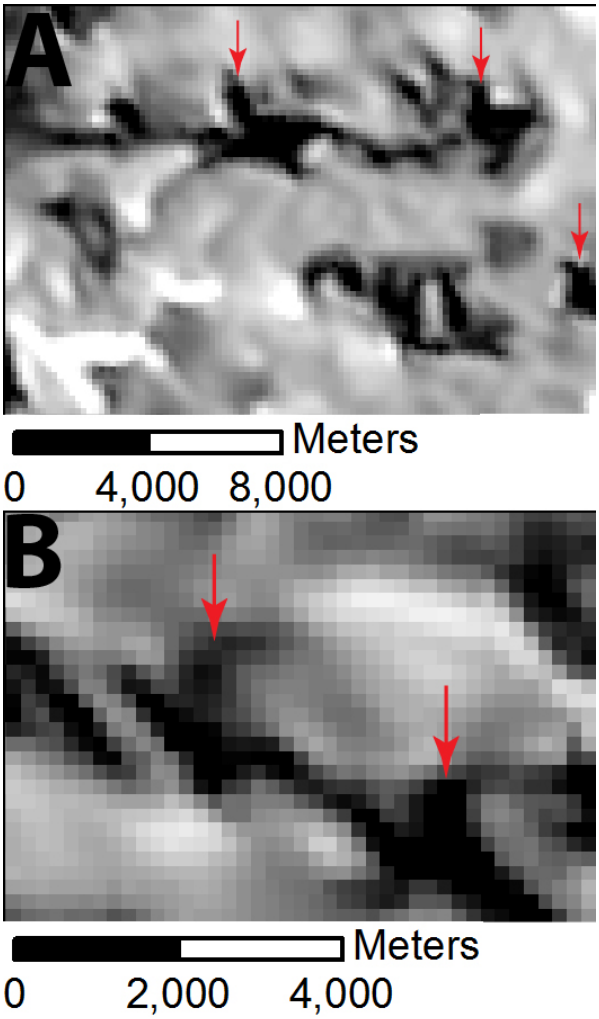

Figure 2: De-noised SAR image showing evidence for two distinct crestlines, incdicating a star dune morphology. Images have been de-noised by A. Lucas using the de-noising algorithm of Deladalle et al. 2009.

pattern maturity and identify areas where changes in dune orientation are likely to occur (or may already be occurring). Measured defect densities are similar to Earth's largest linear dune fields, such as the Namib Sand Sea and the Simpson Desert. We use measured defect densities in the Werner and Kocurek model to estimate crestline reorientation rates. We find reorientation timescales varying from ten to a hundred thousand times the average migration timescale (time to migrate a bedform one meter, ~1 Titan year according to Tokano 2010)). Well-organized patterns have the longest reorientation time scales (~10^5 migration timescales), while the topographically or spatially isolated patches of dunes show the shortest reorientation times (~10^3 migration timescales).

Morphologically, we find that barchanoid and star dunes occur in areas of the dune fields where the primary linear dune pattern is degraded (Fig 2. A and B) and that reoriented portions of the linear dune crestlines are found in both degraded and non-degraded areas. The most likely explanations for crestline reorientation are a change in wind regime or a reorientation resulting from the cycling of one component of a bimodal wind regime. Coupled to the results of the reorientation modeling, which suggested timescales of tens to hudreds of thousands of Titan years, this suggests that Titan's dunes may develop under bimodal winds that have a duty cycle greater than seasonal (e.g. 1 Titan season = 29 Earth years), an idea that is fundamentally distinct from current dune formation hypothesis.

Summary: Our preliminary results suggest that Titan's dunes may react to gross bedform transport over orbital timescales, relaxing the requirement that a single modern wind regime is necessary to produce the observed well-organized dune patterns. We find signals of environmental change within the smallest patterns suggesting that the dunes may be recently reoriented or are reorienting to one component of a longer timescale wind regime with a duty cycle that persists over many seasonal cycles.

References: **[1]** Anderson, R. S. (1990). *Earth Science Reviews*, *29*, 77-96 **[2]** Deledalle, C. A., et al. (2009).IEEE Transactions Image Processing, vol. 18. **[3**] Ewing, R. C., & Kocurek, G. (2010). *Geomorphology*, *114*(3), 175-187. **[4]** Ewing, R. C., et al. (2006). *Earth Surface Processes and Landforms*, *31*(9), 1176-1191 **[5]** Le Gall, A., et al. (2012).*Icarus*, *217*(1), 231-242. **[6]** Lorenz, R. D., et al. (2006). *Science 312*(5774), 724-7. **[7]** Lucas, A., et al. (2012) 43rd Lunar and Planetary Science Conference, the Woodlands, Texas. **[8]** Radebaugh, J., et al. (2008). *Icarus*, *194*(2), 690-703. **[9]** Radebaugh, J., et al. (2010). *Geomorphology*, *121*(1-2), 122-132. **[10]** Rubin, D. M., & Hesp, P. A. (2009). *Nature Geoscience*, *2*(9), 653-658. **[11]** Rubin, D. M., & Hunter, R. E. (1987). *Science*, *237*(4812), 276-278. **[12]** Savage, C. J., et al. (2010) 41st Lunar and Planetary Science Conference, the Woodlands, Texas. **[13]** Schneider, T., et al. (2012) *Nature*, 481**. [14]**Tokano, T. (2010). *Aeolian Research*, *2*(2-3), 113-127. **[15]** Werner, B. (1999). *Science*, *284*(5411), 102-4. **[16]** Werner, B. T., & Kocurek, G. (1997). *Geology*, *25*, 771-774**. [17]**Werner, B. T., & Kocurek, G. (1999). *Geology*, *27*, 727-730.

SOUTH POLAR REGION OF MARS GLOBAL DIGITAL DUNE DATABASE: WIND DIRECTION ANALYSIS AND SAND VOLUME ESTIMATES IN MC-30 R. K. Hayward[1], L. K. Fenton[2], and T. N. Titus[1] [1]U.S.G.S., Astrogeology Science Center, 2255 N. Gemini Dr., Flagstaff, AZ 86001, rhayward@usgs.gov. [2]Carl Sagan Center/Ames Research Center, Moffett Field, CA.

Introduction: The south polar (SP) region (65ºS to 90ºS) of the Mars Global Digital Dune Database (MGD[3]) will add ~55,000 km^2 of medium- to large-size dark dunes and ~15,000 km^2 of smaller dune fields and sand deposits to the previously released equatorial (EQ) and north polar (NP) portions of the database [1, 2, 3]. Here we discuss and compare wind directions, as derived from ground-based features and winds from a global climate model (GCM). We also report preliminary estimates of sand volume in the SP region.

Wind Direction Evidence: *Wind Streaks (WS).* WS were first recognized in Mariner imagery [e.g. 4]. WS orientation may be influenced by strong near-surface winds and can potentially record seasonal wind variations. Thomas and Veverka [5] compared Mariner 9 and Viking images, described the fluctuation in light and dark streaks separated by 3 Martian years, and found varying degrees of change. Researchers [e.g., 6, 7] have compared Viking-derived WS to GCM-simulated winds. Since then, repeat orbital imagery [e.g., 8], as well as Mars Exploration Rover data, have been used [e.g., 9] to further study changes in wind streaks. For this study, we measured ~85 WS identified in the Arizona State University THEMIS daytime IR global mosaic (115 m/pixel resolution) [10].

Slipface (SF) Orientation. SF orientation probably indicates the direction of prevailing wind during the latest period of major dune modification [3]. Thus SF preserves a local record that integrates wind effects over a longer period of time than WS. Assignment of SF direction does not imply that dunes are currently active. SF measurements (~400) were made based on either high-resolution images where SFs are clearly visible, or the gross morphology of dunes formed by unidirectional winds (i.e. barchan, barchanoid and transverse dunes). For ease of plotting and comparison, we averaged the individual SFs of similar azimuth (< 45º difference) within each dune field.

Dune Centroid Azimuth (DCA). DCA, a measure of a dune field's relative location within a crater, may indicate the prevailing wind direction during the period of dune field migration across a crater floor, thus preserving a regional record that integrates wind effects over a longer period of time than WS or SF [3]. Nearly 300 DCAs have been calculated for the 65°S to 90°S region. Dune fields with nearly central locations, dune fields located in topographically complex craters, and dune fields in craters with multiple widely scattered dune fields were not assigned a DCA because they would likely not yield meaningful azimuths.

GCM Wind Direction. WS, SF, and DCA azimuths are compared to wind directions simulated by the NASA Ames GCM (model description [11]). We used a GCM with low spatial resolution (5° latitude x 6° longitude) and high temporal resolution (8 outputs per Martian sol, for one Martian year). We filtered the output to obtain winds with shear stresses > .0225 N/m^2. Haberle et al. [12] have shown that setting this threshold shear stress in the NASA Ames GCM will lift dust in spatial patterns that qualitatively agree with observed dust storm occurrences. Because relatively few modeled winds (~2000) exceed shear stresses > .0225 N/m^2, we also consider modeled wind speeds with magnitudes > 10 m/sec (~100,000 winds).

Discussion: In Figure 1, wind directions are represented by arrows pointing in the direction of sediment transport. WS directions (yellow) display the simplest pattern with wind direction predominantly toward the west and north (Fig. 1). SF direction (red) is mainly to the west, with a secondary flow toward the east. DCA direction (not displayed) is similar to WS, with predominant winds to the north and west. If we take a

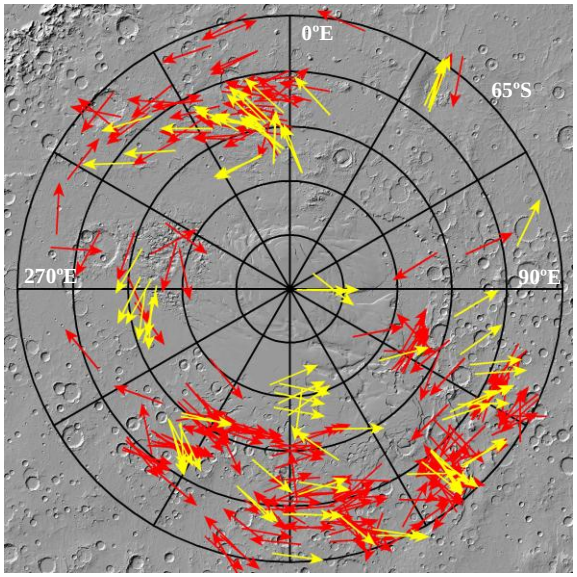

Figure 1. Yellow arrows represent WS-derived winds (majority flowing toward the west and north). Red arrows represent SF-derived winds (majority flowing toward the west and east). Background is MOLA hillshade. South Stereographic projection.

broad overview of the GCM, over 80% of the modeled winds that exceed the .0225 N/ m^2 threshold flow to the north and <15% flow to the west. When the less stringent 10 m/sec threshold is used, about 55% flow to the north and <15% flow to the west (Fig. 2). Thus the WS- and DCA-derived flow toward the north is consistent with GCM-simulated winds. This is interesting because, as mentioned above, the DCA is thought to preserve long-term wind trends while a WS may change seasonally. The majority of SF-derived winds flow to the west, which is compatible with WS and DCA evidence, but is not largely supported by GCM output. In contrast, only a small percentage of SF-derived winds flow to the north (the direction of flow that is quite strong in WS, DCA and GCM evidence). It is possible that local winds, modified by topography, may have a large influence on SF direction.

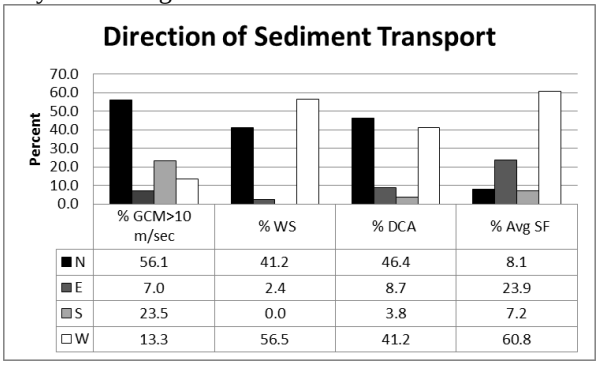

	% GCM>10 m/sec	% WS	% DCA	% Avg SF
N	56.1	41.2	46.4	8.1
E	7.0	2.4	8.7	23.9
S	23.5	0.0	3.8	7.2
W	13.3	56.5	41.2	60.8

Figure 2. Comparison of GCM-modeled winds greater than 10 m/sec and wind direction as measured from windstreak (WS), dune centroid azimuth (DCA), and slipface (SF). Wind directions are given in the direction of sediment transport. N represents winds flowing toward the north with an azimuth of 315º to 45º, E = azimuth of 45º to 135º, S = azimuth of 135º to 225º, W = azimuth of 225º to 315º. GCM, WS and DCA share a strong N component, while WS, DCA and SF share a strong W component.

Preliminary Sand Volume Estimates: Estimating sand volume over a large area, such as the 65ºS to 90ºS region of the Mars, can be challenging. The types of dune fields, and therefore the methods best suited to estimate volume, vary in the EQ, NP, and SP regions [1, 2, 13]. Here we present preliminary estimates from two methods used for the SP. The first is a modification of one of the methods used in the EQ region [1] and the second is a modification of one of the methods used in the NP region [2]. The first method calculates "mean dune height" by subtracting the minimum elevation within a dune field from the mean elevation of a dune field. This method is prone to overestimation because dune fields are often not located on flat surfaces. Thus elevation differences due to underlying topography may be wrongly attributed to sand thickness. We address overestimation by assigning a "mean dune height" based on dune type (calculated using dune fields with less topographic relief) and by accounting for empty space within dune fields. The result is a preliminary SP volume estimate of ~1700 km^3. We exclude sand sheets from the volume estimate. In the second, more subjective method, we measure MOLA profiles across selected dune fields to obtain the height of the dunes or, where appropriate, the overall thickness of a dune field. We average the dune heights, again based on dune type, and assign those averages to dune fields with similar dune types. As a first order approximation of sediment thickness, we use half the dune height. After accounting for dune field area and empty space within dune fields, Method 2 yields a preliminary estimate of ~250 km^3. Both Method 1 and 2 volumes would be reduced by converting dune height to Estimated Sediment Thickness (EST) [14], a more realistic measure of the amount of sediment in dunes.

Summary/Conclusions: 1. The wind directions indicated by the WS and DCA data are most similar. Both show wind directions split almost evenly between winds flowing to the north and to the west. 2. GCM-modeled winds are consistent with the winds flowing north. 3. Like WS and DCA, SF also shows a high percentage of winds flowing to the west (>60%), but unlike WS and DCA, shows only a low percentage of winds flowing north. 4. GCM-simulated winds are not consistent with the SF-derived wind directions, suggesting SF-forming winds are strongly influenced by local topography. 5. Preliminary sand volume estimates for the SP region range from ~250 km^3 to ~1700 km^3.

References: [1] Hayward R.K., et al. (2007) U.S.G.S. Open File Rep., 2007–1158. [2] Hayward R.K., et al. (2010) U.S.G.S. Open File Rep., 2010–1170. [3] Hayward R.K., et al. (2007) JGR, 112, E11007, doi 10.1029/2007JE002943. [4] Sagan et al. (1972) Icarus, 17, 346-372. [5] Thomas, P. and Veverka, J. (1979) JGR, 84, 8131 - 8146. [6] Greeley et al. (1993) JGR 98, 3183-3196. [7] Fenton L.K. and Richardson, M. (2001) JGR, 106(E12), 32, 885-32,902. [8] Toyota, et al. (2011) Planetary & Space Science, doi:10.1016/j.pss.2011.01.015. [9] Geissler et al. (2008) JGR, doi:10.1029/2008JE003102. [10] Christensen, et al., THEMIS Public Data Releases, Planetary Data System node, Arizona State University, http://themis-data.asu.edu. [11] Haberle, R.M., et al. (1999) JGR, 104, 8957-8974. [12] Haberle, R.M., et al. (2003) Icarus 161, 66-89, doi:10.1016/S0019-1035 (02)00017-9. [13] Hayward, R.K. (2011) Earth Surface Processes and Landforms, DOI: 10.1002/esp.2219. [14] Lancaster N. and Greeley R. (1990) JGR 95, 921-927.

MELTWATER-INDUCED DEBRIS FLOWS ON COLD-CLIMATE AEOLIAN DUNES AND THE IMPLICATIONS FOR ANALOGOUS PROCESSES ON MARS. Donald M. Hooper, Cynthia L. Dinwiddie, and Ronald N. McGinnis. Geosciences and Engineering Division, Southwest Research Institute®, 6220 Culebra Road, San Antonio, TX 78238-5166 (DHooper@swri.org).

Introduction: We observed small meltwater-induced debris flows on the lee slopes of large dunes at the 67° N latitude Great Kobuk Sand Dunes (GKSD) in Kobuk Valley, Alaska. They bear a striking resemblance to debris flows with fresh-appearing gullies or erosion tracks that occur on the slopes of several mid- to high-latitude dune fields in both Martian hemispheres. Snow partially to fully blankets the GKSD for ~70% of the year, which likely has direct analogy to hydrocryospheric factors that generate debris flows on Mars. The high-latitude, cold-climate GKSD are a valuable terrestrial system within which to conduct an analog study focused on understanding the integrated factors that generate debris-flow gullies on the slopes of Martian aeolian dunes. In this abstract we build upon our related work presented at the 43rd Lunar and Planetary Science Conference [1].

Martian Gullies: Recent analysis of High Resolution Imaging Science Experiment (HiRISE) and Mars Orbiter Camera (MOC) images by several researchers has revealed the possibility of niveo-aeolian deposits, denivation features, and debris-flow gullies on Martian sand dunes [2–11]. Whether contemporary meteorological conditions on Mars are capable of generating liquid water on the surface is a complex matter yet to be resolved to the satisfaction of most researchers [2, 3, 9, 12–15]. Other hypotheses employ liquid CO_2, CO_2 frost, or dry granular flows as the primary agent driving the formation of these gullies [11–12, 14–15].

Kobuk Valley Climate and Meteorology: The climate at the GKSD is subarctic and semiarid (mean annual air temperature: –4°C; mean annual precipitation: 360 mm) with long, cold winters (January mean: –20°C) and brief, warm summers (July mean: 15°C) [16, 17]. Meteorological data from the Kavet Creek remote automated weather station (located 3.6 km from the northern edge of the GKSD) indicate a bimodal wind regime from the east-southeast during November to April and from the west during May to July [17]. Our field work (March 16–31, 2010) coincided with a period of abundant sunshine, but mean daily temperatures did not rise above the melting point of water [18].

Niveo-aeolian deposits composed of interbedded sand, snow, and ice are a common attribute of cold-climate dunes [19–20]. At the GKSD, these wind-transported sand and snow deposits accumulate on the lee slopes of large transverse, longitudinal, and barchanoid dunes. Distinctive morphologic and sedimentologic phenomena called denivation features are produced by the melting of snow and ice present in these deposits. These include spongy and hummocky surfaces, extension cracks, deformed strata, slumping, and compressional structures.

Field Observations at the GKSD: During March 2010, we observed niveo-aeolian deposits, denivation features, and small debris flows at the GKSD (Figs. 1 and 2). Small debris flows originate in shallow alcoves near dune crests, become channelized down lee faces, and terminate with depositional fans. Melting niveo-aeolian deposits provide a source of liquid water for alluvial processes. Slope aspect and insolation are two factors that control the rate of thawing on south- and west-facing slopes.

Figure 1. A small meltwater-induced debris flow was observed on the lee slope of a large dune at the GKSD. Note niveo-aeolian (sand and snow) deposits and lobate depositional fan. Scale is 10 cm long.

Figure 2. A small debris flow with meltwater has created a shallow, incipient gully on the lee slope of a large dune. Denivation has produced spongy and hummocky microtopography.

Conceptual Model: We propose that these small debris flows are generated when high pore-water pressures develop in thawed, near-surface niveo-aeolian deposits due to impeded infiltration by frozen sand and pore ice. The thawing of niveo-aeolian deposits, perhaps aided by solar insolation, is one possible trigger for generating both terrestrial and Martian debris flows and is a likely mechanism in the formation of the associated gullies [2–3, 9, 21–23] (Fig. 3). Comprehensive surveys are needed at the GKSD to measure debris flow and gully morphologies, volumetric analysis, viscosity, slope angle, porosity, niveo-aeolian stratigraphy, net solar radiative flux, and multipositional and multilevel subsurface temperature and moisture flux profiles.

Conclusions: The GKSD are an important Mars analog site. Small debris flows on dune slopes at the GKSD are activated by seasonal thawing more than a month before the mean daily surface temperature approached 0ºC [18]. The flows consist of a mixture of sand and liquid water cascading down the dune slipface. The debris-flow gullies observed in Martian dune fields may be formed by an analogous process. The presence of Martian gullies with a youthful appearance is a topic of considerable importance because of the possible presence of liquid water. Furthermore, detailed data involving niveo-aeolian transport, deposition, and reworking are sparse and these processes are poorly understood. Our investigation provides insights into the interactions between niveo-aeolian deposition, thawing, insolation, slope aspect, and initiation of alluvial processes.

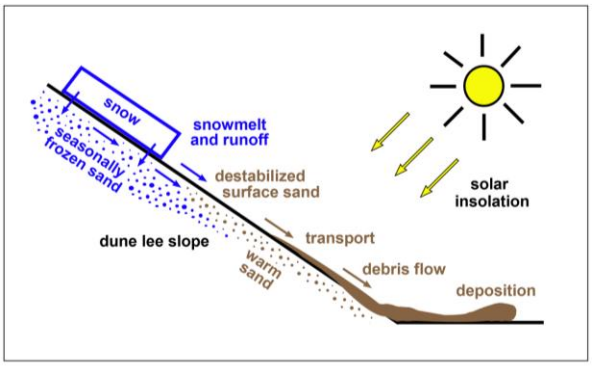

Figure 3. Our conceptual model illustrated as a time series of key slope processes and mechanisms.

Acknowledgments: Field work to the Great Kobuk Sand Dunes was funded by SwRI®'s Internal Research and Development Program (20.R8136) and by NASA MFR grant NNX08AN65G. We thank J. Myers and E. Pearcy for constructive reviews.

References: [1] Hooper, D. M. et al. (2012) *LPS XLIII*, Abstract #2040. [2] Reiss, D. and Jaumann, R. (2003) *GRL 30*, 1321. [3] Mangold, N. et al. (2003) *JGR 108*(E4), 5027. [4] Bourke, M. C. (2004) *Eos Trans. AGU, 85*(47), Abstract #P21B-01. [5] Miyamoto, H. et al. (2004) *GRL 31*, L13701. [6] Bourke, M. C. (2005) *LPS XXXVI*, Abstract #2373. [7] Diniega, S. et al. (2010) *Geology 38*, 1047–1050. [8] Dundas, C. M. et al. (2010) *GRL 37*, L07202. [9] Reiss, D. et al. (2010) *GRL 37*, L06203. [10] Horgan, B. et al. (2010) *LPS XLI*, Abstract #1325. [11] Hansen, C. J. et al. (2011) *Science 331*, 575–578. [12] Musselwhite, D. S. et al. (2001) *GRL 28*, 1283–1286. [13] Hecht, M. H. (2002) *Icarus 156*, 373–386. [14] Treiman, A. H. (2003) *JGR 108*(E4), 8031. [15] Shinbrot, T. et al. (2004) *Proc. Natl. Acad. Sci. 101*(23), 8542–8546. [16] Gibson, W. (2009) Mean Precipitation for Alaska 1971–2000. NPS, AK Regional Office GIS Team. Geospatial Dataset 2170508. [17] Western Regional Climate Center (2011) Kavet Creek, Alaska (Climate Summary, March 2010). WRCC: Desert Research Institute, Reno, NV. [18] Dinwiddie et al. (this volume). [19] Koster, E. A. (1988) *J. Quat. Sci. 3*(1), 69–83. [20] Koster, E. A. and Dijkmans, J. W. A. (1988) *Ear. Surf. Proc. Land. 13*, 153–170. [21] Williams, K. E. et al. (2009) *Icarus 200*, 418–425. [22] Kereszturi, A. et al. (2009) *Icarus 201*, 492–503. [23] Hugenholtz, C. H. et al. (2007) *J. Sediment. Res. 77*, 607–614.

EVIDENCE FOR GLASS-RICH PYROCLASTICS IN MARTIAN DUNES. B. Horgan, D. Clarke, and J.F. Bell, III, School of Earth and Space Exploration, Arizona State University (briony.horgan@asu.edu).

Introduction: One possible origin for sand-sized sediments on Mars is explosive volcanism [*e.g.*,1,2], but direct evidence for explosive volcanic products in martian sand has not been previously identified. Low albedo sediments mantle the northern lowlands of Mars and form the north polar sand sea, which encircles the north polar cap, making this region an excellent location to use composition to constrain possible origin scenarios for these sediments. Here we show that the NIR spectra of the northern plains, the north polar sand sea, and several other dune fields on Mars are consistent with iron-bearing glass partially obscured by a leached glass rind, potentially implying widespread acidic leaching and that explosive volcanism is a major source of martian sand [3].

Methods: We have analyzed Mars Express OMEGA visible and NIR (0.36–2.5 μm) spectra. Spectra were converted to estimated Lambert albedo and mapped into regional mosaics [4] prior to analysis. While most martian spectra have concave down shapes between 0.7 and 2.5 μm, we have found a class of spectra that exhibit unusually strong concave up slopes between 0.7 and 1.5 μm (Fig. 1). We parameterize this concavity by comparing a ratio in the concave part of the spectrum to a ratio at longer wavelengths: A(0.73)/A(1.54) – A(1.54)/A(2.30), where *A* is the average albedo of three channels near the indicated wavelength. Positive values of this parameter indicate a concave up continuum. The position of the spectral peak in these concave spectra is also shifted to lower wavelengths: near 0.68 μm, as opposed to 0.72-0.74 μm in basaltic spectra and 0.78 μm in dusty spectra. So far, these parameters have been calculated for all mosaics between ±30°N and above 45°N.

Typical mafic minerals may be discriminated based on the wavelength position and shape of the 1 μm iron absorption band [5]. In this study, we have examined the position of the 1 μm band center in OMEGA spectra, after contributions from the atmosphere, dust, instrumental artifacts, and the overall continuum shape were suppressed or removed. The band center is derived by locating the reflectance minimum between 0.75 and 1.3 μm, fitting a second-order polynomial to the channels within 0.075 μm of the minimum, and finding the wavelength of the minimum of the fit. So far, we have applied this 1 μm band analysis technique to our mosaics above 45°N.

Results: One of the largest dune fields in the north polar sand sea (Siton Undae), outcrops of the Cavi Unit (hypothesized to be an indurated sand sea) on Planum Boreum, and much of Acidalia and Utopia Planitiae exhibit high concavity values and relatively broad, shallow, and symmetric bands centered between 1.10 and 1.16 μm (Fig. 2). This is beyond the band center range for olivine or pyroxene, but is consistent with high abundances (80-90%) of iron-bearing glass (Fig. 1) [6]. We hypothesize that the concave spectral slope we observe associated with the glass-rich deposits is consistent with the spectra of thin (3–10 μm) silica-enriched leached glass rinds (Fig. 1), formed when silicate glass is exposed to acidic fluids [10]. Leached glass rinds are distinct from depositional silica coatings, which are formed by dissolution of silicates and precipitation of amorphous silica [7]. While rinds retain the loosely bound structure of the host glass, coatings have an opaline structure distinctly different from their substrate [8]. Also, coatings do not exhibit concave up spectral signatures [9].

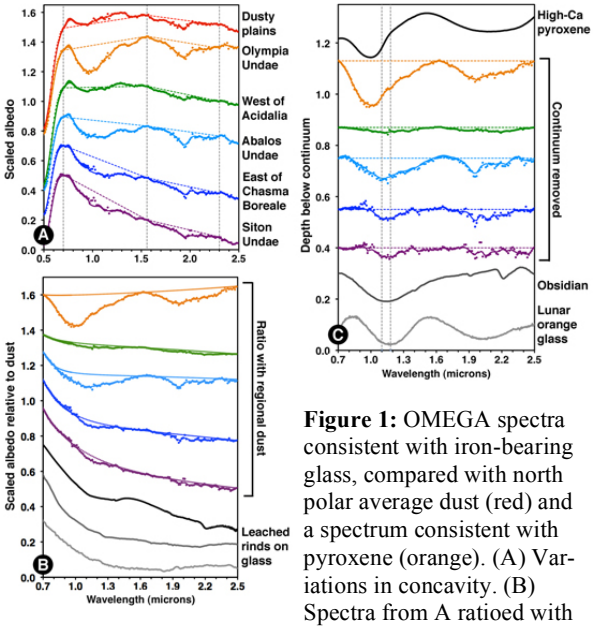

Figure 1: OMEGA spectra consistent with iron-bearing glass, compared with north polar average dust (red) and a spectrum consistent with pyroxene (orange). (A) Variations in concavity. (B) Spectra from A ratioed with average regional dust spectra, compared to leached glass rinds [10,18]. (C) Spectra from B after continuum removal, compared to lab spectra of mafic phases. Vertical lines indicate range of glass band centers in lab spectra.

Proposed origin: We have detected spectra consistent with iron-bearing glass in pixels totaling over one million sq. km north of 45°N on Mars in both exposed surfaces (*e.g.*, Acidalia) and in sand dunes (*e.g.*, Siton Undae), and several million additional sq. km of glass-rich surfaces may be obscured under a dusty mantle. Because the glass is durable enough to form

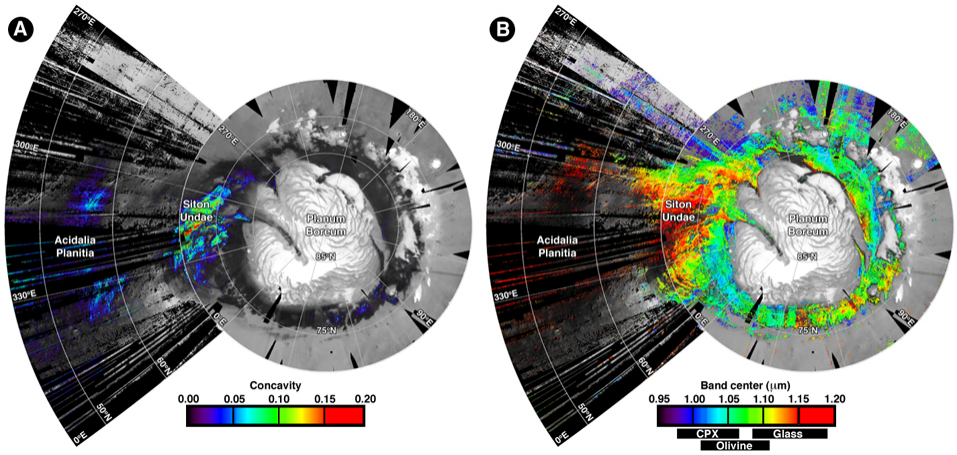

Figure 2: (A) Concavity parameter mapped over the Mars north polar region and northern Acidalia Planitia, showing only positive values. (B) 1 μm band center mapped over the same region. Blue and green regions are consistent with pyroxene (CPX) or olivine, while yellow and red regions are consistent with iron-bearing glass. 1°N ≈60 km.

sand dunes, some fraction of the glass must be sand-sized with minor vesicle content. An analog for these deposits are the extensive sand sheets and dune fields of Iceland, which cover ~25% of the island and contain 50-90 wt.% glass [10]. These deposits are formed during ice-magma interactions, and are emplaced through airfall, fluvial processes, and massive glacial outburst floods. This combination of processes is more consistent with the deposits we see on Mars, as neither dry explosive eruptions or impacts are known to produce such extensive, glass-rich, low vesicularity, sand-size deposits, but such materials are common products of ice-magma interactions [11]. Where these martian glass-rich materials were originally created is not yet known, but possibilities include sub-glacial volcanism in Southern Acidalia [12] as well as ice-magma interactions related to chaos terrain formation. Deposition into the northern plains is also an issue, as models indicate that sand-size grains are not deposited far beyond the immediate vicinity of the vent [13]. Thus, unless high-latitude volcanic sites can be identified, deposition in the northern lowlands may require either aeolian or fluvial transport.

We interpret the leached glass rinds on the northern lowlands glass as the result of post-depositional periglacial weathering [3]. These rinds are a common weathering product on glassy materials in arid volcanic environments on Earth, and exhibit concave up slopes in aerial spectra similar to those observed at lab scale [7,8,14]. Based on the fluid chemistry required to create these rinds [7], we propose that the weathering fluid is melt from surface ice sheets or snow packs, acidified due to oxidizing conditions [15].

Glass in equatorial dunes: To evaluate the glass content of dunes at lower latitudes, we have completed a preliminary search for weathered glass spectra in dune fields between +-30°N. Based on the median values of the concavity parameter, albedo, and spectral peak position for dune fields in this region listed in the Mars Global Digital Dunes Database, we have identified a number of dune fields that may contain weathered glass, based on a median peak position <0.72μm and a median concavity >0.1. These dune fields are concentrated in the Syrtis Major, Valles Marineris, and Arabia Terra regions (Fig. 3). Further detailed analysis of OMEGA spectra of these dune fields will help to constrain the presence of glass. However, even these preliminary results suggest that glass may be common in dunes across the martian surface.

References: [1] Edgett, K. (1997) *Icarus*, *130*, 96. [2] Tirsch, D. *et al*. (2011), *JGR*, *116*, E03002. [3] Horgan, B. and Bell, J.F. III (2012) *Geology*, in press, doi:10.1130/G32755.1. [4] Horgan, B. *et al*. (2009) *JGR*, *114*, E01005. [5] Cloutis, E.A. and Gaffey, M.J. (1991) *Earth Moon and Planets*, *53*, 11-53. [6] Adams, J.B. *et al*. (1974), Proc. 5th Lunar Conf., *1*, 171-186. [7] Minitti, M.E. *et al*. (2007) *JGR*, *112*, E05015. [8] Chemtob, S.M. *et al*. (2010) *JGR*, *115*, E04001. [9] Kraft, M.D. *et al.* (2007) LPSC XXXVIII, #2241. [10] Arnalds, O. *et al*. (2001) *J. Arid Env.*, *47*, 359. [11] Heiken, G. and Wohletz, K. (1991) *Sedimentation in Volcanic Settings*, SSG Spec. Pub. 45, 19-26. [12] Martínez-Alonso, S. *et al*. (2011) *Icarus*, *212*, 597-621. [13] Kerber, L. *et al*. (2012) *Icarus,* in press, doi: 10.1016/j.icarus.2012.03.016. [14] Seelos, K.D. *et al*. (2010) *JGR*, *115*, E00D15. [15] Hurowitz, J.A. *et al*. (2010) *Nat. Geo.*, *3*, 323-326.

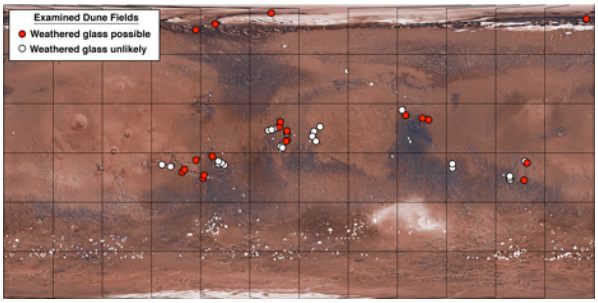

Figure 3: Distribution of dune fields with known or possible weathered glass content (red dots) compared to all examined dune fields (white dots).

COMPARING ACTIVE MODES OF MASS MOVEMENT ON MARTIAN DUNES. B. Horgan[1], L. Fenton[2], and P. Christensen[1], [1]School of Earth and Space Exploration, Arizona State University (briony.horgan@asu.edu), [2]Carl Sagan Center, SETI Institute.

Introduction: High-resolution monitoring of martian sand dunes over the past decade has revealed a variety of modes of mass movement on martian dunes [*e.g.*, 1-10, 13-17]. Various combinations of water, water ice, CO_2 frost, dry sand flow, dust avalanches, and induration have all been proposed as contributing to the origin of these features. In some cases, similar processes have been proposed to cause mass movements with different morphologies, and vice-versa. In an effort to constrain the possible origins of these features, here we summarize their characteristics and evaluate the possible contribution of various volatile, aeolian, and rheologic processes to their development.

Leveed channels: Sinuous, leveed channels with no depositional aprons [1,2] that are the Type I features of [3,4]. They appear to initiate both at dune crests in intermediate alcoves (10-20m wide) as well as further down slope, and extend out onto dune aprons. Levees are found primarily on south-facing slopes south of 45°S. The properties of the levees are consistent with sediments incorporating liquid water, but not CO_2 [1]. New levees have been observed during the spring season [5]. Sediments fluidized by liquid water have also been proposed to explain branching streak-like features on CO_2 covered dunes in the north polar sand sea [6], but morphologic signatures like the leveed channels have not been observed in this region.

Dendritic channels: Large (100m+ wide) alcoves composed of dendritic channels, which merge into a single sinuous channel ending in a depositional apron. These features are only found on south-facing slopes poleward of 45°S, and are Type II features in [4]. Based on channel morphology, [4] proposed that these features were formed by a fluid, but further work is needed to constrain how fluids could be involved.

Dune gullies: While there is some variation in morphology of these features, they are generally characterized by large (100+ meters wide), often channeled alcoves, with sinuous and long to short and straight channels terminating in large (100+ meters long) alluvial fan-like deposits [3,4,7,8]. Dune gullies are primarily found south of 45°S on E/W slopes [4,7], and correspond to Type III features of [3,4]. New dune gullies have been observed [8], and new flows have been identified within several existing gullies during the winter or spring seasons [7]. Based on the seasonal and latitudinal correlation with CO_2 frost, [7] proposed that fluidization due to CO_2 sublimation promoted mass wasting in the gullies; however, the triggering mechanism for the failure in this scenario is not well constrained. Instead, [3] proposed that failure and fluidization may have been triggered by melting ice/snow (denivation) in the subsurface, based on a strong morphologic similarity to denivation features on terrestrial cold-climate dunes [9].

Slumps: Partial or full translational or rotational collapse of the slipface, as opposed to flows [9]. So far, slumps have only been reported in the north polar sand sea [10,11], where new slumps have also been observed [10]. Similar slumps occur on terrestrial dunes with layers of melting ice or snow incorporated into the slipface [12], and this scenario is consistent with evidence for ice-cemented dune interiors in the north polar region [9,12]. While this process is similar to that proposed for the gullies, the difference in morphology may be related to the steepness and length of the slipface – slumps tend to occur on barchans with short, steep slipfaces [3] while gullies tend to occur on large, complex dunes with long, relatively shallow slopes [4].

Streaks: These long, rectilinear albedo features exhibit little to no apparent relief. Streaks are identified by their contrasting albedo with the surrounding slipface (and thus are only apparent on dusty slipfaces), and can appear either darker or lighter in tone. Some streaks brighten down slope. These features correspond to Type II features in [3] and Type IV features in [4]. Streaks are actively forming in mid-latitude and equatorial dune fields [14-16], and here we report streaks forming in early summer in the north polar sand sea. Streaks have been interpreted to be grain flows, similar to rectilinear grain flows on terrestrial dune slipfaces [14-16]. Some streaks occur on very dusty dunes that clearly have not experienced saltation recently, and in these cases, appear to be triggered by dust devils (*e.g.*, HiRISE ESP_014426_2070). This observation raises the question of whether streaks represent flow of sand, dust, or both. Dust streaks are common features on martian slopes [17]. Bright streaks and streaks with bright termini may indicate flows incorporating significant dust. However, some dark streaks on short slipfaces clearly deposit dark sand at their termini, suggesting that at least some streaks are indeed sand flows.

Simple alcoves: These features are characterized by wedge-shaped, un-channeled, shallow alcoves perched above short, symmetrical, fan-shaped deposits (Fig. 1). Alcove widths range from a few meters to a few tens of meters. Alcoves were originally identified in the north polar sand sea [10,18], but are also present

in mid-latitude dune fields in both hemispheres. Alcoves are rare at lower latitudes, but meter-scale structure on the upper portion of slipfaces may be consistent with small alcoves (Fig. 1c). Interestingly, both the linear structure of the equatorial alcoves and the channelized structure of the high latitude alcoves resemble features formed in small-scale granular flow experiments designed to simulate martian gravity [19].

New alcoves have been observed to form in the north polar sand sea between consecutive summer and spring seasons [6]. New alcoves are first observed as outlines beneath the CO_2 frost, implying that they formed prior to the deposition of the thick CO_2 slab in the fall [20], most likely between mid-summer and early fall. The orientations of the alcoves are consistent with recent wind directions [20], suggesting a genetic relationship with aeolian activity. Indeed, the morphology of the alcoves and fans is consistent with channelized dry grain flows [21]. These can form alongside rectilinear flows on terrestrial slipfaces, and the flow morphology may depend on the location of greatest over-steepening on the slipface [22]. However, the large size of alcoves at mid and high latitudes (~10 meters) compared to typical terrestrial flows (tens of cm) suggests that other processes are affecting the martian dunes. One possibility is that the large size, steep walls, and multi-year preservation typical of the alcoves in the north polar erg is due to partial induration of the slipface [20], which would lead to less frequent and therefore larger failures [22], and would help to preserve alcoves and to create steep walls [3].

While most simple alcoves are ~10 meters or less in width, we have identified a few examples of larger alcoves (50-100m) in the north polar sand sea (Fig. 1b). Even these large alcoves still appear fundamentally different from either slumps or the more complex failure features in the south, as they do not exhibit channels within or below the alcove and their depositional fans are small and do not exhibit evidence for multiple events or fluidization. The timing of activity also appears to occur in late summer or fall, compared to winter or spring for the dune gullies. Thus, simple alcoves appear to be less consistent with the presence of volatiles than other mass movement features on martian dunes, supporting a dry grain flow origin.

Comparing hemispheres: It has been suggested that the difference in modes of mass movement between northern and southern mid to high latitude dunes is related to greater frost accumulation during the longer southern winter, causing fluidization of flows [7]. However, in this scenario, high-latitude northern dunes should also exhibit volatilized flows, which are not observed. Our synthesis of available observations suggests that the size and morphology of the dunes themselves may be as important of a factor as seasonality. Dune gullies are only observed on the complex intracrater dunes with long slipfaces and aprons that are common in the southern highlands, but this type of dune is rare in the uncratered northern plains. However, some hemisphere-dependent effect may still be required to explain the pole-facing levees and dendritic channels observed in the south.

References: [1] Mangold, N. *et al*. (2003) *JGR*, *108*, E45027. [2] Reiss, D. and R. Jaumann (2003) *GRL*, *30*, 1321. [3] Bourke, M. (2005) *LPSC XXXVI*, #2373. [4] Reiss, D. *et al*. (2007) *LPSC XXXVIII,* #1993. [5] Reiss, D. *et al*. (2010) *GRL*, *37*, L26203. [6] Kereszturi, A. *et al*. (2011) *P&SS*, *59*, 1413. [7] Diniega, S. *et al*. (2010) *Geology*, *38*, 1047. [8] Malin, M. and K. Edgett (2005) MSSS Captioned Image Release, http://www.msss.com/mars_images/moc/2005/09/20/dunegullies/. [9] Koster, E. and J. Dijkmans (1988) *ESPL*, *13*, 153. [10] Bourke, M. (2012) *LPSC XVIII*, #2885. [11] Horgan, B. *et al*. (2010) *LPSC XVI*, #XXXX. [12] Ahlbrandt, T., and S. Andrews (1978), *Palaeogeo Palaeoclm Paleoeco*, *25*, 327. [13] Feldman, W. *et al*. (2008) *Icarus, 196*, 422. [14] Edgett, K. and M. Malin (2000) *JGR*, *105*, 1623. [15] Fenton, L. (2006) *GRL, 33*, L20201. [16] Silvestro, S. *et al*. (2011) *GRL, 38*, L20201. [17] Sullivan, R. *et al.* (2001) *JGR*, *106*, 23607. [18] Hansen, C. *et al.* (2011) *Science*, *331*, 575. [19] Shinbrot, T. *et al*. (2004) *PNAS*, *101*, 8542. [20] Horgan, B. and J.F. Bell III (2012) *GRL*, in press. [21] Anderson, R. (1988) *Sedimentology*, *35*, 175-188. [22] Breton *et al*. (2008) *Geomorph.*, *95*, 518.

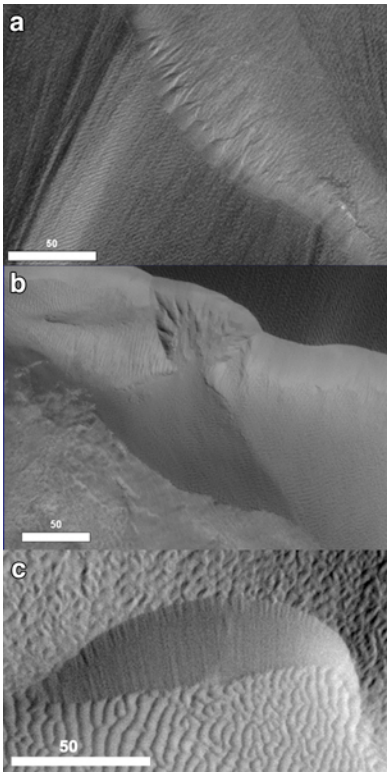

Figure 1: Simple alcove examples. All scale bars are 50 meters, and illumination is from the left.

(a) Overlapping alcoves in the north polar region. (PSP_009252_2640)

(b) A large alcove in the north polar sand sea. (PSP_ 009905_2650)

(c) Small possible alcoves in Herschel Crater, 14°S. (ESP_020384_1650)

HIGH RESOLUTION COMPUTATIONAL FLUID DYNAMIC MODELLING OF AIRFLOW OVER DUNES IN PROCTOR CRATER, MARS. D.W.T. Jackson[1], T.A.G. Smyth[1], M. C. Bourke[2], and J.H.M. Beyers[3], [1] School of Environmental Sciences, University of Ulster, Coleraine, Northern Ireland, BT52 1SA, U.K., d.jackson@ulster.ac.uk; Smyth-TA@email.ulster.ac.uk [2]Planetary Science Institute, 1700 E. Ft. Lowell Rd. #106, Tucson, Arizona, 85719-2395, USA, mbourke@psi.edu, [3]Klimaat Consulting & Innovation Inc., Guelph, Canada, meiring.beyers@klimaat.ca

Introduction: Recent Hi-Rise imagery has presented an opportunity to examine at high resolution the patterns of dune and inter-dune areas inside Proctor's Crater, Mars. Multiple dune crest and ripple formations can be found orientated in distinct directions. To date, these have been used to infer directional components of the wind regimes present with the boundary layer over these features. Using a generated Digital Terrain Surface alongside these clearly defined bedform features compels us to examine the possible wind flow behaviour that has been responsible for these geomorphological patterns. Multiple length scales are present showing progressively smaller bedform features superimposed on and within larger (mega) dunes, giving rise to complex but regular topographical patterns that may be indicative of multi-directional (and magnitude) wind regimes. There is therefore a need to understand the airflow behaviour at an adequate scale over these features to investigate if the formational pattern and orientation of the bedforms correspond to localised wind flow forcing.

Method: Using computational fluid dynamics (OpenFoam CFD code) with a RNG k-ε solver over a 3-D surface mesh, we present preliminary findings within Mars' Proctor Crater (fig.1) to examine a dune area of 4.4km x 3.0km, and a computational cell resolution of 5m x 5m. We ran three wind directions; Primary (WSW), Secondary (ESE) and Tertiary (ENE) winds. Each simulation had a logarithmic inlet with an input of $10ms^{-1}$ at 30m from the surface and a roughness parameter of 0.05m. Kinematic viscosity was assumed to be 0.0019 $m^2 s^{-1}$. Output was presented in the form of surface flow vectors (at 0.5m from the surface) and superimposed over 3-D and Hi-Rise imagery to allow direct comparisons with local bedforms. A cross sectional slice of the boundary layer over the dunes is also presented to show detached and other flow characteristics.

Results: Focusing in on a particular 1km x 1km area where three main megadune ridges are in view and inter-dune trough topography is imaged, results reveal a distinct relationship between steered airflow and localised bedform orientation, clearly mapping orthogonally onto much of the crestal ridges present at multiple scales. Under Primary (WSW) winds, flow vectors were strongly steered orthogonally against the smaller inter-megadune dune ridges in a SW orientation, coincident with re-attached flow coming off the main megadune crests. Winds within the troughs of megadunes were reduced in magnitude by 25-35% from their crestal velocities. Under Secondary (ESE) winds, similar steering patterns were found and clear steered flow and re-attached patterns of airflow were evident with features again lining up at orthogonal directions to these crestal steered flows. Steered winds in the megadunes troughs were from a SE direction and had reductions in velocity of up to 50% compared to crestal wind velocities. Under Tertiary flow conditions (ENE) steered winds inside the megadune troughs travelled from a SE to E direction, and were orthogonal to microdune (ripples) located on the stoss side of the megadunes as well the mesodune ridges inside the megadune troughs. Steered winds were reduced in magnitude by up to 60% compared to crest velocities during tertiary winds.

Within the three wind direction scenarios, detached flow was evident in the Primary and Terriary simulations only whilst the Secondary winds contained largely attached flow only behavior. This has been dictated by the mega-dunes' crestal configuration relative to indicent wind direction. These detached/un-detached flow behaviours in turn induce re-attachment zones or maintain attached wind flow which have morphological implications for localized ripple and dune migration patterns.

This work has important implications for the reconstruction of aeolian dunes within craters on Mars [1] and can help lend further support to studies examining recent activity of Martian dune migration[2].

References:

[1] Fenton, L.K. et al. (2005) *Jour. Geophys. Res.* Vol.110, doi:10.1029/2004JE002309.

[2] Gardin, E. et al. (2011) *Icarus*, 212, 590-596.

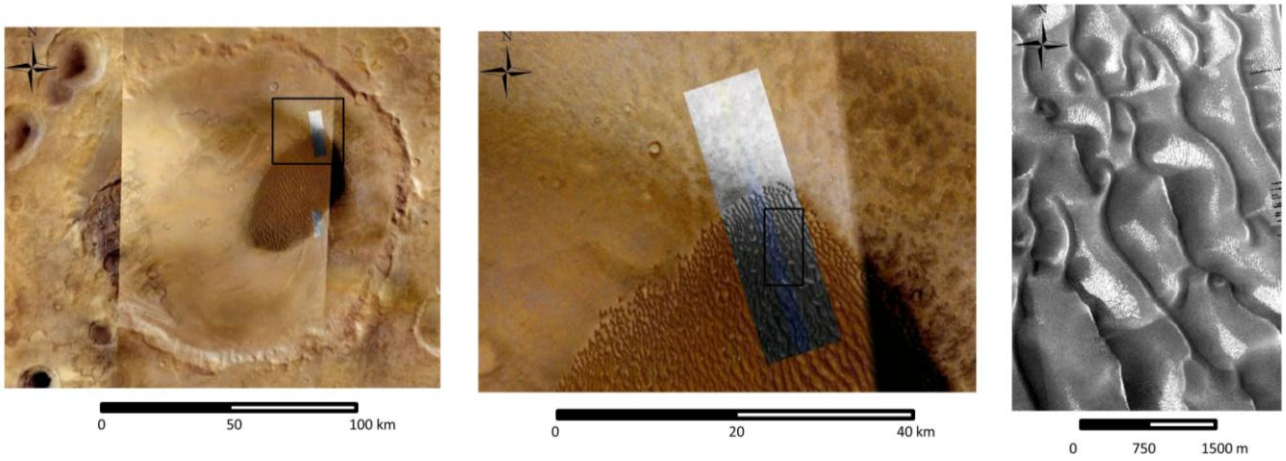

Fig.1 Location of study site within Proctor's Crater, Mars showing area of interest and the DTS used from altimetry data.

AEOLIAN FEATURES IN THE MEDUSAE FOSSAE FORMATION: A HIRISE SURVEY. L. Kerber[1], J. W. Head[2], F. Forget[1] [1]Laboratoire de Météorologie Dynamique du CNRS, Université Paris 6, Paris, France (Kerber@lmd.jussieu.fr), [2]Department of Geological Sciences, Brown University, Box 1846 Providence RI 02912

Introduction: The Medusae Fossae Formation is a voluminous, fine-grained unit located along the equator between the Elysium and Tharsis volcanic complexes [1-4]. While mapped as Amazonian in age, recent stratigraphic analysis has suggested that parts of the unit were emplaced at the latest in the Hesperian [5]. Many different types of aeolian features are present within the formation, including transverse aeolian ridges (TARs) [6] dark-colored dunes [7], yardangs [8], and horseshoe-shaped erosional pits [9]. Unlike other regions of Mars, the Medusae Fossae Formation appears to host a large number of indurated, cratered, and degraded aeolian features [6]. In addition to aeolian geomorphological features, complex inverted fluvial networks have been discovered [10,11], fueling new interest in the deposit and its history. One inherent difficulty in studying particular geomorphological features in a large unit such as the Medusae Fossae Formation is finding appropriate examples of often small-scale features amid the large number of available High Resolution Imaging Science Experiment (HiRISE) images spread across thousands of kilometers. For this reason we have conducted a survey of all of the 427 HiRISE images available as of March 1, 2012 in the region of the Medusae Fossae Formation, noting the appearance of aeolian and other geomorphological features of potential interest to other researchers, including: yardangs, morphologically fresh TARs, indurated TARs, black sand, horseshoe or v-shaped scours, layers, jointing, rootless cones, sublimation terrain, fluvial features, fish-scale terrain, thin, cross-hatched ridges (dubbed "inverted fish-scale terrain"), and "faceted" terrain [as defined in 6].

Methods: Each image was analyzed at high resolution using IAS Viewer or HiView, available from the HiRISE website, and observed geomorphological features were plotted on a map of the Medusae Fossae Formation using the geographical information system software ArcGIS. Type examples of each feature were selected to aid in the consistency of feature identification. In some cases (such as with yardangs), it was found that the morphology of a feature changed across the deposit. In these cases several type examples were chosen to showcase the morphological variability across the deposit.

Results: TARs were found throughout the deposit, as were yardangs, except for in the thickest parts of Eumenides Dorsum and in northwestern Lucus Planum [see also 9]. Fresh TARs were more commonly found in the western parts of the deposit compared with the eastern parts of the deposit (**Figure 1a**). Faceted terrain dominates over both fresh and indurated TARs in the thick, eastern outcrops of the formation. Horseshoe-shaped scours also increase in number in the eastern parts of the deposit (**Figure 1b**). Black sand was found widely in the formation, often inside large craters or next to lava plains (**Figure 1c**). Fluvial features were found dominantly in lower Zephyria Planum region, but several outlying fluvially-modified terrains were discovered elsewhere in the formation.

While dust mantling was not originally a primary feature of interest, it became apparent that much of northwestern parts of the Medusae Fossae, especially in Gordii Dorsum, are heavily mantled with dust. The formation was also found to underlie the thick Olympus Mons aureole in this region. The "reticulate" morphology described by [12] for high altitude regions of Mars is common in these dust-mantled areas. Jointing was found to be much less common than previously hypothesized [3]. The resulting maps of geomorphological features can be used as an aid in finding new instances of a feature of interest as well as providing the spatial context for a feature with respect to other features and surrounding units.

References: : [1] Scott, D.H., Tanaka, K.L. (1986) *USGS Misc. Inv. Series Map* I-1802-B. [2] Greeley, R., Guest, J. (1987) *USGS Misc. Inv. Series* Map I-1802-B. [3] Bradley, B.A. et al. (2002) *JGR 107,* E8. [4] Zimbelman, J.R., Griffin, L.J. (2010) *Icarus 205*, 198-210. [5] Kerber, L., Head, J.W. (2010) *Icarus 206,* 669-684. [6] Kerber, L., Head, J.W. (2011) *Earth Surf. Process. Landforms* doi: 10.1002/esp.2259. [7] Burr, D.M. et al. (2012) *LPSC 43*, Abs. 1692. [8] Ward, A. (1979) *J. Geophys. Res. 84*, B14. [9] Mandt, K. et al. (2009) *Icarus 204*, 471-477. [10] Burr, D.T. et al. (2009) Icarus 200, 52-76. [11] Burr, D.T. et al. (2010) J. Geophys. Res. 115, E07011. [12] Bridges, N.T. et al. (2007) *Geophys. Res. Lett. 34*, L23205.

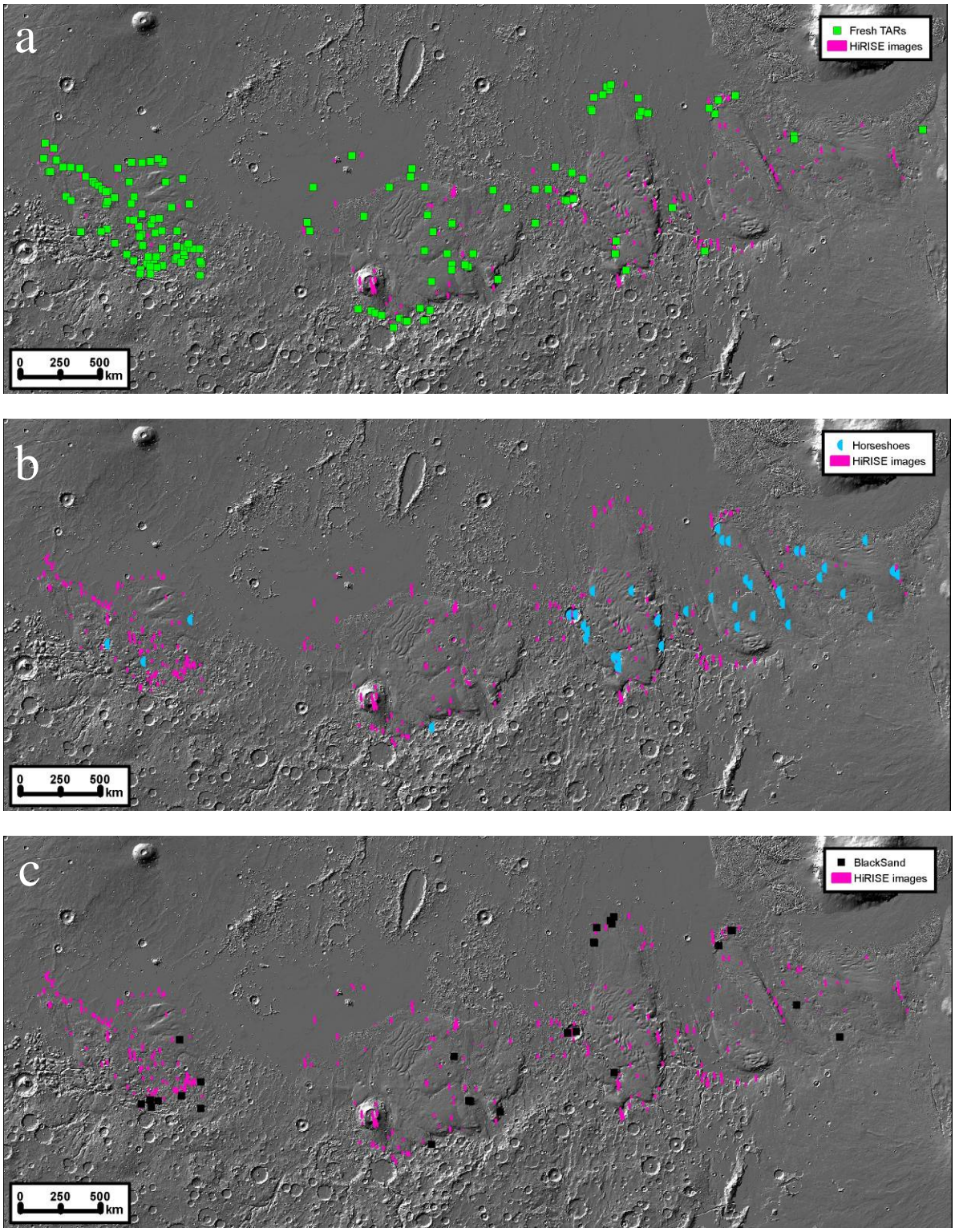

Figure 1. Distribution maps for various aeolian features in the Medusae Fossae Formation. a) Fresh transverse aeolian ridges (TARs). b) Horseshoe or v-shaped depressions. c) Collections of dark-colored sediment. In each case, the fuchsia marks represent the outlines of available HiRISE images used in the survey.

AEOLIAN TRANSPORT AND AEOLIAN DEPOISTS ON VENUS: AN OVERVIEW OF REMOTE SENSING OBSERVATIONS. ***M. A. Kreslavsky*** and ***N. V. Bondarenko***, Earth and Planetary Sciences, University of California - Santa Cruz, CA, USA, mkreslav@ucsc.edu.

Introduction: Data about the surface of Venus are rather scarce. Here we present a concise inventory of known information about aeolian transport and aeolian deposits and summarize the outstanding questions.

Observed aeolian bedforms: Information about the geology and surface properties of Venus has been obtained mostly with microwave remote sensing techniques: radars and radiometers. Imaging radars have revealed a spectacular surface dominated by extensive volcanic plains and deformed by abundant tectonic features. The generally pristine appearance of the volcanic and tectonic features indicates a very low rate of exogenic resurfacing (including aeolian processes) during the last 200 - 500 Ma of geologic history recorded at the surface.

Only the largest aeolian bedforms are resolvable in Magellan SAR images, the highest resolution (100 - 200 m) images of the surface available so far. There are 2 fields of resolved transverse dunes [1-3]. Their total area is ~2×10^4 km^2, or ~4×10^{-5} of the total area of the planet, much less than the area covered by dune fields that would be resolvable with the same technique on Titan (~13%), the Earth land (~1.5%) and Mars (~0.7%). The total amount of sand in these dune fields is a few mm equivalent global layer (EGL). For comparison, Olympia Undae on Mars contain ~5 cm martian EGL of sand. These volume estimates are rough and give only a sensible lower boundaries.

Indirect indications of small-scale, unresolved aeolian bedforms came from azimuthal anisotropy of radar backscattering. The only reasonable explanation for such anisotropy is unresolved decameter-scale asymmetric topography, and in many geological settings aeolian bedforms are the only possible explanation for such asymmetric topography. A few areas of strikingly strong anisotropy have been interpreted as dense fields of microdunes [2] with steep slip faces [4]. Their total area is ~3×10^5 km^2, still small in comparison to the ergs on other planets; the total amount of sand in them is less than a mm EGL. Two different radar remote sensing techniques show independently that weak backscattering anisotropy is ubiquitous [4-6]. It was interpreted as ubiquitous decameter-scale aeolian bedforms without steep slip faces and possibly non-continuous surface coverage [4, 6]. Total amount of sand in these deposits is very poorly constrained between 1 mm - 1 dm EGL.

Radar images reveal also a wide variety of wind streaks [3,7]. It is quite possible that some of them or all of them are formed by fields and chains of small unresolved aeolian bedforms or gaps in such fields. Some wind streaks do correlate with backscattering anisotropy, however, no systematic analysis have been performed. There is a strong trend of concentration of the wind streaks near young large impact craters.

The largest dune field is probably inactive. It is not known, whether the other aeolian bedforms observed directly or indirectly are active now or they record wind action in the geological past. Surface changes in the most active terrestrial dunes hardly would be detectable by repeating Magellan coverage.

Two (2) of 4 Venera landing sites with available images of the surface have abundant loose material ("soil") at the surface; possibly, this soil contains a high fraction of sand-size particles. However, no apparent aeolian bedforms are seen in the panoramas. For comparison, on Mars, all 6 lading sites with available images contain some soil, in 5 of them small-scale aeolian bedforms are obvious, and in 4 of them the bedforms would be seen on images of the same quality as Venera panoramas.

Winds: Venus atmosphere is dense, and the saltation threshold is low, ~0.6 m/s according to wind tunnel experiments [9]. The wind regime in the surface boundary layer of the Venus' atmosphere is essentially unknown. First-principle estimates [10] bracket *typical* wind speeds between a few mm/s and a few m/s; these limits are well below and well above the saltation limit. Day-time wind speed measured [11] at two landing sites was on the order of ~1m/s. Some soil movement apparently caused by wind was noted in repeated Venera panoramas [12]. However, winds at the landing sites might be related to long-living atmospheric disturbances caused by the probe descent and landing and not representative of typical conditions. According to the poor constraints on the typical wind speed, two endmember scenarios for formation of aeolian bedforms can be envisioned.

W*indy regime*. Typical near-surface winds are above the saltation threshold, saltation occurs wherever sand is available. Slip faces and dunes form only when wind speed is close to the threshold, otherwise wind produces slightly undulating sand sheets and small ripples [9] responsible for the observed wind streaks and weak backscattering anisotropy. Statistics of slope streak orientation [7] is consistent with possible circulation pattern and thus with windy regime. The concentration of wind streaks around big craters and the absence of small bedforms in panoramas is explained by

availability of mobile sand (see below). Windy regime predicts significant transport of sand and hence trapping of sand into impact craters, like it occurs on Mars. Such trapping is not observed. Old craters are somewhat shallower than young craters [13], which has been explained through volcanic infill. Unlike craters on Mars, old craters on Venus have no hint of aeolian bedfroms on their floors.

Calm regime. Typical near-surface winds are well below the saltation threshold, and rare short episodes of saltation occur in the aftermath of impact events due to atmospheric and surface thermal disturbances caused by impacts [14]. This naturally explains association of wind streaks with craters, the absence of aeolian bedforms in the panoramas and on the crater floors. The existence of two fields of big dunes (they need much time to form) has no straightforward explanation. They might be relics from ancient climate regime.

Variations. If we do not involve climate change, the presence of only two fields of big dunes might mean a fine tuning of wind regime, which is unlikely to occur by chance. This may point to the existence of some sort of feedback between saltation and winds. Fine dust knocked out by saltation and suspended in the lower atmosphere might be a feedback mechanism.

Sands: Scarcity of sand on Venus has been considered [2, 3] as explanation for the scarcity of observed aeolian bedforms. It has attributed [2, 3] to the fact that erosion by water, the main source of sand-size particles on the Earth, does not operate on Venus, and chemical weathering is not likely to produce sand [15]. On Mars, however, where erosion by water is extremely slow, sand is abundant, because the main terrestrial sink of sand, sedimentation at the sea floor, does not operate on Mars. Unlike Mars, Venus has an efficient sink of sand, lithification of beds accelerated by high surface temperatures. Some "stickiness" of particles at high temperatures has been predicted from the first principles [16] and observed in the wind tunnel experiments under Venus conditions [17]. "Stickiness" and quick lithification of sands can explain lack of saltation of Venus, even if the sand-size particles are abundant.

Impacts have been considered as the main source of sand on Venus; estimates [18] give ~ 1 mm EGL, while from considerations in [15] we got two orders of magnitude more optimistic value (~ 1 dm EGL). Material ejected by young large craters forms extended radar-dark diffuse features (DDFs) of parabolic planform, dm to meters thick. According to [15] they may contain a significant proportion of sand particles, but their surface usually remains flat for tens Ma [19]. Microdunes [2], however, are formed on DDFs, and possibly, from their material. As noted in [20], impacts cause a wave of strong compression of the air followed by rarefaction, which can disintegrate slightly lithified deposits, extract sand from topographic traps, etc. This gives another explanation for concentration of wind streaks around impacts.

In addition to impacts, tectonics and associated mass wasting can disintegrate rocks to produce sand-size particles. No association of wind streaks with the youngest tectonic fractures has been noted. Pyroclastics is obvious and probably rich source of sand-size material, however, there is no unambiguous association of wind streaks with young volcanoes.

Conclusions: Despite abundant morphological observations, is unclear if aeolian activity is / was able to move material for long distances to produce global material mixing, or the observed bedforms reflect only local reworking of the material. There is a set of indications that saltation on Venus is not pervasive, but we do not understand, if this is due to lack of winds or lack of sand.

What new data can help to understand the situation? The most principal point is the order of magnitude of typical winds in the boundary layer. The easiest way to assess it with remote sensing techniques is to measure diurnal variations of the surface temperature with accuracy of ~ 0.1 K. It is possible that advanced analysis of data from IR spectrometers VIRTIS and SPICAV onboard Venus Express can give some new constraints, but probably the right way to achieve required accuracy is well calibrated orbital microwave radiometer.

References: [1] Greeley R. et al. (1992) *JGR, 97,* 13319–13345. [2] Weitz C.M. et al. (1994) *Icarus, 112,* 282-285. [3] Greeley R. et al. (1997) in *Venus II*, Univ. Arizona Press, 547 – 590. [4] Kreslavsky M. A. and Vdovichenko R. V. (1999) *Solar System Res.*, *33*, 110 – 119. [5] Tyler G. L.et al. (1992) *JGR*, *97*, 13115 – 13139. [6] Bondarenko N. V.et al. (2006) *JGR*, *109*, E09004. [7] Greeley R.et al. (1995) *Icarus*, *115*, 399 – 420. [9] Marshall J. R. and Greeley R. (1992) *JGR*, *97*, 1007 - 1016. [10] Gierasch P. J et al. (1997) In *Venus II*, Univ. Arizona Press, 459 – 502. [11] Keldysh V.M. (1977) *Icarus*, *30*, 605-625. [12] Moroz V. I. (1983) In *Venus*, Univ. Arizona Press, 45 – 68. [13] Herrick R. R. and Sharpton V. L. (2000) *JGR*, *105*, 20245 – 20262. [14] Schultz P. H. (1992) *JGR*, *97*, 16183 – 16248. [15] Basilevsky et al. (2004) *JGR*, *109*, E12003. [16] Starukhina L. (2000) *Solar System Res.*, *34*, 295. [17] Marshall J. R. et al. (1991), *JGR*, *96*, 1931–1947. [18] Garvin J. B. (1990) *EMP*, *50/51*, 175 – 190. [19] Bondarenko N. V. and Head J. W. (2009) *JRG*, *114*, E03004. [20] Ivanov B. A. et al. (1992) *JGR*, *97*, 16167 – 16181

TITAN'S DUNES BY THE NUMBERS. A. Le Gall[1], S. Rodriguez[2], A. Garcia[2], J. Radebaugh[3], R.D. Lorenz[4], R.M.C. Lopes[5], A. Hayes[6], E. Reflet[2], [1]Laboratoire Atmosphères, Milieux, Observations Spatiales (LATMOS-UVSQ), Paris, France. [2]Laboratoire AIM, Université Paris Diderot, Gif sur Yvette, France. [3]Department of Geological Sciences, Brigham Young University, Provo, UT. [4]Johns Hopkins University Applied Physics Laboratory, Laurel, MD. [5]Jet Propulsion Laboratory, Caltech, Pasadena, CA. [6]Department of Earth and Planetary Science, University of California at Berkeley, CA.

Introduction: Thousands of dunes observed on the surface of Saturn's moon Titan were one of the greatest surprises uncovered by the Cassini spacecraft [1]. Dunes point to the mobility and processing of sediments on Titan – they are the telltale signatures of wind at work. As such, they provide crucial insights into the geology and climatic history of Titan. Being likely mainly composed of solid organics, they also hold clues on the methane and carbon cycles on Titan. In this paper, we will put numbers on dune areal coverage, volume, altitude and latitude distribution and show how these numbers can help understand past and present conditions on Titan.

Dune coverage Dune fields are one of the dominant landfoms on Titan. Using all SAR swaths acquired from the beginning of the mission (from Ta through flyby T77), we have outlined the dune fields of Titan (see Fig. 1). We find that they cover 6.5% of the 48.5% of Titan's surface observed by SAR so far. This suggests that the dunes may be present on as much as ~13.5% of Titan's surface which corresponds to an area of ~10 million km^2, that is roughly the area of the United States. For comparison, the seemingly featureless plains on Titan likely cover 14.2% of the surface while the hummocky radar-brigth terrains (including the puzzling Xanadu region) extend over 17.6% of the surface observed by SAR.

Next step will include the global mapping of the dune fields using VIMS (Cassini Visual and Infrared Mapping Spectrometer) dataset.

Dune volume Assuming 100 m-high dunes, accounting for the variability in dune height (30-180m, [2,3]) and dune/interdune area coverage fraction (25-50% as derived from [4]) and considering a maximum thickness for the interdune sand cover of 5 m, we find that the volume of sediments in the dune fields should be within the range 0.5-5×10^5 km^3 which represent an equivalent layer of ~0.6-6 m covering Titan. The sand budget is therefore most probably higher than the volume of liquid hydrocarbons on Titan which is currently estimated to be ~0.3×10^5 km^3, accounting for the up-to-date distribution of the lakes and seas, assuming a conservative depth of 20 m (as proposed by [5]) and neglecting a potential subsurface reservoir. If dune sand-sized particles are mainly composed of solid organics as suggested by VIMS observations [2] and atmospheric modeling and supported by radiometry data [6], dune fields are the largest known organic reservoir on Titan.

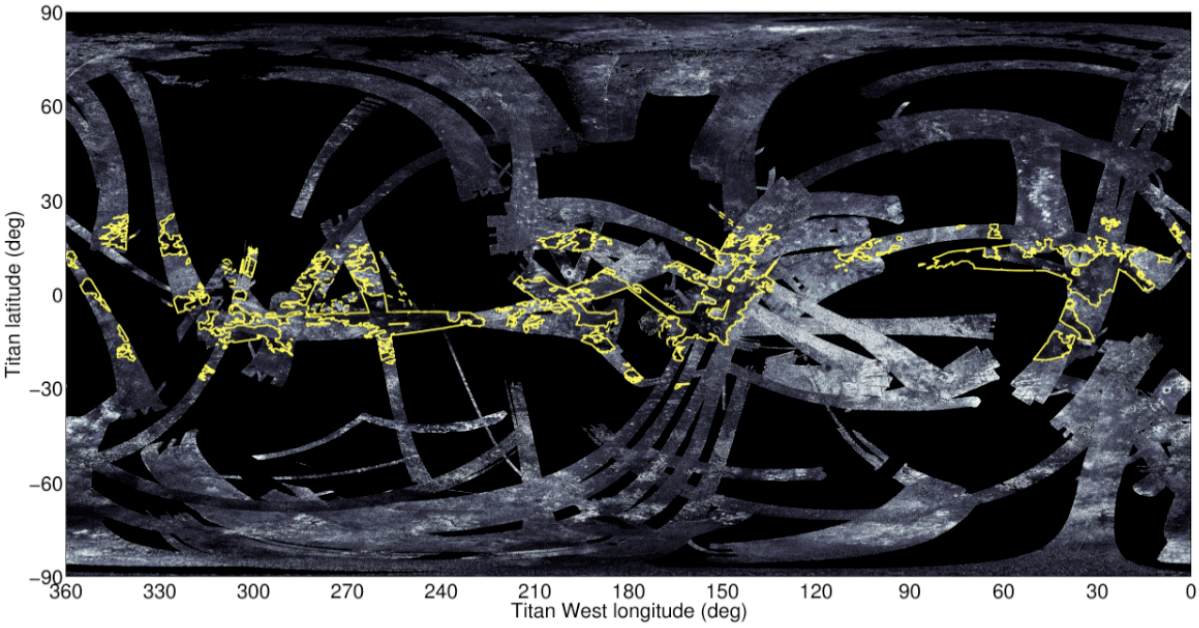

Figure 1: Mosaic of the Cassini SAR (Synthetic Aperture Radar) swaths. Dune fields are outlined in yellow. They are confined to the Equatorial belt.

Dune altitude Using the SAR-Topography data [7], we have investigated the height distribution of Titan's dune fields. The hypsometric profile of the dune regions extends from ~-400 m to ~200 m with a center of mass of ~-163 m and a 95% interval of confidence of 352 m (see Fig. 2). None of Titan's dune fields are located in the most elevated areas where the rate of erosion by aeolian or pluvial processes [8] may exceed the rate of sediment deposition. Neither do dune fields occur in the lowest terrains on Titan where the surface may be moist due to interaction with a potential subsurface alkanfer (hydrocarbon analog of an aquifer) thus limiting or inhibiting sediment entrainment. However, excluding Xanadu, which is relatively low for unknown reasons and whose nature is still puzzling, the center of mass of the equatorial height distribution, ~-115 m (with a 95% IC of 397 m), is higher than the center of mass of the dune terrain height distribution. Dune fields tend to occupy the lowest regions in the equatorial belt; ~70% of the observed dune regions for which we have topographic information are below -115 m in elevation. In particular, Belet, Aztlan and the dunes north of Senkyo are hosted within topographic depressions that are a few hundred meters lower than their surroundings. Troughs or basins are natural depositional sinks which helps explain the presence of sand seas in these areas.

Dune latitude Fields of linear dunes are confined to Titan's equatorial belt, within 30°N and 30°S latitude (see Fig. 1). On Earth the majority of important sand seas are located in low latitudes hot desert. Important dune areas also occurs in the cold arid and semi arid regions. This suggests that relatively dry conditions may prevail at Titan's tropics.

Furthermore, [9] have shown a definite trend towards narrower or more widely separated dunes and thinner interdunal sand cover in higher northern latitude terrains. This latitudinal correlation could result from a gradual increase in the soil wetness toward the North. A wet soil is indeed less favourable to dune developpement since it requires stronger winds to move sand.

The persistence of a gradual rise in wetness toward the northern latitudes could result from Titan's current orbital configuration: Saturn's eccentric orbit coupled to Titan's solar longitude of perihelion causes southern summers to be both more intense and shorter than northern ones. The less intense northern summers reduce evaporation relative to precipitation, which may increase the dampness of the surface and may well explain the lake distribution dichotomy on Titan [10] as well as the dune morphometry asymmetry. Much like the Croll-Milankovitch cycles on Earth, the asymmetry in Titan's hemispherical seasons is expected to reverse as orbital parameters vary with periods of tens of thousands of years (~32 kyrs).

It remains that the variations observed among Titan's dunes are relatively small which suggests that they were all built at the same time, forming a single generation.

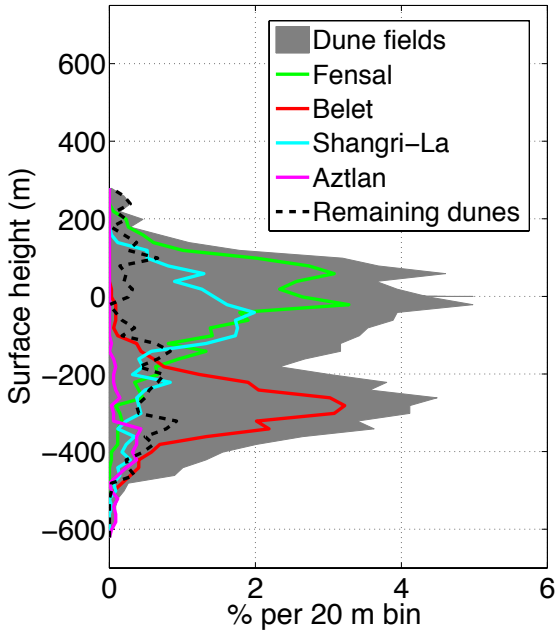

Figure 2: Surface height distributions (with a bin size of 20 m) of all considered dune terrains on Titan (gray), Fensal, Belet, Shangri-La and Aztlan dune regions. The dashed black line represents the height distribution of the remaining dune terrains. The surface heights are referenced to Titan's geoid as defined in [11].

References:

[1] Lorenz, R.D. et al. (2006), Science 329, 519-520 [2] Barnes, J. et al. (2008), Icarus 186, 242-258. [3] Neish, C. et al. (2010), Icarus 208, 385-394. [4] Savage and Radebaugh (2011), LPSC #2530. [5] Lorenz, R.D. et al. (2008), GRL 35, L02206 [6] Le Gall, A. et al. (2011), Icarus 213, 608-624. [7] Stiles et al. (2009), Icarus 202-2, 584-598. [8] Turtle et al. (2011), Science 331, 1414-1417. [9] Le Gall, A. et al. (2012), Icarus 217, 231-242. [10] Aharonson, O. et al. (2009), Nature Geosciences 2. [11] Iess et al. (2010), Science 327.

Timescales of Dune Obliteration and Repair on Titan

Ralph D. Lorenz[1]. [1]Johns Hopkins University Applied Physics Laboratory, 11100 Johns Hopkins Road, Laurel, MD 20723 (Ralph.lorenz@jhuapl.edu)

Abstract:

A process perspective is given on Titan's dunes, by integrating model rates of Aeolian sand transport with modeled and observed rates of pluvial activity on Titan. Heavy low-latitude rainfall likely occurs at ~100-1000yr intervals, but pluvial sediment transport is generally exceeded by Aeolian by a factor of 5-500 if Global Circulation Model winds are adopted and the threshold wind speed is 0.9-1.1m/s.

Introduction:

We find massive seas of sand [1] on Titan. We lack observational data of sufficient resolution to characterize the activity associated with these predominantly linear dunes, although the maintenance of apparently sand-free interdunes implies present-day or at least recent Aeolian transport.

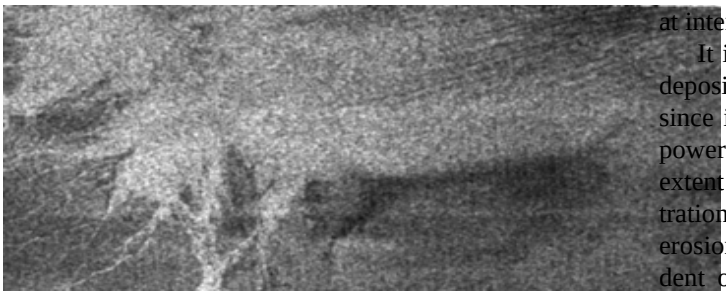

Figure 1. 250kmx150km section of T3 radar image : dunes at right are superposed on bright outwash plain from Elivagar Flumina branching river system. Dunes form in the eastern part away from the rivers - does this imply that rivers outcompete dunes at the left (yes - see discussion on next page).

Although on Mars there is now observational data of sufficient fidelity and resolution [2] to identify ripples have been superposed by small (few m diameter) impact craters, as well as of course many craters that have been superposed by ripples and dunes, on Titan we only have examples of the latter. Atmospheric shielding on Titan essentially eliminates small craters, so the few (~50) craters known are large and thus old. However, while Aeolian and impact craters compete on Mars, fluvial activity is essentially zero in the present-day, whereas Titan is hydrologically-active. Thus dunes compete against rain and rivers on that world. While Aeolian change has not (and likely cannot) be detected with Cassini, the widespread presence of apparently active/unmodified dunes, and the observation of clouds and rain, allow quantification of process rates.

Fluvial Processes:

Cassini has observed two events of surface darkening associated with cloud activity; these are best interpreted as rainfall events. In 2004 Arrakis Planitia (34,000km^2, 80°S) and in 2010 Concordia Regio (510,000km^2, 20°S). Together, these represent ~0.7% of Titan's surface, in 6 years. Crudely, 100% of the surface would then be rained on in 6*100/0.7~860 years [3]. These rates are reassuringly consistent with the notion that ~1cm per Earth year of rain falls on average [4], but that this average reflects infrequent events that correspond to ~1m of rainfall, and that rain occurs preferentially (x10) at the poles, thus in the low latitudes at which dunes are found, there may be ~10s of cm to meters of rainfall in an event a few hours long at intervals of some centuries.

It is of course not a given that even 1m of rainfall deposited in a short time can destroy a duneform : since individual drops fall rather slowly, their erosive power by splash transport is quite modest [4]. The extent to which rain may be simply absorbed by infiltration, versus runoff and thus sheet flow and gully erosion, is essentially unknown (and is likely dependent on a variety of factors such as cementation by solute transport, as is the case on Earth).

By terrestrial analogy, we might consider that on average, pluvial liquid may transport some fraction (say 1-10%) of its volume of loose sediment. If this is the case, then we can simply equate the implied average destructive pluvial effect (~0.01-0.1cm/yr) to the average sand transport rate in order to allow dunes to be preserved.

Sand Transport:

A key difficulty in estimating bulk sand transport rates is that sand transport usually doesn't happen : the saltation threshold is higher than the average winds. Thus the sand transport is a convolution of a skewed windspeed distribution (e.g.[5]) and a windspeed-transport relationship that is typically assumed to be proportional to the cube of windspeed when that speed is above some threshold.

Tokano [6] shows the probability density distribution of windspeeds (noting that the curves for westerly and easterly winds cross - although winds are generally easterly, the fastest winds are more likely to be westerlies (especially around the equinox season): this solves [7] the apparent paradox that low-latitude zonal winds should be predominantly east-west, yet dunes

are observed invariably suggesting west-east transport [8]. Approximately, winds of 1.0m/s are encountered ~0.2% of the time, while 1.2m/s are seen only 0.02%, and 1.4m/s only 0.002%, etc. (these values being referred to 300m altitude.) Essentially, this high-speed tail of the probability distribution is exponential, each 0.2 m/s increment causing an order of magnitude drop in relative frequency.

The sand volume transport rate ($m^3/m/s$) is typically written [5,6] in the form

$q_v \sim 2.6(\rho_a/\rho_d g)(u_* - u_{*t})(u_* + u_{*t})^2$

where u* is the friction speed (assumed to be ~1/25 of the windspeed at 300m.) Note that this expression is roughly linear for winds just above the threshold, but roughly cubic for winds well above the threshold.

Thus if we consider a threshold (300m) speed of 0.9m/s, and add up the contributions of the different fractions of time at different speeds, we find that the major contribution is from winds at 1m/s - the cubic dependence of sand transport due to faster winds is less significant than the exponential rarity of such winds. It therefore follows that the overall (annual-average) sand transport rate is acutely dependent on the choice of threshold. Some simple numerical trials indicate a transport rate, given the wind probabilities above, of ~5cm/yr for a threshold of 0.9 m/s, falling to ~1cm/yr for a threshold of 1.0 m/s, and about half that for a threshold of 1.1 m/s.

The optimum threshold friction speed u_{*t} estimated from the 'classical' empirical expressions [5] is ~4cm/s for 250um particles, or freestream speed of 1.0 m/s. Clearly if cohesion is higher on Titan than Earth, then the threshold would be higher; similarly, pushing the particle size by a factor of two in either direction would increase the threshold by about 20%. A threshold of 1.0m/s seems reasonable. It should also be noted that thresholds of >0.9m/s are required for the net sand transport to be eastwards in Tokano's model, and <1.4m/s to avoid forming transverse, rather than longitudinal, dunes.

Adopting a range of 0.9-1.1 m/s indicates overall transport rates are ~5 to ~500 times higher than the fluvial transports estimated previously, which would be consistent with Aeolian transport generally dominating. If, on the other hand, the threshold were e.g. 1.3 m/s, the transport is ~0.6mm/yr which is likely less than fluvial.

Dune Repair:

The foregoing discussion establishes the likely overall dominance of Aeolian processes. However, pluvial/fluvial effects are episodic on ~1000yr timescales, while sand movement likely occurs seasonally (i.e. every 15 years). If local flow on a dune carves a ~1m deep gully, we might crudely expect it to repair on timescales of ~100 years.

On the other hand, if a dune of height H is washed out (creating a gap H wide) by a river, it can grow back in a timescale $\sim H^2/q_v$: for H=10-100m, this implies timescales of 10kyr-1Myr. Thus a where a streambed width d that can wash 1% of its liquid volume flow away, that drains a watershed of area A, a 1m rainfall can remove .01A/d of material. If we consider Elivagar Flumina (fig.1) with $A \sim 10^5 km^2$ and d~100km, then the sediment that can be removed by a single typical rainfall event corresponds to a 100m high, 100m wide dune. Thus every time it rains here (1kyr) the dunes are destroyed, but take much longer to grow back, and thus the area (especially to the West) remains dune-free. The situation seems rather similar to, for example, the dune-free Sossusvlei gap in the Namib sand sea due to the ephemeral Tsauchab river.

Conclusions :

Relative rates of fluvial/pluvial and Aeolian transport have been considered. The widespread presence of largely unmodified dunes is consistent with continual Aeolian transport and low rain rates, but in areas where rainfall is concentrated by terrain, dunes may be obliterated faster than they can reform. These processes are consistent with GCM winds for saltation thresholds of 0.9-1.1m/s.

Acknowledgement :

This work was supported by the Cassini project.

References

[1] R. Lorenz et al., The Sand Seas of Titan, Science, 312, 724-727, 2006 [2] Golombek et al., Constraints on Ripple Migration and Meridiani Planum from Opportunity and HiRise Observations of fresh craters, Journal of Geophysical Research, 115, E00F08, 2010 [3] Lorenz, R. D. and E. P. Turtle, How Often does it Rain on Titan, LPSC, 2012 [4] Lorenz, R. D. and J. I. Lunine, Erosion on Titan, Icarus, 122, 79-91, 1996 [5] R. D. Lorenz et al.,Prediction of Aeolian Features on Planets : Application to Titan Paleoclimatology, Journal of Geophysical Research (Planets), 88, 26,377-26,386, 1995 [6] Tokano, T., Relevance of fast westerlies at equinox for the eastward elongation of Titan's dunes, Aeolian Research, 2, 113–127, 2010 [7] Lorenz, R. D., Winds of Change on Titan, Science, 329, 519-520, 2010 [8] R. Lorenz and J. Radebaugh, Global pattern of Titan's dunes: Radar survey from the Cassini prime mission, Geophysical Research Letters, 36, L03202, 2009

Observations of Niveo-Aeolian Activity at Great Sand Dunes National Park and Preserve (GSDNPP).

Ralph D. Lorenz[1] and Andrew Valdez[2], [1]Johns Hopkins University Applied Physics Laboratory, 11100 Johns Hopkins Road, Laurel, MD 20723 (Ralph.lorenz@jhuapl.edu) [2]Great Sand Dunes National Park and Preserve, 11500 Highway 150, Mosca, CO 81146-9798, USA

Introduction: Here we report on Aeolian movement of snow and sand at GSDNPP. The site is a large parabolic dune at 37°41'35.30"N 105°35'11.25"W. This area is within GSDNPP but is far from the main dunefield and is not in an area frequented by visitors, nor is it an NPS wilderness area. The site is where the dirt road west from the Lodge on the Desert is blocked by the dune. The interior of the dune has prominent granule ripples that have been the subject of a recent timelapse imaging ripple migration rate study [1].

Buried Snow: During the retrieval of timelapse equipment in January 2011, it was noted that the dune sand was substantially frozen. An interbedded deposit of snow and sand was literally stumbled upon (figure 1) and is investigated here.

Figure 1. Looking down front of parabolic dune, buried snow was encountered beneath a damp rippled patch of sand.

Close examination of the layer (figure 2) shows many fine layers of sand and snow, suggesting alternating snowfall/snow transport and sand transport. The weather records (figure 3) support two main episodes of snowfall. The deposit appears to be ~3 weeks old.

Figure 2. Close inspection shows two principal snow layers, each with sand-rich substrata

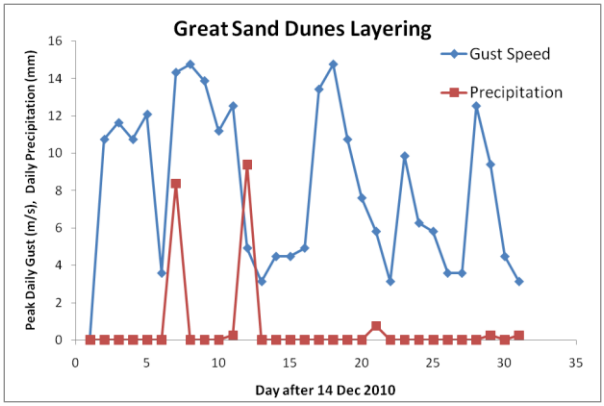

Figure 3. Inspection of weather records at a nearby RAWS station indicates two days of precipitation. Winds exceeded the saltation threshold much of the time.

Mixed blowing sand and snow: During subsequent timelapse imaging, mixed snow/sand movement was observed in action. Images are recorded at 10 minute intervals during daylight by a timelapse digital camera. The camera is mounted about 2.5m above the ground on a fencepost and looks in a downwards-northward direction. A selection of images of combined snow and Aeolian activity follows.

Reference [1] Lorenz, R. D. and A. Valdez Variable Wind Ripple Migration at Great Sand Dunes National Park, Observed by Timelapse Imagery, Geomorphology, 133, 1-10, 2011

.

Figure 4. Initially (Jan 31, 2011) pre-existing sand ripples are highlighted by snow deposition.

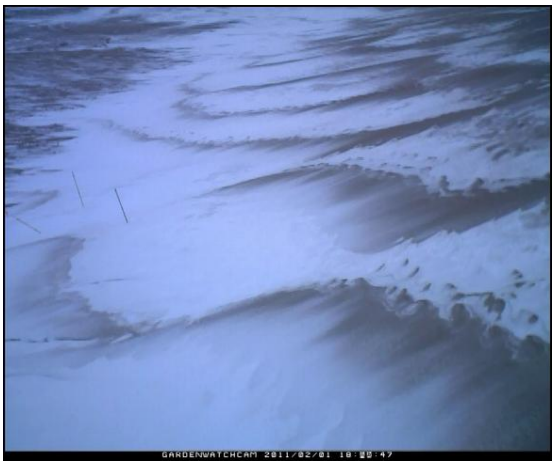

Figure.5 Sand and snow blowing ~08.20am on Feb 1, 2011. The snow forms regular drifts with interbedded layers of snow and sand.

Figure 6. Next day after saltation and overnight snowfall structures are visible as rippled patches at right, despite the uniform albedo. Note coyote tracks.

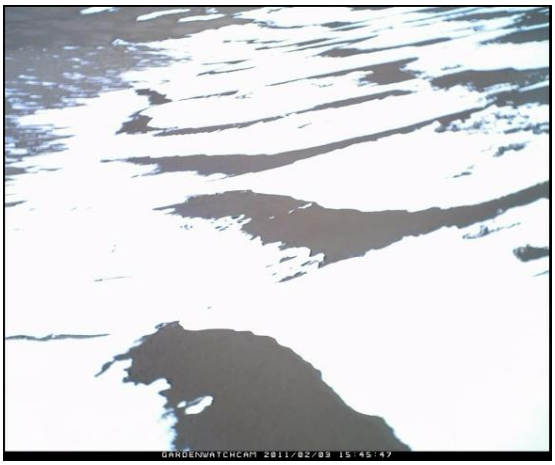

Figure 7. One day later, as snow melts, regular snow patches are left due to snow thickness/texture in the original structures.

Figure 8. Sand deposited with snow, presumably colder and moister, leaves residual regular structures with distinct texture.

Figure 9. A second episode of mixed snow-sand blowing was observed on 8th February

STUDYING MARTIAN DUNE CHANGES WITH HIRISE DTMS AND ORTHOIMAGES. Sarah Mattson[1], N. T. Bridges[2], R. L. Kirk[3], E. Howington-Kraus[3], N. Mogk[1], L. Ojha[1], and the HiRISE Team. [1]Lunar and Planetary Laboratory, University of Arizona, Tucson, AZ, USA (smattson@pirl.lpl.arizona.edu), [2]Space Department, Johns Hopkins University Applied Physics Laboratory, Laurel, MD, USA, [3]Astrogeology Science Center, U. S. Geological Survey, Flagstaff, AZ, USA.

Introduction: Aeolian bedforms are common on Earth and Mars. On Mars, several types of dune forms have been identified [e.g. 1-3]. A current area of research is to understand the state of activity, if any, of the various types of Martian dunes. Dunes composed of relatively dark material have been observed to be active on Mars [4-7]. This fact has been shown with repeat high resolution imaging with the Mars Orbital Camera [8] that operated on Mars Global Surveyor from 1997-2006, and the High Resolution Imaging Science Experiment (HiRISE) operating onboard Mars Reconnaissance Orbiter (MRO) since 2006 [9]. Studies of dune activity with HiRISE images include gully formation, seasonal frost changes, ripple migration and sand flux [5,10-13].

The availability of HiRISE (nominal 25 cm pixel scale) time series images makes the study of Martian dune activity possible. HiRISE stereo image pairs are used to generate Digital Terrain Models (DTMs) of 1 m horizontal scale, with a vertical precision within tens of centimeters [14]. It is important to note that small ripples on dunes are not resolvable in the topography. Repeat images over an area where a DTM has been produced can be orthorectified to that DTM. Time series of these orthoimages are critical to measuring dune activity on Mars. There are many factors to consider in successfully targeting stereo over dunes, producing accurate DTMs, and orthorectifying images for change detection studies.

Targeting HiRISE stereo over dunes: HiRISE stereo images are acquired on different orbits by rolling, or slewing, MRO off-nadir for at least one of the observations. The ideal stereo viewing geometry has a convergence angle of 12º to 25º [12]. The timing of stereo acquisition over dunes should be as close as possible, as we now know that small changes can occur on relatively short time scales [7]. Additionally, changes in lighting between the first and second stereo image are more apparent in small-scale surface textural features such as dune ripples. Successful stereo targeting over dunes also requires sufficient signal-to-noise ratio (SNR), which can be challenging as the surfaces of the dunes tend to be dark and low contrast.

DTM Production: The HiRISE team primarily uses the commercial photogrammetry software SOCET Set (© BAE Systems, Inc.) for terrain extraction and orthorectification, using the processes fully described in [14]. The success of this method depends on inputting stereo images that have high SNR, good contrast, and minimal lighting differences. The surface of dark dunes pose challenges to this method in that they tend to be low contrast, smooth and dark, and also may contain brightly lit, relatively featureless slopes. Additionally, any small changes between the images, such as ripple movement and dust devil tracks, can cause the stereo matching algorithm to fail. SOCET Set provides editing tools to correct the DTM where such failures occur, providing the human operator can identify the ground surface successfully where the automated stereo matching algorithm failed. An additional preprocessing step of taking the difference of Gaussian filters of an image can bring out the ripple and dune feature edges, thereby allowing the SOCET Set stereo matcher more information to correlate to.

Editing DTMs. Improvements in the terrain extraction strategy and editing tools in SOCET Set (as of version 5.5.0) result in better success over bland areas, which cuts down on editing time. Manually editing a DTM is a time-consuming process (a HiRISE DTM contains millions of posts), so it is desirable to balance time spent editing with benefit to the end user. Therefore, editing is devoted primarily to the areas of highest scientific interest. The editing tools that are the most successful on dunes are the area editor with a snap-to-ground algorithm, the area editor using a first order interpolation algorithm, the Triangulated Irregular Network (TIN) editing tool and the geomorphic editing tool. Snap-to-ground works best where the lighting is sufficient and the surface has not changed in the stereo pair, but the stereo matcher failed, causing a large error. This tool re-runs the stereo matcher over a smaller area, isolating failed points, which may result in a much smaller error area (Fig. 1). If successful,

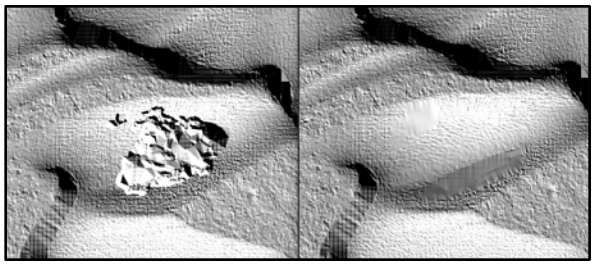

Figure 1. Example of error in the DTM and edits performed with the snap-to-ground and first order interpolation area editing tools in SOCET Set. Detail of HiRISE DTM shaded relief over Nili Patera Dunes, DTEEC_017762_1890_018039_1890_A01 [15].

elevation posts show as well-correlated, not interpolated, terrain. The first order interpolation area tool works well on planar areas, such as the steep flat sides of dunes, where shadows, or slight ripple changes have caused the stereo matcher to fail. The TIN editing tool temporarily converts a given area of the gridded terrain model to a triangulated network, allowing for a better estimation of the surface of the dune shape overall.

Figure of Merit Maps: The quality of the stereo correlation is recorded in an output product from SOCET Set called the Figure of Merit (FOM) map. This map, to be provided in the PDS released HiRISE DTM products [16] in the near future, codes each elevation post with a value indicating correlation quality, and if a post was manually edited or interpolated (Fig. 2). The FOM map is an important piece of information for understanding the quality of the model and any artifacts or errors.

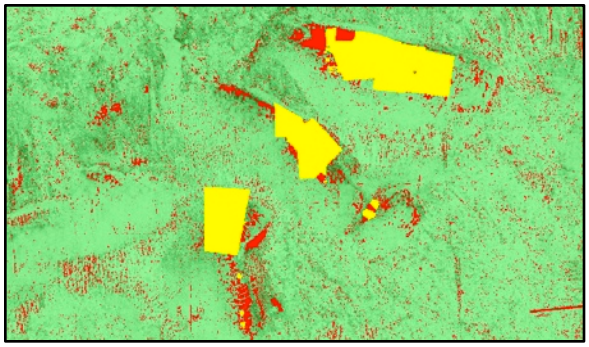

Figure 2. Detail of FOM map for a HiRISE DTM where increasing values of green indicate better correlation, red indicates poor correlation, yellow indicates manually edited or interpolated areas.

Orthoimages: Orthorectification is the reprojection of the image pixels onto the topographic model in order to produce an orthographic (overhead) view from which parallax distortions have been removed. Orthorectification removes the parallax effect caused by topographic features, given that those features are well resolved in the DTM, both horizontally and vertically. The purpose of orthorectification in this context is to facilitate comparison of small scale changes from image to image, without the confusing effects of different viewing geometry. Below the post-spacing of the DTM, parallax effects may not be removed and distortions can even be increased compared to the non-orthorectified image. To derive topography of features at these scales, photoclinometry using nadir or near-nadir images is recommended. The source stereo pair for a DTM is orthorectified at the time of production. Once the DTM is made, any other image acquired over the same area can be orthorectified. We use the same project in SOCET Set to import other images for orthorectification. There is no lighting or geometric observing constraints on such images. Significant lighting differences can make tie point measurements difficult, but the process of orthorectification is not dependent on photometric or geometric similarity of the images. Tie points are measured through all images, using the original stereo pair as a reference. The source stereo pair (which was controlled before DTM production) is held fixed, while the other images are adjusted for alignment. In the case of scenes containing dunes, tie points must be placed in areas that are non-dune material, such as the surrounding bedrock exposures, or any parts of the scene that are not moving or changing. HiRISE orthoimages are produced at two pixel scales: one matching the DTM (usu. 1 m/px), and the other at the nominal mapped full resolution of the source image (usu. 25 cm/px). All orthoimages are georeferenced with the same mapping definition as the DTM. One caveat to using orthoimages that have been rectified to a given DTM is that large changes (i.e. significant dune advancement or gully changes) in the surface will not be accurately shown. This implies that multiple stereo pairs should be acquired to produce DTMs that can effectively measure these topographic changes.

Conclusion: HiRISE DTMs and orthoimages are powerful tools for conducting change detection studies on Mars, particularly of aeolian bedforms. Improvements in DTM production are giving better results, which cuts down on the need for manual editing, although it is typically still required for portions of terrain that include dark dunes. Techniques have been developed by the HiRISE team for orthorectifying sequences of images, specifically using DTMs generated in SOCET Set. These products improve our ability to study Mars in high spatial and temporal resolution, leading to new discoveries about current active processes including dune and ripple movement.

References: [1] Malin, M. C. and K. S. Edgett (2001) *JGR, 106*, 23,429-23,570. [2] Hayward, R. K. et al. (2007) *JGR, 112*, E002943. [3] Balme M. et al. (2011) *Icarus, 213,* 116-130. [4] Bourke M. C. et al. (2008) *Geomorphology, 94,* 247-255. [5] Hansen C. J. et al. (2011) *Science, 331,* 575-578. [6] Bridges N. T. et al. (2012) *Geology, 40,* 31-34. [7] Silvestro S. et al. (2010) *GRL, 37,* L20203. [8] Malin M. and K. Edgett (2001) *JGR, 106,* E10. [9] McEwen A. S. et al. (2007) *JGR, 112,* E05S02. [10] Dundas C. M. et al. (2010) *GRL, 37,* L07202. [11] Diniega S. et al. (2010) *Geology, 38,* 1047-1050. [12] Golombek M. et al. (2010) *JGR, 115,* E00F08. [13] Bridges N. T. et al. (2012) *Nature,* in press. [14] Kirk R. L. et al. (2008) *JGR, 113,* E00A24. [15] http://hirise.lpl.arizona.edu/dtm/dtm.php?ID=ESP_017762_1890. [16] Mattson S. et al. (2011) *LPSC XLII,* abstract #1558.

TOWARDS A BETTER UNDERSTANDING OF LONGER-TERM AEOLIAN PROCESSES ON EARTH VIA DYNAMICAL DOWNSCALING. T. I. Michaels[1], [1]Southwest Research Institute, 1050 Walnut St Suite 300, Boulder, CO 80302, USA, tmichael@boulder.swri.edu.

Introduction: Dunes and other aeolian surface features are the net product of a complex time-series of winds and other surface/atmosphere conditions. Time-scales important to the creation, maintenance, and evolution of such surface features range from less than one second to tens of years or more. In particular, larger-volume particulate bedforms such as dunes often have response/evolution time-scales (i.e., the characteristic time required to significantly change their shape/orientation) that are conveniently measured in months, years, or even decades. Furthermore, conditions that support significant aeolian transport commonly occur only episodically and/or stochastically (e.g., 2 months out of 12, or 1 year out of 4; as opposed to quasi-continuously) – and thus are perhaps best described/characterized by more complex/advanced statistical methods, not simple averages and variances.

Clearly then, understanding the longer-term (months to decades) evolution of dunes and other aeolian surface features requires atmospheric time-series of comparable duration and relevant temporal/spatial resolution. Unfortunately, many locations on Earth that are particularly interesting from an aeolian surface interaction perspective lack any *in situ* (or even nearby) environmental measurements. Even among those sites that do have such information available, the duration, continuity, and/or self-consistency of the data is often less than satisfactory. In spite of numerous limitations, is there a practical way to procure/generate such datasets relevant to aeolian processes from whatever meteorological measurements were gathered/preserved by humankind in years past?

Infused with actual measurements: By the mid-1990s scientific computing capabilities were sufficient to enable the construction of so-called "reanalysis datasets", spanning multiple decades. Examples of such projects include the NCEP/NCAR Reanalysis I (1948-present; [1]), the ECMWF reanalyses (1957-present; [2], [3]), and the NOAA/CIRES 20CRv2 (1871-present; [4]). These datasets are created by running a global numerical weather/climate model forward in time from a past year, folding in all appropriate worldwide historical observational data as it marches forward. In a sense, the model is performing a type of interpolation on the observational data in a manner consistent with known physical principles.

These datasets are lower-resolution, with typical grid-spacings in the 60-240 km range and information every 6 hours. Quality of the reconstruction varies with time and space, with larger uncertainties within observational data "voids" (e.g., the southern Pacific Ocean) and during the pre-meteorological-satellite era (i.e., before 1979). Inherent caveats and limitations aside, such datasets are substantially better than nothing – the focus of this discussion now pivots to "improving" their temporal and spatial resolution.

Increased resolution in time and space: Dynamical downscaling is a process in which higher-resolution limited-area (i.e., not global) numerical weather/climate models are used to better resolve/predict environmental conditions in an area of interest. For the reconstruction of historical conditions, a lower-resolution reanalysis dataset provides initial and boundary conditions for the limited-area mesoscale model – this is known as Type 2 dynamical downscaling (as defined in [5]). This allows important smaller-scale topography and processes to be taken into account, while the solution as a whole remains substantially constrained by the copious historical observational data used to generate the reanalysis dataset.

It has been demonstrated that such a process can yield meaningful information [6] that is unavailable otherwise. The results are infused with and guided by actual measurements, but not unnecessarily limited by them. However, it should be noted that significant amounts of computational time (and related data storage and processing) are required for each area of interest.

Preliminary results: The work presented will concentrate on an area that includes the Grand Falls, Arizona dunes, due to their relevance to the meeting. The historical reanalysis time-series and dynamically downscaled output show important day-to-day, seasonal, and multi-year variabilities in estimated saltation strength, direction, and duration, among other quantities.

References:

[1] Kalnay E. et al. (1996) *Bull. Amer. Met. Soc.*, *77*, 437–470. [2] Uppala, S. et al. (2005) *Quart. J. R. Meteorol. Soc.*, *131*, 2961–3012. [3] Dee D. et al. (2011) *Quart. J. R. Meteorol. Soc.*, *137*, 553–597. [4] Compo G. et al. (2011) *Quart. J. R. Meteorol. Soc.*, *137*, 1–28. [5] Castro C. et al. (2005) *JGR*, *110*, D05108. [6] Feser F. et al. (2011) *Bull. Amer. Met. Soc.*, *September issue*, 1181–1192.

THE PDS4 ARCHIVE: NEW STRUCTURE, NEW POSSIBILITIES

Lynn D. V. Neakrase[1], Lyle Huber[1], Shannon Rees[1], Matias Roybal[1], Reta Beebe[1], Daniel J. Crichton[2], J. Steven Hughes[2], Mitchell K. Gordon[3], Joseph Mafi[4]
[1]Planetary Data System Atmospheres Node, Department of Astronomy, New Mexico State University, Las Cruces, NM 88003
[2]Planetary Data System Engineering Node, Jet Propulsion Laboratory, Pasadena, CA, 91109
[3]Planetary Data System Rings Node, SETI Institute, Mountain View, CA, 94043
[4]Planetary Data System Planetary Plasma Interactions Node, University of California, Los Angeles, CA 90095-1567

Introduction: The NASA Planetary Data System (PDS) is the distributed system of discipline nodes responsible for the archive of all planetary data acquired by robotic missions, manned missions, and observational campaigns through ground/space-based observation systems. Beginning late in 2012, the PDS will be publicly moving from version 3 to version 4 of its archival system. Of greatest concern moving forward is the preservation of the integrity of older data sets, while achieving improved accessibility and streamlined processes for new data entering the archive. Migration of the older data is of the utmost importance while maintaining seamless usability during the transition. New missions, approved for flight after 1 November 2011 will archive under the new standards.

The Past (PDS3): The PDS3 system implemented a label/product duet for each item within the archive [1]. The labels were implemented in the Object Description Language (ODL) developed and maintained by JPL/Caltech (used only by the PDS), which could be used as attached or detached labels. ODL allowed for a human-readable, "KEYWORD = VALUE" structure, that was not always the easiest for software to parse or use efficiently. Directory structures were organized specifically with physical media in mind (e.g., Magnetic Tape, CDs, DVDs, etc.) [1]. Data sets were organized into *volumes* that could easily be written onto physical media, which were designed specifically for transfer from archive to user (or user to user). Retrieval of data was based on search routines maintained by the individual discipline nodes and was not well-suited for overlapping datasets present within the archive in possibly piecemeal fashion between different nodes.

The Future (PDS4): PDS4 is the latest incarnation of the PDS archiving system. With PDS4, many of the perceived problems and shortcomings of the PDS3 system have been addressed. Organization and implementation are designed around the modern idea of all data being delivered to users across internet-based systems. PDS4 is an object-oriented system based on a central core Information Model, from which everything within the system is defined explicitly [2]. This differs greatly from past incarnations and provides continuity across discipline nodes, which has not been present in the past. The catalog system has been replaced by the new central registry, which allows more information to be ingested and tracked across the system. PDS4 is product-centric. A "product" is defined as a label file and the object (data, document, etc.) it describes. The registry allows metadata to be registered across the PDS, allowing better cross-referencing between various data products and between other discipline nodes. This approach also facilitates search and retrieval at the individual product level. The new system replaces the use of ODL (managed by JPL/Caltech, used only by PDS) with the publicly available eXtensible Markup Language (XML)[2,3]. XML is widely accepted as a modern standard for encoding data for use on the Internet by providing enhanced machine readability, focused on simplicity and generality [3]. XML allows publicly available software to use the PDS archive without extensive modification, which should allow for better, more wide-spread usage of PDS data. The first public release of the PDS4 system should be expected in Q4 of 2012.

XML and the PDS: As in many web-based markup languages, XML employs a tag-based system of designating meta-attributes used to distinguish differences in the data [3]. Tags simply bracket the assigned value:

```
<title>This is XML for PDS4</title>
  tag          value          end-tag
```

The tags can be arranged in a specific fashion into a blueprint or *schema* for the entire label. The structure of this schema is determined and generated by the Information Model ensuring that 'valid' labels are 'consistent' with respect to the framework of the Information Model. This approach is a more rigorous approach than in PDS3, in which validation was done by a tool and not against a model.

Contents Organization: PDS4 products are organized into focused "Collections" with separate collections for observational data products, calibration products, browse products, document products, etc. PDS currently identifies nine broad collection types. Related collections are then organized into logical bundles. A bundle, for example, might consist of the collections, which together contain all products from an instrument on a specific mission. Within the Bundle, there could be one collection for raw, calibrated, and reduced data products, or there might be three separate collections (one each for raw, calibrated, and reduced data products), a collection for calibration products, a collection for document products, and a collection for browse products. Different from past iterations, Bundles and collections need not be solely comprised of primary products archived by missions or primary data providers. Specialized communities such as the Dune Database group or Planetary Volcanology groups could create groupings of data that span missions, instruments, and/or targets providing specialized bundles and collections that are useful to associated user communities. These specialized bundles could then be

registered within the PDS4 registry system and made searchable by users worldwide.

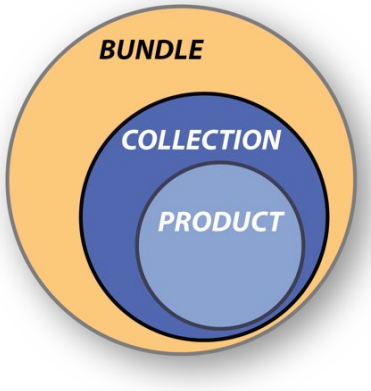

Figure 1. Bundle architecture diagram showing the nested structure for PDS4.

Transitioning to PDS4: In order to be released for public use, the PDS4 system is being tested extensively with previously archived data that are *migrated* into the new system. Exercising many of the new features is a primary goal of migration efforts in late 2011 and early 2012. Many "test-case" holdings, of rather less complicated, complete data sets will be migrated into the new format from end-to-end. Currently migration efforts are occurring across the discipline nodes with the focus on testing all the fundamental data structures. At the Atmospheres Node for example, Python has been employed to bridge the two systems. We've constructed an XML translator that takes the validated blueprints (the schemas) and produces XML label templates and then populates the label by translating PDS3 keyword/value pairs into valid XML tags.

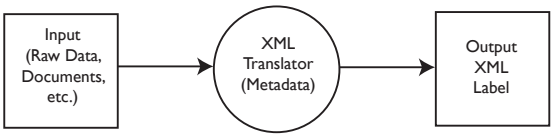

Figure 2. Simplified diagram of the migration process strategy.

This simple modular architecture for migration is also useful for designing data pipelines for new data coming into the PDS as well, in which the input data would be ingested directly from a data provider instead of a PDS3 archived product.

Our strategy has been two-fold using this modular approach as Step 1 and then using progressively more complicated data sets as Step 2. We began testing migration by working with the five atmospheric instruments of the Mars Phoenix Lander mission and have been refining the process over the last year. We chose this mission set because the data types are relatively simple, well-behaved files (ASCII tables or in PDS4 terminology, Table_Character objects), and the mission is finished. We have moved on to prototype binary table files from recently archived (restored) Galileo UVS/EUV data, and simple FITS images from a ground-based observing campaign for Jupiter and Saturn.

Conclusions: PDS4 allows the PDS Archive to begin to transition into a modern, efficient system by using XML as the implementation of a product-centric, object-oriented, Information Model approach. We see this as being an improvement over previous versions of the archive as well as a step in the right direction for moving PDS into the future.

References: [1] PDS Standards Reference, version 3.8 (2009); [2] Data Preparers Handbook, version 4.0, *in prep.*; [3] Extensible Markup Language, http://www.w3.org/XML, (2011)

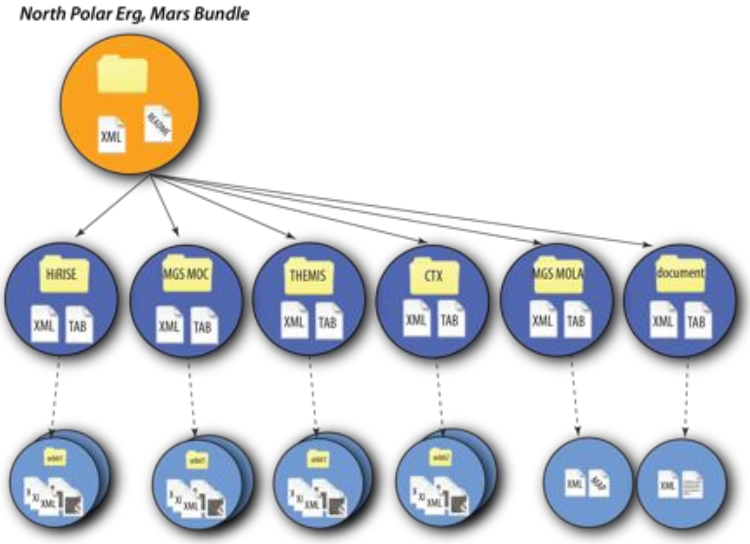

Figure 3. An example of a specific bundle for a hypothetical grouping of data pertaining to the North Polar Erg on Mars. The bundle would consist of XML file listing the member collections and perhaps a description README file. Each member collection would be an XML list of its products, which would contain pointers to the permanent location of the primary files. Bundles like this could help in organization of research across disciplines for common targets of interest within specific communities and could be searchable under the new PDS4 architecture.

GENERAL CIRCULATION MODEL PREDICTIONS OF DUNES ON MARS AND TITAN USING PLANETWRF. C. E. Newman[1], M. I. Richardson[1], N. Lancaster[2] and D. M. Rubin[3], [1]Ashima Research (600 S. Lake Ave., Ste. 104, Pasadena, CA 91106, USA; claire@ashimaresearch.com), [2]Desert Research Institute, [3]US Geological Survey Pacific Science Center.

Introduction: Over the past decade, high-resolution imaging of Mars and Titan has revealed unprecedented detail of dune features on their surfaces. A Mars Global Digital Dunes Database (MGD[3]) is now available and covers much of the martian surface [1], and Cassini Radar continues to improve our coverage of dunes on Titan [2].

At the same time, General Circulation Models (GCMs) of Mars and Titan's atmospheres have continued to improve, as increased datasets and increased understanding leads to improved representations of physical processes in these models and hence increased realism. These GCMs simulate the near-surface wind field that is so critical to the distribution of sediment on the surface and the formation of dunes, and hence to dune locations and morphologies.

Predicting dune features using GCM winds: Dunes represent the time-integrated result of a non-linear, threshold-dependent, wind-driven process (particle saltation). For this reason, while dune orientations can be used to *guess* the dominant wind direction(s), a far better approach is to *predict* the wind regime and use this to predict dune orientations, with a good match to observations thus providing confidence in the predicted winds. The Gross Bedform-Normal Transport (GBNT) approach [3] provides a way of predicting dune orientations given the long-term wind field as either measured or as predicted by numerical models. Using GCM winds to predict dune orientations in this way is relatively new, but is starting to be applied to Mars [4] and Titan [5]. The GBNT approach uses the idea that dunes grow via particle transport perpendicular to their crests in *either* direction, thus looks for the crest orientation with the greatest *gross* particle transport perpendicular to it over a long time period. Other dune characteristics that may be compared to GCM predictions include the dune-centroid azimuth, which should be related to the predicted resultant (*i.e.*, the net rather than gross) sediment transport direction.

Dune observations may thus be used to test or 'validate' the GCM-simulated winds, which is particularly useful for planetary bodies in the almost total absence of *in situ* observations of the near-surface environment. Disagreement between predictions and observations may be due to a variety of causes. For example: the GCM is missing (or incorrectly representing) some key physical process (*e.g.* dust storms) that strongly affects peak near-surface winds and hence saltation rates; the resolution of the GCM is insufficient to capture high-resolution features (especially topography) critical to the near-surface wind regime; the dunes formed in a past orbital epoch when the circulation was quite different; the dunes formed in cohesive rather than loose sediment; *et cetera*.

The GCMs used in this work: MarsWRF and TitanWRF are respectively the Mars and Titan versions of the planetWRF GCM, and both are described in detail in [6]. The impact of resolution on MarsWRF's predictions of the martian atmosphere is discussed in [7], with special emphasis on the impact on saltation processes. Recent results from TitanWRF, which include the maintenance of realistic superrotation in the stratosphere due to large but rather infrequent equatorward eddy transports of angular momentum, are described in [8].

Nesting in planetWRF: Crucial to this work is planetWRF's ability to embed or 'nest' high-resolution regions within the global domain. The simulation thus captures highly localized, small-scale flows (*e.g.* associated with topography) yet also feels the effects of the larger-scale circulation (*e.g.* mean meridional winds; thermal tides) in a wholly consistent manner. This nesting capability is thus far superior to running a limited area (or 'mesoscale') model which is not forced by a GCM, and is also superior to running a separate model that *is* forced by a GCM, as in planetWRF feedbacks are possible between the nested region and global domain ('two-way nesting').

Global, low-resolution predictions of dunes: We will present GCM global predictions of dune resultant transport directions and bedform orientations at 5° and 2° horizontal resolution for Titan and Mars respectively, and compare our results with available observations, discussing the limitations and usefulness of this relatively low-resolution approach. For Mars, we will also present results for (i) varying dust storm conditions and also (ii) at higher orbital obliquities, to explore whether areas of strong disagreement with observations show significant improvement in each case.

Mesoscale predictions of dunes: We will also present high-resolution predictions of dune resultant transport directions and bedform orientations at ~10s of km horizontal resolution for locations on Mars. Figure 1 shows preliminary results for a present day Gale Crater simulation. Surface winds were output every Mars minute over an entire martian year from the innermost

nermost of three nests centered on Gale Crater (each nest having increasingly high resolution). The black arrows show the resultant transport direction predicted using the modeled winds to predict the net sand flux over the year, and assuming a saltation threshold of zero (*i.e.*, with no threshold requirement for sand transport). The white lines show the predicted bedform orientation using the GBNT approach (*i.e.*, the white lines are aligned with the predicted dune crest).

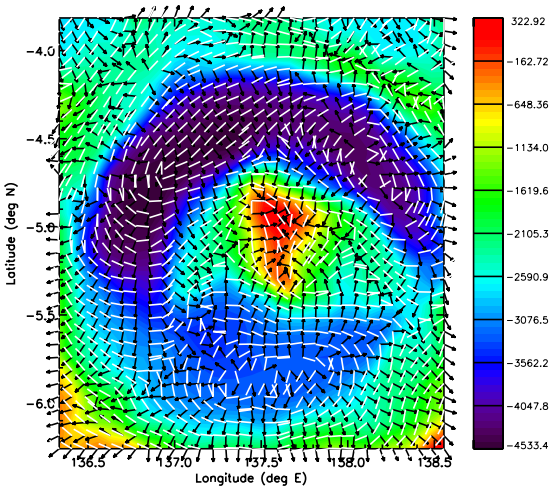

Figure 1: The black arrows show resultant transport directions, and the white lines predicted bedform orientations, predicted using near-surface winds simulated in a MarsWRF nest over Gale Crater. Topography (in m above the geoid) is shown as background shading. See text for more details.

In most regions, the dune crests are oriented almost perpendicular to the resultant transport direction, indicating that transverse dunes are expected to dominate. In our presentation we will discuss the agreement with observations, how it is impacted by changing the assumed saltation threshold, and how it is affected by varying the planet's obliquity or the dust loading of the atmosphere, focusing on whether such changes remove any areas of strong disagreement with observations.

References:

[1] Hayward R. K. et al. (2007), *J. Geophys. Res.*, 112: E11007, doi:10.1029/2007JE002943.

[2] Radebaugh J. et al. (2008), *Icarus*, 194, 2, 690–703.

[3] Rubin D. M. and Hunter R. E. (1987), *Science*, 237, 276-278.

[4] Christian S. and Kocurek G. (2012), *LPS XLIII,* Abstract #1402.

[5] Tokano T. (2011), *Aeolian Res.*, 2, 113-127.

[6] Richardson M. I. et al. (2007), *J. Geophys. Res.*, 112, E09001, doi:10.1029/2006JE002825.

[7] Toigo A. D. et al. (2012), submitted to *Icarus*.

[8] Newman C. E. et al. (2011), *Icarus*, 213, 636-654.

THERMAL EFFECTS OF PHYSICAL HETEROGENEITY IN OLYMPIA UNDAE. N. E. Putzig [1,†], L. M. Bowers[2], M. T. Mellon [1], K. E. Herkenhoff [3], and R. J. Phillips [1]. [1] Southwest Research Institute, Boulder, CO; [2] University of Colorado, Boulder, CO; [3] United States Geological Survey, Flagstaff, AZ. [†] Contact: nathaniel@putzig.com.

Synopsis: The vast dune fields of Olympia Undae exhibit anomalous thermal properties, which led earlier workers to suggest that the dunes are composed of sand-sized agglomerations of dust. More recently, it has been shown that the thermal discrepancy is consistent with ~20 cm of normal basaltic sand overlying shallow ground ice [1,2]. Here, we show that the horizontal mixtures of materials observed in the erg and the slopes of the dune facets are not significant contributors to the thermal behavior. We also find that thermal inertia derived from morning THEMIS images is consistent with that derived from MGS-TES observations and provides a substantial improvement in lateral resolution. Unfortunately, afternoon THEMIS imaging occurs at times of day that precludes deriving unique values of thermal inertia.

Background: Dark dune fields collectively known as the circum-polar erg surround the north polar layered deposits, features which have been linked to climate variations [3,4]. Neutron data suggest that water ice is present within a meter of the erg's surface [5], providing an additional constraint on climate. In Olympia Undae, low values of thermal inertia (~75 tiu, where tiu ≡ J m^{-2} K^{-1} $s^{-1/2}$) suggestive of dust-sized rather than sand-sized grains are reported from both Viking [6,7] and TES [1]. Dunes of similar morphology, color, and albedo at lower latitudes [8] have thermal inertia (~250 tiu) consistent with sand-sized basaltic grains [9,10,11]. An earlier solution to this discrepancy involving the bonding of fines into larger, low-density aggregate particles capable of forming dunes [12,13] has been obviated by the revelation from thermal models [14,15] that heterogeneous surfaces may produce anomalous thermal behavior, including apparent thermal inertia values lower than the intrinsic thermal inertia of model components. Thus, the current explanation for the thermal properties of the erg allows that they are in fact formed of ordinary basaltic sand (perhaps with a varying admixture of gypsum [16]) that is ice-cemented at depth with an ice-free surface layer. This geometry is capable of producing very low values of apparent thermal inertia [17,1].

Horizontal heterogeneity in Olympia Undae: While the earlier modeling work [1] included a qualitative assessment of the thermal effects of horizontal mixtures of materials, a more quantitative analysis and the inclusion of the effects of slope was needed to evaluate the thermal effects of these features.

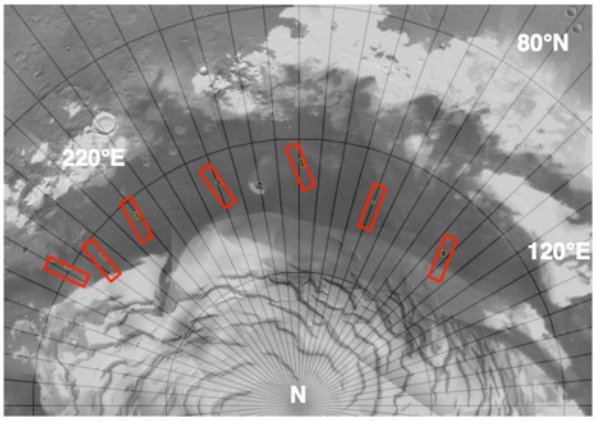

Figure 1. Location map of HiRISE images within Olympia Undae. Background is MOC wide-angle mosaic overlain on MOLA shaded relief. From [18].

Using a representative set of HiRISE images of the erg (e.g., Fig. 1), we measured the relative area of light-toned inter-dune deposits and the orientation of crest lines (Fig. 2). MOLA data and terrestrial observations were used to constrain the dune-face slope angles (a HiRISE DEM for the dunes should be available soon). Interdune deposits cover ~2–8% of the surface area and crest lines are consistently oriented across Olympia Undae at an azimuth of 350° ± 20°. MOLA provides a lower bound on slope angle of 2°–3° and terrestrial studies show angles of repose anywhere from 15° to 45°, depending on the dune materials.

The small area of interdune deposits will have a minimal effect on apparent thermal inertia [14]. Depending on the slope angle, the geometry of the dunes will have a more substantial effect. However, we

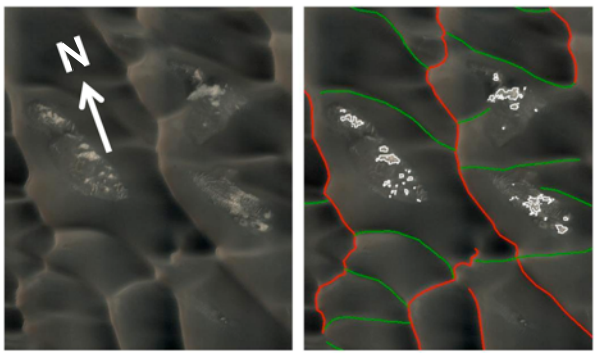

Figure 2. Section of HiRISE image PSP_001432_2610 showing dune crests and inter-dune deposits within Olympia Undae. From [18].

find that potential deviations in apparent thermal inertia induced by slopes oriented as those in the erg have the opposite sense to the observed values (Fig. 3). Thus, these other forms of heterogeneity are not major factors, and the layering of dry sand over an ice-cemented substrate remains the most viable explanation of the observed thermal behavior.

THEMIS thermal inertia: At 100 m/pixel, THEMIS images provide higher spatial resolution than TES (~3 km/pixel), and may enable better discrimination between heterogeneity models. To that end, we derived thermal inertia from THEMIS Band 9 images of Olympia Undae. In earlier work, we had found that such THEMIS results were equivocal [1], with morning observations showing only a rough correlation to TES results and afternoon observations producing extremely high values of doubtful accuracy. In 2009, the Mars Odyssey orbit was moved to an earlier local time, with equator crossings now at about 3:30AM and 3:30PM. During Mars Year 30, the first after the orbit change, afternoon images were acquired over a broad range of seasons, but morning imaging was restricted to late summer (L_S 171–182). Upon deriving thermal inertia for the new images, we find that the afternoon results remain of little use. The erg's high latitude and the spacecraft's inclination combine to place local times near 5:15PM, still a poor time of day for thermal inertia derivation (Fig. 4). Despite the restricted season of the morning images, we find a good correspondence between their results and those of TES at the same season (Fig. 5). Thermal modeling suggests that CO_2 may be freezing diurnally at these seasons (Fig. 4). We have requested acquisition of morning THEMIS images in MY31 during L_S 140–160, hoping to obtain more optimal seasonal coverage.

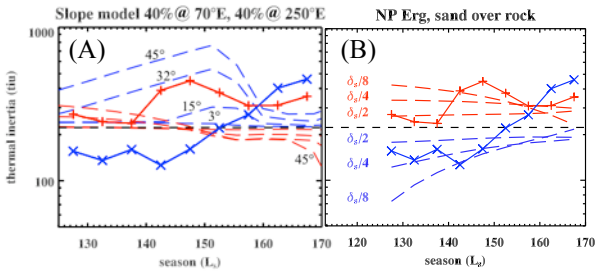

Figure 3. Seasonal apparent thermal inertia as derived from TES data (solid lines and symbols) and as derived from model dune surfaces for the site shown in Fig. 2. (A). Models with various slope angles. Deviations from the model sand value (225 tiu) are progressively larger for greater slope angles, and the sense of deviation for nightside (blue) and dayside (red) differs strongly from the TES-observed behavior, indicating that the dune slopes are not responsible for the thermal anomaly. (B). Models with various thicknesses of dry sand over "rock" (i.e., ice-cemented sand). Best fit to TES data is a dry layer of ~ $\delta_S/4$ (18 cm).

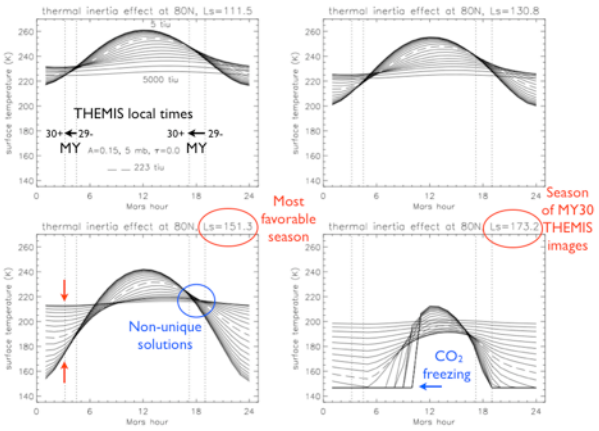

Figure 4. Model temperature at 80°N for a range of thermal inertia at 4 seasons. THEMIS PM image times yield non-unique solutions before and after the Odyssey orbit change. The optimal season for morning images is near L_S 150 when curve separations are greatest (red arrows). AM imaging in MY30 may include frost cover for surfaces of low thermal inertia (blue arrow).

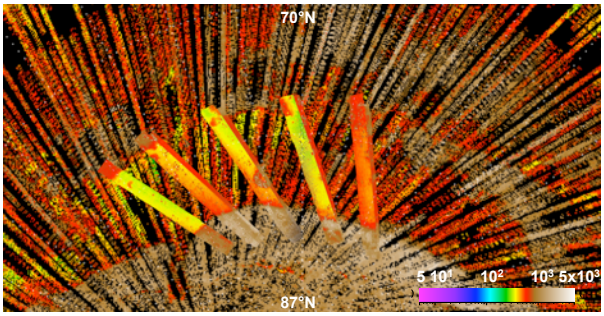

Figure 5. Map of apparent thermal inertia as derived from TES data (background) for L_S 170–180, overlain with images of thermal inertia derived from morning (~3:15AM) THEMIS images acquired in Mars Year 30.

References: [1] Putzig N.E. et al. (2010) *Second Dunes Workshop*, LPI Cont. No 2037. [2] Titus T.N. et al. (2011) *Fifth Mars Polar Sci. Conf.*, LPI Cont. No. 1323.[3] Thomas P. et al. (1992) in: *Mars*, Kieffer H.H. et al. (1992) U. AZ Press. [4] Clifford S.M. et al. (2000) *Icarus 144*, 210–242. [5] Feldman W.C. et al. (2008) *Icarus* 196, 422-432. [6] Paige D.A. et al. (1994) *JGR 99*, 25,959–25,991. [7] Vasavada A.R. et al. (2000) *JGR 105*, 6961–6969.[8] Thomas P. & Weitz C. (1989) *Icarus 81*, 185-215. [9] Sagan C. & Bagnold R.A. (1975) *Icarus 26*, 209-218. [10] El-Baz F. et al. (1979) *JGR 84*, 8205-8221. [11] Breed C.S. et al. (1979) *JGR 84*, 8183-8204. [12] Herkenhoff K.E. & Vasavada A.R. (1999) *JGR 104*, 16,487–16,500. [13] Cutts J.A. et al. (1976) *Science 194*, 1329-1337. [14] Putzig N.E. & Mellon M.T. (2007) *Icarus 191*, 52-67. [15] Mellon M.T. & Putzig N.E. (2007) *LPS XXXVIII*, Abstract #2184. [16] Horgan et al. (2009) *JGR* 114, E01005. [17] Putzig N.E. & Mellon M.T. (2007) *Icarus 191*, 68-94. [18] Bowers L.M. and Putzig N.E (2011) *LPS LXII*, Abstract 2819.

DUNES ON TITAN AT THE BEGINNING OF THE CASSINI SOLSTICE MISSION. J. Radebaugh[1], R. D. Lorenz[2] and A. Le Gall[3], [1]Department of Geological Sciences, Brigham Young University, Provo, UT 84602, janirad@byu.edu, [2]Johns Hopkins University Applied Physics Laboratory, Laurel, MD, [3]Laboratoire Atmosphères, Milieux, Observations Spatiales (LATMOS-UVSQ), Paris, France.

Introduction: Dunes on Titan, a dominant landform comprising 12-20% of the surface, represent the end product of many surface processes acting in foreign conditions. Winds in a nitrogen-rich atmosphere with Earth-like pressure transport sand that is likely to have been derived from complex organics produced in the atmosphere. These sands then accumulate into large linear dunes in planet-encircling sand seas concentrated near the equator.

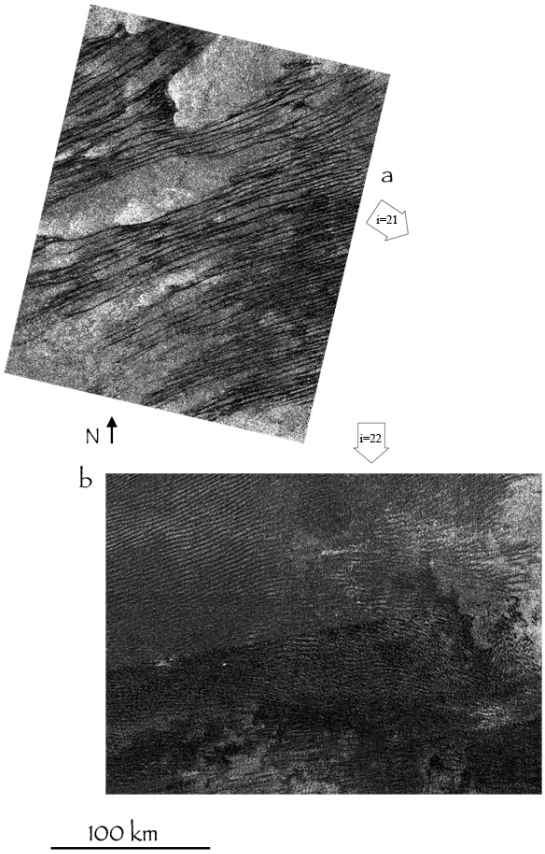

Fig. 1. Dunes on Titan from high latitudes (a) where interdune fraction is high, and from low-latitude sand-rich seas.

Dune Morphology and Distribution: Dunes on Titan are found between 30° N and S latitude and nearly encircle the globe at the equator [1,2,3]. They are generally organized into large sand seas, regions of relatively high sand volume. Dunes on Titan generally appear as SAR-dark lines against muted or bright substrate (Fig. 1) because dune sands are absorbing to the SAR signal. The dunes are predominantly linear in form, being parallel over great distances with lengths much greater than widths. Linear dunes comprise an estimated 50% of all dunes on Earth and fill much of the vast Saharan, South West African, Australian, and Saudi Arabian deserts [4]. From 6000 measurements of dunes across Titan, dunes are 0.7-3.8 km wide with a mean of 1.3 km (SD 0.4), and are spaced 1.6-5 km with a mean of 2.9 km (SD 0.5 km) [5]. These sizes and spacings are comparable to the largest terrestrial linear dune sizes and spacings [6].

Dune Sand Origin and Composition: Given that dune morphologies on Titan are so similar to those of linear dunes on Earth, it is assumed these dunes are formed by saltation of sand-sized particles. Morphologies are not consistent with these features being erosional, rather than depositional forms, such as yardangs, which may be carved out of fine, cohesive sediments. Dunes in general are formed by saltation of a narrow range of particle sizes, given that fine particles are either suspended and removed or remain anchored to the bed, and coarse particles are too large to be lofted or rolled by winds. Dune sands on Titan are likely indeed sand-sized, slightly smaller than for most dunes on Earth at ~0.06 to 0.25 mm [7], this being the optimal size for saltation in Titan's gravity (1/7 Earth) and air density (4x Earth) assuming particle cohesion is similar on the two bodies.

Material compositions on Titan's surface have been difficult to constrain, not least because spectroscopy is hampered by atmospheric absorptions [8]. Titan's dune sands, based on observations and modeling, are thought to be composed of complex hydrocarbons and/or nitriles ultimately derived from atmospheric haze particles [9,10]. Dune sands are dark to visible and near-IR instruments, and their spectra from VIMS are consistent with organics [11,9,12]. In addition, microwave radiometry [13] implies a bulk dielectric constant more consistent with organics than with water ice.

Most dunes on Earth derive their sediments from fluvial and deltaic deposits, ultimately eroded from bedrock, although other sources can include dry lake bed deposits, beaches, and interdunes within the dune regions [14]. It is known that a constant organic `snow' from Titan's atmosphere must lead to vast deposits of organic solids on Titan's surface [10]. These may form sedimentary layers that become hardened, through sintering or diagenesis via an introduced, organic cement, and then eroded by methane rainfall and channel formation into particulate sands. These sands may be carried by eolian or fluvial processes to sand sinks, either regional topographic lows or wind traps, and then blown into dunes by globe-encircling winds [15].

Another sand source may be lake beds that dry seasonally, exposing sediments to erosion and transport by wind [16,17,18].

Wind Directions: Dunes on Earth and other planets have been used as regional wind indicators, given their direct morphological relationship with dominant winds. Dunes on Titan are classified as linear, based on the commonalities in their morphologies compared with this dune type on Earth [7,19]. Linear dunes can form from at least two different wind conditions, wide unimodal winds, coming from one broad direction and blowing down the dune long axis [e.g., 20], or bimodal winds, wherein at least two strong winds blow from widely separated (>90°) directions [e.g., 21]. Controlled experiments and numerical models by Reffet et al. [22] reveal that bimodal winds separated by at least 130° generate longitudinal dune forms, and that sand transport occurs down the dune long axis. It is generally agreed upon that even wide unimodal wind regimes have important seasonal winds from different directions [23], and that the time-averaged vector sum of winds, weighted by strength, in the bimodal wind model is generally down the dune long axis [6]. Thus, it has been assumed that strength-weighted-time-averaged winds are parallel to Titan's dunes and that sand transport occurs in the direction of mean wind flow [15,12,19,2]. Measurements of the long axes of over 16,000 dunes covering ~4% of the surface revealed Titan's dunes are broadly parallel with lines of latitude across the globe, with variations of about 30° on their orientation of 90° from north [2]. The mean direction of wind flow, globally to the east, was determined from the interaction of dunes with topographic obstacles [15,2,19]. This is in agreement with the model by Tokano [24] that allows for fast westerlies near the surface seasonally.

Dune Maturity and Climate: Morphological studies, in the form of pattern analysis of various dune parameters, are starting to yield important results concerning dune field maturity on Earth and other planets [e.g., 25]. The strength in these studies for planetary surfaces is that many characteristics of a region can be determined from spatial analyses alone. If Titan has undergone a recent change in climate or wind direction, for example, superposed forms or variations in overall size would be evidence of this change. At Cassini Radar's resolution of 300 m at best (capable of resolving intermediate to large forms), with the exception of disrupted or cross-cutting forms seen upwind of some obstacles, very few superposed forms are evident in dune fields on Titan. Preliminary studies of dune parameters numerically corroborate this observation [5]. Interdune fraction, the ratio of interdune width to dune spacing, increases toward the north, indicating sand availability is decreased northward, and perhaps dunes are restricted from movement. It is possible moisture increases toward the north, as indicated by vast lakes and seas at the north pole, and that the liquids help stabilize the dunes [16,26].

The uniformity of dune type across Titan, coupled with emerging pattern analysis results, indicate dunes on Titan may reside in an equilibrium condition that has persisted for a long time. Sand seas are relatively long lived on Earth, as the transport and accumulation of sand can occur over tens of thousands of years in some regions, in many cases episodically [6]. Just how these processes might scale to Titan conditions of lower atmospheric energies and other parameters is the subject of current modeling [e.g., 16].

Dunes are the result of a long sequence of surface evolutionary processes, including atmospheric chemisty, volcanism/tectonism, formation of sedimentary layers, erosion by rainfall, erosion by wave action, fluvial transport, and finally atmospheric dynamical processes. They are relatively ephemeral, and thus highlight current processes. Dunes on Titan can therefore reveal many aspects of past and present processes on the surface of Titan.

References: [1] Elachi, C. et al. (2006) *Nature* 441. [2] Lorenz, R.D. and J. Radebaugh (2009) *Geophys. Res. Lett.* 36, L03202. [3] Le Gall, A. et al. (2011) *Icarus* 213. [4] Lancaster, N. (1982) *Prog. Phys. Geog* 6. [5] Savage, C. (2011) Thesis, BYU. [6] Lancaster, N. (1995) The Geomorphology of Desert Dunes, 290 pp. [7] Lorenz, R. D. et al. (2006) *Science* 312, 724-727. [8] Griffith, C.A. et al. (1991) *Icarus* 93. [9] Soderblom, L. et al (2007) *Planetary and Space Science* 55. [10] Clark, R.N. et al. (2010) *J. Geophys. Res.* 115. [11] Porco, C.C. et al. (2005) *Nature* 434. [12] Barnes, J.W. et al. (2008) *Icarus* 195. [13] Janssen, M.A. et al. (2009) *Icarus* 200. [14] Kocurek, G. et al. (1991) *Sedimentology* 38. [15] Radebaugh, J. et al. (2008) *Icarus* 194, 690-703. [16] Aharonson, O. et al. (2009) *Nature Geoscience* 2, 851-854. [17] Lorenz, R.D. (2010) *Science* 329. [18] Barnes, J.W. et al. (2011) *Icarus* 216. [19] Radebaugh, J. et al. (2010) *Geomorphology* 121, 122-132. [20] Fryberger, S.G. and G. Dean (1979) U.S. Geol. Surv. Prof. Pap. 1052. [21] Rubin, D.M. and H. Ikeda (1990) *Sedimentology* 37. [22] Reffet, E. et al. (2010) *Geology* 38. [23] Lancaster 1981. [24] Tokano, T. (2010) *Aeolian Research* 2. [25] Ewing, R.C. et al. (2010) *J. Geophys. Res* 115. [26] Le Gall, A. et al. (2012) *Icarus* 217.

EVOLUTION OF LABORATORY DUNEFIELDS ANALOGS. E. Reffet[1,2,3], S. Courrech du Pont[3], P. Hersen[3], S. Douady[3]. [1]Laboratoire AIM Paris-Saclay, Université Paris-Diderot CEA/Irfu CNRS/INSU, F-91191 Gif-sur-Yvette. [2]LESIA, Université Paris-Diderot / Observatoire de Paris / CNRS, 92195 Meudon, France. [3]Laboratoire MSC, Université Paris-Diderot / CNRS, 75013 Paris, France. (reffet.erwan@gmail.com / erwan.reffet@cea.fr)

Introduction : Dunes result of the complex interaction of the wind regime with the topography of the dunes themselves. Variations of wind strength and direction are responsible for the types of morphologies sculpted and the evolution of dunefields. In the field, for the aeolian case, the time-scales involved in their evolution from their initial states to a mature dunefield make it difficult to have access to the whole history of the sandbed. When the study of the dunes stratigraphy gives access to a part of their history [1,2], laboratory and numerical modeling can provide the whole time-line for ideal case-study analogs that can be used to complete and better understand the ground truth observations. Recent works, whether experimental or numerical, have allowed to study and constrain the relation between dunes morphology and wind regime under controlled conditions [3,4,5,6,7]. However, the evolution of dunefields has been rarely studied using these new tools so far. Here, laboratory experiments have been realized to form dunefields under symmetrical bidirectional wind regimes, i.e with a wind switching between 2 distinct directions of identical weight. The evolution of these experimental dunefields has been monitored.

Data: The experimental setup consists of a moving baseplate immersed in a water tank. By conducting the experiments underwater, the typical length-scale and consequently the corresponding time-scale of evolution are reduced and centimeter-scale dunes analogs are formed [4,8]. The motion of the baseplate produces a unidirectional wind by successive strokes combining a fast active translation phase to a slow translation to bring it back to its initial position. A disk on which the sand is placed and which orientation can be modified is located in the middle of the baseplate. By changing its orientation, respectively to the direction of the translation of the baseplate, the direction of the simulated wind can be selected. This setup allows then to apply controlled wind regimes that can be tuned at will by choosing the orientations of the wind relative to the sandbed and the number of strokes spent in each of these orientations. Here, a set of laboratory experiments has been conducted for a wind regime composed of 2 wind directions of same number of strokes. The influence of θ, the angular separation between the 2 directions of wind, has been explored for values ranging from 0° to 172°. The evolution of an initial flat sandbed under these conditions of winds and without external sand flux has been monitored.

Dunefields evolution : In agreement with previous works, transverse and longitudinal dunefields are formed for small and large angular separations respectively. For intermediate values of θ, both transverse and longitudinal structures are clearly observed within the same sandbed and squared pattern dunefields are formed. For all of the angular separations, the evolution of the dunefields is accompanied by the growth of the amplitude of the dunes, the coherence of the dune pattern and of its main wavelength. However, one can notice that longitudinal structures develop more rapidly than transverse ones until saturation is eventually reached. The evolution of the main wavelength, taken before the saturation, is presented in figure 1 and illustrates this difference of coarsening rate.

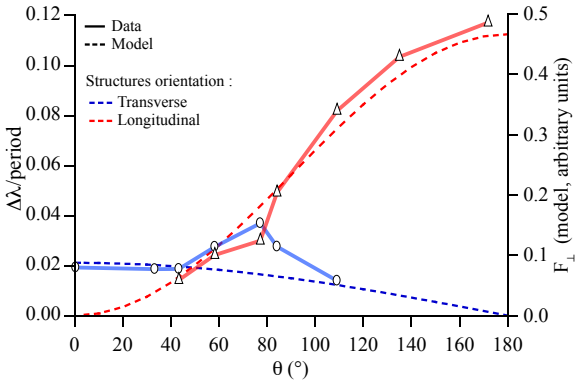

Figure 1: Variation of the wavelength in transverse and longitudinal modes for various values of θ, the angular separation between the 2 directions of wind. The observed slower evolution of the transverse structures in comparison to evolution of the longitudinal can be understood using a simple model.

The coarsening of a dune is proportional to the flux perpendicular to its crest. In order to explain the observed asymmetric behavior, the role of the angular separation in this perpendicular flux appears not suffi-

cient. One has to also consider the role of the slope of the dune viewed by the wind in the contribution to the flux feeding the dune and therefore participating to its growth. In the case of transverse structures, the wind blows always on the back of the dunes which is more adapted to the wind. On the contrary, it changes periodically of side for longitudinal dunes and blows on the slipface developed under the previous wind orientation. The slipface is steeper than the back of the dune and is not adapted to the current wind direction. This higher slope viewed by the wind implies more efficiency to make the structures grow. In a first order approach, this perpendicular flux can therefore be written, for the transverse and longitudinal structures respectively, as $f_{\perp}^{T} \propto \cos(\theta/2) \times \cos(\theta/2)\tan(\mu_b)$ and $f_{\perp}^{L} \propto \sin(\theta/2) \times \sin(\theta/2)\tan(\mu_s)$, where μ_b is the slope of the back of the dune and μ_s the slope of its slipface. This model is compared to the experimental data in figure 1 for the values of μ_b and μ_s measured in our experiments. This simple model provides a satisfactory match to the difference observed between transverse and longitudinal structures. However, one has to notice that this is valid because the period duration of the wind regime used here is small in comparison to the time of adaptation of the dunes to a change in wind conditions. For longer period durations, as the slope of the dunes evolves as the wind blows and the dunes adapt to the current wind direction, the expressions are likely to be more complex. Nevertheless, this simple model suggests that longitudinal structures will develop more rapidly and could be predominant even for angular separations smaller than 90° for small period durations. For longer periods, a more symmetrical behavior relatively to $\theta/2$ is expected with a coarsening of longitudinal structures of the same order than the one observed for their transverse counterparts.

Conclusion : The evolution of dunefields produced in the laboratory for symmetrical bidirectional wind regimes has been followed. Based on indicators of the evolution such as the wavelength, the laboratory experiments suggest that transverse and longitudinal structures within dunefields develop at different rates under symmetrical bidirectional wind regimes. The longitudinal structures appear to grow faster than transverse ones. For the former, the larger is the angular separation between the wind and the more the pattern evolves rapidly. This distinction can be understood by the consideration of the wind efficiency and the resulting sand flux that feeds the structures. A simple model taking into account the slope of the dunes viewed by the wind for the various angular separations reproduces convincingly the observed ratio measured between the growth of the wavelength of transverse and longitudinal structures. This discrepancy in coarsening will depend on the angular separation between wind directions and the duration of the period of the wind regime. One of the consequences, is the potential variation of the transition angle between a dunefield mainly composed of transverse dunes and a dunefield dominated by longitudinal structures. It will be particularly interesting to better constrain the role of this wind efficiency for further studies on more complex wind conditions such as asymmetrical bidirectional wind regimes.

References : [1] Bristow C. et al., Nature 406, 2000. [2] Rubin D. M. and Hunter R. E., Sedimentology 32, 2000. [3] Rubin D. M. and Ikeda H., Sedimentology 37, 1990. [4] Hersen P., JGR 110, 2005. [5] Parteli et al., PNAS 106, 2009. [6] Reffet et al., Second Planetary Dunes Workshop, 2010. [7] Reffet et al., Geology 38, 2010. [8] Claudin P. and Andreotti B., EPSL 252, 2006.

EQUINOCTIAL ATMOSPHERIC ACTIVITY OVER TITAN DUNE FIELDS REVEALED BY CASSINI/VIMS. S. Rodriguez[1], S. Le Mouélic[2], J.W. Barnes[3], M. Hirtzig[4], P. Rannou[5], C. Sotin[2,6], R.H. Brown[7], J. Bow[3], G. Vixie[3], T. Cornet[2], O. Bourgeois[2], C. Narteau[8], S. Courrech du Pont[9], A. Le Gall[10], E. Reffet[1], C.A. Griffith[7], R. Jaumann[11], K. Stephan[11], B.J. Buratti[6], R.N. Clark[12], K.H. Baines[13], P.D. Nicholson[14], A. Coustenis[4], *[1]Laboratoire AIM, Université Paris Diderot – Paris 7/CNRS/CEA-Saclay, DSM/IRFU/SAp, 91191 Gif sur Yvette, France (sebastien.rodriguez@cea.fr), [2]Laboratoire de Planétologie et Géodynamique, CNRS-UMR 6112, Université de Nantes, 2 rue de la Houssinière, 44322 Nantes, France ; [3]Department of Physics, University of Idaho, Engineering-Physics Building, Moscow, ID 83844, USA ; [4]LESIA, Observatoire de Paris, section de Meudon, 5 place Jules Janssen, 92195 Meudon Cedex, France ; [5]Groupe de Spectroscopie Moléculaire et Atmosphérique, UMR CNRS 6089, Université de Reims, U.F.R. Sciences Exactes et Naturelles, Moulin de la Housse B.P. 1039, 51687 Reims Cedex 2, France ; [6]Jet Propulsion Laboratory, California Institute of Technology, 4800 Oak Grove Dr., Pasadena, CA 91109, USA ; [7]Department of Planetary Sciences, University of Arizona, Lunar and Planetary Laboratory, 1629 E. University Blvd., Tucson, AZ 85721, USA ; [8]Institut de Physique du Globe de Paris, Laboratoire de Dynamique des Fluides Geologiques, Paris, France ; [9]Laboratoire Matière et Systèmes Complexes, Université Paris Diderot, Paris, France ; [10]Laboratoire Atmosphères, Milieux, Observations Spatiales (LATMOS-UVSQ), Paris, France ; [11]DLR, Institute of Planetary Research, Rutherfordstrasse 2, D-12489, Berlin, Germany ; [12]United States Geological Survey, Mail Stop 964, Box 25046, Denver Federal Center, Denver, CO 80225, USA ; [13]Space Science and Engineering Center, University of Wisconsin-Madison 1225 West Dayton St., Madison, Wisconsin 53706, USA ; [14]Department of Astronomy, Cornell University, 418 Space Sciences Building, Ithaca, NY 14853, USA.*

Introduction: Titan, the largest satellite of Saturn, is the only satellite in the solar system with a dense atmosphere. The close and continuous observations of Titan by the Cassini spacecraft, in orbit around Saturn since July 2004, bring us evidences that Titan troposphere and low stratosphere experience an exotic, but complete meteorological cycle similar to the Earth hydrological cycle, with hydrocarbons evaporation, condensation in clouds, and rainfall. Cassini monitoring campaigns also demonstrate that Titan's cloud coverage and climate vary with latitude. Titan's tropics, with globally weak meteorological activity and widespread dune fields, seem to be slightly more arid than the poles, where extensive and numerous liquid reservoirs and sustained cloud activity were discovered.

Only a few tropospheric clouds have been observed at Titan's tropics during the southern summer [1-4]. As equinox was approaching (in August 2009), they occurred more frequently and appeared to grow in strength and size [5-7].

VIMS observations: We present here the observation of intense brightening at Titan's tropics, very close to the equinox. These detections were conducted with the Visual and Infrared Mapping Spectrometer [8] (VIMS) onboard Cassini. Figure 1 presents the VIMS color composite images of the three individual events detected so far, observed during the Titan's flybys T56 (22 May 2009), T65 (13 January 2010) and T70 (21 June 2010). T56, T65 and T70 observations show an intense and transient brightening of large regions very close to the equator, right over the extensive dune fields of Senkyo, Belet and Sangria-La. They all appear spectrally and morphologically different from all transient surface features or atmospheric phenomena previously reported. Indeed, these events share in particular a strong brightening at wavelengths greater than 2 µm (especially at 5 µm), making them spectrally distinct from the small tropical clouds observed before the equinox [1,3,7] and the large storms observed near the equator in September and October 2010 [6].

Discussion: In this paper, we will discuss the possibility that these singular events may have occurred very close to the surface, having a strong link with the underlying dune fields. Radiative transfer calculations indeed show that these singular brightenings are due to the transient appearance of an additional atmospheric layer, confined at very low altitudes and loaded with few but large particles. Gathering all the observational and modeling constraints, we conclude that the most probable explanation for these events is the local and transient occurrence of huge dust storms, directly originating from the underlying dune fields. We will also discuss the possible implications of the equinoctial occurrence of such events for Titan's tropical wind regimes and for the present-day activity of equatorial dunes.

References: [1] Griffith et al. Astrophys. J. Letters 702, L105-L109, 2009. [2] Turtle et al., Geophys. Res. Lett. 36, CiteID L02204, 2009. [3] Rodriguez et al., Nature 459, 678-682, 2009. [4] Schaller et al., Nature 460, 873-875, 2009. [5] Turtle et al., Geophys. Res. Lett. 38, CiteID L03203, 2011. [6] Turtle et al., Science 331, 2011. [7] Rodriguez et al., Icarus 216, 89-110, 2011. [8] Brown et al., Space Sci. Rev. 115, 111–168, 2004.

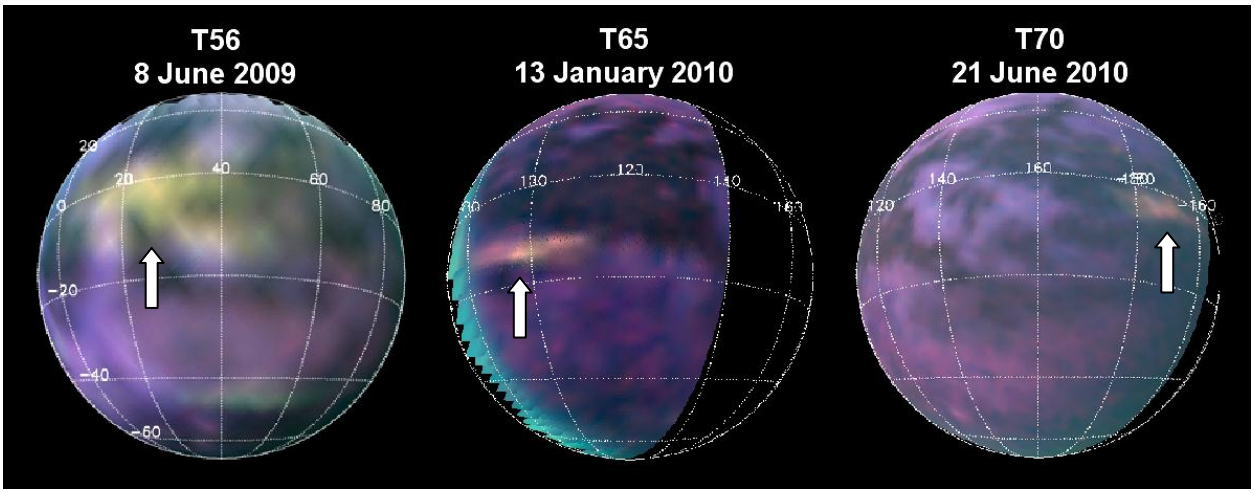

Figure 1. Orthographic reprojection of VIMS observations of Titan during the T56, T65 and T70 flybys. These images are RGB color composites, using the VIMS 5 μm channel as red, the 2.78 μm as green and 2 μm as blue. The yellowish/pinkish areas, also marked by the white arrows, denote the unusual spectral behaviour of large regions within Titan's tropics, very close to the equinox.

A UNIFYING MODEL FOR PLANFORM STRAIGHTNESS OF RIPPLES AND DUNES IN AIR AND WATER. David. M. Rubin, USGS, 400 Natural Bridges Dr., Santa Cruz, CA 95060; drubin@usgs.gov.

Introduction: Geologists, physicists, and mathematicians have studied ripples and dunes for more than a century, but little attention has been directed at explaining one of the morphologic properties that is most visible in remotely collected images: why are some bedforms straight, continuous, parallel, and uniform in planform geometry (i.e. two-dimensional) whereas others are barchanoid and irregular, with discontinuous crests and troughs (three-dimensional)? We argue that physical coupling along the crest of a bedform is required to produce straight crests and that along-crest flow and sand transport provide effective physical mechanisms for that coupling [1].

Discussion:

Planform geometry in simple unidirectional flows. In unidirectional flows, bedforms generally have crescentic, barchanoid, or irregular planform geometry [2-7]. For a ripple or dune to have a straight continuous crest, some physical mechanism must operate to couple the topography at different along-crest locations. Without such coupling, different sites along a crest need not remain locked in phase and are free to form breaks, bends, or junctions. Hypothetically, if flow and topography along every streamline were completely decoupled from adjacent streamlines, "bedform" crests would be randomly phased from one streamline to another, and coherent bedforms could not exist. The presence of coherent continuous crests implies some degree of along-crest coupling, and straight continuous crests require a greater degree of along-crest coupling.

Situations that enhance two-dimensionality. Ripples and dunes with the straightest and most continuous crests include longitudinal and oblique dunes in unidirectional flows, wave ripples, dunes in reversing flows, wind ripples, and ripples migrating along a slope. At first glance, these bedforms appear quite different (ripples and dunes; air and water; transverse, oblique, and longitudinal orientations relative to the net sand-transport direction), but they all have one property in common: a process that increases the amount of along-crest sand transport (that lengthens and straightens their crests) relative to the across-crest transport (that makes them migrate and take the more typical three-dimensional planform geometry). In unidirectional flows that produce straight bedforms, along-crest transport of sand is caused by along-crest flow (non-transverse bedform orientation), gravitational transport along an inclined crest, or ballistic splash in air. Bedforms in reversing flows (wave ripples, tidal dunes, and eolian dunes in seasonally reversing winds in Figure 1d-f) tend to be straighter than their unidirectional counterparts (Figure 1a-c) because reverse transport across the bedform crest reduces the net across-crest transport (that causes the more typical irregular geometry) relative to the along-crest transport (that smoothes and straightens planform geometry.

Unresolved issues. A variety of processes that might influence planform geometry remain unresolved, including: (a) intersection of two or more sets of bedforms such as those that form in bi-directional flows diverging by ~90° [7-9], (b) formation of superimposed bedforms that become so large that they effect the geometry of the main bedforms [10]), (c) formation of bedforms in flows with three or more vectors, such as combined waves and currents [11] or intersecting sets of waves, (d) formation of bedforms in flows with directional modes that individually transport enough sand to substantially alter bedform morphology, and (e) sorting of sediment by grain size into patches of sediment that respond differently to flow. Nevertheless, the model reviewed here [1] identifies the unifying underlying process that causes two-dimensionality in a wide variety of diverse situations.

References:

[1] Rubin, D. M. (in press) *Earth-Science Reviews*. [2] Bagnold, R. A. (1941) *The Physics of Blown Sand and Desert Dunes*, Methuen, London. [3] Allen, J. R. L. (1966) *Sedimentology*, 6, 153-190. [4] Middleton, G. V., and Southard, J. B. (1984) *Mechanics of Sediment Movement*, Society for Sedimentary Geology, Tulsa. [5] Baas, J. H. (1994) *Sedimentology*, 41, 185–209. [6] Venditti, J. G., Church, M., Bennett, S. J. (2005) *Sedimentology*, 52, 1343-1359. [7] Reffet, E., Courrech du Pont, S., Hersen, P., Douady, S. (2010) *Geology*, 38, 491-494. [8] Dalrymple, R. W., Rhodes, R. N. (1995) *Developments in Sedimentology.* Elsevier, Amsterdam, 53, 359-422. [9] Werner, B. T., Kocurek, G. (1997) *Geology*, 27, 771-774. [10] Brookfield, M. E. (1977) *Sedimentology*, 24, 303-332. [11] Lacy, J. R., Rubin, D. M., Ikeda, H., Mokudai, K., Hanes, D. M. (2007) *J. Geophys. Res*., 112, C10018, doi:10.1029/2006JC003942. [12] Kaplinski, M., Hazel, J. E., Jr., Parnell, R., Breedlove, M., Kohl, K., and Gonzales, M. (2009) *U.S. Geological Survey Open-File Report* 2009–1207. [13] Barnard, P. L., Erikson, L. H., Kvitek, R. G. (2011) *Geo-Marine Letters*, 31, 227-236.

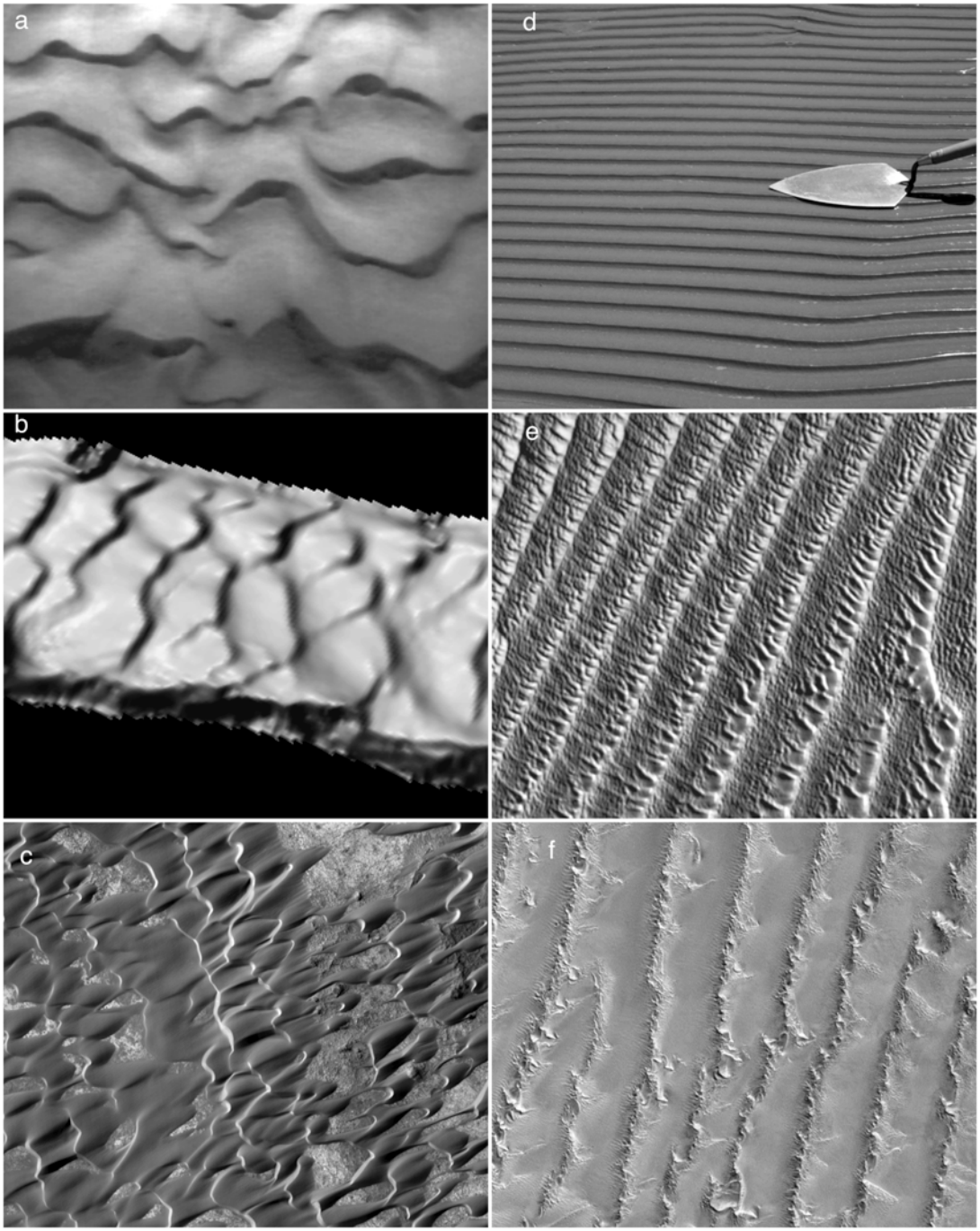

Figure 1. Three-dimensional ripples and dunes in unidirectional flows (left column a-c) and two-dimensional counterparts in reversing flows (right column d-f). (a) Ripples formed by unidirectional flow in a lab flume; flow is from top to bottom; field of view is 40 cm from right to left. (b) Dunes in unidirectional flow in the Colorado River in Grand Canyon viewed by multibeam sonar [12]; channel width is approximately 70 m. (c) Crescentic eolian dunes on Mars (winds roughly from right to left; field of view ~6 km x 6 km); (Image: NASA/JPL/University of Arizona; Nili Patera Ripples ESP_017762_1890). Right column shows straight-crested bedforms created by reversing flows. (d) Ripples formed by reversing wave-generated flow on a sand bar in Colorado River in Grand Canyon. (e) Dunes formed by reversing tidal currents, San Francisco Bay, California [13]; wavelength is 60 m. Superimposed dunes demonstrate along-crest sand transport (from bottom to top in image). (f) Eolian dunes formed by seasonally reversing winds, Namib Desert; dune wavelength is 2 km. Superimposed dunes demonstrate along-crest sand transport (from bottom to top in image). Landsat Earth as Art series; USGS and NASA.

SAND TRANSPORT PATHWAYS OF DARK DUNES IN THE SPERRGEBIET: SAND COMPOSITION AND DUNE MIGRATION RATES FROM ASTER DATA. S. P. Scheidt[1], [1]CEPS/NASM MRC 315, Smithsonian Institution, Washington D.C. 20013-7012 (sscheidt77@gmail.com).

Introduction: The Coregistration of Optically Sensed Images and Correlation (COSI-Corr) software [1] has shown to be a useful tool for measuring the migration of dunes on Earth [2,3] and detecting the movement of aeolian bedforms on the surface of Mars [4,5]. Linear spectral unmixing of thermal infrared (TIR) has been used as an effect tool for extracting the mineralogical composition of both Mars and Earth surface materials as well [6,7]. Using these techniques together, a great deal of information can be exploited about an aeolian system, regardless of the planet.

Geologic Background: The Namib Sand Sea is an ancient and modern sand accumulation area [8, and others]. It is a large group of south-north-trending complex linear dunes at its core, located along the Atlantic coast of Namibia between 23º and 26.5º S (Figure 1). Other complex and spatially varied dune patterns exist, including transverse ridges and barchan forms at the southern margin (8,9). Studies of sands have shown that the Namib Sand Sea has probably persisted for the past one million years [10], and the primary source of sand, past and modern, has been the Orange River at the southernmost edge of the Sperrgebeit, a large deflation basin and source area of sand [10,11]. North-migrating convoys of dark-colored barchan dunes make up well-defined sand transport corridors in the Sperrgebiet deflation basin [8, 12, and others] which are sourced from south-facing reentrant coastal embayments along the Atlantic shoreline [12].

Methods: The migration rates of dunes at the southern margin of the Namib Sand Sea were recently measured using COSI-Corr from Advanced Spaceborne Thermal Emission and Reflection Radiometer (ASTER) sensor data [13]. These results were recently improved and the study area was expanded using ASTER L1A data products as the data source. COSI-Corr is a change detection method, described here in simple terms. The ASTER satellite images from multiple dates were orthorectified and co-registered in a common geographic coordinate system. Areas of correlation (no change) and decorrelation (lateral land surface movement) were determined between the "before" and "after" image data from years 2001, 2002, 2006, 2007, 2008 and 2009. New image data was produced containing the relative N/S and E/W displacement fields at each pixel location for each image pair processed. Where these pixels are associated with dunes, the pixel values represent the migration rate of that dune or part thereof. All the COSI-Corr results were thoroughly evaluated at the dune scale for

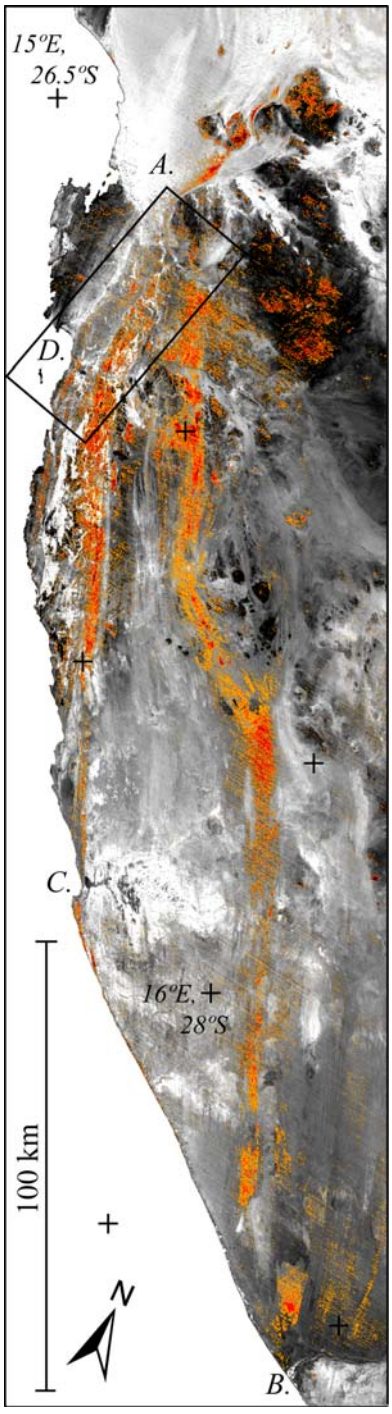

Figure 1. Dark sand transport pathways in the Sperrgebiet (orange and red color scale). Quartz abundance from ASTER shown by underlain image (white = quartz rich). A. Namib Sand Sea. B. Mouth of the Orange River. C. Chamais Bay. D. COSI-Corr study area (box) and Elizabeth Bay.

accuracy and filtered to contain only valid dune migration rates. These data were compiled to generate statistics of the dune field's migration rate, direction and frequency distribution of dune velocity by area.

Composition mapping using ASTER thermal infrared image data. The spatial pattern of dune migration shown by COSI-Corr data revealed the distinct pattern of sand transport corridors described by past researchers[8,12, and others]. These image data were overlain in Google Earth, and the COSI-Corr data corresponded to other dark streaks and convoys of dark-colored barchan dunes. These could be traced to other coastal sand source areas, including the mouth of the Orange River, 260 km south of the Namib Sand Sea.

These observations prompted the mapping of the sand transport pathways of the dark dunes using the sand's unique spectral character and sand composition. A seamless, multispectral, radiometrically balanced mosaic of ASTER TIR data [14] was constructed to cover the Sperrgebiet region between the southern Namib margin and the Orange River. The ASTER instrument has multispectral capabilities (5 bands) in the TIR wavelength region (8.125 - 11.65 μm), and accurate and quantitative compositional mapping was achieved using these data and linear spectral unmixing [6,7,15,16]. Image spectral endmembers were selected from four locations: quartz-rich sand, a coastal source of dark sand, alluvial fan and bedrock.

Results: The underlain black and white image in Figure 1 shows the areal distribution of quartz-rich sand, where bright areas represent high abundance and dark areas are quartz poor. Quartz-rich sand was mapped as the most abundant spectral endmember in the Namib Sand Sea, especially as a transport corridor emanating from Elizabeth Bay (location D). Several quartz-rich corridors in the north-south orientation are visible in the Sperrgebiet basin as well. Dark-colored sand (at visible wavelengths) was also mapped, shown here on a color scale ranging from orange to red, corresponding to an areal abundance of 30% and 100% (Figure 1). This pattern shows two primary sand transport corridors extending across the Sperrgebiet to the Namib Sand Sea from location B (Figure 1) and the other from the Chamais Bay (location C, Figure 1). The dark sand endmember mapped from ASTER TIR corresponded to both dark-colored streaks in Google Earth and the dark-colored migrating barchan dunes in the COSI-Corr study (subset box D, Figure 1).

In the COSI-Corr study area (850 km^2), 12% of the area was consistently identified as active dunes within sand transport pathways. COSI-Corr data from subset box D, Figure 1 were used to show the distribution of direction and magnitude of dunes migrating within the sand transport corridors as a sand rose (Figure 2). Below the sand rose, the percentage of the active dune field moving at different migration rates is also shown (Figure 2). Using COSI-Corr data of dunes in the the Chamais Bay sand transport corridor, sand flux of the dark-colored dunes averaged 520 $m^3\ m^{-1}\ yr^{-1}$, ranging from 170 to 1260 $m^3\ m^{-1}\ yr^{-1}$, between 2001 and 2009. This source of dark colored sand was not mapped further north into the Namib Sand Sea other than a small concentration at the southern margin of 8 km^2 (location A, Figure 1).

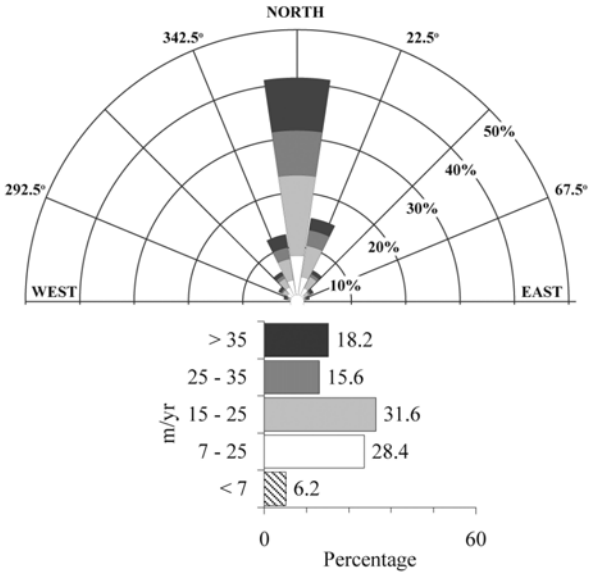

Figure 2. Sand rose showing dune migration direction and magnitude distribution from COSI-Corr data.

References: [1] Leprince et al. (2007), IEEE T. Geosci. Remote, 45, 1529-1558. [2] Vermeesch P. and Drake N. (2008), GRL, 35, L24404, doi:10.1029/2008 GL035921. [3] Necsoiu et al. (2009), Rem. Sens. Environ., 113, 2441-2447. [4] Bridges et al. (2011), EPSC-DPS Joint Meeting 2011, held 2-7 October 2011 in Nantes, France. [5] Bridges et al. (2010), AGU Fall Meeting Abstract 0531. [6] Bandfield J.L. et al (2002), JGR, 107, E11, 5092. [7] Ramsey M.S. et al. (1999), GSA Bull., 111, 646-662. [8] Lancaster (1989), The Namib Sand Sea: Dune forms, processes and sediments. [9] Livingstone et al. (2010), Aeolian Research 2(2-3), 93-104. [10] Vermeesch et al. (2010), Nature Geosci. 3(12), 862-865. [11] Lancaster and Ollier (1983), Zeitschrift für Geomorphologie Supplement B 45, 71-83. [12] Corbett (1993), Int. Asc of Sedimentologists Special Pub 16, 45-60. [13] Scheidt and Lancaster (2010), 2nd Planetary Dunes Workshop, Abstract #2024. [14] Scheidt et al. (2008), Rem. Sens. Environ. 112, 920-933. [15] Scheidt et al. (2010), 2nd Planetary Dunes Workshop, Abstract #2010. [16] Scheiet et al. (2011), GSA Bull., 123(7/8), 1628-1644.

ACTIVE AEOLIAN PROCESSES ALONG CURIOSITY'S TRAVERSE. S. Silvestro[1], D. A. Vaz[2,3], A. P. Rossi[4], J. Flahaut[5], L. K. Fenton[1], R. Ewing[6], and P. E. Geissler[7], [1]SETI Institute, Carl Sagan Center, 189 N. Bernardo Avenue, Mountain View, CA, USA (ssilvestro@seti.org), [2]Center for Geophysics, University of Coimbra, Portugal, [3]CERENA, Instituto Superior Técnico, Av. Rovisco Pais, 1049-001 Lisboa, Portugal, [4]Jacobs University, Bremen, Germany, [5]Laboratoire de Géologie de Lyon, Université Lyon 1, Villeurbanne, France, [6]University of Alabama, Department of Geological Sciences, Tuscaloosa, AL, USA,[7]US Geological Survey, Flagstaff, AZ, USA.

Introduction: Gale Crater is the landing site of the Mars Science Laboratory (MSL) mission to Mars (Fig. 1). This crater has been subject to a wide range of geological processes that gave rise to the dramatic variability of terrains observed from orbit [1]. Among these processes the action of the wind appears to have played a dominant role for much of the crater's history, as indicated by the abundance of aeolian features at this site [1,2,3]. In the NW portion of the crater floor, dark sand dunes are organized in a dune field crossing the landing ellipse from the NE to the SW (Fig. 1a). Recent observations of the migration of dark dunes and ripples throughout the Martian tropics have provided a wealth of new information on the sediment transport dynamics and wind regime at the surface of Mars [4,5,6,7] and similar analyses can provide precious indications about the current wind regime in the landing site. We analyzed three overlapping HiRISE images in MSL's landing site. These data, together with the morphology and orientations of the dark dunes and ripples, allow us to reconstruct the wind regime across the rover traverse, for the first time providing the opportunity to use ground measurements from the MSL Rover Environmental Monitoring Station (REMS) to test the accuracy of a wind regime derived from orbital data.

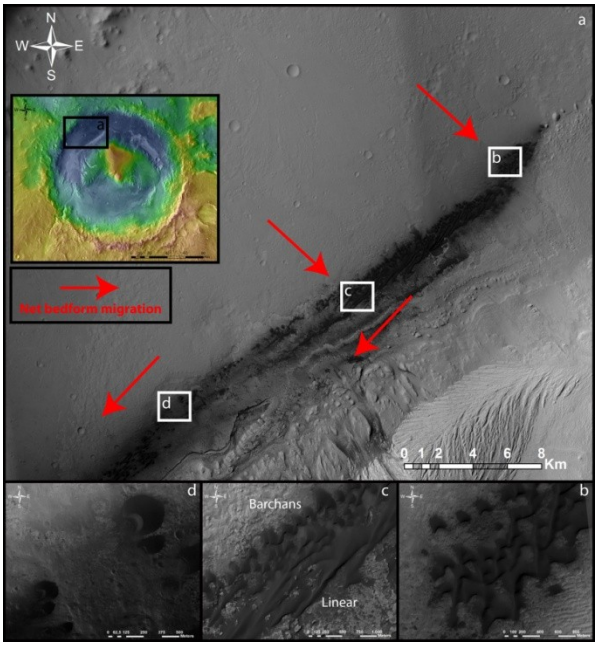

Fig. 1: Dune morphology in the study area

Methods: We performed our analysis over three orthorectified overlapping HiRISE images that were co-registered in ArcGIS using bedrock as reference. The images have been processed in ISIS and were acquired with minimal difference in lighting conditions in 2006 (T1), 2008 (T2) and 2011 (T3). CTX images have been used as context. The ripple pattern is mapped automatically using part of the methodology introduced by [8]. Ripple displacements were calculated along the whole ripple crest for 180 ripples over 5 dunes. CRISM data available over the area were processed as in [9] to derive mineralogical composition for the dunes.

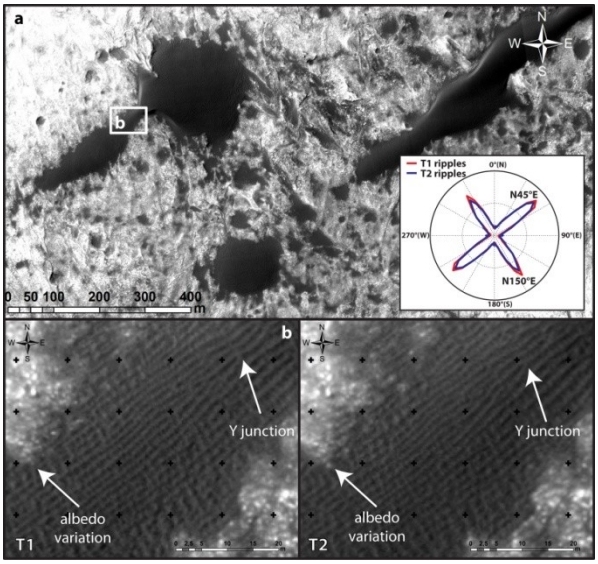

Fig. 2: ripple pattern and sand movement in the Site 1

Dune morphology and ripple pattern: The dark dunes in the MSL landing site consist of dark sand enriched in mafic minerals (olivine and high-calcium pyroxene) as seen with CRISM. Their morphology is quite complex as it changes, moving toward the SW. Simple barchan dunes with SE facing slip faces are visible in the NE margin of the erg (Fig. 1b). In the central part of the erg, barchan dunes evolve to linear or oblique features close to the central mound (Fig. 1c). Further to the SW, the dune field is dominated by simple barchans with SW-facing slip faces (Fig. 1d). A schematic representation of the net sand movement direction solely based on dune morphology is visible in Fig. 1a. However, because the wind regime is not

strictly uni-directional, the dune morphology is not representative of individual wind directions [10]. Ripples rather than dunes give us more precise information about the wind regime in the study area and are analyzed in two different sites. *Site 1:* the ripples superposing three dunes (Fig. 2a) were mapped automatically and their orientations are plotted in the circular diagram shown in the inset. Two orthogonal patterns with modes at N50°E and N150°E are visible. The N150°E ripples migrated consistently and, while such a migration is not so evident for the N50°E pattern, it also displays significant changes (Fig. 2b). *Site 2:* at this site two classes of bedforms (dark and bright dunes-TARs) have accumulated in a canyon (Fig. 3a). The ripples (4-5 m in wavelength) consist of transverse ridges that are locally crossed by linear features (Fig. 3b). The bright bedforms (TARs) have a NW-SE trend and an average wavelength of about 17m (Fig. 3c). A steeper slope facing SW is visible (Profile AB). CRISM spectra indicate a weak hydration band suggesting that these features could be formed of the hydrated material eroded out from the central layered mound outcropping nearby [11].

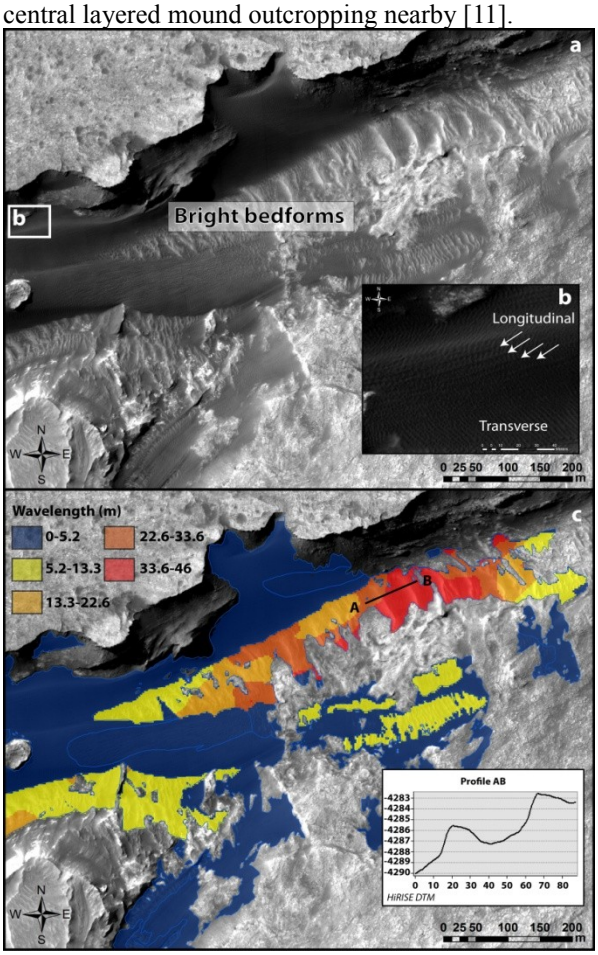

Fig. 3: Dark and bright dunes morphology and wavelength in the Site 2.

Ripple migration: The dark ripple pattern changed consistently between T1 and T2 with the N150°E ripples migrating 1.16 m on average in one Martianyear (0.58 m/Earth year) toward the SW. This value of displacement is comparable to migration rates in other tropical zones of Mars [4,12]. The N50°E ripple pattern is also changing suggesting a multi-directional wind regime. Conversely, the bright bedforms in site 2 didn't display significant movement.

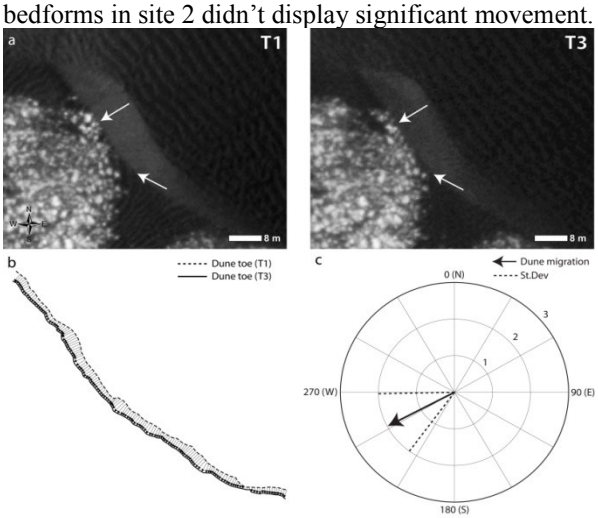

Fig. 4: Dune migration magnitude and direction.

Dune migration: Dune migration is evident comparing the image pair T1-T3 (Fig. 4). The rate of migration for eight dunes in the SW margin of the dune field was calculated averaging the vectors linking the dune toes at T1 and T3 as visible in Fig. 4b. An average migration of two meters toward the SW has been calculated for the study dunes, suggesting a rate of migration of 0.4 meter/Earth year (about 0.8 meter/Mars year) (Fig. 4c).

Conclusion: We identified consistent ripple and dune migration caused by strong winds from the NE in the MSL landing site. Because Curiosity will drive through these dunes, it may eventually experience such winds. This will be an opportunity to measure the threshold friction velocity of sand saltation, a key factor for determining erosion rate and sand fluxes on Mars. Such activity however, could represent a threat to the rover, and care should be taken in selecting the safest traverse.

References: [1] Anderson R. B. and Bell J. F. (2010) *Mars, 5,* 76-128. [2] Hobbs S. W. et al. (2010) *Icar.,210,* 102-115. [3] Silvestro S. et al. (2010) *LPS XLI,* Abstract #1533, 1838. [4] Silvestro S. et al. (2010) *Geophys. Res. Lett., 37,* L20203. [5] Chojnacki M. et al. (2011), *JGR, 116*, E00F19. [6] Silvestro S. et al. (2011) *Geophys. Res. Lett., 38,* L20201. [7] Bridges et al. (2012), *Geology, 40*, no.1. [8] Vaz D. A. (2011), *PSS, 59*, 1210-1221. [9] Murchie S. L. et al. (2009) *JGR, 114*, E00D07.[10] Rubin D. M. and Ikeda H.(1990), *Sedimentology, 37*, 673-684. [11] Milliken R. E. et al. (2010), *GRL, 37,* L04201. [12] Geissler P. E. et al. (2011) *LPS XLII,* 2537.

THE NORTHERN SPIRAL TROUGHS OF MARS AS CYCLIC STEPS: A FRAMEWORK FOR USING OBSERVATIONS OF ACTIVE PROCESSES TO CALCULATE MIGRATION AND ACCUMULATION RATES ON THE NPLD. I. B. Smith, J. W. Holt, University of Texas Institute for Geophysics, Jackson School of Geosciences, University of Texas, Austin, TX 78758 isaac@ig.utexas.edu; jack@ig.utexas.edu.

Introduction: The spiral troughs on Mars' North Polar Layered Deposits (NPLD) contain a rich, detailed stratigraphic record of surface processes in Mars' recent polar history. SHARAD radar data near the center of the NPLD revealed that the troughs have migrated more than 50 km towards the north during the accumulation of the uppermost ~ 600 m of NPLD [1]. It was proposed that katabatic winds are the primary driver of this migration process [1, 2]. Here we test that hypothesis by integrating observations of current surface winds, quantitative radar stratigraphy, and mesoscale model results into a model of trough migration based on cyclic steps. We find that wind transport of ice and vapor is able to account for the observed amount of spiral trough migration. This model makes no assumptions about accumulation on the NPLD, but an average rate of accumulation derived from this analysis compares favorably with rates derived by other means [1].

Model: Surface morphology in and around the spiral troughs indicates a complex system of erosion and deposition. Features such as albedo, surface slopes, terrain (banded vs. layered), and radar reflectors are all asymmetric across the spiral troughs. This observation suggests that either non-uniform deposition or post-deposition transport of material is important during trough evolution.

In terrestrial and submarine environments on Earth, features that resemble the spiral troughs in morphology and stratigraphy have been well characterized. Material transport is responsible for the asymmetries in these systems which belong to a class of features termed cyclic steps [3]. Furthermore, this has been validated in flume experiments and numerical models intended to replicate cyclic steps. The experiments reproduced stratigraphy and morphology qualitatively similar to those associated with the spiral troughs (Fig. 1) [3]. We therefore interpret the spiral troughs as a depositional form of cyclic steps and apply the cyclic step model, modified for Martian atmospheric conditions, to constrain flow parameters of the katabatic winds on the NPLD. Using this technique, we are able to calculate average migration rates of the troughs and deposition rates of the NPLD since trough onset.

Constraints: SHARAD radar stratigraphy associated with spiral troughs has provided both a ratio of lateral trough migration to NPLD accumulation, amount of accumulation since trough onset, and estimates of the required mass transport [1]. THEMIS

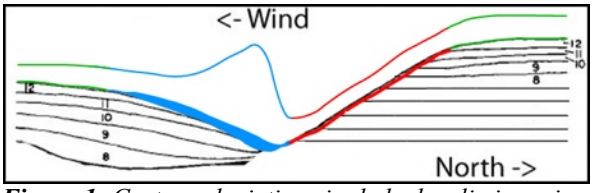

Figure 1: *Cartoon depicting single hydraulic jump in cyclic step model. Flow is right to left. Green indicates no change in topography, red: erosion and supercritical (thin) flow; blue: deposition and subcritical (thick) flow after a hydraulic jump.*

VIS and other optical imagery provide observations of active aeolian processes. From these observations we extract flow parameters required for Froude number calculations. Two physical constraints are necessary for the model: Froude numbers as predicted by cyclic step theory and conservation of flux across a boundary. Existing mesoscale models [4] provide the final constraints necessary to complete the calculations of total mass moved during a katabatic wind storm.

Observations: 9858 THEMIS VIS images covering the NPLD have been examined. Of those images, ~ 260 capture katabatic winds acting on the spiral troughs and fall within solar longitude (L_s) range of 36-98, the majority after L_s 76. Images capture thick, linear clouds that we interpret as hydraulic jumps near the bottom of the troughs. Several images also show linear vortices of entrained ice particles that enter a trough perpendicular to its length, descending from its higher side (Fig. 2). Beyond the hydraulic jump, and along the lower slope, the thick clouds are turbulent and flow downstream. Sequential observations provide constraints on the duration of active winds.

Analysis: The cyclic step model describes and predicts the observed flow (Fig. 2), which alternates between supercritical, shallow flow and subcritical, thick flow [3]. The process repeats in a series of steps. The Froude number (Equation 1) is a dimensionless number defined as the ratio of characteristic velocity to surface wave velocity. It is a measure of the thickness of a flow in comparison to the topography over which

$$Frd = \frac{U}{\sqrt{gHr}} \quad (1)$$

$$r = (\rho_i - \rho_{ia})C + (\rho_{ia} - \rho_a)(1 - C) \quad (2)$$

$$f_1 = H_1 \times U_1 \times C_1 = f_2 = H_2 \times U_2 \times C_2 \quad (3)$$

it flows. Supercritical flow is defined as having a densimetric Froude number greater than 1, while subcritical flow has a Froude number less than one. In the cyclic step model they are associated with erosion and deposition, respectively.

Fr_d is the densimetric Froude number used for two-phase flow; U is the horizontal velocity; g the gravitational acceleration; H the flow depth, and C is the volumetric concentration. ρ_a, ρ_i, and ρ_{ia} are estimated densities of air, ice, and icy-air respectively. Equation 3 is the conservation of flux across a hydraulic jump.

Using these equations with values listed in Table 1, an instantaneous flux can be calculated. An estimate of duration for an event may be derived from one or multiple VIS images. Most events are captured in only one image; however, in a series of 18 images from Mars Year 29, one event lasted longer than 200 hours.

Using the calculated flux and estimated duration of 13 hours, the total two-dimensional mass moved across the hydraulic jump is 92 m^2. Very little mass transfers between adjacent troughs, as can be demonstrated by SHARAD radargrams [5], so we assume all the material flux is deposited on the pole-facing slope, acquired from material carried from the ~ 20 km equator-facing slope. This amounts to ~ 4.6 mm of erosion, and 49 mm of scarp retreat (migration) using a nominal slope of 5°. Alternately, during a 1 hour storm the trough will migrate about 3.8 mm.

	Supercritical$_1$	**Subcritical$_2$**
Fr	1.7	0.4
U (m/sec)	11	4
g (m^2/sec)	3.698	3.698
H (m/sec)	150	293
C	$1.2x10^{-6}$	$1.7x10^{-6}$
Flux (m^2/sec)	$2.0x10^{-3}$	$1.59X10^{-3}$

Table 1: *Estimated values used for Equations 1 and 3. Constraints obtained from the following: Fr: cyclic step model, U: models of katabatic winds on the NPLD [4], H_1: distance between vortices in Fig. 2, H_2 Belanger equation, C: calculated from Eqn. 1.*

Implications: The preponderance of events captured between Ls 76 and 98 and the lack of confirmed events during other times of the year suggest that the poleward migration of troughs occurs during the late spring and first few days of summer. From radar analysis, it is known that the older troughs have migrated more than 50 km [1]. Estimating 3.8 mm of migration per hour, approximately $1.3x10^7$ hours of wind are required to account for the total migration.

We estimate the total migration undergone by a trough in one Earth year to be 26 mm on average. Using the relationship of accumulation to migration found in SHARAD [1], an estimate for accumulation rate may be calculated. Between 550 and 700 m of ice has accumulated during the trough's 50 km migration. Applying these ratios, we calculate that, on average, between 0.29 and 0.37 mm of ice have accumulated on NPLD per year of spiral trough existence. These numbers agree well with published estimates of accumulation between 0.28 and 1.2 mm per year [6].

Based on the best available constraints, average rates, and estimated age of the NPLD (~4 Myr), we find that katabatic storms are sufficient to account for the 50+ km of observed trough migration.

Acknowledgements: This work was supported by NASA ESSF Fellowship NNX10AT24H and NASA MDAP grant NNX10AO26G.

References: [1] Smith, I.B. & Holt, J.W. (2010) *Nature* 465, 450-453. [2] Howard A. D. (1982) *Icarus*, 50, 161-215. [3] Kostic, S. et al., (2010) *Journal of Hydro-enviro Ress* 3, 167–172. [4] Spiga, A. et al. (2011) *Icarus*, 212, 504-519. [5] Smith, I.B. et al, (2011) *LPSC* XLII, Abst #2742. [6] Fishbaugh, K.E. & Hvidberg, C.S. (2006) *JGR Planets* 111 E06012

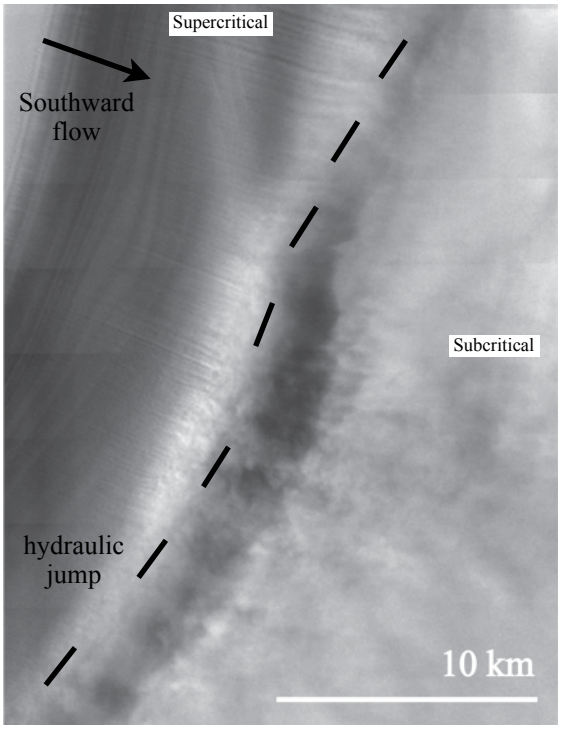

Figure 2: *Portion of THEMIS image V12295001. Katabatic wind event captured with vortices and hydraulic jump where flow thickens by factor of ~ 1.5.*

VARIATIONS IN NORTH POLAR SEASONAL CO_2 ICE: IMPROVED DISTRIBUTION MAPS USING PIXON IMAGE RECONSTRUCTION. Luis F.A. Teodoro[1], William C. Feldman[2], Mary Bourke[2], [1]BAER, NASA Ames Research Center, Moffett Field, CA 94035-1000 (luis.f.teodoro@nasa.gov); [2]Planetary Science Institute, 1700 E. Fort Lowell, Suite 106, Tucson, AZ, 85719, USA.

Introduction: H_2O and CO_2 are exchanged between the atmosphere and the surface of Mars from autumn through spring. Deposition extends from the Poles to the mid latitudes with approximately 30% of CO_2 condensing out of the atmosphere when temperatures reach 148°K [under typical martian pressures, 1]. Work has shown that CO_2 may precipitate as snowfall and although not directly observed due to observational constraints, 'cold spots' [20 μm brightness temperatures as low as 130°K, 2] are considered to be a signature of combined CO_2 atmospheric condensates and freshly fallen CO_2 snow [3-8]. However the majority of CO_2 ice is thought to form directly on the surface as a result of radiative cooling [9] or as direct condensation onto the surface.

Pressurized CO_2 gas that forms beneath the seasonal ice cap during sublimation [10] has been shown to be an important geomorphic process that can transport sand on North Polar sand dunes. Hansen et al, [10] proposed that subsurface pressurized gas can mobilize sediment down avalanche faces, contributing to dune migration. Bourke and Cranford [11] demonstrated that dune 'furrow' formation was linked to the polygonal cracking of the seasonal CO_2 ice and documented that these dune surface morphologies formed seasonally.

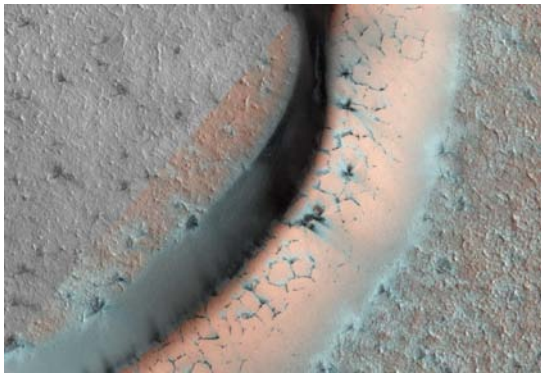

Figure 1: Subset of HiRISE Image ESP_024537_2600 taken at L_s= 18.4. showing polygonal cracking in seasonal CO_2 frost on dune.

It is important therefore to document the distribution, thickness and persistence of the seasonal CO_2 deposit, particularly those that overlap dunes on the North Polar Sand Seas (Figure 1).

Previous estimates of the distribution of CO_2 frost at the North Pole using data from the Neutron Spectrometer on board the Mars Odyssey Spacecraft plotted the deconvolved epithermal neutron count rates and estimated the CO_2 ice column abundance for the North Polar Region [12]. Our work builds upon this. We apply Pixon image reconstruction methods to the North Polar Epithermal Neutron data to increase the spatial resolution of the count rates.

Method: During CO_2 ice-free conditions, the epithermal range of neutron energies is nearly uniquely sensitive to the hydrogen content of surface soils, which should likely be in the form of H_2O/OH molecules/radicals. We therefore convert epithermal counting rates in terms of Water-Equivalent-Hydrogen, WEH. Given the summer count rates as a proxy for water content in the top meter of soil we can compute the CO_2 ice column abundance using Prettyman et al's [12] results. However, MONS counting-rate data have a FWHM of ~550 km., which is sufficiently broad to prevent a close association of WEH variability with images of geological features. In this study, we reduce spurious features in the instrument smeared neutron counting rates through deconvolution. We choose the PIXON numerical deconvolution technique for this purpose. This technique uses a statistical approach [13, 14] which is capable of removing spurious features in the data in the presence of noise. We have previously carried out a detailed study of the martian polar regions applying such a methodology to Martian epithermal neutrons [15,16]. In the present study, we will apply this technique to the recent reanalysis of MONS epithermal data [17], which is marked by significantly lower statistical and systematic uncertainties that have plagued older versions of these data.

Results: Preliminary data are encouraging. Figure 2 shows a pixon reconstruction of the Mars

Odyssey data for 0° <Ls < 30°. It shows the large deposits of CO_2 on the top of the water ice perennial cap. In addition it shows a spatial pattern that is consistent with the spatial distribution of the most dense distributed sand dunes. Previously we have shown a similar pattern of the epithermal count rates for H_2O [17] suggesting a genetic link between the water distribution in the dune subsurface and the spatial variation in the seasonal CO_2 ice deposits.

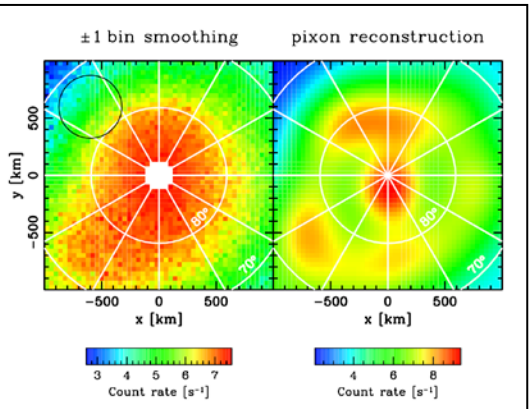

Figure 2: Left Panel Mons epithermal count rates data in 40X40 km bins. The dark circle in the top left corner represents the MONS point spread function. **Right panel** From the left to the right we show the MONS data and pixon reconstruction for 0° < Ls < 30°. The
dark circle in the left panel represents the MONS response function. The red area is the CO_2 polar cap. Whilst the dark blue regions indicate the presence of water ice.

Conclusion:

- The application of the Pixon technique improves the spatial resolution of the MONS data to ~150 km FWHM.
- A heterogeneous distribution in the deconvolved epithermal count data suggest spatial variability associated with the dunes in the CO_2 abundance of the circum-polar area.
- Ongoing work will determine the potential role of buried H_20 ice within the dunes in controlling the build up and decay of seasonal CO_2 ice and its annual variability.

References

[1] James, P.B. *et al.*, The Seasonal Cycle Of Carbon Dioxide On Mars in *Mars*, edited by H.H. Kieffer *et al.* (The University of Arizona, Tucson, Arizona, 1992), pp. 934-968.
[2] Kieffer, H.H. *et al.*, (1976) *Science* 194, 1346-1351.
[3] Neumann, G.A. *et al.*, (2003) *J. Geophys. Res.* 108 (E4), 5023.
[4] Pearl, J.C. *et al.*, (2001) *Journal of Geophysical Research (Planets)* 106 (E6), 12,325-12,338.
[5] Kieffer, H.H. *et al.*, (2001) *Icarus* 154 (1), 162-180.
[6] Titus, T.N. *et al.*, (2001) *Journal of Geophysical Research* 106 (E10), 23,181-23,196.
[7] Forget, F. *et al.*, (1995) *J. Geophys. Res.* 100 (E10), 21219-21234.
[8] Ivanov, A.B. *et al.*, (2001) *Icarus* 154 (1), 190-206.
[9] Forget, F. *et al.*, (1998) *Icarus* 131 (2), 302-316.
[10] Kieffer, H.H., (2007) *Journal of Geophysical Research (Planets)* 112, 08005.
[11] Bourke, M.C. *et al.*, (2011) Fifth International Conference on Mars Polar Science.
[12] Prettyman, T.H. *et al.*, (2009) *Journal of Geophysical Research (Planets)* 114 (E08005).
[13] Pina, e.a., (1992) *PASP* 104 (1096).
[14] Eke, (2001) *MNRAS* 324 (108).
[15] Teodoro, L.F.A. *et al.*, (2011) AGU.
[16] Teodoro, L.F.A. *et al.*, (2012) EGU General Assembly.
[17] Feldman, W.C. *et al.*, (2012) 43rd LPSC Conference, abs# 2170.

ON THE SOURCES OF DARK DUNE SANDS ON MARS. D. Tirsch[1] and R. Jaumann[1,2], [1]Institute of Planetary Research, German Aerospace Center (DLR), Rutherfordstrasse 2, 12489 Berlin, Germany, (Daniela.Tirsch@dlr.de); [2]Institute of Geological Sciences, Freie Universität Berlin, Berlin, Germany.

Introduction and Background: Dark aeolian sediments can be observed almost all over Mars. They are preferably deposited as aeolian dunes on the floor of impact craters and in the north polar erg, but also as thin sand sheets and wind streaks in topographically unconfined places. The sediments are enriched in pyroxene and olivine pointing to a basaltic origin of the dune sands [1, 6]. Hypotheses of material origin include volcaniclastic sediments and volcanic ash [e.g. 1, 2], impact melts [3], and local geologic units, e.g. the Planum Boreum cavi unit [4] or the Medusae Fossae Formation [5].

In previous works [e.g. 6, 7] we have shown that the material seems to have its local source inside the depressions in the form of dark sedimentary layers exposed at crater walls or beneath crater floors – it is not blown into the craters as widely assumed. Similar intra-crater sources have also been described in Noachis Terra [8] and Amazonis Planitia [9].

In this work we present further examples of dark material emerging from local intra-crater sources and provide further spectral evidence for a mineralogical correlation between emerging material and the dune sands. The results will help to refine our view of these aeolian deposits on Mars.

Data and Methods: For feature identification HRSC nadir (12.5 m/px), CTX (6 m/px), and HiRISE (up to 0.25 m/px) image data were examined and provide a database from regional to local scale. Topographical information was gained from HRSC DTMs (up to 50 m/px). CRISM datasets with a spatial resolution of up to 18 m/px were used for the mineralogical analysis of the dark sediments.

Results and Discussion: We found numerous locations (e.g. western Arabia Terra, Noachis Terra, Terra Sirenum) where dark aeolian material emerges from distinct dark layers and is deposited as basaltic dunes nearby. The layers can be exposed at impact crater walls (Fig. 1, 2), along the scarps of channels and plateaus or are located beneath the floors of larger craters, which are blotched by smaller impacts. In the latter case the dark material emerges from these small impact craters, cutting the subsurface dark layer (Fig. 3). It is unlikely that the aeolian material has been blown into these small craters earlier because there are numerous similar craters nearby comprising no dark sand at all. These "clean" craters did not cut the subsurface layer because it is heavily degraded and fragmented. Hence it can take place that craters comprising dark sand and

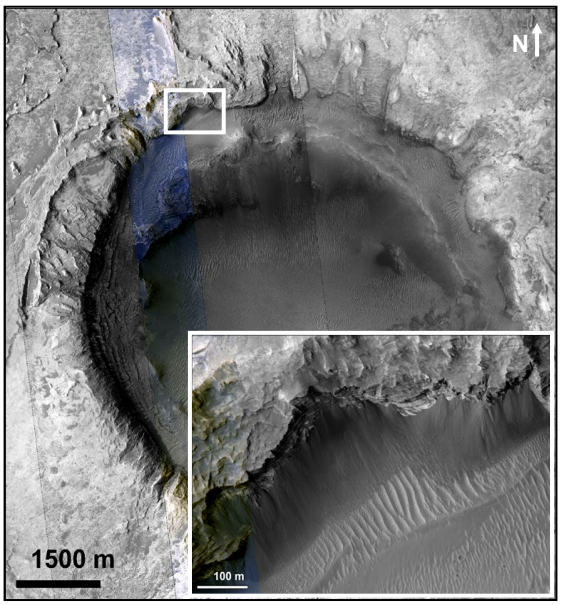

Fig. 1: A 7.8 km crater near Meridiani Planum showing layered structures and dark aeolian sediments emerging from a dark layer exposed in the crater wall. White box indicates location of inset (color and red image of HiRISE observation ESP_011277_1825 superimposed onto CTX P12_005647_1814_XI_01N002W, image center is at 2.5°S; 2.2°E).

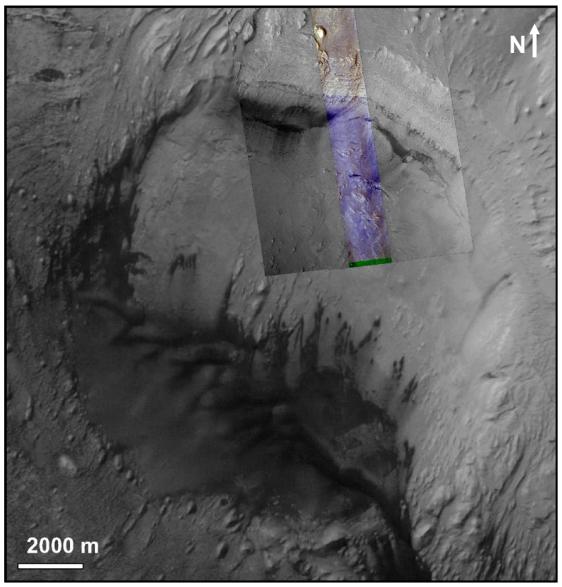

Fig. 2: A 14.3 km crater south of Crommelin crater featuring a dark sedimentary layer exposed at the northern wall and material transport going down-wall. (HiRISE ESP_012385_1825 color and red images on top of HRSC H3253_0002 nadir, image center is at 9.66°S; 2.55°W).

craters lacking dark sand occur right next to each other (Fig. 3, 4). Following our analysis no other regional sources could be identified. Sand transport pathways usually go from the layers to the dunes or start downwind of the dune deposits (Fig. 2, 3).

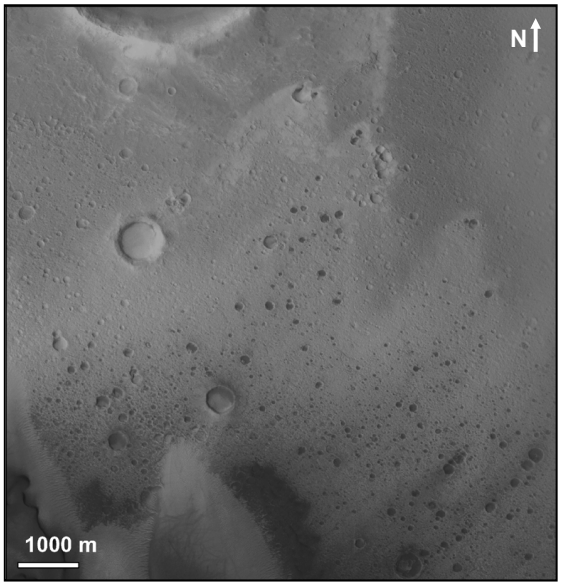

Fig. 3: Close-up of Trouvelot's crater floor, blotched by numerous smaller craters exposing dark aeolian sediments (CTX mosaic, image center is at 13.35°S; 16.17°W).

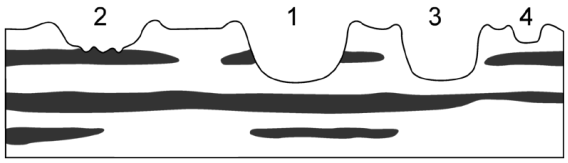

Fig. 4: Crater-Layer-Relationships. 1) Crater cuts dark layer completely, exposing a dark layer at the crater wall. 2) Crater cuts top of dark layer, exposing the dark layer at the crater floor. 3) Impact did not hit dark layer. 4) Impact did not reach the depth of dark layer. [6]

CRISM I/F observations show that the mineralogical composition of the emerging dark material correlates well with the dark dunes and sand sheets. Figure 5 shows rationed spectra of dark sediment emerging from small impact craters and dark dunes deposited on the floor of a crater NW of Crommelin crater. Both spectra show the typical broad absorption bands at 1 µm and around 2 µm indicating a mixture of olivine and pyroxene as it is typical for the dark sediments on Mars [6]. A similar correlation was also observed between wall and dune material [6].

Conclusions: The fact that the source material of the dark basaltic dunes is deposited as distinct geologic layers in many cases weakens the source hypotheses of impact melts because these permanently ongoing processes would not result in a discrete layer unit but produce material which is permanently mixed with bed rock material or regolith. The geologic setting rather points to single (or multiple) distinct source events such as volcanic eruptions producing thick ash layers, which are subsequently buried by regolith and reactivated by impact erosion. The Planum Boreum cavi unit could be the result of ash transport and deposition to the north poplar region as it is a sandy, even, and cross-bedded layer sequence, as typical for aeolian deposits. If the Medusae Fossae Formation hosts similar sedimentary layers acting as a local source for the dunes deposited there, need to be analyzed in detail.

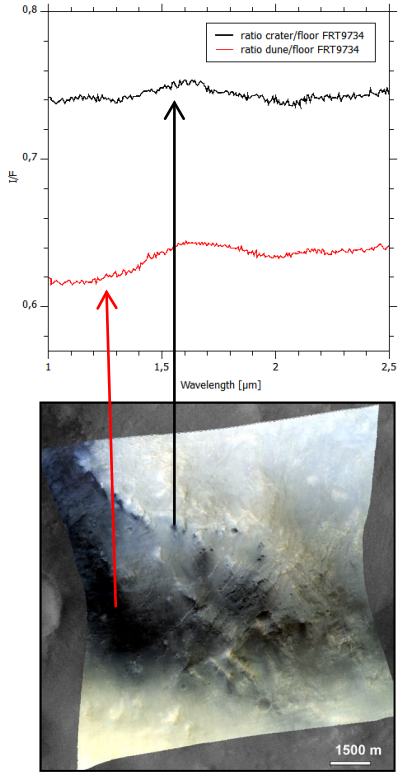

Fig. 5: Rationed near-infrared spectra of material emerging from a dark layer and dune forming material (CRISM FRT00009734_07_if165l_trr3, lower image is VIS RGB, north is to the top).

Acknowledgements: This research has been supported by the Helmholtz Association through the research alliance 'Planetary Evolution and Life'.

References: [1] Tirsch D. et al. (2012) *Earth Surf. Process. Landforms, 37, 434-448*. [2] Edgett, K.S. and Lancaster N. (1993) *J. Arid. Env.* 25(3), 271-297. [3] Schultz P.H. and Mustard J.F. (2004) *JGR*, 109, doi: 10.1029/2002JE002025. [4] Tanaka K.L. and Hayward R.K. (2008) *LPI Contrib.* 1403, 69-70. [5] Burr D.M. et al. (2011) *LPSC XXVII,* Abstract #1582. [6] Tirsch D. (2011) JGR, 116, doi: 10.1029/2009JE003562. [7] Tirsch D. (2009) *LPSC XL*, Abstract 1004. [8] Fenton L.K. (2005) *JGR* 110, doi:10.1029/2005JE002436. [9] Stockstill-Cahill K.R. (2008) *JGR,* 113, doi: 10.1029/2007JE003036.

THERMAL DIFFUSIVITY EXPERIMENT AT THE GRAND FALLS DUNE FIELD. T. N. Titus[1] and G. E. Cushing[1], [1]U.S.G.S. Astrogeology Science Center, 2255 North Gemini Dr., Flagstaff, AZ 86001

Introduction: Thermal inertia is a commonly derived surface property for many terrestrial solar system bodies (e.g. Mars [1,2], Vesta [3], the Moon [4]). Thermal inertia is defined as $I = \sqrt{k\rho c}$, where *k* is thermal conductivity, ρ is the density and *c* is the heat capacity. Thermal inertia, unlike surface temperature, is treated as a surface invariant and can therefore be mapped. High thermal inertia indicates exposed rock while low thermal inertia indicates fine grain material, such as dust or sand. Complicated numerical models are needed to convert observed surface temperatures into thermal inertia; these models include several other input parameters – such as albedo, slopes, and surface roughness. Most models assume that the surface properties are vertically homogeneous. A few models allow for compositional gradients or 2 layers (e.g. [5]). These compositionally multilayered models are usually only used where large differences are expected – such as a layer of ice covered by a thin layer of dust (e.g. [6]). This study will focus on testing the assumption of vertical homogeneity in the top 20 cm of sand in a local dune field.

This study focuses on *in situ* temperature observations of one location on a dune field located in northern Arizona. Because temperatures are measured at the surface and at several depths, the usual complex numerical models that require knowledge of albedo and slope are unnecessary. A simple analytical solution to the thermal diffusion equation is all that is required to test the homogeneity of the top layer of the sand.

Thermal Physical Properties: Temperature as a function of depth can be determined by solving:

$\frac{\partial T}{\partial t} = \alpha \frac{\partial^2 T}{\partial z^2}$, where $\alpha = \frac{k}{\rho c}$, α is the coefficient of thermal diffusion (thermal diffusivity), *T* is temperature and *z* is depth.

Thermal Skin Depth: The thermal skin depth is a measure of how far either a diurnal or annual surface temperature cycle penetrates the regolith. The exact definition is the depth at which the amplitude of the thermal wave is attenuated by a factor 1/e.

$D = \sqrt{\frac{kP}{\pi\rho c}} = \sqrt{\alpha \frac{P}{\pi}}$, where *D* the skin depth, and *P* is the period of the cycle (86,400 sec for the terrestrial diurnal cycle).

Diffusion Equation Solution: Since the surface temperature is cyclic, one convenient and useful solution is:

$$T(t,z) = T_0(z) + \sum_i e^{-z/D_i}(A_i \cos\theta_i(t,z) + B_i \sin\theta_i(t,z))$$

where

$\theta_i(t,z) = \frac{2\pi i}{P} t - \frac{z}{D_i}$ and $A_i^2 + B_i^2 = 1$.

For the diurnal thermal wave, the temperature profiles can usually be described using as few as 3 harmonics (i=1,2,3) using linear regression of sines and cosines. The attenuation of the amplitude between sensors allows the calculation of skin depth as a function of depth.

Data Collection: Temperature data was collected for nearly a week at a single location at the Grand Falls dune field, near Leupp, AZ. A series of temperature probes were attached to a pole. The sensors were separated by 4 cm and the pole was placed in the sand so that the top sensor was at the surface (Fig. 1). The sand in this region was observed to be loose and dry. To allow the temperature probes to reach equilibrium with the sand, we excluded the first50 minutes of data.After about 20 hours of data collection, a sand storm altered the placement of the temperature probes. Therefore, only 19 hours of temperature data were available.

Table 1: Physical Properties of Sand (Source: http://www.engineringtoolbox.com)

	Density (Kg m^{-3})	Heat Capacity	Conductivity (W m^{-1} K^{-1})	Diurnal Skin Depth (cm)
Dry Sand	1281	830	0.15 – 0.25	6.2-8.0
Wet Sand	1922		0.25 – 2	6.6-18.6
Saturated	2082		2 - 4	18-25

Analysis: While most thermal inertia studies are expressed in either units of thermal inertia or thermal conductivity, this study presents the results as units of skin depth in centimeters. Neither the density nor the heat capacity of the sand at the Grand Falls dune field was measured. The results from comparing the amplitude attenuation with depth are thermal diffusivity, α. However, α can be converted to effective skin depths

Figure 1: Equipment layout used to collect temperatures.

which are independent of assumptions about density and heat capacity, but retain results that can easily be compared to Table 1. The results of this analysis is shown in Table 2. A decrease in the thermal diffusivity as a function of depth is quite apparent. There are three possible causes for this effect: (1) an increase in moisture with depth, a decrease in particle size (related to *k*) with depth, or (3) a decrease in density (or heat capacity). Because the sand was observed to be dry, it is unlikely that the sand has a moisture gradient. Particle size variations were not observed either. Therefore the vertical layering of the sand must have a density gradient, which could be caused by compaction at the lower layers. Based on the change in skin depths, the change in density would need to be a factor of 2.

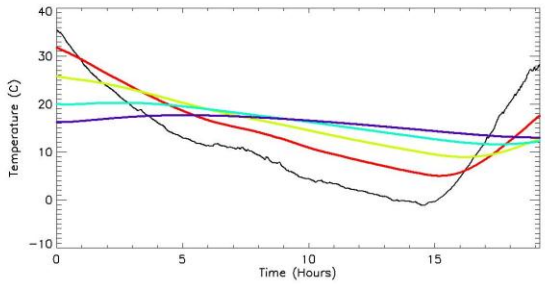

Figure 2: Temperature data collected from Grand Falls dune field over a period of 19 hours. The temperatures were collected at the surface, and at depths 4cm, 8cm, 12cm, and 16cm (black, yellow, cyan, and purple, respectively).

Summary: The top 16 cm of the dune field was not homogeneous with depth, but varied in at least one of the thermal physical parameters: density, heat capacity, and thermal conductivity. The most likely cause is an increase in density with depth, suggesting that the top 8 cm may be a less-dense active layer and the lower layer (depth greater than 8 cm) is a denser, less active layer.

Table 2: Estimated Skin Depth Results for the 1st three harmonics.

	Effective Skin Depth (cm)		
Depth (cm)	P=24 hours	P=12 Hours	P=8 Hours
0-4	9.14	9.38	11.5
4-8	8.39	9.21	15.5
8-12	6.90	7.18	11.1
12-16	6.37	5.34	7.24

Future work: This study was conducted at one location for a short period of time. The authors of this study intend to expand the thermal measurements to multiple locations, at greater depth, over a period of several diurnal cycles.

Acknowledgements: We wish to thank Rose Hayward for her insightful comments.

References: [1] Christensen, P.R. et al. (2001) JGR, 106, 23823-23872. [2] Mellon, M.T. et al. (2000) Icarus, 148, 437. [3] Leyrat, C. et al. (2012) A&A, 539, 154. [4] Paige, D.A. (2010) SSRv, 150, 125. [5] Kieffer, H.H. (1977) JGR, 82, 4249. [6] Titus, T.N. (2003) Sci., 299, 1048.

OBSERVATIONS ON DUNE BEHAVIOR AT GREAT SAND DUNES NATIONAL PARK, COLORADO.

Andrew Valdez, Great Sand Dunes National Park and Preserve, 11500 Highway 150, Mosca, CO 81146, USA (andrew_valdez@nps.gov)

Introduction: Dune migration measurements have been made by the National Park Service (NPS) at Great Sand Dunes, Colorado. The development of GPS satellites as a mapping tool in the 1990s has allowed the NPS to map the position of several index dunes on an annual basis. A time series of aerial imagery has also been used by the NPS and others [1] to measure dune movement from the 1930s to the present. The have also been periodic surveys with a total station to measure dune height on some of the larger dunes at Great Sand Dunes. In October 2011, Great Sand Dunes have been mapped by LiDAR. If that data becomes available, it will be included in the presentation and a comparison will be made of measuring dune heights with LiDAR vs. conventional surveying.

Great Sand Dunes, Colorado is the site of an aeolian system that varies along a topographic gradient [2], Figure 1. It originates at a playa system [3]

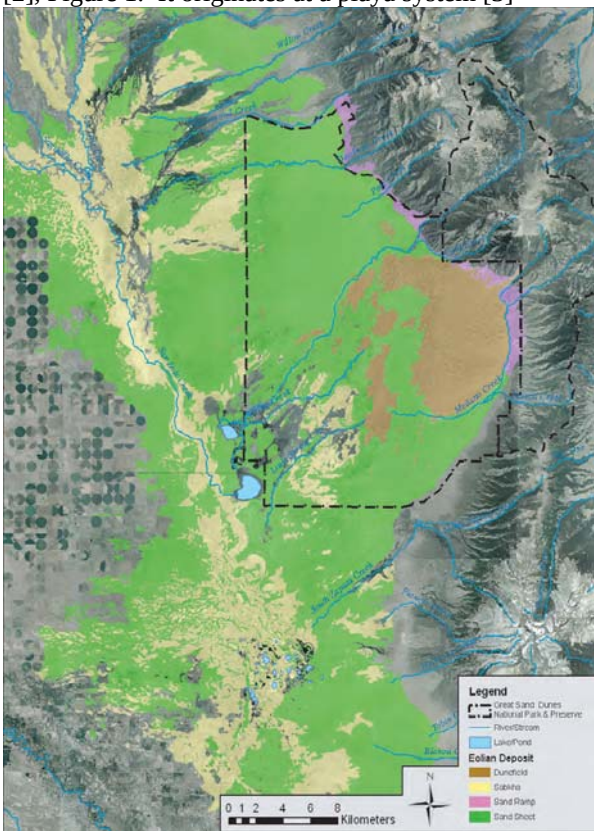

Figure 1: Aeolian Sand Deposits at Great Sand Dunes. The deposits consist of inland sabkhas (yellow), sand sheets (green), active dunefields (brown), and sand ramps (purple).

where sabkha deposits are found. As the land surface rises above the capillary fringe, sand sheets develop. Near the mountain front is the dunefield and along the mountain front are sand ramps. So the playa is the site of aqueous concentration of sand. Once exposed to wind, the sand is transported across the sand sheet. At the mountain front the wind regime changes and creates a depo-center where the dunefield is found. Because of variation in wind regime, sand supply, vegetation, and topography, a variety of dune types have developed [2], Figure 2.

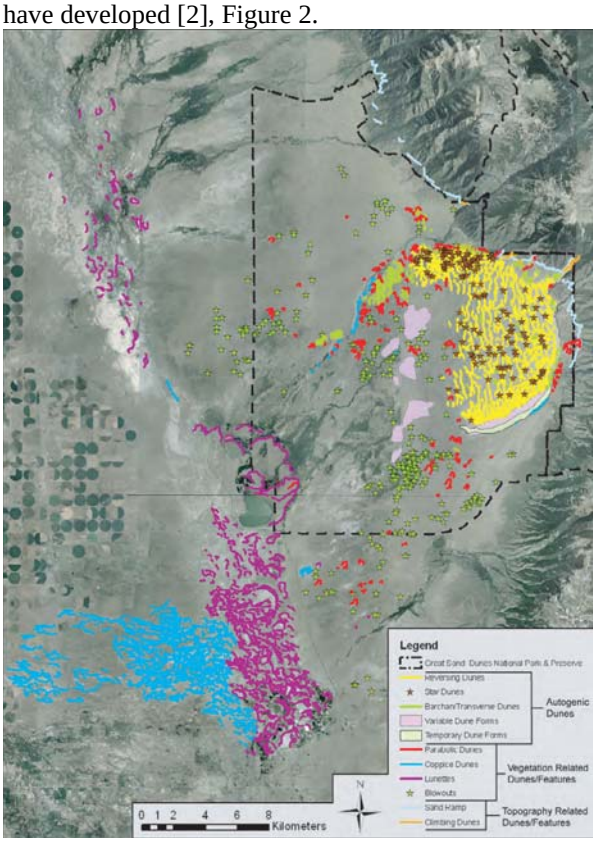

Figure 2. Dune types at Great Sand Dunes.

Problem Statement: The NPS manages Great Sand Dunes and is interested in understanding the behavior of the sand dunes and how the aeolian system works. Essential to that is monitoring dune movement and growth. There are areas with a unimodal wind regime where migratory dunes form and areas with bimodal and complex wind regimes where vertically growing dunes form.

Great Sand Dunes is known for having the tallest dunes in North America, so understanding the vertical

growth component is also important. Elevation changes have been tracked and field observations have also led to ideas about how the vertical growth occurs.

Results: The dunes with the longest period of measure are a barchan/parabolic dune known as the escape dune and the tallest dune in the park knows as the star dune. Up-to-date data is available, but Figure 3 shows that from 1992 to 2006, the escape dune has migrated more then 120 meters toward the northeast. That is an average of 8.6 meters/year. Much of the migration is during the spring where migration as high as 6 meters in 40 days have been measured.

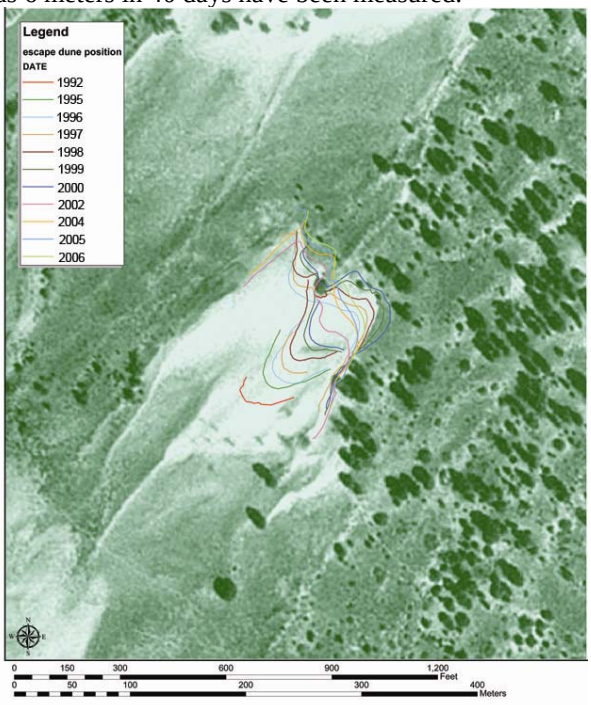

Figure 3. 1992 to 2006 locations of the "escape dune" at Great Sand Dunes, Colorado.

The star dune is in a bi-model wind regime and its position tends to oscillate with some net migration toward the northeast. Elevation measurements suggest that when the dune's crest migrated toward the northeast, the crest elevation drops. When the crest migrates back toward the southwest, it gains elevation.

Data from other dunes would also be presented.

Conclusions: The unimodal dune forms are smaller and have shown more migration, but all show a net migration toward the northeast. Vertical growth on large dunes requires an input of new sand.

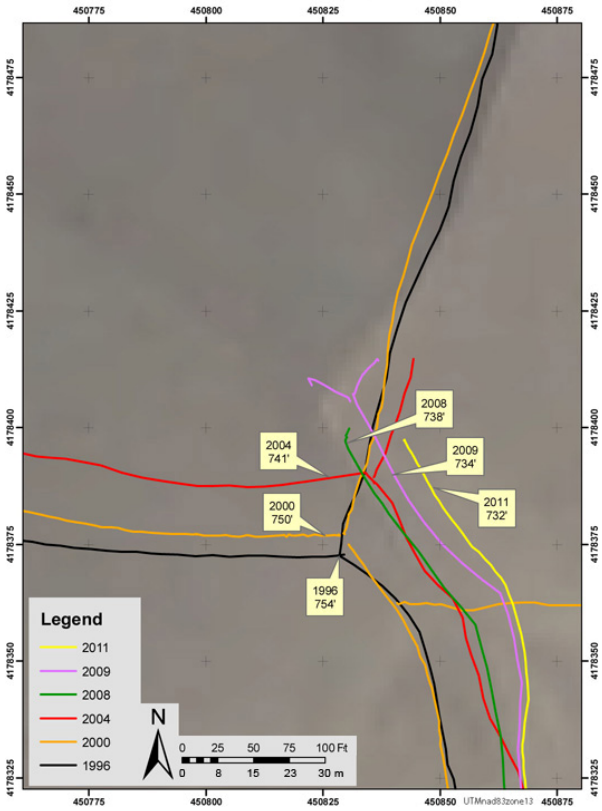

Figure 4. 1996 to 2011 locations and heights of the "star dune" at Great Sand Dunes, Colorado.

References: [1] Foreman, S. L., Episodic Late Holocene dune movements on the sandsheet area, Great Sand Dunes National Park and Preserve, San Luis Valley, Colorado, USA. Quaternary Research 66 p 97–108, 2006

[2] Valdez, A. D., Development and Eolian Geomorphology of Great Sand Dunes in Quaternary Geology of Great Sand Dunes, USGS Open File Report 2007-1193 p 7-10, 2007

[3] Madole, R. F., On the origin and age of the Great Sand Dunes, Colorado, Geomorphology 99 p 99-119, 2008

AN OBJECT BASED APPROACH FOR THE MAPPING AND CHARACTERIZATION OF MARS RIPPLES. D. A. Vaz[1,2] and S. Silvestro[3], [1]Centre for Geophysics of the University of Coimbra, Observatório Astronómico da Universidade de Coimbra, Almas de Freire, 3040-004 Coimbra, Portugal (vaz.david@gmail.com), [2]CERENA, Instituto Superior Técnico, Lisboa, Portugal, [3]SETI Institute, Carl Sagan Center, 189 N. Bernardo Avenue, Mountain View, CA, USA.

Introduction: Mapping and characterization of active aeolian processes from remote sensing data on Mars has been growing after the advent of HIRISE imagery. The spatial resolution of the data (0.25 m/pix) permit the study of even small-scale aeolian features, such has ripples. Ripple migration rates were estimated [1] and dramatic changes of the ripple patterns were described based on the analysis of temporal series of HIRISE observations [2].

We have focused our initial efforts in the human analysis and change detection of ripple patterns, but we have quickly realized that automated image processing tools would be required due to the increasing amount of available data. We have envisioned and started to implement an integrated framework for mapping and characterizing ripple patterns on Martian dunes.

Methodology: Automated ripple pattern characterization techniques are not new [3], and estimates of migration rates were made using the COSI-Corr subpixel correlation on Earth [4] and on Mars [5].

The mentioned approaches rely on a pixel or subpixel based analysis, but the high spatial resolution of the HIRISE imagery is ideal to the application of object based image analysis (OBIA) techniques [6]. We choose this approach because it allows the natural integration of textural, spectral and spatial information. Other important concern was that the targeted framework would have to be able to integrate change analysis using temporal series of images.

Orthorectified HIRISE images and DTMs are the standard input datasets used. The main steps of the proposed methodology are ripple segmentation, vectorization and object characterization. A set of morphological operations using line segments as structuring elements is used in order to achieve ripple segmentation. After that, a hysteresis threshold generates a ripple marker matrix. The applied vectorization process is the same presented in [7]. At this point, we have a set of objects (lines) which mark the spatial location of each ripple. To be more precise, it marks the center of the illuminated side of the ripples.

Several parameters are then computed and linked with each ripple line. Spatial parameters (length, azimuth, and sinuosity) as well as morphometric parameters computed from the DTM (slope, aspect, longitudinal dip) are some of the derived parameters (fig, 1a,b and d). Besides the reflectance data computed from the image, more complex multi-scale textural information is also stored. Morphological orientation fields are computed at different scales and are integrated on the mapped objects.

Application examples: Ripple population circular statistics can be easily analyzed. Length weighted circular distributions can be produced and the main trends identified [8]. The same kind of analysis can be performed locally by deriving a vectorial field from the ripple lines. Assuming that the ripples formed perpendicular to the main wind regimes, an axial vector can be generated for a given area representing the orientation of the main winds. This should be considered a first approximation since complex ripple patterns, with more than one main ripple orientation are common. In those cases, we use the textural parameters to segment ripple populations, and generate a primary and secondary axial fields. This is particularly suited to analyzed areas with more than one set of ripples [9].

Ripple wavelengths can also be estimated, allowing the spatial analysis of the variation of this parameter (fig. 1c), which can be converted to ripple heights, and used to derive sand fluxes [5].

Temporal analysis is not yet fully supported. Ripples are nearly periodic features whose migration can hardly be described has a simple translation. In Gale crater for example, a firm correlation between ripples is not possible everywhere. In localized areas near the dune brinks, the ripple pattern seems to be completely different suggesting that a migration of more than one crest wavelength has occurred. The periodic nature of the ripples, defect migration, re-orientation of the pattern and appearance of secondary ripple sets are important factors that must be considered when a ripple correlation is attempted. If we consider that the migration was higher than one ripple wavelength we could barely assure that a correlation is meaningful [10]. We have adopted the conservative approach of assuming that the displacements were less than half the wavelength, and measure the displacements between neighbor ripples in the two time-lapse images. Those assumptions imply that we are measuring a minimum possible displacement [2].

Conclusions: Work is underway to improve and expand the described object based ripple pattern characterization techniques. Although the mentioned limita-

tions, migration estimates through feature correlation is under development.

References: [1] Silvestro S., et al. (2010) *Geophys. Res. Lett.*, 37, L20203. [2] Silvestro S., et al. (2011) *Geophys. Res. Lett.*, 38, L20201. [3] Skarke A. and A. C. Trembanis (2011) *Cont. Shelf Res.*, 31, 1688-1700. [4] Vermeesch P. and N. Drake (2008) *Geophys. Res. Lett.*, 35, L24404. [5] Bridges N. T., et al. (2012) High sand fluxes and abrasion rates on Mars determined from HiRISE images, *LPSC XLII, Abstract #1322*. [6] Blaschke T. (2010) *ISPRS J. Photogramm. Remote Sens.*, 65, 2-16. [7] Vaz D. A. (2011) *Planet. Space Sci.*, 59, 1210-1221. [8] Silvestro S., et al. (2012) Active Aeolian Processes Along Curiosity's Traverse in Gale Crater, *LPSC XLII, Abstract #1659*. [9] Ewing R. C., et al. (2010) *J. Geophys. Res*, 115, E08005. [10] Lorenz R. D. and A. Valdez (2011) *Geomorphology*, 133, 1-10.

Acknowledgements: This work was supported by FCT (Fundação para a Ciência e a Tecnologia) under grant SFRH/BPD/72371/2010, with Portuguese and European funds.

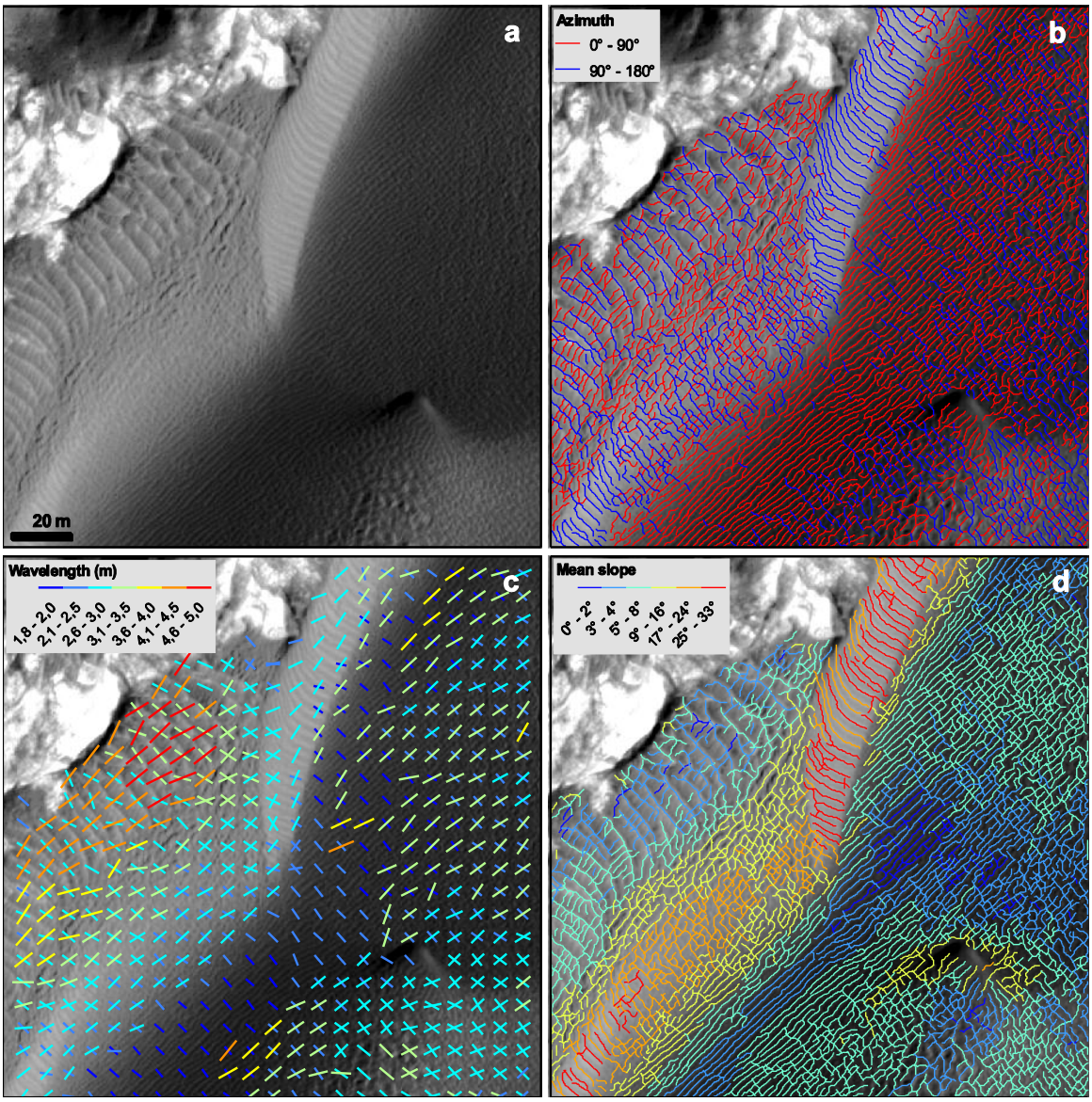

Fig. 1 – a) Gale crater HIRISE image; b) azimuth segmentation of mapped ripple traces; c) axial representation of the ripple wavelengths for the two populations segmented in b); d) ripples regional mean slope extracted from the HIRISE DTM.

Basaltic sand ripples in Eagle crater as indirect evidence for the hysteresis effect in Martian saltation.

H. Yizhaq[1] and J. F. Kok[2], [1]Solar Energy and Environmental Physics, BIDR, Ben-Gurion University, Midreshet Ben-Gurion, Israel (yiyeh@bgu.ac.il), [2]Department of Earth and Atmospheric Sciences, Cornell University, Ithaca, New York, 14853, USA (jasperkok@cornell.edu).

Introduction: Aeolian ripples, which form regular patterns on sand beaches and desert floors and also on Mars, indicate the instability of flat sand surfaces under the wind-induced transport of sand grains. The opportunity rover documented small normal basaltic sand ripples at the bottom of Eagle crater [1]. These ripples are composed of fine sand (100 micron) and their average wavelength and height are 10 cm and 1 cm respectively. Such light particles are thought to be easily suspended by turbulence at the fluid threshold, such that the wind speed at which these bedforms develop must be substantially below the fluid threshold. The occurrence of these bedforms on the Martian surface thus requires the impact threshold to be substantially smaller than the fluid threshold. Recently [2], it was suggested that saltation on Mars can be maintained at much lower wind speeds than the fluid threshold which is needed to initiate it. We used the COMSALT model for saltation [3] together with a dynamic model for sand ripples [4] to show that the small basaltic ripples can develop under wind speeds below the threshold for suspension.

COMSALT includes many of the advances of previous models [e.g., 5], and in addition it includes: (1) a physically based parameterization of the splashing of surface particles that agrees with experimental and numerical studies [3], (2) a generalization of this splashing process to beds of mixed particle sizes, and (3) a detailed treatment of the influence of turbulence on particle trajectories, which agrees with laboratory measurements. Because of these and other advances, COMSALT is the first physically-based numerical saltation model to reproduce a wide range of experimental data. The model has also been recently used to show that saltation can be maintained on Mars by wind speeds an order of magnitude less than those required to initiate it [2].

We used COMSALT to give the basic values of the parameters used by the ripple model for saltation on Mars, specifically the average number of reptating grains per impact of one saltating grain, the number density of saltator impact on a flat surface, and the probability distribution of reptation length.

The ripple model is based on the classic approach of Anderson (1987) [6] and includes a correction to the reptation flux that depends on the local bed slope [4]. According to Anderson's model, the sole role of saltating grains is to bring energy into the system, extracting it from the wind that blows above the surface of the sand. In this view, ripple formation is due entirely to spatial changes in the reptation flux. We thus built a one dimensional heuristic model of sand transport based on the Exner equation [4]:

$$(1-\lambda_p)\rho_p \frac{\partial h}{\partial t} = -\frac{\partial Q}{\partial x}, \qquad (1)$$

where $h(x,t)$ is the local height of the sand surface at point x and time t, λ_p is the porosity of the bed, ρ_p is the grain density and $Q(x,t)$ is the sand flux, which includes both saltation and reptation flux. Here, we assume that saltation flux can be taken as constant and we do not take it into consideration in the Exner equation. Thus, in Eq. 1 we take into account only reptation flux of fine particles, Q_{rf}. The reptation flux at a certain point and time is obtained by the sum of all the grains that pass that point at that time. The grains have a probability distribution of reptation lengths $p_f(\alpha)$. Following Anderson (1987), we derive the explicit expression for reptation flux on a flat surface:

$$Q_{rf}^0 = m_f n_f \int_0^\infty d\alpha\, p_f(\alpha) \int_{x-\alpha}^{x} N_{im}(x')dx', \qquad (2)$$

where the subscript f denotes fine grains, m_f is the mass of each particle, n_f is the average numbers of reptating grains ejected by the impact of one saltating grain, and p_f is the probability distribution of reptating grains. Because saltation flux is uniform and the fixed angle ϕ at which the grains descend back to the ground is assumed to be constant, the number density of impacting grains changes only because of variations in bed slope. Based on geometrical considerations, we obtain,

$$N_{im}(x) = N_{im}^0 \frac{1+h_x \cot\phi}{\sqrt{1+h_x^2}}, \qquad (3)$$

where h_x is the local slope and N_{im}^0 is the number density of impacting grains on a flat surface. We further modify Eq. (2) to take into account correction of the reptation length on an inclined plane [4]. This correction leads to a mean reptation length that is shorter on the windward slope and longer on the leeward slope of the bedform. The full model can be written as:

$$h_t = -Q_0 \partial_x \left[(1-\mu_f) Q_{rf}^0 \right], \qquad (4)$$

where the parameter μ_f heuristically includes the correction to reptation flux discussed above, and $Q_0 = m_f n_{rf} N_{im}^0 \cot\phi / \rho_b (1-\lambda_p)$. The basic parameters

used in the model (N_{im}^{0}, n_f , $p_f(\alpha)$) will be given by COMSALT (see Figure 1), which simulates Martian conditions.

Results: Running COMSALT [2] for the unique Martian conditions (air pressure 700 Pa, air temperature 220 K, gravitational acceleration 3.72 m/s^2, and particle density 3000 kg /m^3) will give us the essential parameters that will then be used in the normal ripple evolution model. We will simulate the ripples for two cases, without any kind of cohesion and with cohesion [7].

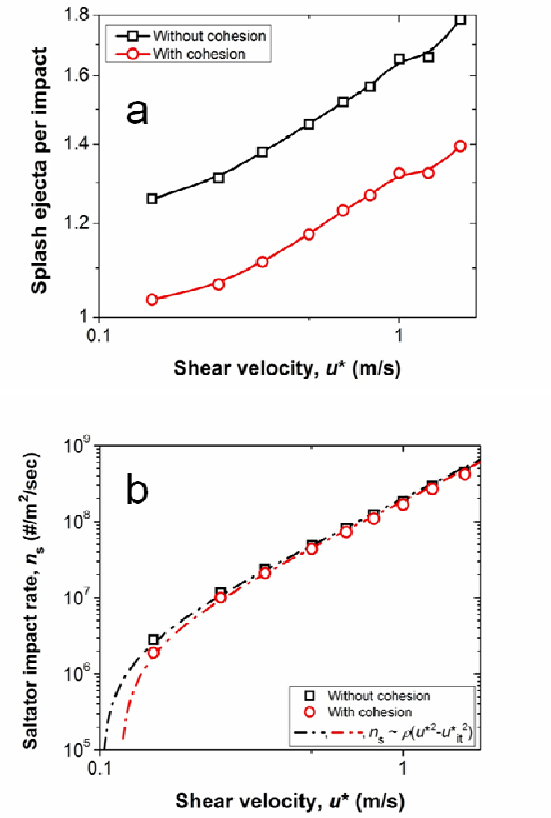

Figure 1: COMSALT simulation results for n_f (panel a) and N_{im}^{0} (panel b) for 100 micron under Martian conditions.

Together with the computed probability distribution of reptation length given by $p_f(\alpha) = s(1-\exp(-\sqrt{x/a}))(b/x)\exp(-\sqrt{x/b})$ where s, a, b are numerical constants.

Figure 1 shows the results of COMSALT simulations for two of the model parameters (Eq. 1): n_f , the average number of reptating particles per impact of saltation impactor (a) and N_{im}^{0} , the average impact number of saltation particles on a flat bed (diameter 100 micron) as a function of shear velocity under Martian conditions with and without cohesion between sand grains.

Figure 2 shows results of the one hour ripples simulations on Mars using the input from COMSALT (Figure 1) for different shear velocities. It looks that the observed basaltic ripples at Eagle crater (height 1 cm and wavelength of 10 cm) can be formed under the action of winds with shear velocities ($0.35 < u^* < 0.8$ m/s) which is much below the fluid threshold on Mars for this grain size which $u_{th}^* \sim 1.6$ m/s. This result is indirect evidence which supports the hysteresis effect in saltation on Mars [2].

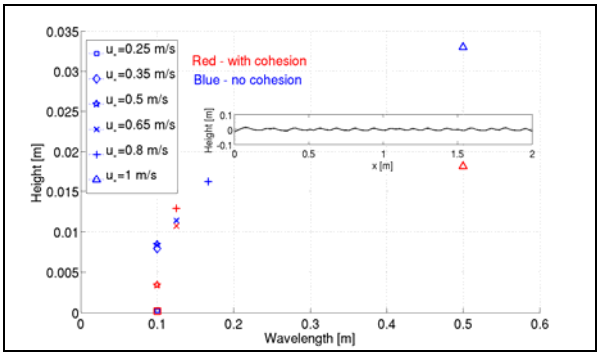

Figure 2: Model simulations (Eq. 1) of normal ripples on Mars with parameters computed by COMSALT for different shear velocities after one hour. The inset shows the final ripples profile for $u^* = 0.65$ m/s. Note that for higher values of shear velocity, the ripples become quite large .

Conclusion: Numerical simulations show that ripples like the basaltic ripples on Eagle crater can be developed by shear velocity of 0.5 m/s, much below the fluid threshold for 100 micron grain on Mars. These findings can be regarded as indirect evidence of the unique saltation mechanism on Mars and support recently observed migration of dunes and ripples [8] .

References: [1] Sulivan, R. et al., (2005) *Nature, 436*, doi: 10.1038 /nature03641. [2] Kok, J. (2010) *PRL,* 104, 074502. [3] Kok, J. and Renno, N. O. (2009) *JGR*, 114, D17204. [4] Yizhaq et al, (2004) *Physica D*, 195, 207-228. [5] Werner, B. T. (1990), *J. Geology*, 98, 1-17. [6] Anderson, R. S. (1987) *Sedimentology*, 34, 943-956. [7] Kok, J. (2010) *GRL*, 37, L12202. [8] Bridges, N. T. et al. (2011) *Geology*, doi:10.1130/G32373.1.

"THE ANSWER IS BLOWIN' IN THE WIND": THE REMARKABLE AEOLIAN CAREER OF RONALD GREELEY. J. R. Zimbelman[1], [1]CEPS/NASM MRC 315, Smithsonian Institution, Washington, D.C., 20013-7012; zimbelmanj@si.edu.

Introduction: In a career that spanned over four decades, Ronald Greeley (Fig. 1) was widely acknowledged as a driving force behind the growth and development of the field of planetary science, particularly planetary geology. He was a Regents' Professor in the School of Earth and Space Exploration at Arizona State University, and he contributed significantly to the scientific exploration of planetary bodies throughout the solar system. He passed away at his home in Tempe, Arizona, on October 27, 2011.

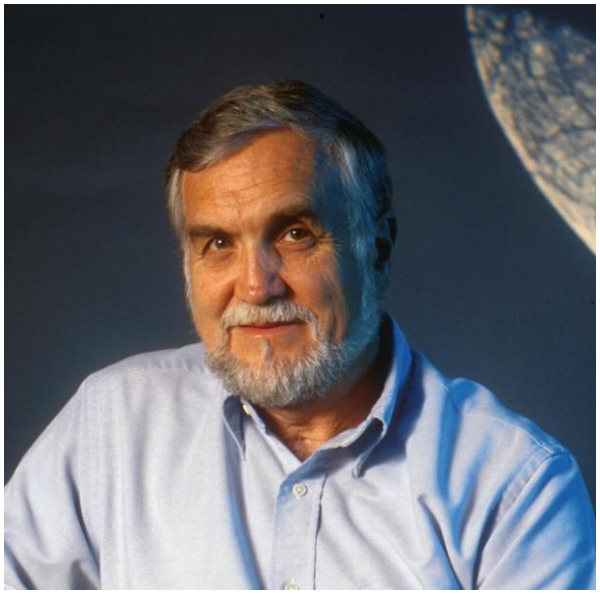

Figure 1. Ronald Greeley at Arizona State University.

Background: Greeley earned undergraduate and graduate degrees in geology from Mississippi State University and his doctorate in geology at the University of Missouri in Rolla in 1966. He worked for Standard Oil Company of California as a paleontologist before military duty assigned him to NASA's Ames Research Center at Moffett Field, California, in 1967. He continued work at Ames in a civilian capacity, studying impact cratering processes in preparation for the Apollo missions to the Moon, as well as the early Mariner investigations of Mars.

Greeley began teaching geology at Arizona State in 1977 while continuing to conduct research related to volcanism, wind-surface interactions, and the photogeological mapping of planets and their satellites. He was a pioneer in the combination of the interpretation of planetary image data with both laboratory experiments and field studies of terrestrial analogs, in order to understand the processes that contributed to the geologic history of planetary surfaces.

Greeley was a member of several science teams for robotic spacecraft missions to Mars, Venus, and the moons orbiting the giant outer planets. He was a Fellow of the American Geophysical Union and the American Association for the Advancement of Science. In 1997, he was awarded the G. K. Gilbert Award by the Planetary Geology Division of the Geological Society of America. He authored or coauthored 16 books and more than 450 scientific papers. Greeley taught a variety of subjects, and through the numerous students he influenced so greatly, he will continue to impact planetary science in general, and aeolian studies in particular, well into the future. Ron was active in many diverse lines of research; here we concentreate on his many contributions to aeolian research, including the expansion of this topic to include planetary bodies other than Earth.

Aeolian Research: In an attempt to restrict the discussion to publications relating specifically to aeolian studies, Greeley's extensive publication list was reviewed, resulting in the identification of more than 140 peer-reviewed publications that deal with this topic. Following is a list of 54 Greeley publications in an attempt to illustrate the diversity of aeolian subjects that his research touched upon; readers will find citations to many other Greeley aeolian publications in the reference lists of the papers listed below.

Greeley's involvment in investigating aeolian problems began with wind tunnel studies designed to understand how wind-related features can form in the current Martian environment [1], which in turn led to important contributions to the theory of particle motion on Mars [2-4]. The combination of laboratory and theoretical work was then applied to the interpretation of features observed in spacecraft images obtained from Mars [5, 6]; the triad of laboratory/field studies, theory, and spacecraft data analysis established a pattern of investigation that typified all of Greeley's subsequent studies.

It is impossible to do justice to the numerous subjects that Greeley's aeolian research dealt with. In lieu of that, below are several broad subjects in planetary aeolian studies along with some of Greeley's published work related to the topic: wind tunnel and laboratory experiments [1, 8-13, 33, 37, 42, 46, 53], erosion and abrasion by wind-blown sand [10, 13, 30, 48, 51], particle motion induced by the wind [2-4, 8, 13, 14, 17,

36, 50], dust mobilization and dust devils [9, 13, 24, 33, 36, 37, 41, 46, 47, 52-54], field investigations of aeolian sites [13, 14, 16, 18, 24, 26, 35], radar studies [13, 17, 20, 27], General Circulation Models [23, 25], Viking [5-7, 13, 19, 21, 23, 34, 38, 39, 41], Pathfinder [29-32, 35], Mars Exploration Rover (MER) missions 40, 44, 45, 47-51, 54], High Resolution Stereo Camera (HRSC) [43, 52], Magellan [20, 22, 25, 28], Mars [1-10, 13, 19, 21, 23, 29, 30, 33-54], Venus [11-13, 15, 20, 22, 25, 28], and Titan [13, 42]. The 1985 book "*Wind as a Geological Process: Earth, Mars, Venus, and Titan*", which Greeley co-authored with J.D. Iversen [13], has become a standard reference for most planetary aeolian studies, comparable in many respects to the continued citation of Bagnold's seminal book.

Greeley's aeolian research either initiated or enhanced many of the topics that will continue to be significant to planetary aeolian research in the decades to come. Greeley's impressive record demonstrates to all of us that often the answer can be found "blowin' in the wind" (with a nod to the Joan Baez song of the 1970s). Ron will be greatly missed by all of us.

References: [1] Greeley, R., et al. (1974) *Science 183*, 847-849. [2] Iversen, J.D., et al. (1976) *Icarus 29,* 381-393. [3] White, B., et al. (1976) *J. Geophys. Res. 81*, 5643-5650. [4] Greeley, R., et al. (1976) *Geophys. Res. Lett. 3*, 417-420. [5] Veverka, J., et al. (1977) *J. Geophys. Res. 82*, 4167-4187. [6] Greeley, R., et al. (1978) *Icarus 34*, 556-567. [7] Tsoar, H., et al. (1979) *J. Geophys. Res. 84*,8167-8180. [8] Greeley, R., et al. (1980) *Geophys. Res. Lett. 7*, 121-124. [9] Greeley, R., et al. (1981) *Geol. Soc. Amer. Spec. Paper 186*, 101-121. [10] Greeley, R., et al. (1982) *J. Geophys. Res. 87*, 10,009-10,024. [11] Greeley, R., et al. (1984) *Icarus 57*, l12-124. [12] Greeley, R., et al. (1984) *Icarus 60*, 152-160. [13] Greeley, R., and Iversen, J.D. (1985) *Wind as a Geological Process: Earth, Mars, Venus, and Titan*, Cambridge Univ. Pr., Cambridge, 333 p. [14] Greeley, R., and Iversen, J.D. (1987) *Geophys. Res. Lett. 14*, 925-928. [15] Greeley, R., et al. (1987) *Nature 327*, 313-315. [16] Lancaster, N., et al. (1987) *Earth Surf. Proc. Landforms 12*, 277-288. [17] Greeley, R., et al. (1988) *Geophys. Res. Lett. 15*, 565-568. [18] Greeley, R., et al. (1989) *Geology 17*, 665-668, 1989. [19] Lancaster, N., and Greeley, R. (1990) *J. Geophys. Res. 95*, 10,921-10,927. [20] Greeley, R., et al. (1991) *Icarus, 90*, 123-128. [21] Greeley, R., et al. (1992) In *Mars*, Kieffer, H.H. and B. Jakosky (Eds.), Univ. Ariz. Pr., 730-766. [22] Greeley, R., et al. (1992) *J. Geophys. Res. 97*,13,319-13,345. [23] Greeley, R., et al. (1993) *J. Geophys. Res. 98*, 3183-3196. [24] Greeley, R., and Williams, S.H. (1994) *Icarus, 110*, 165-177. [25] Greeley, R., et al. (1994) *Science 263*, 358-361. [26] Greeley, R., et al. (1996) *Sediment. 43*, 41-52 [27] Greeley, R., et al. (1997) *J. Geophys. Res. 102*, 10,971-10,983. [28] Greeley, R., et al. (1997) In *Venus II: Geology, geophysics, atmosphere, and solar wind environment*, S.W. Bougher, D.M. Hunten, and R.J. Phillips (Eds.), Univ. Ariz. Pr., 547-589. [29] Greeley et al. (1999) *J. Geophys. Res. 104*, 8573-8584 (with correction in *J. Geophys. Res. 104*, 22,065). [30] Bridges, N., et al. (1999) *J. Geophys. Res. 104*, 8595-8615. [31] Greeley, R., et al. (2000) *J. Geophys. Res., Planets 105*, 1829-1840. [32] Sullivan, R., et al. (2000) *J. Geophys. Res. 105*, 24,547-24,562. [33] Greeley, R., et al. (2000) *Planet. Sp. Sci. 48*, 1349-1355. [34] Greeley, R., et al. (2001) *Sp. Sci. Rev. 96*, 365-392. [35] Greeley, R., et al. (2002) *J. Geophys. Res., 107*, doi: 10.1029/2000JE001481. [36] Greeley, R. (2002) *Planet. Space Sci., 50*, 151-155. [37] Greeley, R., et al. (2003) *J. Geophys. Res.108*(E5), doi: 10.1029/2002 JE001987. [38] Greeley, R., et al. (2003) *J. Geophys. Res., 108*, doi:10.1029/2002JE002006. [39] Greeley, R., and Thompson, S. (2003) *J. Geophys. Res. 108*, doi:10.1029/2003JE002110. [40] Greeley, R., et al. (2004) *Science 305*, 810-821 [41] Greeley, R., et al. (2004) *J. Geophys. Lett. 31*, L24702, doi:10.1029/2004 GL021599. [42] Lorenz, R.D., et al. (2005) *Icarus, 175*, 556-560. [43] Greeley, R., et al. (2005) *J. Geophys. Res., 110*, doi: 10.1029/2005JE002403. [44] Sullivan, R., et al. (2005) *Nature 436*, 58-61, doi: 10.1038/nature03641. [45] Greeley, R., et al. (2006) *J. Geophys. Res. 111*, doi:10.1029/2005JE002491. [46] Neakrase L.D.V., et al. (2006) *Geophys. Res. Lett. 33*, doi:10.1029/2006GL026810. [47] Greeley, R., et al. (2006) *J. Geophys. Res. 111*, E12S09, doi:10.1029/ 2006JE002743. [48] Golombek, M.P., et al. (2006) *J. Geophys. Res., 111*, E12S10, doi:10.1029/2006JE 002754. [49] Greeley, R., et al. (2008) *J. Geophys. Res. 113*, E06S06, doi:10. 1029/2007JE002971. [50] Sullivan, R., et al. (2008) *J. Geophys. Res., 113*, E06S07, doi:10.1029/2008JE003101. [51] Thomson, B.J., et al. (2008) *J. Geophys. Res., 113*, E08010, doi:10.1029/2007JE003018. [52] Stanzel, C., et al. (2008) *Icarus 197*, 39-51. [53] Neakrase, L.D.V. , and Greeley, R. (2010) *J. Geophys. Res. 115*, E05003, doi:10.1029/2009JE003465 [54] Greeley, R., et al. (2010) *J. Geophys. Res. 115*, E00F02, doi:10.1029 /2010JE003608.

TOPOGRAPHIC PROFILES ACROSS A LARGE REVERSING DUNE, TO AID IN EVALUATING THE REVERSING DUNE HYPOTHESIS FOR TARs ON MARS. J. R. Zimbelman[1] and S. P. Scheidt[1], [1]CEPS/NASM MRC 315, Smithsonian Institution, Washington, D.C., 20013-7012; zimbelmanj@si.edu.

Introduction: The Bruneau Dunes in south-central Idaho are an excellent location to examine reversing dunes, at a site that includes the largest single-structured sand dune in North America [1, 2]. Study of reversing dunes is important for evaluating the hypothesis that large Transverse Aeolian Ridges (TARs) on Mars may be formed as reversing dunes [3].

Results: In April 2011, we obtained precision topographic surveys across the southern end of a 115-m-high reversing dune at Bruneau Dunes using a Differential Global Positioning System (DGPS; Fig. 1). The topographic profiles show a steady progression of the dune from a low sand ridge ridge near the end of the dune (Fig. 2) to a symmetric sand dune as one approaches the highest portion of the dune (Figs. 3-5). Profiles were angled at the dune crest as the relief increased, to keep both portions of the survey line perpendicular to the slope of the dune face. Relief of the crest of the dune, obtained from the surveyed profiles relative to the west side of the dune, show the following progression going up the dune: 2.2 m, 5.5 m (Fig. 2), 6.5 m, 10 m, 16 m (Fig. 3), 17 m, 29 m, 37 m (Fig. 4), 80 m (Fig. 5), 115 m. The central portion of the dune, which includes the highest point along the dune crest, is represented by remarkably symmetric profiles, where both flanks at slopes not far below the angle of repose (Fig. 5). At the time of the surveys, we placed an inexpensive commercial timelapse digital camera (GardenWatchCam) to monitor the dune (Fig. 6); see [4, 5] for discussion of timelapse cameras for aeolian studies.

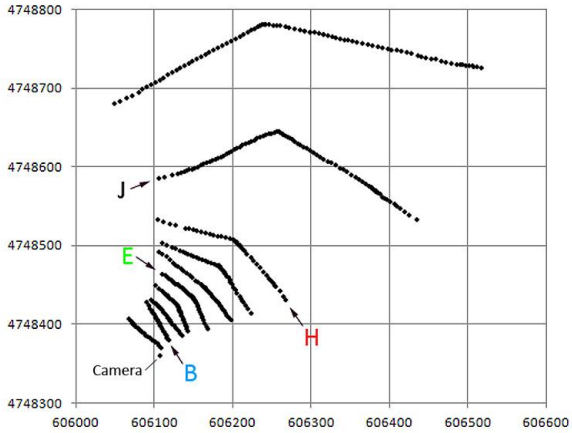

Figure 1. Survey lines over the southern end of a large reservsing dune at Bruneau Dunes, Idaho. Surveys are shown on a UTM grid (zone 11N) with 100-m boxes. Letters indicate profiles shown in Figs. 2 to 5; arrows indicate direction of each profile survey.

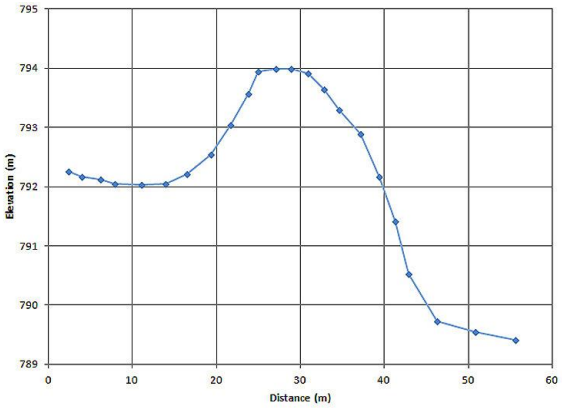

Figure 2. DGPS profile B near the distal end of the dune, going to the NW (see Fig. 1).

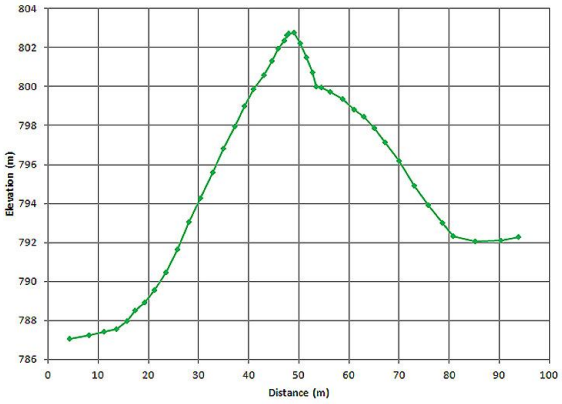

Figure 3. DGPS profile E, showing an enhanced accumulation of sand at the crest as a result of the latest sand-mving winds. Profile goes to SE (see Fig. 1).

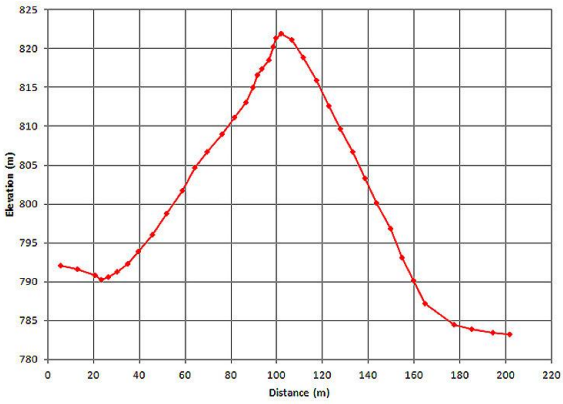

Figure 4. DGPS profile H, where topography is becoming symmetric with respect to both sides of the dune crest. Profile goes to WNW (see Fig. 1).

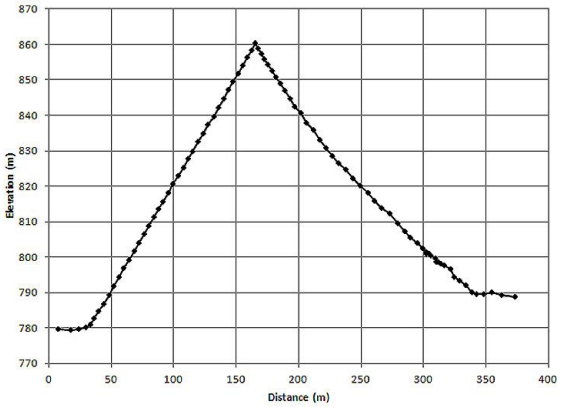

Figure 5. DGPS profile J. Topography here is very symmetric with respect to both sides of the dune crest, which remains the case on all of the central (highest) portion of the dune. Profile goes to E-SE (see Fig. 1).

Figure 6. South end of the Bruneau Dunes, in a photo taken by a GardenWatchCam looking north (see camera location in Fig. 1). Strong saltation, caused by wind blowing to the east, is evident at the dune crest. Timelapse images document movement of dry sand patches over the wet substrate of the main dune. Photo taken on May 5, 2011, at 8:32 pm MDT.

The Remote Automated Weather Station (RAWS) system [6] includes a RAWS installation at the Mountain Home Air Force Base, which is 21 km NW of the Bruneau Dunes. RAWS data has proved useful in studies of wind events at Great Sand Dunes National Park and Preserve in central Colorado [5]. The automatic camera monitoring provides a simple method for relating RAWS wind data from the Moutnain Home AFB site to conditions occurring at the south end of the Bruneau Dunes. Documentation of both the dune topography and the wind regime experienced at Bruneau Dunes will provide a valuable data set for evaluating the reversing dune hypothesis for TARs on Mars.

The work reported here was supported by funds from the Becker Endowment of the Smithsonian Institution.

References: [1] Murphy, J.D. (1973) *The geology of Eagle Cove at Bruneau, Idaho.* M.A. thesis, SUNY - Buffalo. [2] Zimbelman, J.R., and Williams, S.H. (2007) In *The Geology of Mars: Evidence from Earth-based Analogs* (M. Chapman, Ed.), Cambridge Univ. Pr., 232-264. [3] Zimbelman, J.R. (2010) *Geomorph. 121*, 22-29, doi: 10.1016/j.geomorph.2009.05.012. [4] Lorenz, R.D. (2011) *Aeolian Res. 3(2)*, 229-234, doi: 10.1016/j.aeolia.2011.01.004. [5] Lorenz, R.D., and Valdez, A. (2011) *Geomorph. 133(1-2)*, 1-10, doi: 10.1016/j.geomorph.2011.06.003. [6] Zachariassen, J., et al. (2003) *Gen. Tech. Report RMRS-GTR-119*, USDA.